

ELASTIC-PLASTIC SOLUTIONS OF A LONG TUBE SUBJECTED TO A  
TEMPERATURE CYCLE

A THESIS SUBMITTED TO  
THE GRADUATE SCHOOL OF NATURAL AND APPLIED SCIENCES  
OF  
MIDDLE EAST TECHNICAL UNIVERSITY

BY

YASEMIN KAYA

IN PARTIAL FULFILLMENT OF THE REQUIREMENTS  
FOR  
THE DEGREE OF DOCTOR OF PHILOSOPHY  
IN  
ENGINEERING SCIENCES

SEPTEMBER 2014



Approval of the thesis:

**ELASTIC-PLASTIC SOLUTIONS OF A LONG TUBE SUBJECTED TO A  
TEMPERATURE CYCLE**

submitted by **YASEMIN KAYA** in partial fulfillment of the requirements for the degree of **Doctor of Philosophy in Engineering Sciences Department, Middle East Technical University** by,

Prof. Dr. Gülbin Dural  
Dean, Graduate School of **Natural and Applied Sciences**

\_\_\_\_\_

Prof. Dr. Murat Dicleli  
Head of Department, **Engineering Sciences**

\_\_\_\_\_

Prof. Dr. Ahmet N. Eraslan  
Supervisor, **Engineering Sciences Dept., METU**

\_\_\_\_\_

**Examining Committee Members:**

Assoc. Prof. Dr. Zafer Evis  
Engineering Sciences Dept., METU

\_\_\_\_\_

Prof. Dr. Ahmet N. Eraslan  
Engineering Sciences Dept., METU

\_\_\_\_\_

Assoc. Prof. Dr. Yusuf Uludağ  
Chemical Engineering Dept., METU

\_\_\_\_\_

Assist. Prof. Dr. M. Tolga Yılmaz  
Engineering Sciences Dept., METU

\_\_\_\_\_

Assoc. Prof. Dr. Tolga Akış  
Civil Engineering Dept., Atılım University

\_\_\_\_\_

**Date:**

\_\_\_\_\_

**I hereby declare that all information in this document has been obtained and presented in accordance with academic rules and ethical conduct. I also declare that, as required by these rules and conduct, I have fully cited and referenced all material and results that are not original to this work.**

Name, Last Name: YASEMIN KAYA

Signature :

# ABSTRACT

## ELASTIC-PLASTIC SOLUTIONS OF A LONG TUBE SUBJECTED TO A TEMPERATURE CYCLE

Kaya, Yasemin

Ph.D., Department of Engineering Sciences

Supervisor : Prof. Dr. Ahmet N. Eraslan

September 2014, 156 pages

In many engineering applications, cylindrical structures are often subjected to various temperature fluctuations. When the temperature gradient is high enough, the thermal stresses build up in the structure and these stresses may cause the permanent deformation of the body. Therefore, determination and detailed understanding of the thermoelastoplastic stresses in the cylindrical elements are an important issue of engineering design to predict the failures and improve the safety and reliability of the products.

To that end, in this thesis, an uncoupled thermo-elastoplastic problem of a long tube subjected to a temperature cycle from its inner surface is solved. The stress boundary conditions treated are those of stress-free at the inner wall while the outer wall is rigidly constrained. It is presumed that the tube is in a state of generalized plane strain and obeys Tresca's yield criterion and its associated flow rule. After the temperature cycle is applied, the tube experienced three stages; purely elastic, elastic-plastic and finally unloading stage. The analytical formulation of these stages are obtained and the corresponding time-dependent stress, strain and displacement distributions are plotted during the temperature cycle.

The formulation of the problem and the subsequent solutions are cast in general terms and the results may be adapted to a variety of specific applications. In this context, the

present research study will make a theoretical contribution to the literature by giving analytical solution to the problem of thermo-elastoplastic thick-walled tube subjected to temperature cycle.

Keywords: Tube, Thermal Stress, Temperature Cycle, Elastoplasticity

# ÖZ

## SICAKLIK ÇEVİRİMİ ETKİSİ ALTINDAKİ UZUN BİR TÜPÜN ELASTİK-PLASTİK ÇÖZÜMLERİ

Kaya, Yasemin

Doktora, Mühendislik Bilimleri Bölümü

Tez Yöneticisi : Prof. Dr. Ahmet N. Eraslan

Eylül 2014 , 156 sayfa

Bir çok mühendislik uygulamasında kullanılan silindirik yapılar, çeşitli sıcaklık değişimlerine maruz kalmaktadır. Sıcaklık farkı yeteri kadar büyük olduğu zaman, yapıda ısıl gerilmeler meydana gelmektedir. Bu gerilmelerden dolayı, yapı içerisinde sürekli deformasyonlar oluşabilmektedir. Bu sebeple, silindirik yapılarda gelişen bu gerilmelerin detaylarını anlamak ve çözümlenmek, oluşacak deformasyonları tahmin etmek ve yapının güvenilirliği ve sürekliliğini geliştirmek açısından önemli bir mühendislik problemi.

Bu amaçla, bu tezde, iç yüzeyinden bir sıcaklık çevrimine tabi tutulan uzun bir tüpün, ayrık termo-elastoplastik problemi çözülmüştür. Gerilme sınır koşulları olarak, tüpün iç duvarı gerilmeden serbest, ve dış duvarı ise radyal yönde sabitlenmiş olarak ele alınmıştır. Düzlem şekil değiştirme ve Tresca akma kriteri ve ilgili akma kuralı kabul edilmiştir. Tüp, sıcaklık çevrimi uygulandıktan sonra, üç ayrı evreden geçmiştir. Bunlar, elastik, elastik-plastik ve boşaltma evresi olarak adlandırılabilir. Bu evrelere ait analitik formülasyonlar elde edilmiş ve sıcaklık çevrimi boyunca, tüp içerisindeki, bu evrelere karşılık gelen gerilme, gerinim ve yer değiştirme dağılımları grafiğe geçirilmiştir.

Bu problemin formülasyonu ve çözümü genel terimlerle ifade edilmiş olup, problem ve çözümü çeşitli koşullar için uyarlanabilir. Bu bağlamda, bu tez çalışması, kalın

duvarlı silindirik yapıların termo-elastoplastik çözümlenmesini analitik yollarla yaparak, literatüre teorik anlamda bir katkı sağlamaktadır.

Anahtar Kelimeler: Tüp, Isıl Gerilim, Sıcaklık Çevrimi, Elastoplastisite



*To my family*

## ACKNOWLEDGMENTS

I would like to thank my supervisor Prof. Dr. Ahmet N. Eraslan for his advice, guidance and support throughout this study. I would like to particularly express my gratitude to Prof. Dr. Werner Mack (Vienna University of Technology, Austria) for his valuable comments and support.

I am very grateful to all people I know at METU Engineering Sciences Department during my research assistantship.

I am deeply thankful to Memduh Karalar for his love, support and understanding to make the completion of this thesis possible. He was always with me during writing this thesis and the most critical times; and encouraged me in my accomplishment.

Sincerest thanks to each of my family members, my parents Gönül-Ali Kaya, my sisters Derya and Tülin, and my brother Fatih Mehmet, for supporting and believing in me all the way through my academic life. I love them so much, and I would not have made it this far without them.

## TABLE OF CONTENTS

ABSTRACT . . . . .	v
ÖZ . . . . .	vii
ACKNOWLEDGMENTS . . . . .	x
TABLE OF CONTENTS . . . . .	xi
LIST OF TABLES . . . . .	xv
LIST OF FIGURES . . . . .	xvi
LIST OF SYMBOLS . . . . .	xx
CHAPTERS	
1 INTRODUCTION . . . . .	1
1.1 Objective . . . . .	2
1.2 Scope of the Study . . . . .	2
1.3 Research Outline . . . . .	3
1.4 Review of Previous Studies . . . . .	4
1.4.1 Temperature Field in Cylindrical Structures . . . . .	4
1.4.2 Cylindrical Structures under Steady Thermal Loading . . . . .	5

	1.4.3	Cylindrical Structures under Transient Thermal Loading . . . . .	6
2		THEORY . . . . .	9
	2.1	Tensile Test and Stress-Strain Relation . . . . .	9
	2.2	Yield Criteria . . . . .	11
	2.2.1	Tresca Yield Criterion . . . . .	11
	2.2.2	The von Mises Yield Criterion . . . . .	13
	2.3	Flow Rule Associated with the von Mises and Tresca Yield Criteria . . . . .	13
3		DEFINITION OF THE PROBLEM . . . . .	17
	3.1	Basic Equations . . . . .	18
	3.2	Temperature Field . . . . .	20
4		TEMPERATURE DISTRIBUTION . . . . .	23
	4.1	Analytical Solution of Heat Conduction Equation . . . . .	23
	4.2	Numerical Solution of Heat Conduction Equation . . . . .	28
	4.3	Results and Discussion for Temperature Distribution . . . . .	29
5		THERMOELASTIC ANALYSIS OF THE TUBE . . . . .	37
	5.1	Analytical Solution for the Thermoelastic Analysis of the Tube . . . . .	37
	5.2	Numerical Solution Thermoelastic Analysis of the Tube . . . . .	41
	5.3	Results and Discussion of the Analytical and Numerical Solution for the Thermoelastic Analysis . . . . .	45
6		THERMO-ELASTOPLASTIC ANALYSIS OF THE TUBE . . . . .	61
	6.1	Formulation of the Plastic Regions . . . . .	62

6.1.1	Plastic Region 1 . . . . .	62
6.1.2	Plastic Region 2 . . . . .	67
6.1.3	Plastic Region 3 . . . . .	70
6.2	Elastic-Plastic Stages and Numerical Results . . . . .	75
6.2.1	Purely Elastic Stage . . . . .	75
6.2.2	Results and Discussion for Purely Elastic Stage . . . . .	75
6.2.3	Elastic-Plastic First Stage . . . . .	83
6.2.4	Results and Discussion for the Elastic-Plastic First Stage . . . . .	87
6.2.5	Elastic-Plastic Second Stage . . . . .	97
6.2.6	Results and Discussion for the Elastic-Plastic Second Stage . . . . .	103
6.2.7	Elastic-Plastic Third Stage . . . . .	111
6.2.8	Results and Discussion for the Elastic-Plastic Third Stage . . . . .	112
7	UNLOADED STAGE . . . . .	123
7.1	Formulation of the Unloaded Region . . . . .	124
7.2	Results and Discussion for the Unloaded Stage . . . . .	128
8	SUMMARY, CONCLUSIONS AND FUTURE WORK . . . . .	143
8.1	Thesis Summary and Conclusions . . . . .	143
8.2	Future Work . . . . .	145
	REFERENCES . . . . .	147

APPENDICES

A DATA OF PERMANENT PLASTIC STRAINS . . . . . 153

CURRICULUM VITAE . . . . . 155

## LIST OF TABLES

### TABLES

Table 5.1	Axial strain and integration constants obtained from the elastic analytic solution. . . . .	47
Table 6.1	Axial strain and integration constants for the elastic stage . . . . .	76
Table 6.2	Axial strain and integration constants for the elastic-plastic first stage	87
Table 6.3	Axial strain and integration constants for the elastic-plastic second stage . . . . .	103
Table 6.4	Axial strain and integration constants for the elastic-plastic third stage	112
Table 7.1	Axial strain and integration constants for the unloaded stage . . . . .	129
Table A.1	Plastic strains at $\tau = 1.2$ . . . . .	153

## LIST OF FIGURES

### FIGURES

Figure 2.1	Stress-strain curve . . . . .	10
Figure 2.2	Tresca's hexagon with yielding conditions on three-dimensional principal stress space . . . . .	12
Figure 3.1	Tube geometry. . . . .	17
Figure 3.2	Temperature cycle applied to the inner surface of the tube. . . . .	21
Figure 4.1	Description of linear functions of inner surface temperature in time intervals. . . . .	27
Figure 4.2	Temperature cycle applied to inner surface of the tube. . . . .	30
Figure 4.3	Temperature distribution in the tube between $\tau = 0.2 - 1.2$ . . . . .	32
Figure 4.4	Temperature distribution in the tube between $\tau = 1.2 - 1.5$ . . . . .	33
Figure 4.5	Temperature distribution in the tube between $\tau = 1.5 - 2.7$ . . . . .	34
Figure 4.6	Temperature distribution in the tube between $\tau = 2.7 - 3.0$ . . . . .	35
Figure 4.7	Variation of temperature gradient at several time steps during the cycle, $\tau = 0.2 - 3.0$ . . . . .	36
Figure 5.1	Comparison of results of analytical and numerical solution for radial stress distribution in the tube during heating time. . . . .	50
Figure 5.2	Comparison of results of analytical and numerical solution for radial stress distribution in the tube during cooling time. . . . .	51
Figure 5.3	Comparison of results of analytical and numerical solution for tangential stress distribution in the tube during heating time. . . . .	52
Figure 5.4	Comparison of results of analytical and numerical solution for tangential stress distribution in the tube during cooling time. . . . .	53



Figure 5.5 Comparison of results of analytical and numerical solution for axial stress distribution in the tube during heating time. . . . .	54
Figure 5.6 Comparison of results of analytical and numerical solution for axial stress distribution in the tube during cooling time. . . . .	55
Figure 5.7 Comparison of results of analytical and numerical solution for displacement distribution in the tube during heating time. . . . .	56
Figure 5.8 Comparison of results of analytical and numerical solution for displacement distribution in the tube during cooling time. . . . .	57
Figure 5.9 Comparison of Tresca and von Mises' stresses for $q=0.15$ . . . . .	58
Figure 5.10 Comparison of analytical and numerical results for axial strain. . .	59
Figure 5.11 Initial estimates of initial value problem. . . . .	60
Figure 6.1 Radial stress distribution in the tube for purely elastic tube. . . . .	77
Figure 6.2 Tangential stress distribution in the tube for purely elastic tube. . .	78
Figure 6.3 Axial stress distribution in the tube for purely elastic tube. . . . .	79
Figure 6.4 Radial displacement in the tube for purely elastic tube. . . . .	80
Figure 6.5 Response variables in the tube at the end of the elastic stage. . . . .	81
Figure 6.6 Ratio of equivalent stress to yield stress during purely elastic stage.	82
Figure 6.7 Stresses and displacement in elastic-plastic first stage at $\tau = 0.88$ .	89
Figure 6.8 Stresses and displacement in elastic-plastic first stage at $\tau = 0.92$ .	90
Figure 6.9 Stresses and displacement in elastic-plastic first stage at $\tau = 0.96$ .	91
Figure 6.10 Stresses and displacement at the end of elastic-plastic first stage, $\tau = 0.99773$ . . . . .	92
Figure 6.11 Plastic strains in elastic-plastic first stage at $\tau = 0.88$ . . . . .	93
Figure 6.12 Plastic strains in elastic-plastic first stage at $\tau = 0.92$ . . . . .	94
Figure 6.13 Plastic strains in elastic-plastic first stage at $\tau = 0.96$ . . . . .	95
Figure 6.14 Plastic strains at the end of elastic-plastic first stage at $\tau = 0.99773$	96
Figure 6.15 Stresses and displacement in elastic-plastic second stage at $\tau = 1.05$	105
Figure 6.16 Stresses and displacement in elastic-plastic second stage at $\tau = 1.1$	106

Figure 6.17 Stresses and displacement at the end of elastic-plastic second stage, $\tau = 1.12757$ . . . . .	107
Figure 6.18 Plastic strains in elastic-plastic second stage at $\tau = 1.05$ . . . . .	108
Figure 6.19 Plastic strains in elastic-plastic second stage at $\tau = 1.1$ . . . . .	109
Figure 6.20 Plastic strains at the end of elastic-plastic second stage, $\tau = 1.12757$	110
Figure 6.21 Stresses and displacement in elastic-plastic third stage at $\tau = 1.14$ .	113
Figure 6.22 Stresses and displacement in elastic-plastic third stage at $\tau = 1.16$ .	114
Figure 6.23 Stresses and displacement in elastic-plastic third stage at $\tau = 1.18$ .	115
Figure 6.24 Stresses and displacement at the end of elastic-plastic third stage at, $\tau = 1.2$ . . . . .	116
Figure 6.25 Plastic strains in elastic-plastic third stage at $\tau = 1.14$ . . . . .	117
Figure 6.26 Plastic strains in elastic-plastic third stage at $\tau = 1.16$ . . . . .	118
Figure 6.27 Plastic strains in elastic-plastic third stage at $\tau = 1.18$ . . . . .	119
Figure 6.28 Plastic strains at the end of elastic-plastic third stage at, $\tau = 1.2$ . .	120
Figure 6.29 Evolution of elastic and plastic regions with respect to time. . . . .	121
Figure 6.30 Elastic-plastic stages during temperature cycle . . . . .	122
Figure 7.1 Stresses and displacement in unloaded stage at $\tau = 1.2$ . . . . .	130
Figure 7.2 Stresses and displacement in unloaded stage at $\tau = 1.3$ . . . . .	131
Figure 7.3 Stresses and displacement in unloaded stage at $\tau = 1.4$ . . . . .	132
Figure 7.4 Stresses and displacement in unloaded stage at $\tau = 1.5$ . . . . .	133
Figure 7.5 Stresses and displacement in unloaded stage at $\tau = 1.7$ . . . . .	134
Figure 7.6 Stresses and displacement in unloaded stage at $\tau = 1.9$ . . . . .	135
Figure 7.7 Stresses and displacement in unloaded stage at $\tau = 2.1$ . . . . .	136
Figure 7.8 Stresses and displacement in unloaded stage at $\tau = 2.3$ . . . . .	137
Figure 7.9 Stresses and displacement in unloaded stage at $\tau = 2.5$ . . . . .	138
Figure 7.10 Stresses and displacement in unloaded stage at $\tau = 2.7$ . . . . .	139

Figure 7.11 Ratio of equivalent stress to yield stress between  $\tau = 1.2$  and  $\tau = 2.7$  in unloaded stage . . . . . 140

Figure 7.12 Evolution of elastic and plastic regions during the temperature cycle. 141

## LIST OF SYMBOLS

$a, b$	inner and outer radii of tube
$G$	modulus of rigidity
$J_0, Y_0$	Bessel functions of order zero of first and second kinds
$J_1, Y_1$	Bessel functions of first order, of first and second kinds
$k$	thermal conductivity
$q$	heat load parameter
$r$	radial coordinate
$t$	time
$T$	temperature
$T_0$	initial temperature
$T_m$	maximum temperature
$u$	displacement
$z$	axial direction
$\alpha$	coefficient of thermal expansion
$\beta$	temperature dependent yield parameter
$\varepsilon_r, \varepsilon_\theta, \varepsilon_z$	radial, tangential, and axial strains
$\kappa$	thermal diffusivity
$\lambda$	eigenvalue
$\nu$	Poisson's ratio
$\sigma_r, \sigma_\theta, \sigma_z$	radial, tangential, and axial stresses
$\sigma_0$	yield strength
$\sigma_{th}$	temperature dependent yield stress
$\tau$	dimensionless time variable

# CHAPTER 1

## INTRODUCTION

In various engineering applications, cylindrical structures such as heat generators, nuclear power plants, internal heat generating elements such as spherical shells, tubes, cylinders and rods are often subjected to temperature fluctuations. When the temperature gradient is high enough, the thermoelastoplastic stresses build up in the structure and these stresses may cause the permanent deformation of the body. To that end, determination and detailed understanding of the thermoelastoplastic stresses in the cylindrical elements are an important issue of engineering design to predict the failures and improve the safety and reliability of the products [1]-[4].

Historically, cylinder problems involving mechanical and/or thermal load have been studied extensively due to their practical importance. In the pure elastic domain, solutions with great accuracy have existed [1]-[4]. However, the addition of material yield and plastic deformation greatly increase the complexity of the solution procedure.

Recently numerous research studies have been conducted to analyze the deformation of the cylindrical structure under thermal load. However, there are limited research on the cylindrical structures subject to the cyclic thermal loading. Most of these researches are interested in elastic solution. Further, the elastoplastic analysis of the tube under thermal load is handled by the numerical solution procedures.

The most remarkable research among the recent studies is performed by Arslan et al. [5]. In this research, an elastoplastic analysis of a long solid cylinder subjected to a temperature cycle from its outer surface is examined. However, this research study does not include the tube geometry, which brings along difficulty in the analysis

compared to solid cylinder since the distribution and gradient of temperature in a tube affects the locations of elastic plastic boundaries. Therefore, the tube under thermal load is more difficult to treat than the problem of a thick-walled tube under pressure or mechanical loads [6]. Therefore, this research study is aim to extend the Arslan et al.'s previous work [5] to the tubular geometry. To that end, analytical solutions are derived to determine the stresses, strains, and displacement in a long tube subjected to a temperature cycle. In this context, the present work will make a significant theoretical contribution to the literature. The solution is also applicable to a wide variety of thermal transients.

## **1.1 Objective**

The main objectives of this research study are:

- To determine the temperature field in the tube for the radial direction.
- To investigate the thermoelastic behavior of the tube during one temperature cycle and to verify the analytical model with a numerical model in the elastic analysis of the tube.
- To analyze the thermo-elastoplastic deformation of the tube under higher thermal load during one temperature cycle.

## **1.2 Scope of the Study**

In this study, the research is limited to the thermo-elastoplastic analysis of a hollow circular cylinder subject to a temperature cycle from its inner surface and isolated on its exterior surface. As a mechanical boundary condition, the tube is stress free on the its inner wall and radially constrained from the outer wall.

### 1.3 Research Outline

As a first step, an extensive literature review has been done on the cylindrical structures under thermal load. Next, the literature review is restricted to tubular geometry. Furthermore, the literature review is conducted for the transient thermal loading. Additionally, elastic and elastoplastic studies are performed. As a last step of the literature review, analytical and numerical solutions to the tube problem under the transient thermal loading are investigated.

In the second phase of the research, the temperature cycle applied to the inner surface of the tube is determined to solve the heat conduction equation for the temperature distribution in the tube in the radial direction. As mentioned above, the tube is subjected to the temperature cycle from its inner surface while the outer surface is isolated. And then, the analytical solution of the heat conduction equation is produced by the application of Duhamel's theorem.

Furthermore, as a next step, to verify the analytical solution, a numerical solution is performed by a finite element collocation procedure. Once the temperature function is obtained, it is used to determine the stresses, strains and displacement in the tube.

In the third phase of the research, the results of the temperature solutions obtained earlier section are used to analyze the elastic behavior of the tube. In this part, the analytical model is verified against a numerical model. The tube is examined in terms of thermoelastic behavior during the entire temperature cycle.

In the fourth phase of the research, the analytical model is developed to determine the plastic deformation of the tube by increasing the thermal load. For this purpose, Tresca's yield criterion and a linearly temperature dependent yield stress are used to determine the onset of the plastic yield.

As a last step of the study, the unloading phenomenon is investigated during the temperature cycle.

After all formulations are completed, the corresponding stress, strain and displacement distributions of the tube for the elastic, elastic-plastic and unloaded stages are obtained and evaluated.

The formulation of the problem and the subsequent solutions are cast in general terms and the results may be adapted to a variety of specific applications.

#### **1.4 Review of Previous Studies**

Preliminary studies on thermoelastic stresses in circular cylinders have received a great deal of attention in the past as appeared in the references [7]-[14].

In thermal stress problems, in general, the heat conduction problem is solved first, and the result can be used in determining the stresses. Hence, first, a literature review is given for the solution of temperature field in cylindrical structures. Then, the studies including elastic and plastic deformation of the cylindrical structures under thermal load are presented.

##### **1.4.1 Temperature Field in Cylindrical Structures**

Cylindrical structures subject to thermal load are widely used in the engineering applications. To be able to determine the failures due to temperature gradient in the long term, the detailed analysis of temperature distribution is essential. Considerable research studies on temperature distribution in the cylindrical structures have been done on heat conduction problems including time dependent boundary conditions. Carslaw and Jaeger [51], and Ozisik [15]-[16] presented generalized analytical solutions to basic heat conduction problems.

Transient temperature distributions in tubular structures have been studied various researchers, the most remarkable of which are presented below.

Vedula et al. [17] derived an analytical solution to hollow cylinder with an exponential boundary condition on the inner surface and with external convection to the external environment. In this study, they also performed a series of thermal transient calculations using finite element analysis to verify the accuracy of the derived equations.

The transient response of a thick walled pipe under polynomial thermal loading was



derived using the Duhamel's relationship by Segall [18]. Due to the flexibility of the polynomial used, the derived solution has many practical research and industrial applications.

Kandula [19] presented a closed form approximated solution for the transient temperature distribution in a hollow cylinder with a linear variation in thermal conductivity with temperature. At the end of this study, it is shown that resulting solution agrees closely with the finite difference numerical solution.

#### **1.4.2 Cylindrical Structures under Steady Thermal Loading**

Noda presented governing equations for some basic structures like spherical shells, cylinders, tubes, and thin plates [20]. In his work representative results of temperature dependent computations in comparison to constant properties are depicted.

Eraslan and Argeso extended their previous study [21] by considering temperature dependent physical properties [22]. Various numerical examples were presented for heat generating cylinders and tubes based on plain strain assumption. Numerical solution procedure was handled by a shooting method technique combined with Newton iterations. As a result of this work, the differences between constant and variable physical property behavior of material were shown. The strength of the material decreases with decreasing elastic modulus with temperature. Therefore, the material having temperature dependent physical properties more rapidly deforms plastically than those of having constant properties. It is emphasized that in thermal stress calculations, temperature dependency of physical material properties should be taken into account.

Same authors assessed the temperature dependency of modulus of elasticity, Poisson's ratio, yield strength, the coefficient of thermal expansion, and the thermal conductivity of steel for cylinders and tubes. At the end of this study, they found that among these five physical properties, Poisson's ratio can be taken as constant in the calculations, since the effect of temperature dependency of Poisson's ratio in thermal stress calculations is found not significant [23].

Orcan and Gamer [24] described the elastic-plastic stress distribution of a centrally

heated cylinder with fixed ends based on Tresca's yield criterion and its associated flow rule. They considered a uniform temperature its inside of the cylinder and zero surface temperature. Plastic region first appears at the center and expands towards the surface of the cylinder.

### **1.4.3 Cylindrical Structures under Transient Thermal Loading**

Thermo-elastoplastic analysis of cylindrical structures has received considerable attention in recent years. Analytical and numerical solutions exist in the literature for different temperature and mechanical boundary conditions. The plain strain assumption is valid for long cylinders. Elastic-plastic interfaces are predicted by mostly Tresca or Von Mises' yield criteria. In the plastic solution Neuman's stress-strain temperature relations are used. Prandtl-Reuss' incremental stress-strain relations are assumed to be valid at any point in the plastic region. In most cases, temperature dependent material properties are assumed.

Chu presented an incremental theory to a problem of elastoplastic thick-walled tube subjected to transient thermal loading [6]. On the basis of von Mises' yield criterion, compressibility and strain hardening properties of a material, the solution was performed by using finite difference method. It is shown that the effective stress in a thick-walled tube subjected to transient thermal loading is not a monotonic function of the radius, but depends upon the temperature distribution and gradient in the tube.

Thermal stresses in the cylinders due to the internal heat generation have been widely studied by various authors [25], [28].

Orcan and Eraslan [29], also examined the transient solution of the thermoelastic-plastic deformation of internal heat-generating tubes by considering the thermomechanical coupling effect and the temperature-dependent physical properties of the material. It is seen that the thermomechanical coupling effect is negligible for this specific problem. However, it should be included at early times of the unsteady behavior of systems due to rapid increasing in temperatures. Additionally, it is shown that the temperature dependence of the mechanical and thermal properties of the material affects the computed profiles significantly, therefore, it should be taken into

account in similar models. Furthermore, they also observed at high temperatures that the difference between the effect of constant and variable material properties on stresses, displacement, and plastic strains is significant [30].

Mack and Plöchl [31] presented a semi-analytical solution to the stress distribution in a rotating shrink fit with solid shaft subject to a temperature cycle based on Tresca's yield criterion and associated flow rule.

Jahanian extended his previous studies [32], [33] to a cyclic thermal and mechanical loading [34]. He considered a long hollow cylinder with temperature dependent material properties subject to rapid heating and cooling and axial tension and torsion. The incremental plastic shear strains emerged at second, third and fourth cycles. Plastic stresses were calculated numerically.

Mukhopadhyay and Kumar [35] investigated a problem of an infinitely long annular cylinder with temperature dependent material properties like modulus of elasticity and thermal conductivity. They solved a coupled nonlinear governing equations by using the finite difference method for copper material. As a result of this study, it is seen that the temperature dependency of the material properties can be taken into account in practical applications. Additionally, the transient solution at any time can be evaluated directly from the model.

Zenkour and Abbas compared the results of finite element calculations for cylinders with temperature dependent and independent material properties subjected to a decaying thermal load over time [36].

Shahani and Nabavani [37] solved the quasi-static thermoelasticity problem in a thick-walled cylinder using the finite Henkel transform for the differential equations of both temperature and displacements.

Segall [38] derived the close-form solution for the axisymmetric thick-walled tube under an arbitrary internal thermal loading which is of the form a polynomial and with convection on the surrounding external environment.

Kim and Noda [39] analyzed a thermoelastic problem with two-dimensional unsteady temperature field and associated thermal stress in an infinite hollow circular cylinder.

Kim and Noda used a Green's function approach based on the laminate theory to obtain the temperature field and thermoelastic potential function and Mitchell's function to obtain the thermoelastic stresses.

Radu et al. [40] developed a set of analytical solutions for temperature field and the associated elastic thermal stress distributions in a hollow circular cylinder with traction free surfaces. The cylinder is subjected to sinusoidal transient thermal loading on its inner surface. They compared the analytical solutions with the results from finite element analysis. The sinusoidal thermal load is applied on the inner surface of the cylinder and the solution of temperature distribution is achieved by applying Henkel transform to the integral form.

As mentioned the related literature, there have been numerous research studies to solve the thermoelastic or thermoelastoplastic behavior of cylinders under transient loading. In the elastic domain, the solutions were carried out by the analytical methods whereas the elastoplastic analysis was performed by numerical solution techniques under the transient temperature loading. In this context, the present research study will make a theoretical contribution to the literature by giving analytical solution to the problem of thermo-elastoplastic thick-walled tube subjected to temperature cycle.

## CHAPTER 2

### THEORY

#### 2.1 Tensile Test and Stress-Strain Relation

The most common and easiest test to measure the mechanical properties of a material is the tension test. A cylindrical test specimen is inserted into the test machine and load is applied. Increasing the load, the elongation of the specimen over some distance is measured [41]. A typical load extension diagram is shown in Fig. 2.1. In this figure, nominal stress is represented by  $\sigma_n$  and defined by the load divided by the original cross-section of the specimen. It is represented by

$$\sigma_n = \frac{P}{A}. \quad (2.1)$$

The increase in specimen length per unit original length is defined as conventional or engineering strain and represented by

$$\epsilon = \frac{l - l_0}{l_0}, \quad (2.2)$$

where  $P$  is load,  $A$  is original cross-sectional area,  $l_0$  is unit original length, and  $l$  is the final length after the test. The stress-strain curve indicates the applied stress to the resulting strain and each material has its own unique stress-strain curve.

According to the Fig. 2.1, when the load is increased, length of the specimen increases linearly up to point A, which is known as proportional limit. This portion of the stress-strain diagram is a straight line and the material obeys the Hooke's law. If a

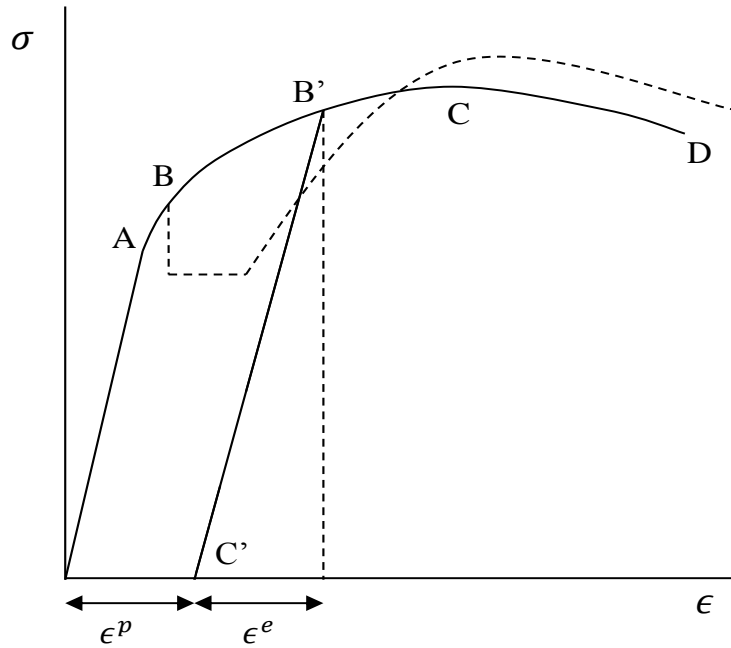


Figure 2.1: Stress-strain curve

further increase occurs after this point, the strain no longer increases linearly but the material is still elastic. In other words, upon release of the load the specimen returns to its original length. This condition continues up to the point B, which is called as elastic limit or yield point. The difference between proportional limit A and elastic limit B is very little, hence, they are assumed the same for many materials. Point B indicates the end of the elastic straining and the initiation of plastic deformation. Beyond the point B, the strain increases at a greater rate. However, the specimen will not deform further unless the load is increased. This condition is defined as work hardening or strain hardening, which is defined as the strengthening of a metal by plastic deformation. At point C, a maximum load is reached. Beyond the point C, at a point D, the specimen neck down and fractures. The maximum load point C is called the tensile strength or ultimate strength. In the Fig. 2.1, line B'C' shows the unloading path when the load is removed at any point between B and C. Some part of strain is recovered, which is elastic part of the strain whereas the other part remains permanently, which is plastic part of the strain. Therefore, total strain is presented by

$$\epsilon = \epsilon^e + \epsilon^p. \quad (2.3)$$

The stress-strain curve can be considered in an ideal form due to the complexity of its natural form. Among the various types of idealization, the elastic-linear strain hardening stress-strain curve is considered in this thesis research.

## 2.2 Yield Criteria

The yield criterion is the combination of multiaxial stresses causing the yielding [42]. It defines the limit of elasticity of the material and the onset of plastic deformation with the any combination of stresses. Numerous criteria have been proposed for the yielding of solid materials. Some of them are maximum stress of Rankine theory, maximum strain or Saint-Venant theory, maximum shear or Tresca criterion, maximum strain energy or Beltram's energy theory, distortion energy or the von Mises yield criterion, Mohr's theory of yielding and international friction theory [41]. Among these criteria, Tresca and von Mises are the more common ones and mostly used. Therefore, these theories are briefly explained below.

### 2.2.1 Tresca Yield Criterion

Tresca yield criterion is also known as the maximum shear theory introduced by tresca in 1868 [43]. Yielding occurs when the highest of the maximum shear stresses attains a critical value  $k$ , which is a material property obtained easily from the tension test as half of the yield strength,  $\sigma_y/2$ . Maximum shear stresses are equal to half the difference between the maximum and minimum principle stresses given by

$$\tau_1 = \pm \frac{1}{2} (\sigma_2 - \sigma_3), \quad (2.4)$$

$$\tau_2 = \pm \frac{1}{2} (\sigma_1 - \sigma_3), \quad (2.5)$$

$$\tau_3 = \pm \frac{1}{2} (\sigma_1 - \sigma_2). \quad (2.6)$$

The maximum shear stress at yielding is  $\sigma_y/2$ , hence any one of the following conditions is reached at the yield point

$$\sigma_1 - \sigma_2 = \pm\sigma_y, \quad (2.7)$$

$$\sigma_2 - \sigma_3 = \pm\sigma_y, \quad (2.8)$$

$$\sigma_3 - \sigma_1 = \pm\sigma_y. \quad (2.9)$$

In other words, yielding occurs when the half of the highest absolute value of the differences of stress pairs is equal to  $k$  [49],

$$\text{Max} \left( \frac{1}{2} |\sigma_1 - \sigma_2|, \frac{1}{2} |\sigma_2 - \sigma_3|, \frac{1}{2} |\sigma_1 - \sigma_3| \right) = k \quad (2.10)$$

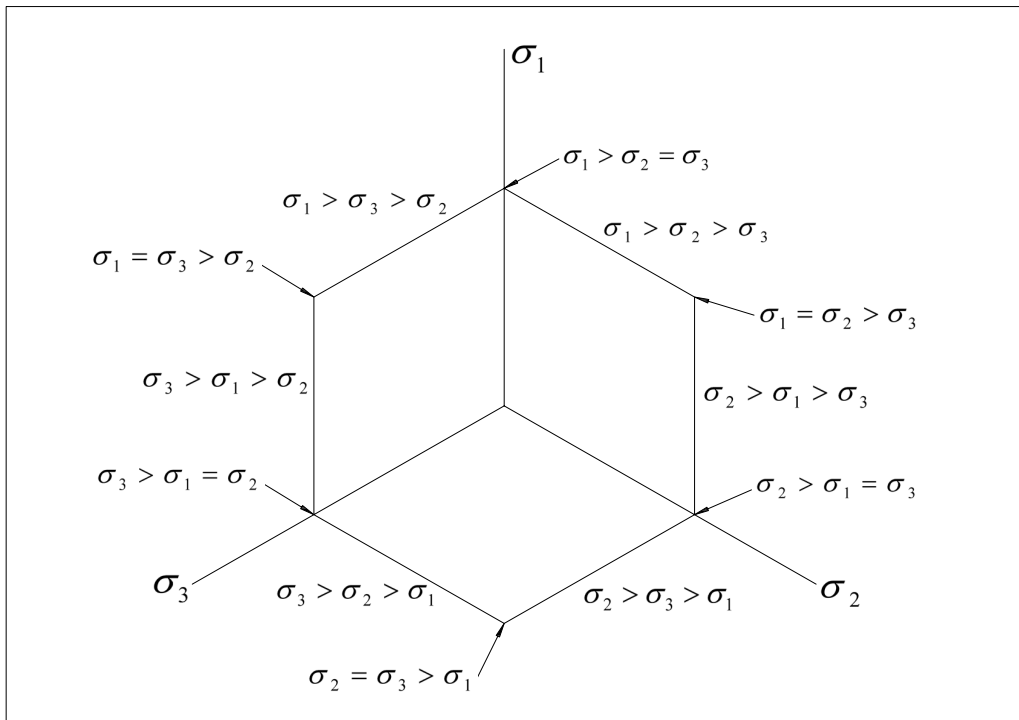


Figure 2.2: Tresca's hexagon with yielding conditions on three-dimensional principal stress space

Fig.2.2 expresses Tresca's criterion in the  $\pi$ -plane. Each of the six sides of the locus is relevant to that which of  $\sigma_1, \sigma_2, \sigma_3$  is the maximum and which is the minimum,



and whether they are tensile or compressive. The onset of yielding is defined at the boundary of the hexagon. The state of stress of inside the yield surface is elastic while the outside of the hexagon states the yielded material [3].

Tresca's yield criterion has a good agreement with experimental results for ductile materials and the theory offers an additional advantage in its ease of applications [3]. The criterion is mostly chosen for the theoretical treatment of the yielding problem since it generally makes a closed form solution possible.

### **2.2.2 The von Mises Yield Criterion**

The von Mises yield criterion is also known as the distortion energy theory introduced by von Mises in 1913 [44]. The yielding occurs in a material when the distortion energy per unit volume equals or exceeds the distortion energy per unit volume in a specimen at yield in tension [48]. This criterion considers both shear and principle stresses whereas most others take into account the effect of either one. The von Mises criterion predicts that the yielding occurs when  $k = \sigma_y/\sqrt{3}$ . This means that, at the onset of yielding, the shear stress in pure shear is  $1/\sqrt{3}$  times the tensile stress in simple tension. The von Mises yield criterion is expressed in principal stresses for pure shear stress as [49]

$$(\sigma_1 - \sigma_2)^2 + (\sigma_2 - \sigma_3)^2 + (\sigma_1 - \sigma_3)^2 = 6k^2 = 2\sigma_y^2.$$

The application of the von Mises criterion is usually easier than the Tresca criterion since Tresca criterion is needed the knowledge of the relative magnitude of the principle stresses. It is also in a good agreement with the experimental data compared to other theories.

### **2.3 Flow Rule Associated with the von Mises and Tresca Yield Criteria**

It is mentioned previously the stress states of Tresca and von Mises criteria at which yielding begins. Here, the stress-strain relations are given in the case of plastic flow.

In the elastic range the strain are linearly vary with the stresses by Hooke's law, however the relation is not linear in the plastic range [41]. Plastic stress-strain relation of material is explained with the flow rules. The flow rule defines the plastic behavior of the material. The first relation between plastic stress-strain relation was introduced by Saint-Venant in 1870 [45]. The ratios of total strain increment to the stress deviations in a general three dimensional equations were given

$$\frac{d\epsilon_x}{S_x} = \frac{d\epsilon_y}{S_y} = \frac{d\epsilon_z}{S_z} = \frac{d\epsilon_{xy}}{S_{xy}} = \frac{d\epsilon_{xz}}{S_{xz}} = \frac{d\epsilon_{yz}}{S_{yz}} = d\lambda, \quad (2.11)$$

or in tensor notation,

$$d\epsilon_{ij} = S_{ij}d\lambda, \quad (2.12)$$

where  $S_{ij}$  is the stress deviator tensor and  $d\lambda$  is a non-negative constant which may vary during the loading [41]. However, in these equations, the elastic strains are ignored, therefore they can only be used in the case of large deformation. Hence, Prandtl [46] and Reuss [47] suggested a more general relation including both elastic and plastic strains as

$$\frac{d\epsilon_x^p}{S_x} = \frac{d\epsilon_y^p}{S_y} = \frac{d\epsilon_z^p}{S_z} = \frac{d\epsilon_{xy}^p}{S_{xy}} = \frac{d\epsilon_{xz}^p}{S_{xz}} = \frac{d\epsilon_{yz}^p}{S_{yz}} = d\lambda. \quad (2.13)$$

They can be expressed with indicial notation,

$$d\epsilon_{ij}^p = S_{ij}d\lambda, \quad (2.14)$$

which assumes that the plastic strain increment  $d\epsilon_{ij}^p$  is related to the deviatoric stress components. The Prandtl -Reuss relations are associated with the von Mises criterion. More generally,

$$d\epsilon_{ij}^p = G_{ij}d\lambda, \quad (2.15)$$

where  $G_{ij}$  is a symmetric tensor since the strain is symmetric and it is function of stresses and some other quantities, i.e. strain hardening or loading history [50]. By using this general form, plastic behavior of many materials can be modeled,

$$d\epsilon_{ij}^p = \frac{\partial g}{\partial \sigma_{ij}} d\lambda, \quad (2.16)$$

where  $g$  is a scalar function and called as plastic potential. Its differentiation with respect to the stresses,  $\partial g / \partial \sigma_{ij}$ , gives the plastic strains. The flow rule Eq. 2.16 is called a non-associative flow rule. When the yield function and the plastic potential function coincide,  $f = g$ , following relation is obtained [50]

$$d\epsilon_{ij}^p = \frac{\partial f}{\partial \sigma_{ij}} d\lambda. \quad (2.17)$$

These relations show that plastic flow develops along the normal to the flow surface  $\partial f / \partial \sigma_{ij}$ . Eq. 2.17 is known as associated flow rule since the flow rule is associated with a yield criterion. It can also be written for several yield functions as

$$d\epsilon_{ij}^p = \frac{\partial f_1}{\partial \sigma_{ij}} d\lambda_1 + \frac{\partial f_2}{\partial \sigma_{ij}} d\lambda_2 + \dots + \frac{\partial f_n}{\partial \sigma_{ij}} d\lambda_n. \quad (2.18)$$

The associated flow rule in terms of principle stresses,

$$d\epsilon_i^p = \frac{\partial f}{\partial \sigma_i} d\lambda. \quad (2.19)$$

As an example, if Tresca yield function is taken as the plastic potential and by considering that the relation of the magnitude of the principal stresses is  $\sigma_1 > \sigma_2 > \sigma_3$ , the yield function is written as

$$f = \sigma_1 - \sigma_3 - 2k = 0. \quad (2.20)$$

By using the associated flow rule Eq. 2.19, the principal plastic strain increments,  $d\epsilon_1^p, d\epsilon_2^p, d\epsilon_3^p$ , can be calculated as

$$d\epsilon_1^p = \frac{\partial f}{\partial \sigma_1} d\lambda = d\lambda, \quad (2.21)$$

$$d\epsilon_2^p = \frac{\partial f}{\partial \sigma_2} d\lambda = 0, \quad (2.22)$$

$$d\epsilon_3^p = \frac{\partial f}{\partial \sigma_3} d\lambda = -d\lambda. \quad (2.23)$$

Similar results can be obtained for the other five possible combinations in algebraic orders of magnitude of the principal stresses.

## CHAPTER 3

### DEFINITION OF THE PROBLEM

In this study, a long tube with outer radius  $b$  and inner radius  $a$  is considered. The surfaces and ends of the tube are traction-free. The problem treated by using a standard cylindrical polar coordinate system, i.e.  $r$  is radial,  $\theta$  circumferential, and  $z$  axial directions shown in Fig. 3.1. Since the length of the tube is very long compared to its thickness, a state of generalized plane strain condition is presumed. Small deformations theory has been taken into account.

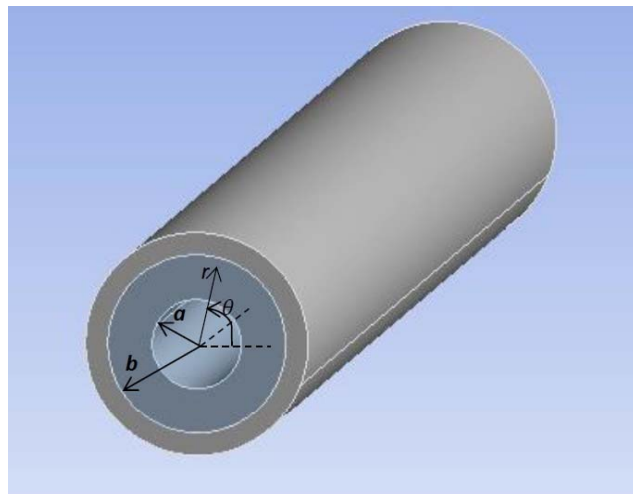


Figure 3.1: Tube geometry.

End effects are ignored for such a long tube and circular symmetry is presumed. This assumption leads to that the stress components dependent on  $r$  only, while the other stress components vanish.

The tube is initially at zero temperature and free of stress. For times  $t > 0$ , the tube is

subjected to a temperature cycle from its inner surface, Fig. 3.2, therefore, thermally induced stresses are developed in the tube.

The objective of this thesis is to investigate the deformations in the tube arising from these thermal stresses. To that end, an elastoplastic analysis of the tube is carried out. As the tube is heated slowly, an uncoupled solution procedure is adopted. The temperature solution, elastic and the plastic stages are formulated separately.

### 3.1 Basic Equations

In the formulation, Timoshenko and Goodier notation is followed [1]. Hence  $\sigma_i$  denotes normal stress,  $\epsilon_i$  normal strain, where ( $i : r, \theta, z$ ), and  $u$  is the radial component of the displacement vector.

Equation of motion in the radial direction:

$$(r\sigma_r)' - \sigma_\theta = 0 \quad (3.1)$$

The relation between stress and strain is linear and expressed with Hooke's law in the elastic range, however this relation is nonlinear in the plastic range. Although the strains can be determined directly by stresses in the elastic range by using Hooke's law, the strain are not uniquely calculated by stresses in the plastic range since they depend on the history of loading or the conditions of the stress state reached.

Experimental results show that the plastic strains are dependent upon the loading path for different materials. Therefore, to compute the differential and the plastic strain increments throughout the loading history are necessary. Thus, the total strains are obtained by summation or integration. However, in the case of radial or proportional loading paths, the stresses increase in the same rate and depend only on the final state of stress [3]. The plastic strain- stress relationships for cylindrical coordinates read

$$\epsilon_r = \frac{1}{2G(1+\nu)}[\sigma_r - \nu(\sigma_\theta + \sigma_z)] + \epsilon_r^p + \alpha T(r, t) \quad (3.2)$$

$$\epsilon_\theta = \frac{1}{2G(1+\nu)}[\sigma_\theta - \nu(\sigma_r + \sigma_z)] + \epsilon_\theta^p + \alpha T(r, t) \quad (3.3)$$

$$\epsilon_z = \frac{1}{2G(1+\nu)}[\sigma_z - \nu(\sigma_r + \sigma_\theta)] + \epsilon_z^p + \alpha T(r, t) \quad (3.4)$$

where,  $G$  represent the modulus of rigidity,  $\nu$  Poisson's ratio, and  $\alpha$  the coefficient of thermal expansion of the material.  $T$  denotes the temperature, and  $\epsilon_i^p$  is the plastic strain components.

The axial strain is independent of the geometric coordinates and as a state of generalized plain strain, it is constant

$$\epsilon_z = \epsilon_0. \quad (3.5)$$

The radial and tangential strains are functions of radial distance  $r$ , and related to the radial displacement by

$$\epsilon_r = u', \quad \epsilon_\theta = \frac{u}{r}. \quad (3.6)$$

The inner surface of the tube is stress free, which is stated as

$$\sigma_r = 0, \quad \text{at } r = a. \quad (3.7)$$

Since the outer wall of the tube is rigidly constrained in the radial direction, at this surface, the boundary condition is defined as

$$u = 0, \quad \text{at } r = b. \quad (3.8)$$

Ends of the tube are free, thus, the total axial force vanishes in any cross-section along the tube. This condition is stated as

$$F_z = 2\pi \int_a^b r \sigma_z dr = 0, \quad (3.9)$$

which is used to determine the constant axial strain  $\epsilon_0$  at any time instant.

Yield stress is defined as a linear function of temperature with the following equation

$$\sigma_{th} = \sigma_0(1 - \beta T). \quad (3.10)$$

where  $\sigma_0$  represents uniaxial yield limit at reference temperature,  $\beta$  is the temperature dependent yield parameter of the material, and  $T$  denotes the difference between the absolute and reference temperature.

The plastic behavior of the tube material is determined by the Tresca yield criterion

$$f = \max(|\sigma_z - \sigma_r|, |\sigma_{theta} - \sigma_r|, |\sigma_z - \sigma_{theta}|) - \sigma_{th} = 0. \quad (3.11)$$

### 3.2 Temperature Field

Before the analysis of stress, strain and displacement distribution, the temperature field in the tube in  $r$ -direction is determined. Temperature cycle applied to inner surface of the tube is shown in Fig. 3.2. As depicted in this figure, the temperature is increased slowly to a maximum temperature,  $T_m$  in time  $t_t$ , then held constant at this temperature for a while,  $t_c$ , and finally, decreased linearly at the same rate to the reference temperature. One cycle is completed in time  $2t_t + t_c$ . The analysis are performed for this single temperature cycle Fig. 3.2.

The temperature field  $T(r, t)$  in the tube is defined by the time dependent, one-dimensional ( $r$ -direction) heat conduction equation for cylindrical coordinates [15], [16]

$$\rho C \frac{\partial T}{\partial t} = \frac{1}{r} \frac{\partial}{\partial r} \left( r k \frac{\partial T}{\partial r} \right), \quad a < r < b, \quad t > 0, \quad (3.12)$$



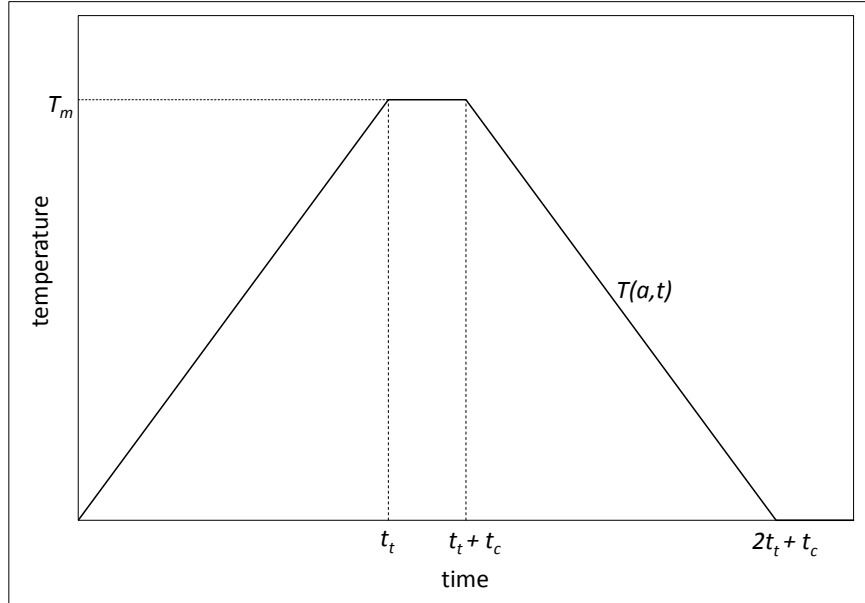


Figure 3.2: Temperature cycle applied to the inner surface of the tube.

where  $\rho$  is the mass density,  $C$  the heat capacity,  $k$  the thermal conductivity of the material. The surface boundary condition prescribed in Fig. 3.2 is expressed mathematically as

$$T(a, t) = \begin{cases} (T_m/t_t)t & \text{for } 0 < t \leq t_t \\ T_m & \text{for } t_t < t \leq t_t + t_c \\ T_m - (T_m/t_t)(t - t_t - t_c) & \text{for } t_t + t_c < t \leq 2t_t + t_c \\ 0 & \text{for } t > 2t_t + t_c. \end{cases} \quad (3.13)$$

The tube is isolated from its outer surface, hence the outer boundary condition is defined as

$$\frac{\partial T(b, t)}{\partial r} = 0, \quad t > 0.$$

Since the tube is assumed initially at zero temperature, the initial condition reads

$$T(r, 0) = 0, \quad a \leq r \leq b. \quad (3.14)$$

Analytical and numerical treatment of heat conduction equation Eq. 3.12 for different purposes is given the next chapter, Ch. 4.

In summary, the problem is solved based on the following assumptions:

- Tube material is homogeneous and isotropic and material properties are independent of temperature.
- Material is incompressible.
- Small deformation theory is adopted.
- Prandtl-Reuss' incremental stress-strain relation is adopted.
- End effects are ignored and plane strain assumption is made for such a long tube.
- Tresca criterion is valid.

## CHAPTER 4

### TEMPERATURE DISTRIBUTION

In this chapter, the solution of heat conduction equation is explained. Analytical and numerical treatment are introduced. The tube is heated from its inner surface by a temperature cycle (Fig. 3.2) and its outer surface is isolated as previously mentioned in Ch. 3. It is assumed that the tube material is initially at zero temperature, and all mechanical and physical properties of the material are independent of the temperature. Once the formulations are developed, the results of the analytical model are compared with those of the results of the numerical solution.

#### 4.1 Analytical Solution of Heat Conduction Equation

In this section, analytical treatment of heat conduction equation is performed by using Duhamel's theorem. Duhamel's theorem is used to derive an analytical heat conduction solution for a body exposed to time variable medium temperatures using a normalized analytical solution of the same body [51]. The details are given below.

In analytical solution, all material properties are assumed to be independent of temperature. Hence, the heat conduction equation can be written as

$$\frac{\partial^2 T}{\partial r^2} + \frac{1}{r} \frac{\partial T}{\partial r} = \frac{1}{\kappa} \frac{\partial T}{\partial t} \quad \text{in } a < r < b, t > 0, \quad (4.1)$$

where  $\kappa (= k/\rho C)$  is thermal diffusivity. Corresponding boundary conditions are

$$T = f(t) \quad \text{at } r = a, \quad (4.2)$$

$$k \frac{\partial T}{\partial r} = 0 \quad \text{at } r = b, \quad (4.3)$$

and the initial condition is

$$T = 0 \quad \text{for } t = 0 \text{ in the region,} \quad (4.4)$$

where  $f(t)$  is a known function of time defining the temperature cycle applied to the inner surface of the tube.

Solution of this problem can be obtained by means of solution of an auxiliary problem by Duhamel application. The auxiliary problem for the main problem is chosen as

$$\frac{\partial^2 \Phi}{\partial r^2} + \frac{1}{r} \frac{\partial \Phi}{\partial r} = \frac{1}{\kappa} \frac{\partial \Phi}{\partial t},$$

with the boundary conditions

$$\begin{aligned} \Phi &= 1 \quad \text{at } r = a, \\ k \frac{\partial \Phi}{\partial r} &= 0 \quad \text{at } r = b, \end{aligned}$$

and the initial condition

$$\Phi = 0 \quad \text{for } t = 0.$$

Generalized solution of the auxiliary problem an infinite hollow circular cylinder is given by Carslaw and Jaeger [51] as

$$\Phi(r, t) = 1 + \pi \sum_{n=1}^{\infty} e^{-\kappa \lambda_n^2 t} \frac{C_0(r, \lambda_n)}{F(\lambda_n)} P(\lambda_n) \quad (4.5)$$

where

$$C_0(r, \lambda_n) = J_0(r\lambda_n)Y_0(a\lambda_n) - Y_0(r\lambda_n)J_0(a\lambda_n), \quad (4.6)$$

$$F(\lambda_n) = J_0(a\lambda_n)^2 - J_1(b\lambda_n)^2, \quad (4.7)$$

$$P(\lambda_n) = J_1(b\lambda_n)^2 \quad (4.8)$$

$\lambda_n$  are the positive roots of

$$k\lambda [J_0(a\lambda)Y_1(b\lambda) - Y_0(a\lambda)J_1(b\lambda)] = 0. \quad (4.9)$$

where  $J_0$  and  $Y_0$  are Bessel functions of order zero of first and second kinds,  $J_1$  and  $Y_1$  are Bessel functions of first order, of first and second kinds.

The main problem Eq.(4.1) is solved by applying Duhamel's theorem to the auxiliary problem as explained by Ozisik in [15], [16].

Duhamel's Theorem,

$$T(r, t) = \int_{t^*=0}^t f(t^*) \frac{\partial \Phi(r, t - t^*)}{\partial t} dt^*. \quad (4.10)$$

Applying Duhamel's theorem to the auxiliary problem Eq.(4.5)

$$\Phi(r, t - t^*) = 1 + \pi \sum_{n=1}^{\infty} e^{-\kappa\lambda_n^2(t-t^*)} \frac{C_0(r, \lambda_n)}{F(\lambda_n)} P(\lambda_n), \quad (4.11)$$

$$\frac{\partial \Phi(r, t - t^*)}{\partial t} = \pi \sum_{n=1}^{\infty} (-\kappa\lambda_n^2) e^{-\kappa\lambda_n^2(t-t^*)} \frac{C_0(r, \lambda_n)}{F(\lambda_n)} P(\lambda_n). \quad (4.12)$$

Substituting the Eq.(4.12) into Eq.(4.10)

$$T(r, t) = \int_{t^*=0}^t f(t^*) \left\{ \pi \sum_{n=1}^{\infty} (-\kappa\lambda_n^2) e^{-\kappa\lambda_n^2(t-t^*)} \frac{C_0(r, \lambda_n)}{F(\lambda_n)} P(\lambda_n) \right\} dt^*$$

and rearranging the solution is obtained as

$$T(r, t) = \pi \sum_{n=1}^{\infty} (-\kappa \lambda_n^2) e^{-\kappa \lambda_n^2 t} \frac{C_0(r, \lambda_n)}{F(\lambda_n)} P(\lambda_n) \int_{t^*=0}^t f(t^*) e^{\kappa \lambda_n^2 t^*} dt^*. \quad (4.13)$$

Since the solution is expressed in the close-form, the temperature field can be adapted for different boundary conditions by means of defining the temperature cycle function  $f(t^*)$  applied on the inner surface.

In this problem, the time-dependent thermal boundary condition is defined on the inner surface as

$$f(t^*) = (T_m/t_t) t^*, \quad (4.14)$$

and substituting it in the Eq.(4.13)

$$T(r, t) = \pi \sum_{n=1}^{\infty} (-\kappa \lambda_n^2) e^{-\kappa \lambda_n^2 t} \frac{C_0(r, \lambda_n)}{F(\lambda_n)} P(\lambda_n) \int_{t^*=0}^t (T_m/t_t) t^* e^{\kappa \lambda_n^2 t^*} dt^* \quad (4.15)$$

and taking the integral,

$$\int_{t^*=0}^t t^* e^{\kappa \lambda_n^2 t^*} dt^* = \frac{1}{\kappa^2 \lambda_n^4} \left[ 1 - e^{-\kappa \lambda_n^2 t} + \kappa \lambda_n^2 t \right]$$

$$T(r, t) = \frac{T_m}{t_t} \pi \sum_{n=1}^{\infty} (1 - e^{-\kappa \lambda_n^2 t} - \kappa \lambda_n^2 t) \frac{C_0(r, \lambda_n)}{\kappa \lambda_n^2 F(\lambda_n)} P(\lambda_n). \quad (4.16)$$

Rearranging this equation

$$T(r, t) = -\frac{T_m}{t_t} t \pi \sum_{n=1}^{\infty} \frac{C_0(r, \lambda_n)}{F(\lambda_n)} P(\lambda_n) + \frac{T_m}{t_t} \pi \sum_{n=1}^{\infty} (1 - e^{-\kappa \lambda_n^2 t}) \frac{C_0(r, \lambda_n)}{\kappa \lambda_n^2 F(\lambda_n)} P(\lambda_n) \quad (4.17)$$

For  $t = 0$ , solution of the auxilary problem Eq.(4.5) should be equal to the initial temperature  $\Phi(r, 0) = 0$ ; thus,

$$0 = 1 + \pi \sum_{n=1}^{\infty} \frac{C_0(r, \lambda_n)}{F(\lambda_n)} P(\lambda_n) \quad (4.18)$$

which gives the close-form expression for the first series on the right-side of Eq.(4.17),

$$\pi \sum_{n=1}^{\infty} \frac{C_0(r, \lambda_n)}{F(\lambda_n)} P(\lambda_n) = -1 \quad (4.19)$$

Substituting Eq.(4.19) into Eq.(4.17) , then the final solution becomes

$$T(r, t) = \frac{T_m}{t_t} t + \frac{T_m}{t_t} \frac{\pi}{\kappa} \sum_{n=1}^{\infty} (1 - e^{-\kappa \lambda_n^2 t}) \frac{C_0(r, \lambda_n)}{\lambda_n^2 F(\lambda_n)} P(\lambda_n). \quad (4.20)$$

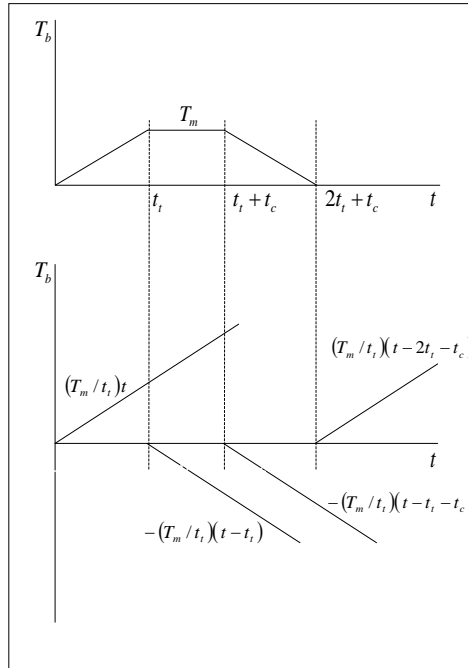


Figure 4.1: Description of linear functions of inner surface temperature in time intervals.

In this case, the hollow cylinder is subjected to the temperature cycle from its inner surface given by Eq.(3.13). On the other hand, the solution obtained for  $T(r, t)$  should be adapted to the all time intervals in the cycle by making superposition as

$$T(r, t) = \begin{cases} T(r, t) & \text{for } 0 < t \leq t_t \\ T(r, t) - T(r, t - t_t) & \text{for } t_t < t \leq t_t + t_c \\ T(r, t) - T(r, t - t_t) - T(r, t - t_t - t_c) & \text{for } t_t + t_c < t \leq 2t_t + t_c \\ T(r, t) - T(r, t - t_t) - T(r, t - t_t - t_c) \\ \quad + T(r, t - 2t_t - t_c) & \text{for } t > 2t_t + t_c \end{cases} . \quad (4.21)$$

Superposition is achieved by defining the linear functions of temperature, which are depicted in Fig. 4.1, in each time steps.

## 4.2 Numerical Solution of Heat Conduction Equation

The numerical solution of heat conduction equation is carried out by using a computer code PDECOL [52]. To that end, the heat conduction equation Eq.(4.1) is written in the nondimensional form in terms of the dimensionless variables  $\bar{r} = r/b$ ,  $\bar{T} = T/T_m$ ,  $\tau = \kappa t/b^2$ . The dimensionless heat conduction equation and the accompanying conditions become after some algebra

$$\frac{\partial^2 \bar{T}}{\partial \bar{r}^2} + \frac{1}{\bar{r}} \frac{\partial \bar{T}}{\partial \bar{r}} = \frac{\partial \bar{T}}{\partial \tau} \quad \text{in } \bar{a} < \bar{r} < 1, \quad \tau > 0, \quad (4.22)$$

subject to

$$\bar{T}(\bar{a}, \tau) = f(\tau), \quad \frac{\partial \bar{T}(1, \tau)}{\partial \bar{r}} = 0, \quad \tau > 0, \quad (4.23a)$$

$$\bar{T}(\bar{r}, 0) = 0, \quad \bar{a} \leq \bar{r} \leq 1, \quad (4.23b)$$

It should be noted that because of the existence of the square term and powers of temperature, the conduction equation, Eq.(4.22), is nonlinear. At any time instant, the temperature distribution in the tube is obtained by the numerical solution of this nonlinear equation, Eq.(4.22), with the accompanying conditions by Eqs. (4.23a) and (4.23b). The robust nonlinear parabolic partial differential equation solver PDECOL is used for this purpose. PDECOL is based on the method of lines and uses a finite



element collocation procedure for the discretization of the spatial variable [52]. The numerical solution involves an approximation in the form

$$\bar{T}(\bar{r}, \tau) = \sum_{i=1}^N C_i(\tau) S_i^B(\bar{r}), \quad (4.24)$$

where the coefficients  $C_i(\tau)$  depend only on time and  $S_i^B(\bar{r})$  are the  $B$ -spline basis functions that depend on the radial coordinate  $\bar{r}$  only.  $N$  in the preceding sum designates the number of collocation points in the  $\bar{r}$  - direction. At time  $\tau$  the unknown coefficients  $C_i(\tau)$  are computed by requiring that the solution satisfy the differential equation and the boundary conditions at a set of  $N$  collocation points. The advantages of this technique are that higher order accuracy is obtained with a very small number of collocation points and the solution is continuous.

### 4.3 Results and Discussion for Temperature Distribution

The numerical results of the analytical solution are obtained for the nondimensional and normalized variables. These variables are defined in the form of

$$\bar{r} = r/b, \quad \bar{a} = a/b \quad (4.25)$$

$$\bar{T} = T/T_m \quad (4.26)$$

$$\tau = \kappa t/b^2 \quad (4.27)$$

$$\tau_t = \kappa t_t/b^2 \quad (4.28)$$

$$\bar{\lambda}_n = \lambda_n b \quad (4.29)$$

and Eq.(4.20) becomes,

$$\bar{T}(r, t) = \frac{1}{\tau_t} \left\{ \tau + \pi \sum_{n=1}^{\infty} (1 - e^{-\bar{\lambda}_n^2 \tau}) \frac{P(\bar{\lambda}_n)}{\bar{\lambda}_n^2 F(\bar{\lambda}_n)} C_0(\bar{r}, \bar{\lambda}_n) \right\} \quad (4.30)$$

where

$$\begin{aligned}
C_0(\bar{r}, \bar{\lambda}_n) &= J_0(\bar{r}\bar{\lambda}_n)Y_0(\bar{a}\bar{\lambda}_n) - Y_0(\bar{r}\bar{\lambda}_n)J_0(\bar{a}\bar{\lambda}_n), \\
F(\bar{\lambda}_n) &= J_0(\bar{a}\bar{\lambda}_n)^2 - J_1(\bar{\lambda}_n)^2, \\
P(\bar{\lambda}_n) &= J_1(\bar{\lambda}_n)^2
\end{aligned} \tag{4.31}$$

and the characteristic equation is

$$\bar{\lambda} [J_0(\bar{a}\bar{\lambda})Y_1(\bar{\lambda}) - Y_0(\bar{a}\bar{\lambda})J_1(\bar{\lambda})] = 0. \tag{4.32}$$

For the temperature cycle introduced in Fig. 3.2, the nondimensional time parameters are determined as  $\tau_t = 1.2$  and  $\tau_c = 0.3$ . Fig. 4.2 shows the numerical nondimensional values of the temperature cycle applied to the inner surface of the tube. As shown in this figure, the inner surface of the tube is heated until  $\tau_t = 1.2$ , kept constant at a maximum temperature for a while,  $\tau_c = 0.3$ , and, cooled with the same heating rate until  $\tau = 2\tau_t + \tau_c = 2.7$ . Finally, the temperature of the inner surface decreases to the reference temperature and it remains there after  $\tau \geq 2.7$ . Thus, the cycle is completed. The inner boundary condition is defined with this temperature cycle, while the outer surface of the tube is isolated.

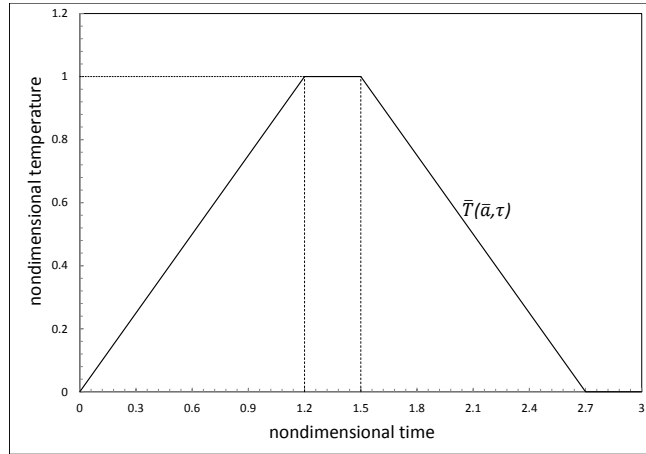


Figure 4.2: Temperature cycle applied to inner surface of the tube.

For this time period, the temperature distributions along the radial direction are obtained. The results of analytical and numerical solutions are presented. The variations of temperature at several time steps are plotted in Figures 4.3-4.6.

As shown in these figures, at the inner surface,  $\bar{r} = \bar{a}$ , the boundary temperature is dictated by the cycle depicted in Fig. 3.2 whereas at the outer surface the insulation boundary condition holds.

In these figures, the results of the analytical solution are represented with the solid lines, while the dots show the results of the numerical computation.

Fig. 4.3 shows the temperature distribution in the tube at the heating time interval until  $\tau = 1.2$ . At the maximum temperature value of the inner wall of the tube, the temperature distribution in the  $r$ -direction in the tube is plotted in Fig. 4.4 at different time steps. Cooling section is depicted in Fig. 4.5. Finally, the tube reaches to almost initial value at  $\tau = 10$ , shown in Fig. 4.6. It is observed that in these figures the tube reaches the its maximum temperature at time  $\tau = 1.5$ .

Fig. 4.7 shows the variation of temperature gradient at several time steps. As seen in this figure, positive temperature gradients are observed in the time interval  $\tau = 0.2$  and  $\tau = 1.5$  due to the heating, while between  $\tau = 1.5$  and  $\tau = 2.7$  gradients are negative due to the cooling. At time  $\tau = 1.5$ , temperature gradient is almost linear, and as seen in Fig. 4.4, the temperature distribution in the tube approaches to isothermal case at this time. As seen in Fig. 4.7, the temperature gradient reaches its peak value at the inner surface of the tube whereas it is equal to zero at the outer surface since the outer surface of the tube is isolated.

As a result of these comparisons, the analytical solution has been verified with the numerical solution. As a result, analytical and numerical solutions are in a good agreement. In the next calculations, the analytical expressions will be used to calculate the stress field of the tube.

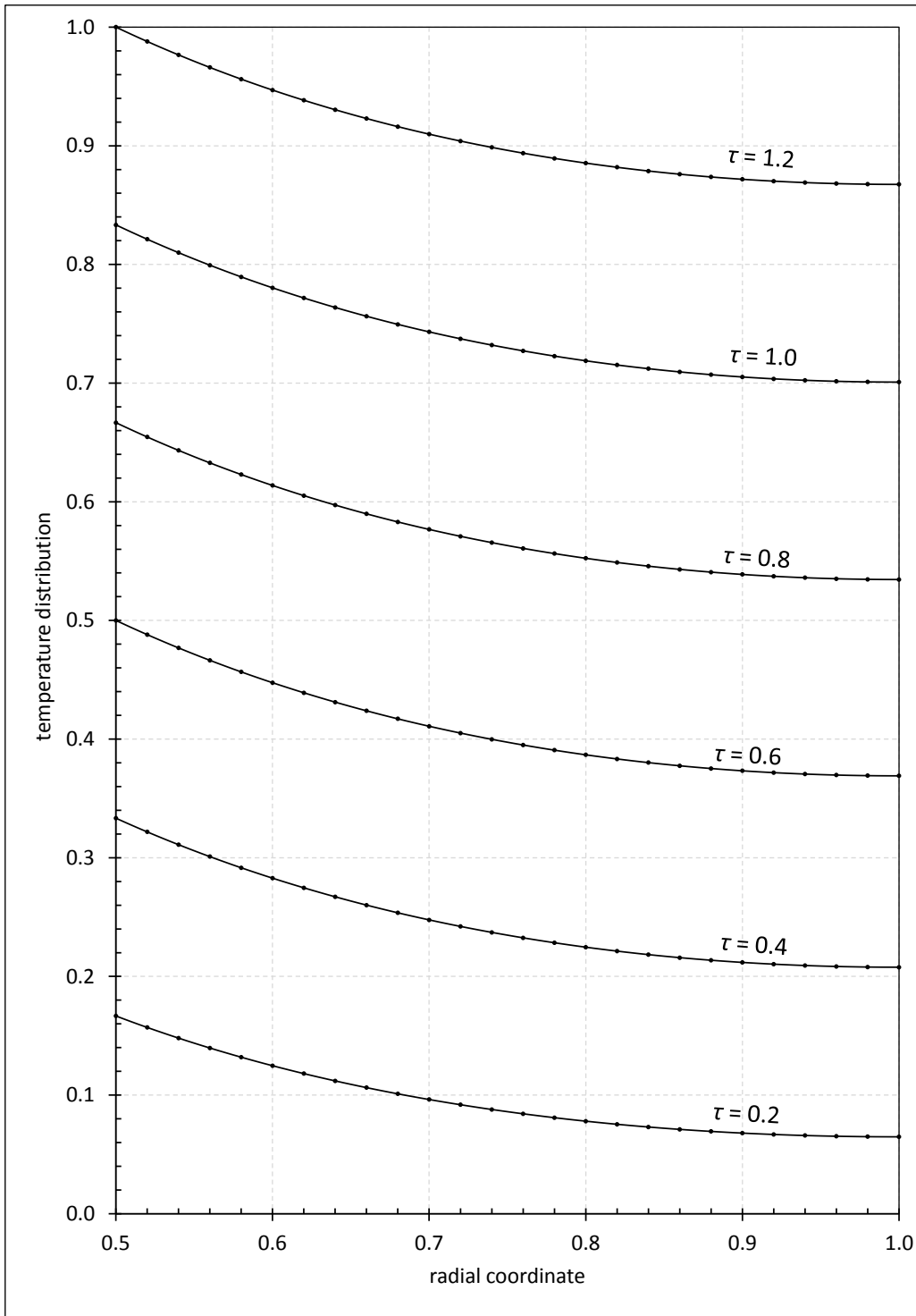


Figure 4.3: Temperature distribution in the tube between  $\tau = 0.2 - 1.2$ .

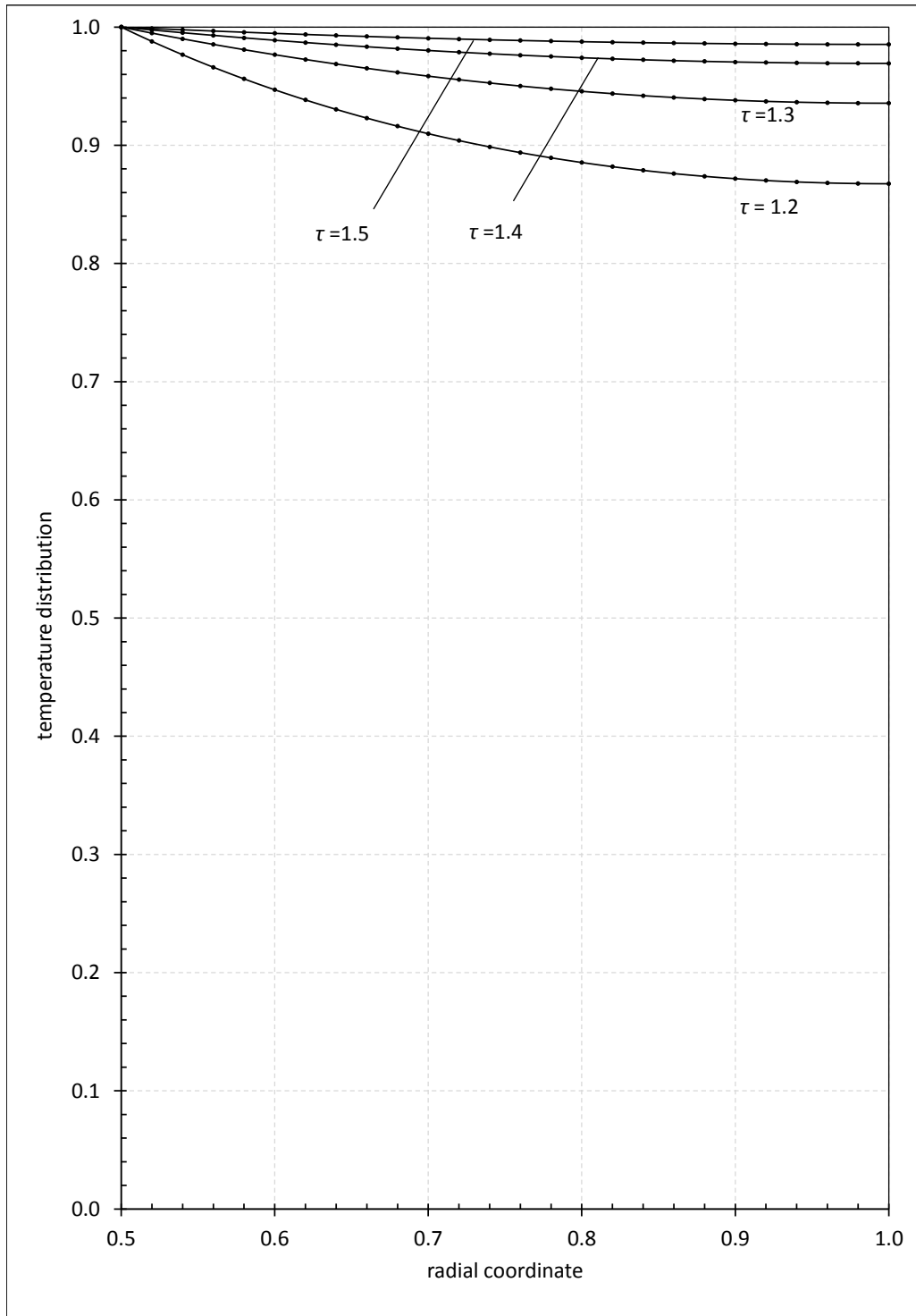


Figure 4.4: Temperature distribution in the tube between  $\tau = 1.2 - 1.5$ .

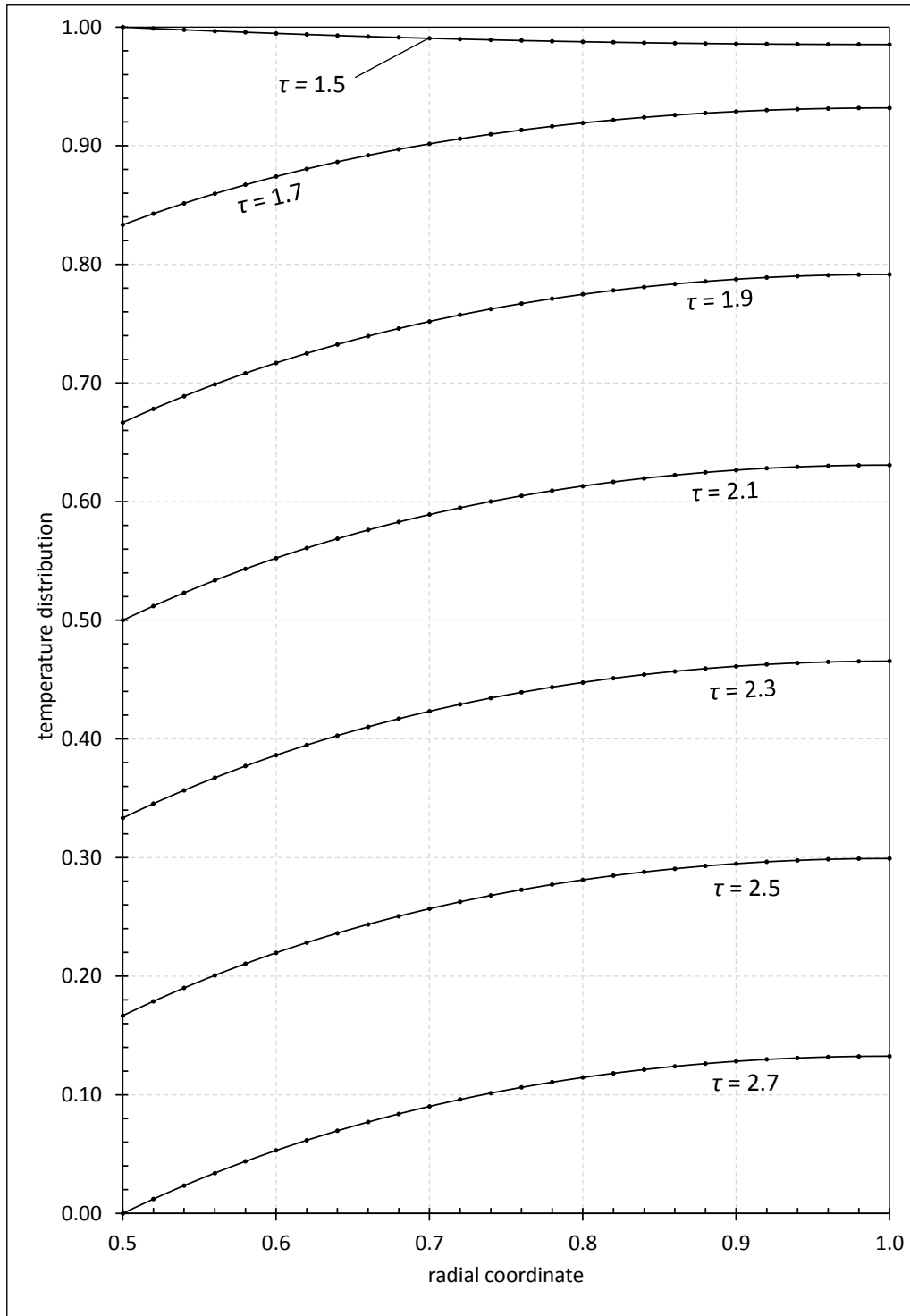


Figure 4.5: Temperature distribution in the tube between  $\tau = 1.5 - 2.7$ .

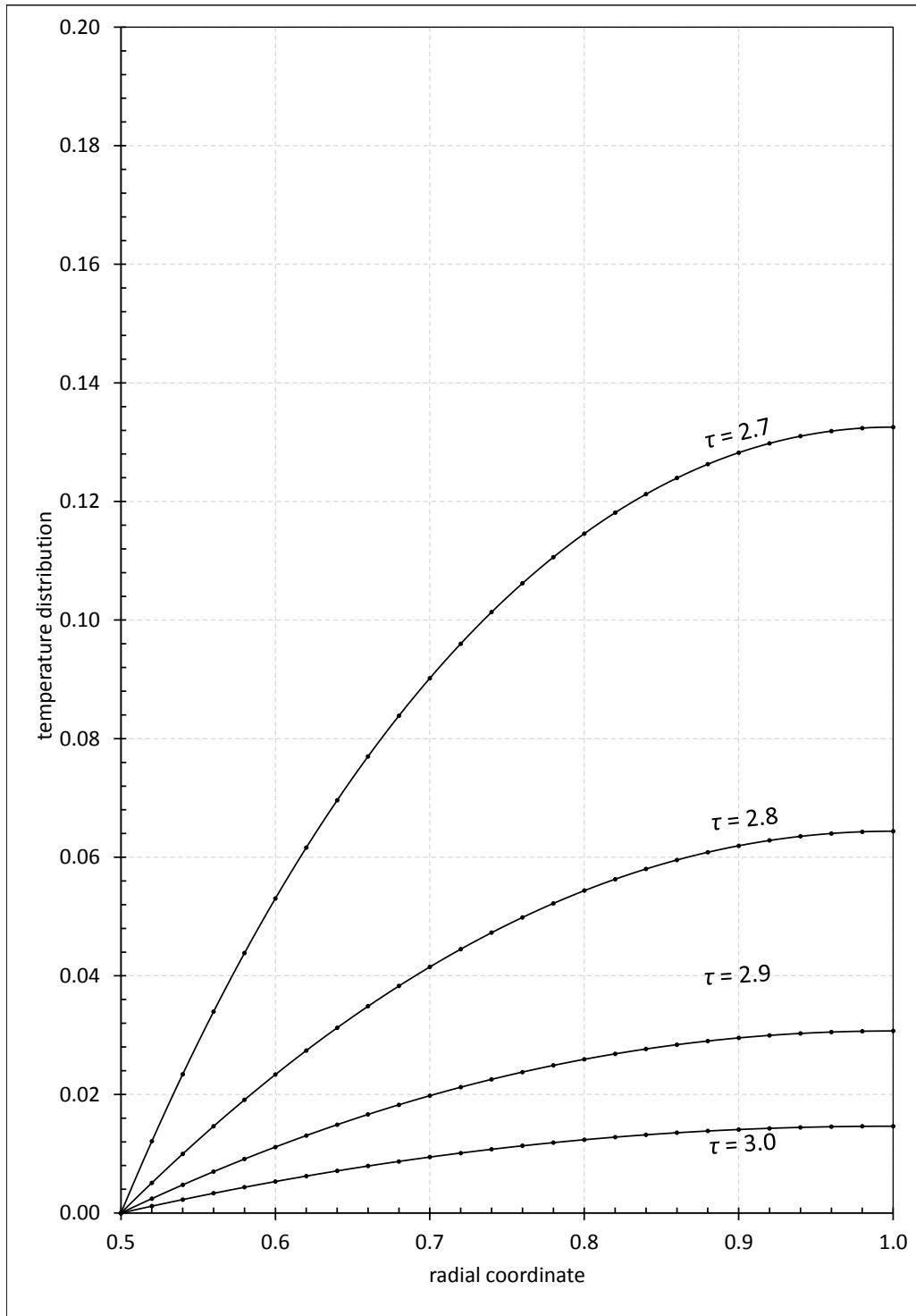


Figure 4.6: Temperature distribution in the tube between  $\tau = 2.7 - 3.0$ .

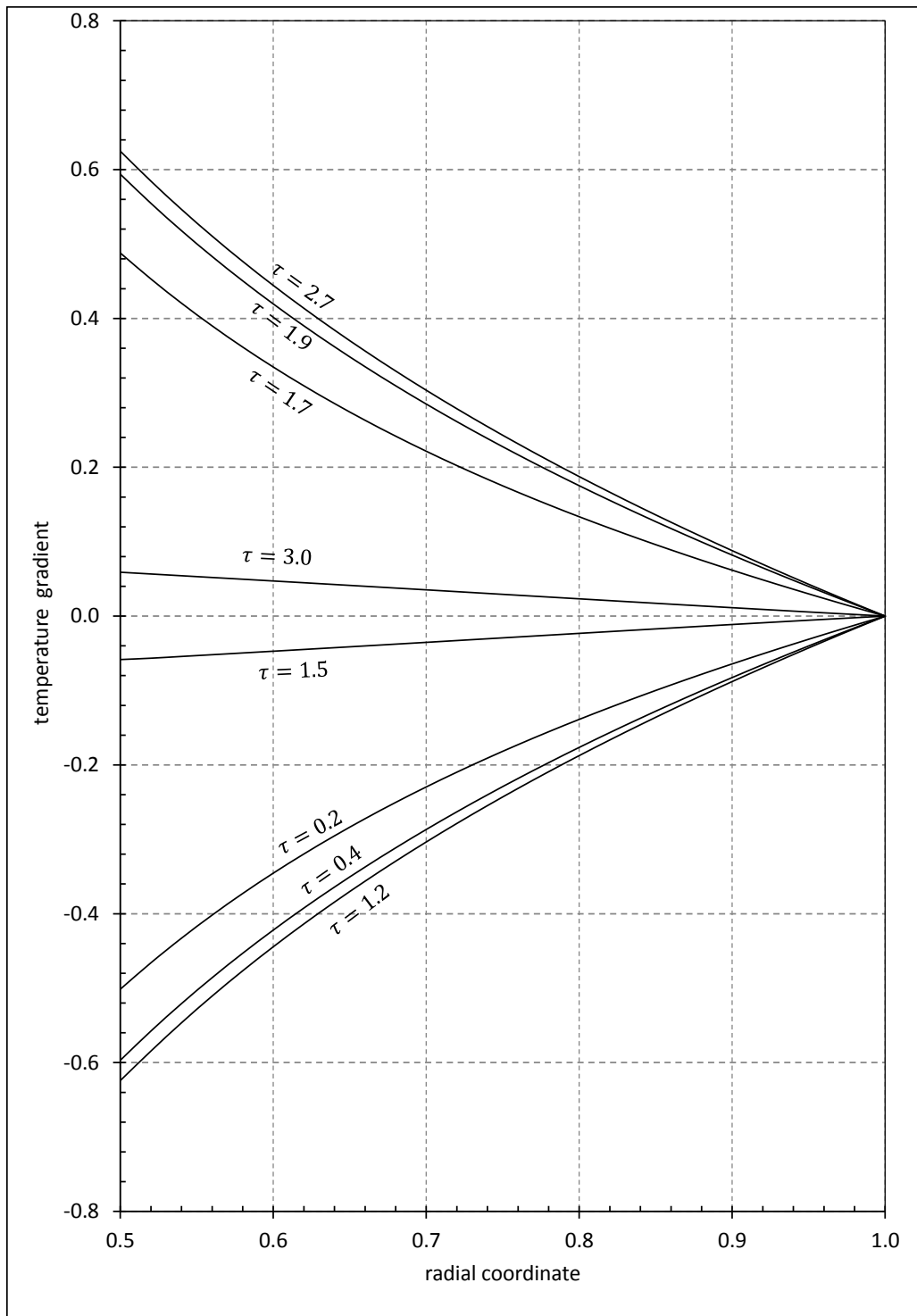


Figure 4.7: Variation of temperature gradient at several time steps during the cycle,  $\tau = 0.2 - 3.0$ .



## CHAPTER 5

### THERMOELASTIC ANALYSIS OF THE TUBE

In this chapter, thermoelastic behavior of the tube during the temperature cycle is studied. Temperature distribution in the tube is achieved by the solution of heat conduction equation explained in the previous chapter. For this temperature distribution, the elastic analytical solution is derived. Then, the verification of the analytical solution is achieved by the comparison with a numerical solution.

#### 5.1 Analytical Solution for the Thermoelastic Analysis of the Tube

In the elastic part, plastic strains,  $\epsilon_i^p$ , drops in the basic equations, Eqs. 3.2-3.4. The solution is performed with dimensional variables, then the numerical results are given in non-dimensional form.

Starting with solving Eq.(3.4) for axial stress

$$\sigma_z^e = \nu(\sigma_r^e + \sigma_\theta^e) + 2G(1 + \nu) [\epsilon_0 - \alpha T], \quad (5.1)$$

and, by using geometric relations and Hooke's law, elastic stresses are written in terms of radial displacement as

$$\sigma_r^e = \frac{2G}{r(1 - 2\nu)} [\nu u + (1 - \nu)ru' + (\epsilon_0\nu - \alpha(1 + \nu))rT] \quad (5.2)$$

$$\sigma_\theta^e = \frac{2G}{r(1 - 2\nu)} [(1 - \nu)u + \nu ru' + (\epsilon_0\nu - \alpha(1 + \nu))rT] \quad (5.3)$$

Substituting the stresses into the equation of motion Eq.(3.1), the non-homogeneous Euler equation is obtained in the radial direction as

$$r^2 \frac{d^2 u}{dr^2} + r \frac{du}{dr} - u = \frac{r^2 \alpha (1 + \nu)}{1 - \nu} T' \quad (5.4)$$

For the solution of homogeneous part of the above equation is

$$r^2 \frac{d^2 u}{dr^2} + r \frac{du}{dr} - u = 0, \quad (5.5)$$

and homogeneous solution for the radial displacement is derived as

$$u_h^e = \frac{C_1}{r} + C_2 r, \quad (5.6)$$

where  $C_1$ ,  $C_2$  are arbitrary integration constants. Particular solution of the problem is obtained by applying the method of variation of parameters.

$$u_{par}^e = Y_1(r)C_1(r) + Y_2(r)C_2(r) \quad (5.7)$$

$Y_1$  and  $Y_2$  are written via the homogeneous solution:

$$Y_1(r) = \frac{1}{r}, \quad (5.8)$$

$$Y_2(r) = r. \quad (5.9)$$

$$C_1(r) = - \int \frac{Y_2(r)F(r)}{W(r)} dr, \quad (5.10)$$

$$C_2(r) = \int \frac{Y_1(r)F(r)}{W(r)} dr, \quad (5.11)$$

where  $W$  is the Wronskian obtained as

$$W(r) = \begin{vmatrix} Y_1(r) & Y_2(r) \\ Y_1'(r) & Y_2'(r) \end{vmatrix} = \frac{2}{r} \quad (5.12)$$

and  $F(r)$  is the non-homogeneous part of the Eq.(5.4)

$$F(r) = \frac{\alpha(1+\nu)}{1-\nu}T' \quad (5.13)$$

$$C_1(r) = -\frac{\alpha(1+\nu)}{2(1-\nu)} \int r^2 T' dr, \quad (5.14)$$

$$C_2(r) = \frac{\alpha(1+\nu)}{2(1-\nu)}T. \quad (5.15)$$

$$u_{par}^e = \frac{\alpha(1+\nu)}{2(1-\nu)}T - \frac{\alpha(1+\nu)}{2r(1-\nu)} \int r^2 T' dr \quad (5.16)$$

Apply integration by parts to  $\int r^2 T'(r) dr$

$$\int r^2 T' dr = r^2 T - 2 \int r T dr$$

Particular solution obtained as

$$u_{par}^e = \frac{\alpha(1+\nu)}{r(1-\nu)} \int_a^r \xi T d\xi \quad (5.17)$$

and the solution is

$$u^e = u_h^e + u_{par}^e$$

Finally the radial displacement integrated as

$$u^e = \frac{C_1}{r} + C_2 r + \frac{\alpha(1+\nu)}{r(1-\nu)} \int_a^r \xi T d\xi \quad (5.18)$$

Substituting displacement into the stress equations, elastic stresses are obtained as

$$\sigma_r^e = -\frac{2GC_1}{r^2} + \frac{2G}{1-2\nu}(C_2 + \nu\epsilon_0) - \frac{2G\alpha(1+\nu)}{(1-\nu)r^2} \int_a^r \xi T d\xi \quad (5.19)$$

$$\sigma_\theta^e = \frac{2GC_1}{r^2} + \frac{2G}{1-2\nu}(C_2 + \nu\epsilon_0) - \frac{2G\alpha(1+\nu)}{(1-\nu)r^2} \left( r^2 T - \int_a^r \xi T d\xi \right). \quad (5.20)$$

Total axial force vanishes  $F_z^e = 2\pi \int_a^b r\sigma_z dr$ :

$$F_z^e = -\frac{2G\alpha(1+\nu)}{(1-\nu)} \int_a^b rT dr - \frac{(a^2 - b^2)G}{1-2\nu} [(1-\nu)\epsilon_0 + 2\nu C_2]$$

If we substitute  $\sigma_r$  and  $\sigma_\theta$  into  $\sigma_z$ , Eq.(7.4), axial stress is obtained as

$$\sigma_z^e = \frac{2G}{1-2\nu} (2\nu C_2 + (1-\nu)\epsilon_0) - \frac{2G\alpha(1+\nu)}{1-\nu} T. \quad (5.21)$$

In these equations  $C_1$ ,  $C_2$ , and  $\epsilon_0$  are the unknowns to be calculated. For the purely elastic state boundary conditions are;

$$\sigma_r^e = 0, \quad \text{at } r = a, \quad (5.22)$$

$$u^e = 0, \quad \text{at } r = b, \quad (5.23)$$

$$F_z^e = 2\pi \int_a^b r\sigma_z dr = 0. \quad (5.24)$$

Hence, the integration constants are obtained by means of the boundary conditions as

$$C_1 = \frac{a^2\alpha(1+\nu)(b^2(1-\nu) - a^2(1+\nu))}{(a^2 - b^2)(1-\nu)(b^2(1-\nu) + a^2(1+\nu))} \int_a^b rT dr, \quad (5.25)$$

$$C_2 = -\frac{\alpha(1+\nu)(a^2(1-3\nu) - b^2(1-\nu))}{(a^2 - b^2)(1-\nu)(b^2(1-\nu) + a^2(1+\nu))} \int_a^b rT dr, \quad (5.26)$$

$$\epsilon_0 = -\frac{2(a^2 + b^2)\alpha(1+\nu)}{a^4 - b^4 + (a^2 - b^2)^2\nu} \int_a^b rT dr. \quad (5.27)$$

## 5.2 Numerical Solution Thermoelastic Analysis of the Tube

At the beginning of the numerical solution, the elastic stress-strain relations are converted to the nondimensional form by using the previously defined dimensionless variables  $\bar{T} = T/T_m$ ,  $\bar{\sigma}_r = \bar{\sigma}_r/\sigma_0$ . These nondimensional equations are

$$\bar{\epsilon}_r = \frac{1}{2(1+\nu)} [\bar{\sigma}_r - \nu(\bar{\sigma}_\theta + \bar{\sigma}_z)] + q\bar{T}, \quad (5.28)$$

$$\bar{\epsilon}_\theta = \frac{1}{2(1+\nu)} [\bar{\sigma}_\theta - \nu(\bar{\sigma}_r + \bar{\sigma}_z)] + q\bar{T}, \quad (5.29)$$

$$\bar{\epsilon}_z = \frac{1}{2(1+\nu)} [\bar{\sigma}_z - \nu(\bar{\sigma}_r + \bar{\sigma}_\theta)] + q\bar{T}. \quad (5.30)$$

where  $\bar{\epsilon}_j = \epsilon_j G/\sigma$  is a normalized strain component, and  $q = G\alpha T_m/\sigma_0$  is the dimensionless heat load. In terms of dimensionless variables the equation of equilibrium is

$$\frac{d\bar{\sigma}_r}{d\bar{r}} + \frac{\bar{\sigma}_r - \bar{\sigma}_\theta}{\bar{r}} = 0. \quad (5.31)$$

The compatibility relation

$$\bar{\epsilon}_r = \frac{d}{d\bar{r}}(\bar{r}\bar{\epsilon}_\theta), \quad (5.32)$$

and the strain-displacement relations

$$\bar{\epsilon}_\theta = \frac{\bar{u}}{\bar{r}}, \quad \bar{\epsilon}_r = \frac{d\bar{u}}{d\bar{r}}, \quad (5.33)$$

complete the list of basic equations. Here  $\bar{u} = Gu/(\sigma_0 b)$  represents the dimensionless radial displacement.

Remembering the state of generalized plane strain  $\bar{\epsilon}_z = \bar{\epsilon}_0$ , the axial stress  $\bar{\sigma}_z$  is determined from the axial strain equation Eq. (5.30) as

$$\bar{\sigma}_z = 2(1 + \nu)\bar{\epsilon}_0 + \nu(\bar{\sigma}_r + \bar{\sigma}_\theta) - 2(1 + \nu)q\bar{T}. \quad (5.34)$$

This equation is used to eliminate the axial strain wherever it is necessary. Bringing in a stress function  $Y(\bar{r})$  of the form

$$Y(\bar{r}) = \bar{r}\bar{\sigma}_r, \quad (5.35)$$

we find from the equation of equilibrium, Eq. (5.31),  $\bar{\sigma}_\theta = Y'(\bar{r})$ , and as a result the equation of equilibrium is satisfied by the use of  $Y(\bar{r})$  in the equations. The radial and circumferential strain expressions become after eliminating the axial stress

$$\bar{\epsilon}_r = -\nu\bar{\epsilon}_0 - \frac{\nu Y'(\bar{r})}{2} + \frac{(1 - \nu)Y(\bar{r})}{2\bar{r}} + (1 + \nu)q\bar{T}, \quad (5.36a)$$

$$\bar{\epsilon}_\theta = -\nu\bar{\epsilon}_0 + \frac{(1 - \nu)Y'(\bar{r})}{2} - \frac{\nu Y(\bar{r})}{2\bar{r}} + (1 + \nu)q\bar{T}. \quad (5.36b)$$

By the substitution of these strains into the compatibility relation, Eq. (5.32), we obtain

$$\frac{d^2 Y}{d\bar{r}^2} + \frac{1}{\bar{r}} \frac{dY}{d\bar{r}} - \frac{Y}{\bar{r}^2} = -2 \left( \frac{1 + \nu}{1 - \nu} \right) q \frac{d\bar{T}}{d\bar{r}},$$

which is the governing thermoelastic equation. This is a second order, linear, non-homogeneous differential equation. As noted before, the inner surface  $\bar{r} = \bar{a}$  of the tube is free of stress, i.e.  $\bar{\sigma}_r(\bar{a}) = 0$ , and the outer surface  $\bar{r} = 1$  is radially constrained implying  $\bar{u}(1) = 0$ . Under these circumstances, the boundary conditions that accompany the thermoelastic equation are

$$Y(\bar{a}) = 0 \quad (5.37)$$

and, by using Eq.(5.36b) strain-displacement relation ,  $\bar{u} = \bar{\epsilon}_\theta \bar{r}$  , one can write the outer boundary condition as

$$\frac{\nu}{2}Y(1) - \left[ \frac{(1-\nu)}{2} \right] Y'(1) = -\nu\bar{\epsilon}_0 + (1+\nu)q\bar{T}. \quad (5.38)$$

Since the ends in the axial direction are free, we have one additional condition to be satisfied:

$$\int_{\bar{a}}^1 \bar{\sigma}_z dA = 2\pi \int_{\bar{a}}^1 \bar{r} \bar{\sigma}_z d\bar{r} = 0, \quad (5.39)$$

which is used to determine the constant axial stress  $\bar{\epsilon}_0$  at any time instant.

Finally, the thermoelastic equation can be cast into the form

$$Y''(\bar{r}) + \Gamma_1(\bar{r})Y'(\bar{r}) - \Gamma_2(\bar{r})Y(\bar{r}) = \Psi(\bar{r}), \quad (5.40)$$

where

$$\Gamma_1(\bar{r}) = \frac{1}{\bar{r}}, \quad (5.41)$$

$$\Gamma_2(\bar{r}) = \frac{1}{\bar{r}^2}, \quad (5.42)$$

and

$$\Psi(\bar{r}) = -2 \left( \frac{1+\nu}{1-\nu} \right) q \frac{d\bar{T}}{d\bar{r}}. \quad (5.43)$$

Introducing two new variables:  $\phi_1(\bar{r}) = Y(\bar{r})$  and  $\phi_2(\bar{r}) = Y'(\bar{r})$  we may write

$$\frac{d\phi_1}{d\bar{r}} = Y', \quad (5.44a)$$

$$\frac{d\phi_2}{d\bar{r}} = Y'', \quad (5.44b)$$

or by making use of Eq.(5.40)

$$\frac{d\phi_1}{d\bar{r}} = \phi_2, \quad (5.45a)$$

$$\frac{d\phi_2}{d\bar{r}} = -\Gamma_1\phi_2 + \Gamma_2\phi_1 + \Psi. \quad (5.45b)$$

These equations form a system of initial value problems (IVP) and should be solved starting with the initial conditions  $\phi_1(\bar{a}) = Y(\bar{a}) = 0$  and  $\phi_2(\bar{a}) = Y'(\bar{a})$ . Since normally the gradient of  $Y'$  at  $\bar{r} = \bar{a}$  is not known, a Newton iteration scheme is used to obtain the correct value of this gradient by requiring that

$$\left(\frac{\nu}{2}\right) \phi_1 - \left[\frac{(1-\nu)}{2}\right] \phi_2 = -\nu\bar{\epsilon}_0 + (1+\nu)q\bar{T}, \quad (5.46)$$

is satisfied at  $\bar{r} = 1$ . Runge-Kutta-Fehlberg fourth-fifth order integration is used to solve numerically Eqs. (5.45a)-(5.45b). Just a few iterations turn out to be sufficient to reach the correct  $\phi_2(\bar{a}) = Y'(\bar{a})$ . Thereafter, the IVP system is solved once more with converged  $\phi_2(\bar{a})$  to get the distributions of stress and displacement.

On the other hand, an outer iteration loop is performed to determine the value of  $\bar{\epsilon}_0$ . At each iteration, the problem is solved 3 times using  $\bar{\epsilon}_0^k$ ,  $\bar{\epsilon}_0^k + \Delta_\epsilon$  and  $\bar{\epsilon}_0^k - \Delta_\epsilon$ , respectively and corresponding net axial forces

$$F_z(\bar{\epsilon}_0) = \int_{\bar{a}}^1 \bar{\sigma}_z dA, \quad (5.47)$$

are calculated. A better approximation  $\bar{\epsilon}_0^{k+1}$  to the axial strain is then obtained from

$$\bar{\epsilon}_0^{k+1} = \bar{\epsilon}_0^k - \frac{2\Delta_\epsilon F_z(\bar{\epsilon}_0^k)}{F_z(\bar{\epsilon}_0^k + \Delta_\epsilon) - F_z(\bar{\epsilon}_0^k - \Delta_\epsilon)}, \quad (5.48)$$

where  $\Delta_\epsilon$  stands for a small increment of the order  $\bar{\epsilon}_0^k/100$ . Equation (5.48) approaches  $\bar{\epsilon}_0$  in the direction of vanishing net axial force. Starting with a reasonable initial estimate  $\bar{\epsilon}_0^0$ , this iteration scheme converges to the result with a sufficient accuracy in only a few iterations. Further details of the computation is given in Eraslan and Kartal [53].



### 5.3 Results and Discussion of the Analytical and Numerical Solution for the Thermoelastic Analysis

The problem is solved for the non-dimensional and normalized variables. These variables are defined as:

$$\bar{\sigma} = \frac{\sigma_i}{\sigma_0}, \bar{u} = \frac{uG}{b\sigma_0}, \epsilon_i = \frac{\epsilon_i G}{\sigma_0}. \quad (5.49)$$

Heat load parameter is defined as,

$$q = \frac{\alpha T_m G}{\sigma_0}. \quad (5.50)$$

Thus, the stress, strain and displacement expression take the form of

$$\bar{\sigma}_r^e = -\frac{2\bar{C}_1}{\bar{r}^2} + \frac{2}{1-2\nu}(\bar{C}_2 + \nu\bar{\epsilon}_0) - \frac{2q(1+\nu)}{(1-\nu)\bar{r}^2} \int_{\bar{a}}^{\bar{r}} \xi \bar{T} d\xi \quad (5.51)$$

$$\bar{\sigma}_\theta^e = \frac{2\bar{C}_1}{\bar{r}^2} + \frac{2}{1-2\nu}(\bar{C}_2 + \nu\bar{\epsilon}_0) - \frac{2q(1+\nu)}{(1-\nu)\bar{r}^2} \left( \bar{r}^2 \bar{T} - \int_{\bar{a}}^{\bar{r}} \xi \bar{T} d\xi \right) \quad (5.52)$$

$$\bar{\sigma}_z^e = \frac{2}{1-2\nu} (2\nu\bar{C}_2 + (1-\nu)\bar{\epsilon}_0) - \frac{2q(1+\nu)}{1-\nu} \bar{T} \quad (5.53)$$

$$\bar{u}^e = \frac{\bar{C}_1}{\bar{r}} + \bar{C}_2 \bar{r} + \frac{q(1+\nu)}{\bar{r}(1-\nu)} \int_{\bar{a}}^{\bar{r}} \xi \bar{T} d\xi \quad (5.54)$$

$$\bar{F}_z^e = -\frac{2q(1+\nu)}{(1-\nu)} \int_{\bar{a}}^1 \bar{r} \bar{T} d\bar{r} - \frac{(\bar{a}^2 - 1)}{1-2\nu} [(1-\nu)\bar{\epsilon}_0 + 2\nu\bar{C}_2] \quad (5.55)$$

where

$$\bar{C}_1 = \frac{C_1 G}{b^2 \sigma_0}, \bar{C}_2 = \frac{C_2 G}{\sigma_0}.$$

Nondimensional integration constants:

$$\bar{C}_1 = \frac{\bar{a}^2(1+\nu)(-1+\nu+\bar{a}^2(1+\nu))}{(1-\nu)(1-\bar{a}^4-(1-\bar{a}^2)^2\nu)} q \int_{\bar{a}}^1 \bar{r} \bar{T} d\bar{r}, \quad (5.56)$$

$$\bar{C}_2 = \frac{(1+\nu)(-1+\nu+\bar{a}^2(1-3\nu))}{(1-\bar{a}^2)(1-\nu)(1-\nu+\bar{a}^2(1+\nu))} q \int_{\bar{a}}^1 \bar{r} \bar{T} d\bar{r}, \quad (5.57)$$

$$\bar{\epsilon}_0 = \frac{2(1+\nu)(1+\bar{a}^2)}{1-\bar{a}^4-(\bar{a}^2-1)^2\nu} q \int_{\bar{a}}^1 \bar{r} \bar{T} d\bar{r}. \quad (5.58)$$

Temperature integrals are calculated as

$$\bar{T} = \bar{T}_1 + \bar{T}_2 \quad (5.59)$$

$$\bar{T}_1 = \frac{\tau}{\tau_t} \quad (5.60)$$

$$\bar{T}_2 = \frac{\pi}{\tau_t} \sum_{n=1}^{\infty} (1 - e^{-\bar{\lambda}_n^2 \tau}) \frac{C_0(\bar{r}, \bar{\lambda}_n)}{\bar{\lambda}_n^2 F(\bar{\lambda}_n)} P(\bar{\lambda}_n) \quad (5.61)$$

$$\int_{\bar{a}}^{\bar{r}} \xi \bar{T}_1 d\xi = \frac{\tau}{\tau_t} \left\{ \frac{(\bar{r}^2 - \bar{a}^2)}{2} \right\}$$

$$\int_{\bar{a}}^1 \bar{r} \bar{T}_1 d\bar{r} = \frac{\tau}{\tau_t} \left\{ \frac{(1 - \bar{a}^2)}{2} \right\}$$

$$\begin{aligned} \int_{\bar{a}}^{\bar{r}} \xi \bar{T}_2 d\xi &= \frac{\pi}{\tau_t} \sum_{n=1}^{\infty} (1 - e^{-\bar{\lambda}_n^2 \tau}) \frac{P(\bar{\lambda}_n)}{\bar{\lambda}_n^2 F(\bar{\lambda}_n)} \int_{\bar{a}}^{\bar{r}} \bar{r} C_0(\bar{r}, \bar{\lambda}_n) \\ &= \frac{\pi}{\tau_t} \sum_{n=1}^{\infty} (1 - e^{-\bar{\lambda}_n^2 \tau}) \frac{P(\bar{\lambda}_n)}{\bar{\lambda}_n^3 F(\bar{\lambda}_n)} \left\{ Y_0(\bar{a}\bar{\lambda}_n) [\bar{r} J_1(\bar{r}\bar{\lambda}_n) - \bar{a} J_1(\bar{a}\bar{\lambda}_n)] \right. \\ &\quad \left. - J_0(\bar{a}\bar{\lambda}_n) [\bar{r} Y_1(\bar{r}\bar{\lambda}_n) - \bar{a} Y_1(\bar{a}\bar{\lambda}_n)] \right\} \end{aligned}$$

$$\begin{aligned} \int_{\bar{a}}^1 \bar{r} \bar{T}_2 d\bar{r} &= \frac{\pi}{\tau_t} \sum_{n=1}^{\infty} (1 - e^{-\bar{\lambda}_n^2 \tau}) \frac{P(\bar{\lambda}_n)}{\bar{\lambda}_n^2 F(\bar{\lambda}_n)} \int_{\bar{a}}^1 \bar{r} C_0(\bar{r}, \bar{\lambda}_n) \\ &= \frac{\pi}{\tau_t} \sum_{n=1}^{\infty} (1 - e^{-\bar{\lambda}_n^2 \tau}) \frac{P(\bar{\lambda}_n)}{\bar{\lambda}_n^3 F(\bar{\lambda}_n)} \left\{ Y_0(\bar{a}\bar{\lambda}_n) [J_1(\bar{\lambda}_n) - \bar{a} J_1(\bar{a}\bar{\lambda}_n)] \right. \\ &\quad \left. - J_0(\bar{a}\bar{\lambda}_n) [Y_1(\bar{\lambda}_n) - \bar{a} Y_1(\bar{a}\bar{\lambda}_n)] \right\}. \end{aligned}$$

In this section, the thermoelastic behavior of tube along the temperature cycle is investigated. Additionally, the analytical model is verified against the numerical solution. In the calculations, a tube of inner radius  $\bar{a} = 0.5$  is considered under the heat load  $q = 0.15$ .

Stress and displacement distributions in the tube are obtained for the temperature distribution given in Ch.4 and the analytical and numerical results are plotted at the same figures. The distributions of the radial, tangential, and axial stresses as well as the displacement are depicted in the Figures 5.1-5.8, respectively. In these figures, the results of the analytical model are shown with solid lines whereas the numerical solutions are represented by dots.

As a result of the analytical solution, integration constants and axial strain at different time steps are given in Table 5.1. By using these constants, the corresponding stress and displacement distributions are obtained with the analytical solution.

Table 5.1: Axial strain and integration constants obtained from the elastic analytic solution.

$\tau$	$\bar{\epsilon}_0$	$\bar{C}_1$	$\bar{C}_2$
0.2	0.02106	-0.01603	-0.00116
0.4	0.05592	-0.04256	-0.00307
0.6	0.09388	-0.07145	-0.00515
0.8	0.13255	-0.10088	-0.00727
1	0.17137	-0.13043	-0.00940
1.2	0.21023	-0.16000	-0.01153
1.3	0.22235	-0.16922	-0.01220
1.5	0.23076	-0.17562	-0.01266
1.7	0.21161	-0.16105	-0.01161
1.9	0.17718	-0.13485	-0.00972
2.1	0.13932	-0.10603	-0.00764
2.3	0.10068	-0.07662	-0.00552
2.5	0.06186	-0.04708	-0.00339
2.7	0.02300	-0.01750	-0.00126

Fig. 5.1 shows the results of the analytical and numerical solutions for the radial stress distribution at the heating time period. Fig. 5.2 shows the radial stress distribution at the cooling time period. As seen in these figures, the radial stresses in the tube build

up and increase with the increasing temperature. The radial stress is equal to zero at the inner wall of the tube whereas it has the maximum value at the outer wall due to the described boundary conditions.

Fig. 5.3 shows the results of the analytical and numerical solutions for the tangential stress distribution at the heating time period. Fig. 5.4 shows the tangential stress distribution at the cooling time period. These figures show that the tangential stress rapidly increases and very remarkable at the inner wall of the tube with the increasing temperature.

Fig. 5.5 shows the results of the analytical and numerical solutions for the axial stress distribution at the heating time period. Fig. 5.6 shows the axial stress distribution at the cooling time period. As depicted in these figures, the axial stress variation with time is not very significant compared to radial and tangential stresses. It is noted that it changes sign in the tube.

Fig. 5.7 shows the results of the analytical and numerical solutions for the displacement distribution at the heating time period. Fig. 5.8 shows the displacement distribution at the cooling time period. Since the tube is radially constrained, the displacement is equal to zero on the outer surface of the tube while on the inner surface, the displacement increases with the increasing temperature.

Additionally, in this section, the distributions of von Mises stresses:

$$\sigma_{vM} = \sqrt{\frac{1}{2} [(\bar{\sigma}_r - \bar{\sigma}_\theta)^2 + (\bar{\sigma}_r - \bar{\sigma}_z)^2 + (\bar{\sigma}_\theta - \bar{\sigma}_z)^2]},$$

are calculated and compared with the analytical results based on Tresca criterion at various time instants along the cycle. In Fig. 5.9 solid lines represent the results of the ratio of Tresca equivalent stress to yield stress and dots represent the results of the von Mises stresses to yield stress. As seen in this figure, the ratio of both stresses to yield stress imply that the tube behave elastic during the temperature cycle since Tresca and von Mises stresses don't reach the value of yield stress,  $\sigma_{th}$ . Additionally, as seen in this figure, Tresca condition is more conservative compared to the von Mises' criterion in determining the onset of the yielding.

Finally, the variation of axial strain with respect to time is investigated. The axial strain is independent of space coordinates, it is only a function of time. As seen in Fig. 5.10, variation of axial strain with time follows the similar trend of temperature cycle applied to the inner surface. The axial strain reaches to its maximum value at the end of the time for the maximum temperature interval.

As a computational detail the converged values of  $\phi_2(\bar{a})$  along the cycle are plotted in Fig. 5.11. On average, three iterations are performed to reach convergence for  $\epsilon_0$ , and only a few iterations are required to reach the correct  $\phi_2(\bar{a})$ .

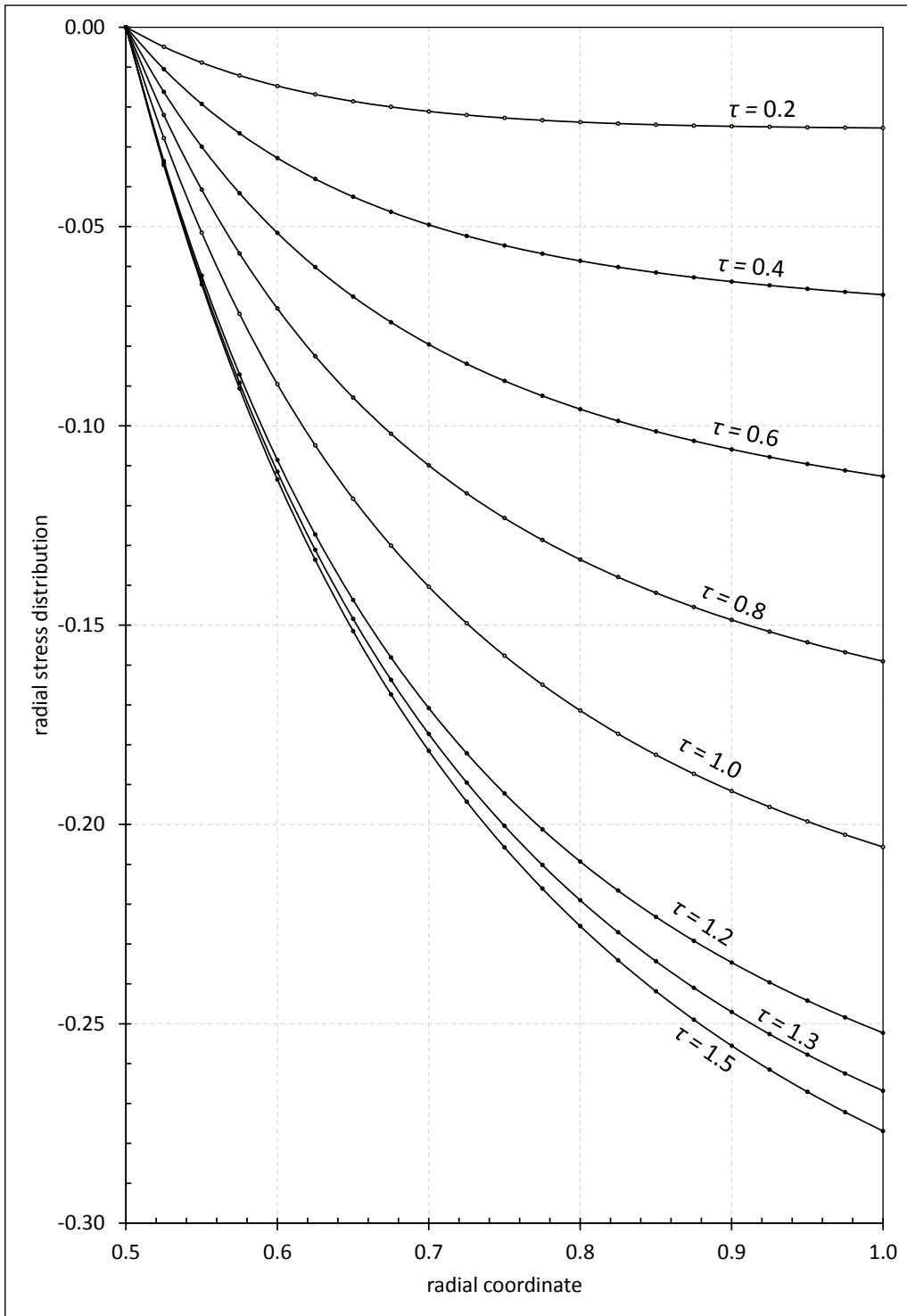


Figure 5.1: Comparison of results of analytical and numerical solution for radial stress distribution in the tube during heating time.

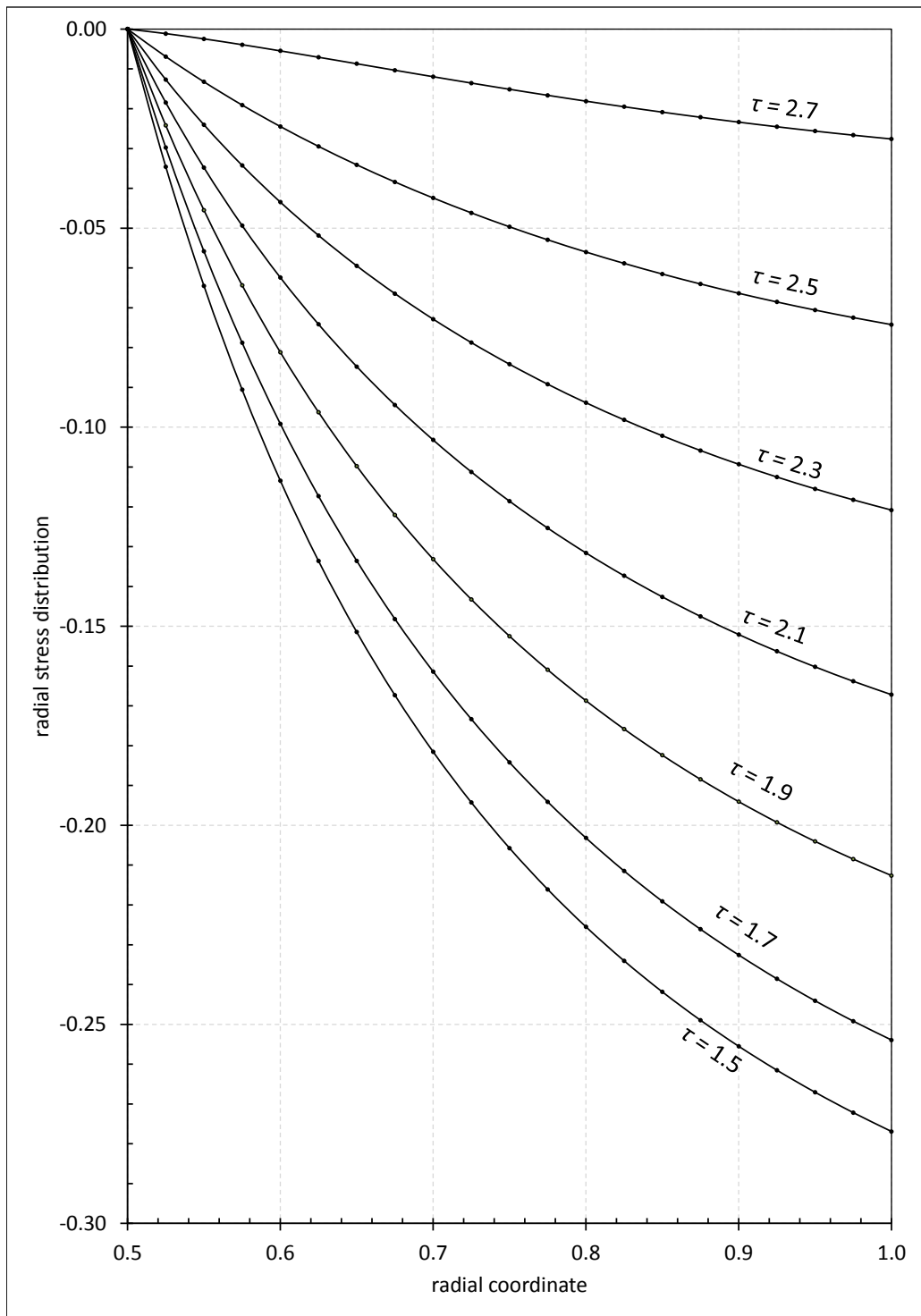


Figure 5.2: Comparison of results of analytical and numerical solution for radial stress distribution in the tube during cooling time.

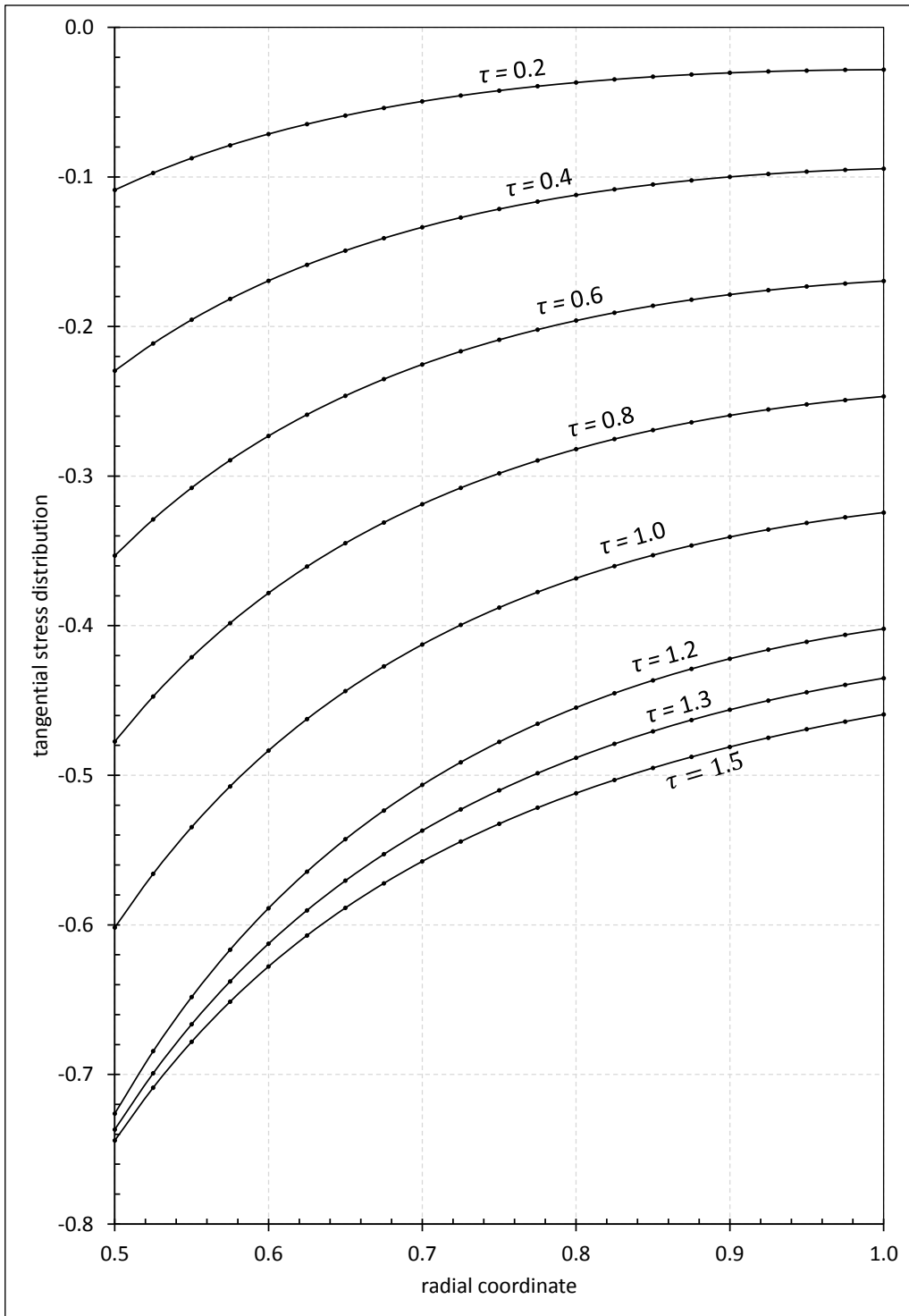


Figure 5.3: Comparison of results of analytical and numerical solution for tangential stress distribution in the tube during heating time.



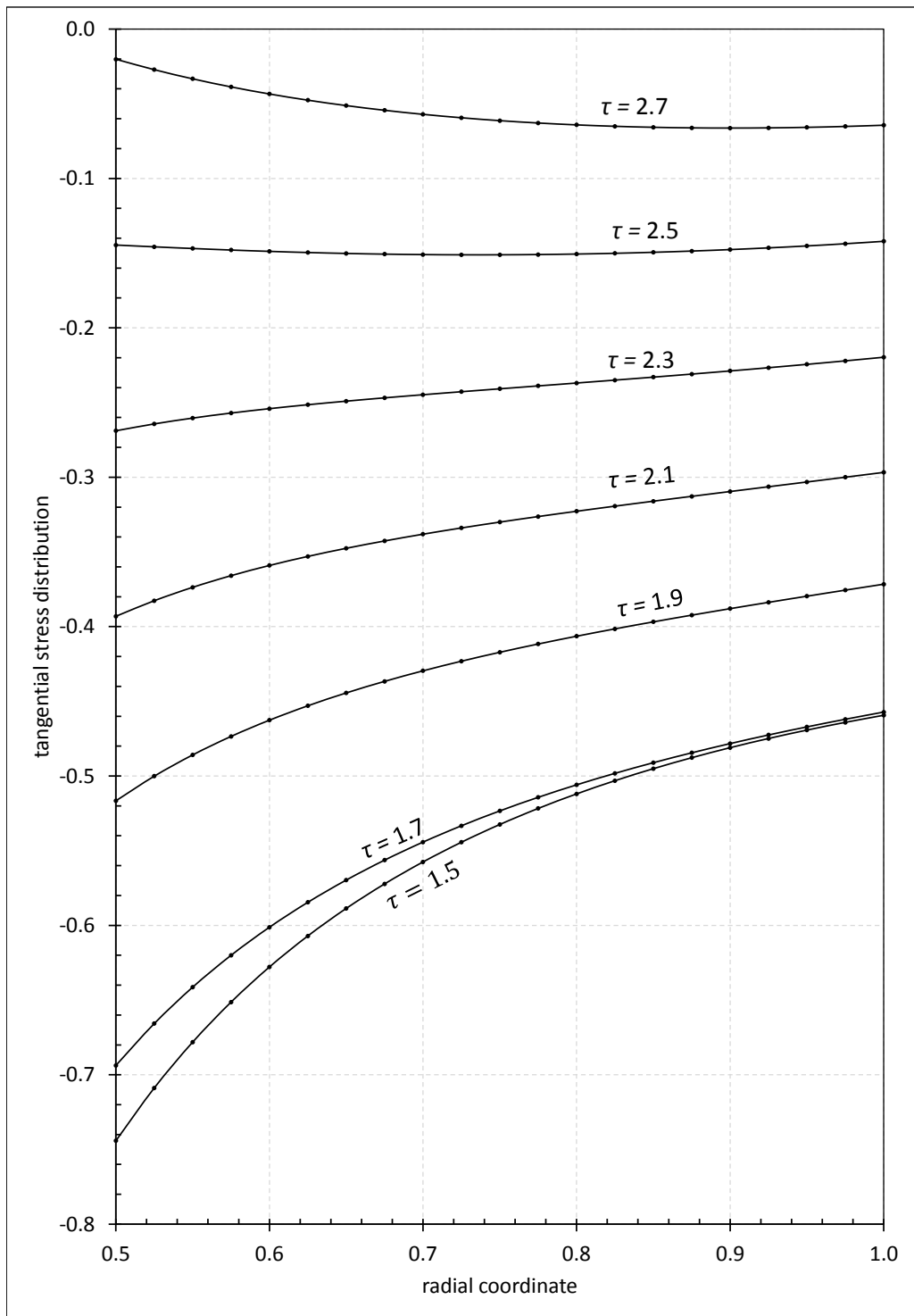


Figure 5.4: Comparison of results of analytical and numerical solution for tangential stress distribution in the tube during cooling time.

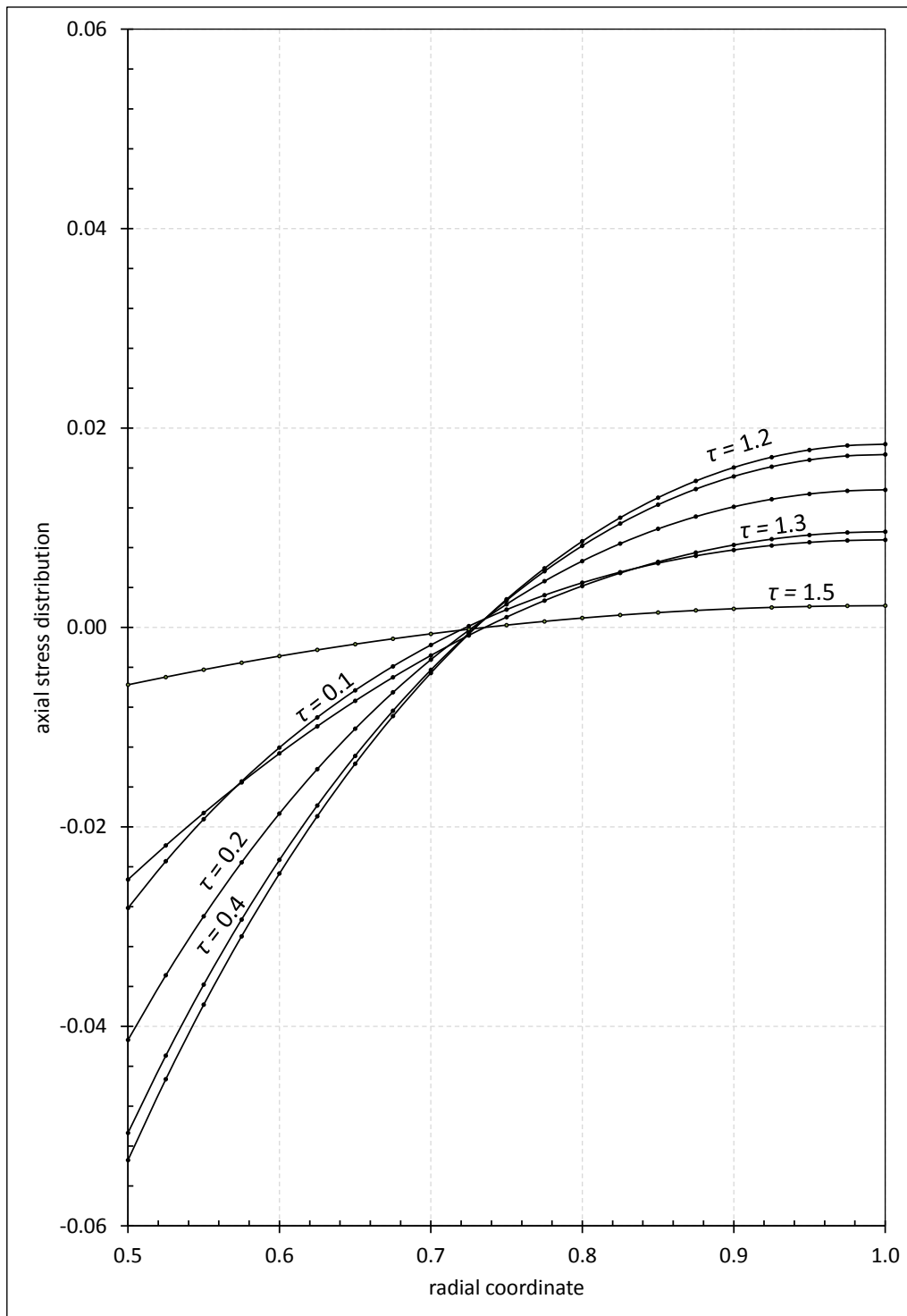


Figure 5.5: Comparison of results of analytical and numerical solution for axial stress distribution in the tube during heating time.

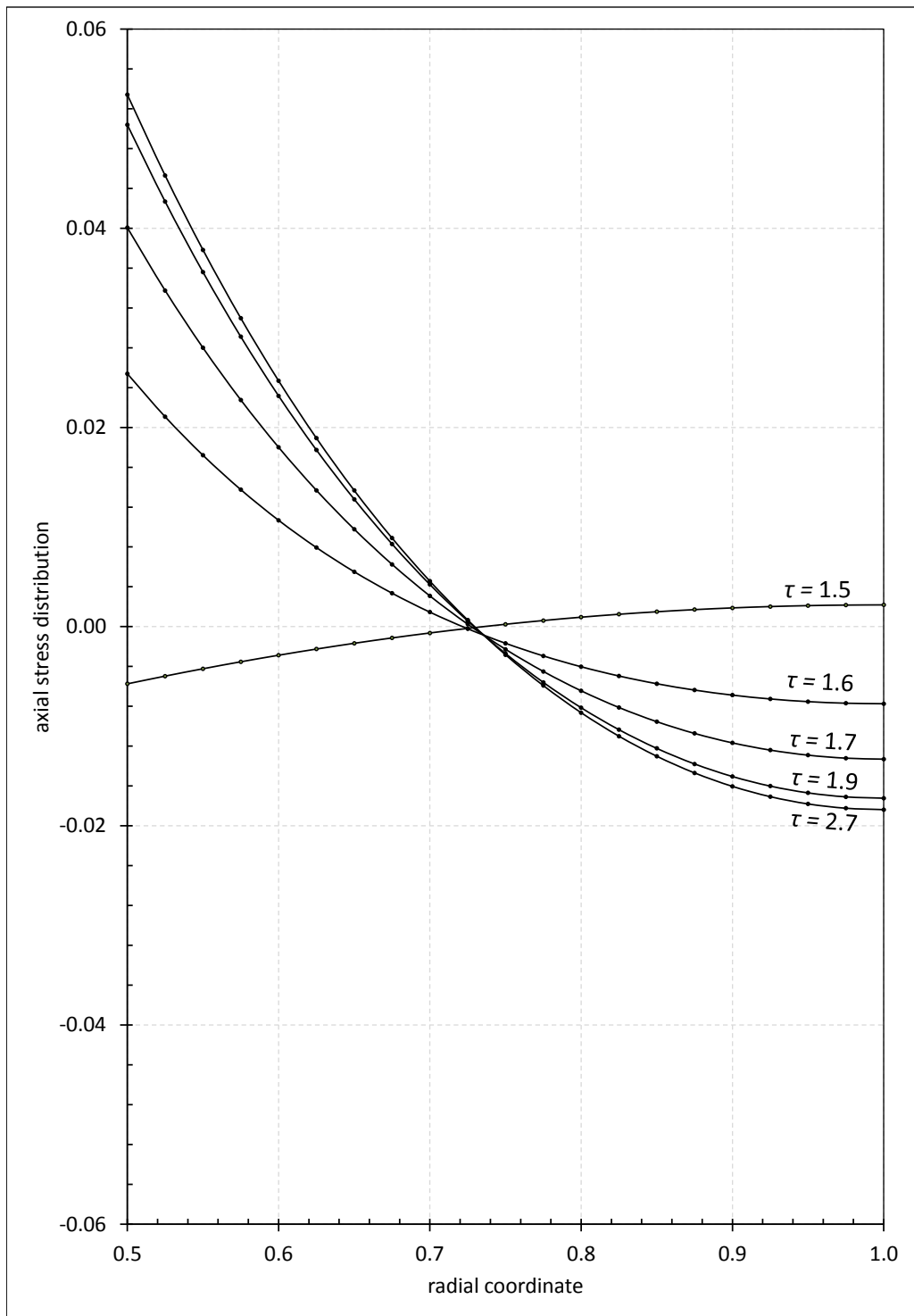


Figure 5.6: Comparison of results of analytical and numerical solution for axial stress distribution in the tube during cooling time.

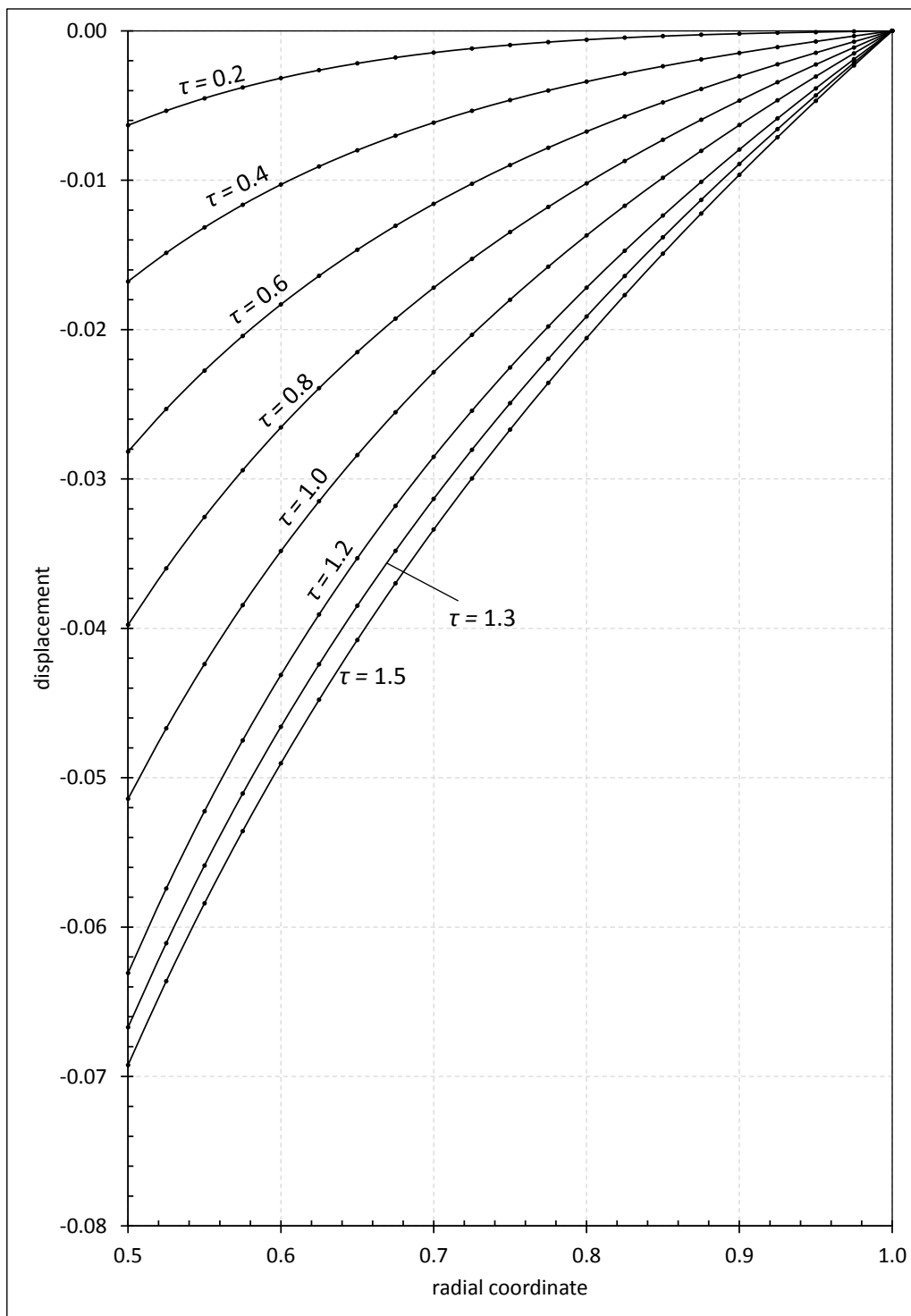


Figure 5.7: Comparison of results of analytical and numerical solution for displacement distribution in the tube during heating time.

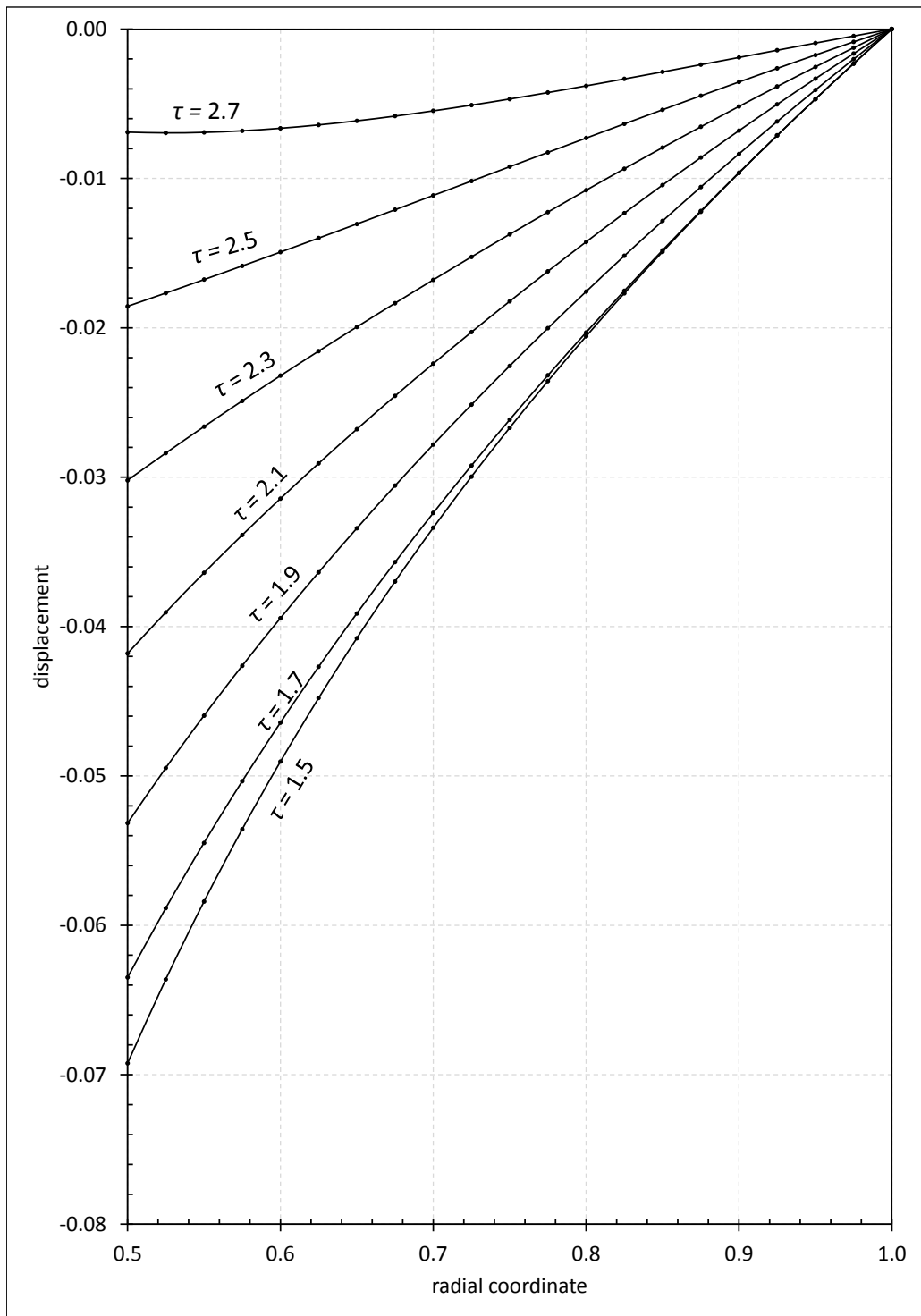


Figure 5.8: Comparison of results of analytical and numerical solution for displacement distribution in the tube during cooling time.

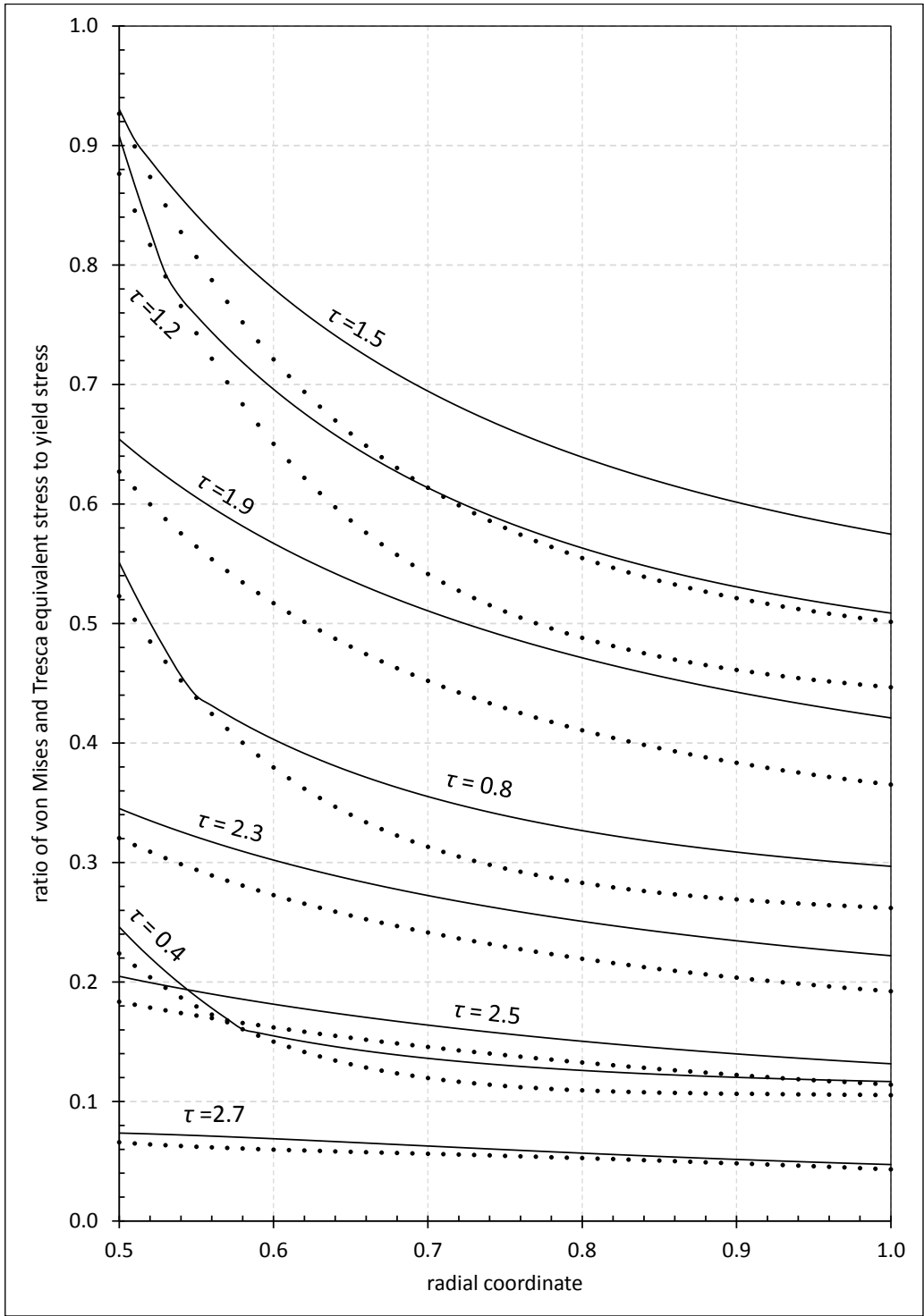


Figure 5.9: Comparison of Tresca and von Mises' stresses for  $q=0.15$ .

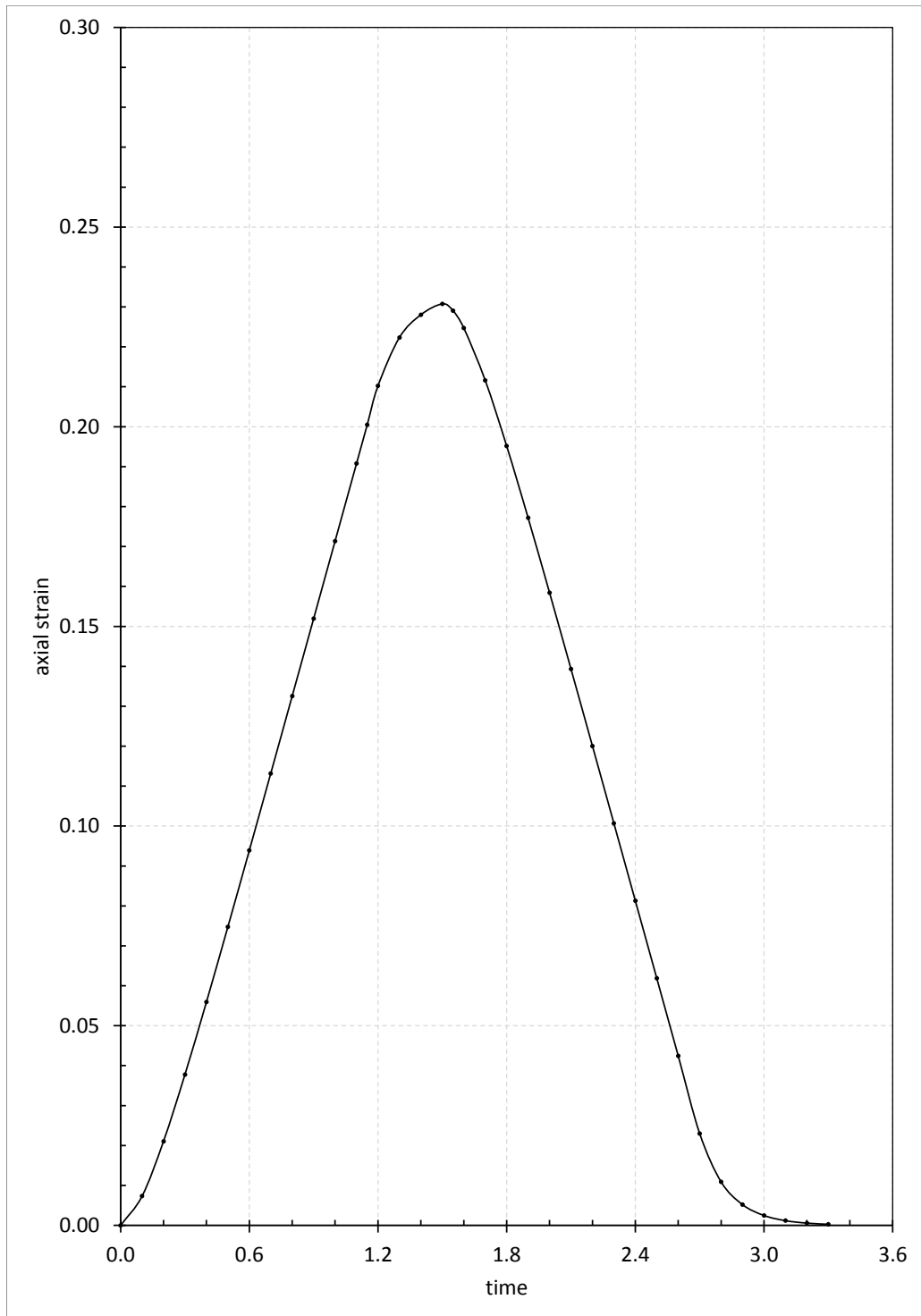


Figure 5.10: Comparison of analytical and numerical results for axial strain.

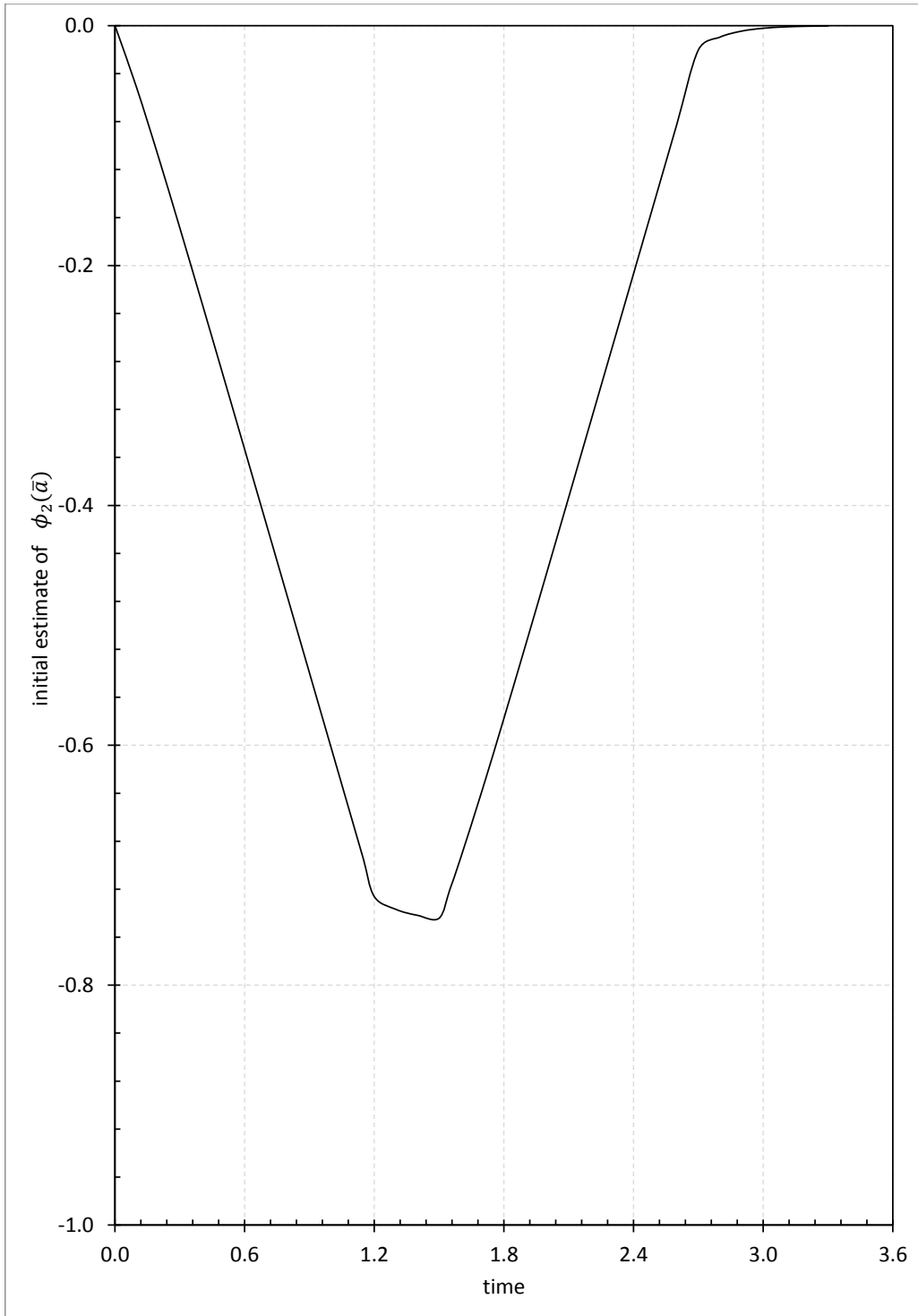


Figure 5.11: Initial estimates of initial value problem.



## CHAPTER 6

### THERMO-ELASTOPLASTIC ANALYSIS OF THE TUBE

In this chapter, analytical solutions are introduced for the tube problem by increasing the heat load parameter in order to determine the plastic behavior of the tube under temperature cycle. All other parameters are chosen as in the problem of the previous section. Thermal and material properties are assumed constant. The elastic-plastic behavior of the tube under the heat load can be divided into four parts:

**Purely Elastic Stage:** Firstly, the tube behaves elastic to a certain time, which is called elastic stage.

**Elastic-Plastic First Stage:** After some time, the plastic deformation starts from the inner wall of the tube, which is called as elastic-plastic first stage. This plastic region expands through the elastic region.

**Elastic-Plastic Second Stage:** When time elapses, in the plastic-elastic border, another two plastic regions (second and third plastic regions) emerge at the same time, which is named as elastic-plastic second stage. One of the plastic regions spreads into the first plastic region to the inner boundary of the tube while the other region expands to the outer boundary.

**Elastic-Plastic Third Stage:** After some time, first plastic region is completely covered by the second plastic region and disappears. Thus, second and third plastic regions are seen in the tube from the inner wall to the outer wall, while the outer wall still remains elastic, which is elastic-plastic third stage.

In these stages, an elastic and three different plastic regions exist. Formulation of

the elastic region is given in the previous chapter, Ch.5. In this chapter, formulations of the three plastic regions are presented. By this means, the stages of the tube experienced (elastic, elastic-plastic first stage, elastic-plastic second stage, and elastic-plastic third stage) are treated.

## 6.1 Formulation of the Plastic Regions

The basic equations given in theory Ch.2 are used to derive the plastic stress, strain and displacement expressions.

### 6.1.1 Plastic Region 1

In the plastic region 1, the principal stresses satisfy  $\sigma_r > \sigma_z > \sigma_\theta$ . Tresca yield condition in this stage is:

$$\sigma_r - \sigma_\theta = \sigma_{th} \quad (6.1)$$

where the yield stress is  $\sigma_{th} = \sigma_0 (1 - \beta T)$ . Tresca's yielding function in this region reads

$$f_1 = \sigma_r - \sigma_\theta - \sigma_{th} = 0. \quad (6.2)$$

Associated flow rule is written as

$$d\epsilon_i^p = \frac{\partial f_1}{\partial \sigma_i} d\lambda_1. \quad (6.3)$$

According to the flow rule, the plastic strain increments are written as

$$d\epsilon_r^p = \frac{\partial f_1}{\partial \sigma_r} d\lambda_1 = d\lambda_1, \quad (6.4)$$

$$d\epsilon_\theta^p = \frac{\partial f_1}{\partial \sigma_\theta} d\lambda_1 = -d\lambda_1, \quad (6.5)$$

$$d\epsilon_z^p = \frac{\partial f_1}{\partial \sigma_z} d\lambda_1 = 0. \quad (6.6)$$

Finally, from the flow rule associated with the yield condition one can derive the relations between the strains as  $\epsilon_r^p = -\epsilon_\theta^p$ ,  $\epsilon_z^p = 0$ . Total strains become

$$\epsilon_r = \epsilon_r^p + \frac{1}{2G(1+\nu)} [\sigma_r - \nu(\sigma_\theta + \sigma_z)] + \alpha T, \quad (6.7)$$

$$\epsilon_\theta = -\epsilon_r^p + \frac{1}{2G(1+\nu)} [\sigma_\theta - \nu(\sigma_r + \sigma_z)] + \alpha T, \quad (6.8)$$

$$\epsilon_z = 0 + \frac{1}{2G(1+\nu)} [\sigma_z - \nu(\sigma_r + \sigma_\theta)] + \alpha T. \quad (6.9)$$

Solving the Eq.(6.9) for  $\sigma_z$  by considering the generalized plain strain condition,  $\epsilon_z = \epsilon_0$ , the axial stress is obtained as

$$\sigma_z = 2G(1+\nu) [\epsilon_0 - \alpha T] + \nu(\sigma_r + \sigma_\theta). \quad (6.10)$$

Inserting axial strain Eq.(6.10) into Eqs. (6.7) and (6.8),

$$\epsilon_r = \epsilon_r^p + \frac{1}{2} [\sigma_r(1-\nu) - \nu\sigma_\theta] - \epsilon_0\nu + \alpha(1+\nu)T, \quad (6.11)$$

$$\epsilon_\theta = -\epsilon_r^p + \frac{1}{2} [\sigma_\theta(1-\nu) - \nu\sigma_r] - \epsilon_0\nu + \alpha(1+\nu)T. \quad (6.12)$$

Inserting the final forms of the total strains, Eq.(6.11) and (6.12), into strain-displacement relations given by Eq.(3.6), the radial and circumferential stresses can be expressed in terms of displacement as

$$\begin{aligned} \sigma_r = \frac{2G}{r(1-2\nu)} [r(\epsilon_0\nu - (1-2\nu)\epsilon_r^p + (1-\nu)u') \\ + \nu u - \alpha r(1+\nu)T], \end{aligned} \quad (6.13)$$

$$\begin{aligned} \sigma_\theta = \frac{2G}{r(1-2\nu)} [r(\epsilon_0\nu + (1-2\nu)\epsilon_r^p + \nu u') \\ + (1-\nu)u - \alpha r(1+\nu)T], \end{aligned} \quad (6.14)$$

where  $u'$  denotes the derivative of displacement with respect to the radial coordinate. By using yield criterion,  $\sigma_r - \sigma_\theta = \sigma_0(1 - \beta T)$ , the plastic strain  $\epsilon_r^p$  is derived in terms of the displacement as

$$\epsilon_r^p = -\frac{1}{2r}(u - ru') - \frac{1}{4G}\sigma_0(1 - \beta T) \quad (6.15)$$

Inserting the radial and tangential stresses into the equation of motion Eq.(3.1), the nonhomogeneous Euler equation is obtained for the radial displacement as

$$r^2 \frac{d^2 u}{dr^2} + r \frac{du}{dr} - u = \frac{r}{2G} \{2\sigma_0(1 - 2\nu) [\beta T - 1] + [4G\alpha(1 + \nu) + \sigma_0\beta(1 - 2\nu)] rT'\}, \quad (6.16)$$

where  $T'$  represents the derivative of temperature with respect to the radial coordinate. Solution of the Eq.(6.16) can be expressed as:

$$u = u_h + u_{par}$$

where  $u_h$  is homogeneous part of the solution and easily derived as

$$u_h = \frac{C_3}{r} + C_4 r, \quad (6.17)$$

where  $C_3$  and  $C_4$  are the integration constants for the first plastic region. The particular solution of Eq.(6.16),  $u_{par}$ , is obtained by the application of variation of parameters method.

$$u_{par} = Y_1(r)u_1(r) + Y_2(r)u_2(r). \quad (6.18)$$

By means of homogeneous solution,  $Y_1(r)$  and  $Y_2(r)$  are defined as

$$Y_1(r) = \frac{1}{r} \text{ and } Y_2(r) = r. \quad (6.19)$$

Thus

$$u_1(r) = - \int \frac{Y_2(r)F(r)}{W(r)} dr, \quad (6.20)$$

$$u_2(r) = \int \frac{Y_1(r)F(r)}{W(r)} dr, \quad (6.21)$$

where  $F(r)$  is the nonhomogeneous part of the Eq.(6.16),

$$F(r) = \frac{1}{r^2} \frac{r}{2G} \{2\sigma_0(1-2\nu) [\beta T - 1] + [4G\alpha(1+\nu) + \sigma_0\beta(1-2\nu)] rT'\}, \quad (6.22)$$

and  $W(r)$  is Wronskian calculated as follows

$$\begin{aligned} W(r) &= \begin{vmatrix} Y_1(r) & Y_2(r) \\ \frac{dY_1(r)}{dr} & \frac{dY_2(r)}{dr} \end{vmatrix} = Y_1(r) \frac{dY_2(r)}{dr} - Y_2(r) \frac{dY_1(r)}{dr} \\ &= \frac{2}{r}. \end{aligned} \quad (6.23)$$

After calculating the integral Eq.s (6.20) and (6.21) and substituting into the Eq.(6.18), particular solution is obtained as

$$\begin{aligned} u_{par} &= \frac{r\beta\sigma_0(1-2\nu)}{2G} \int_a^r \frac{T}{\xi} d\xi + \frac{2\alpha(1+\nu)}{r} \int_a^r \xi T d\xi \\ &+ \frac{(a^2 - r^2) [4G\alpha(1+\nu) + \beta\sigma_0(1-2\nu)]}{4Gr} T(a) \end{aligned} \quad (6.24)$$

$$+ \frac{\sigma_0(1-2\nu) [r^2 - a^2 + 2r^2 \ln(a/r)]}{4Gr}, \quad (6.25)$$

and the total displacement is the summation of the homogeneous and particular solutions

$$\begin{aligned} u_r^{p1} &= \frac{C_3}{r} + C_4 r + \frac{r\beta\sigma_0(1-2\nu)}{2G} \int_a^r \frac{T}{\xi} d\xi + \frac{2\alpha(1+\nu)}{r} \int_a^r \xi T d\xi \\ &+ \frac{(a^2 - r^2) [4G\alpha(1+\nu) + \beta\sigma_0(1-2\nu)]}{4Gr} T(a) \\ &+ \frac{\sigma_0(1-2\nu) [r^2 - a^2 + 2r^2 \ln(a/r)]}{4Gr}, \end{aligned} \quad (6.26)$$

where superscript  $p1$  denotes the "plastic region 1".  $T(a)$  is temperature of the inner surface of the tube. Substituting the displacement into stress equations, one obtains the radial and tangential stresses:

$$\sigma_r^{p1} = \frac{2GC_4}{1-2\nu} + \beta\sigma_0 \int_a^r \frac{T}{\xi} d\xi + \frac{1}{2}(1+2\ln(a/r)) \quad (6.27)$$

$$+ \frac{2G\nu\epsilon_0}{1-2\nu} - \left( \frac{2G\alpha(1+\nu)}{1-2\nu} + \frac{\beta\sigma_0}{2} \right) T(a) \quad (6.28)$$

$$\begin{aligned} \sigma_\theta^{p1} &= \frac{2GC_4}{1-2\nu} + \beta\sigma_0 \left( \int_a^r \frac{T}{\xi} d\xi + T \right) \\ &- \frac{\sigma_0}{2}(1+2\ln r) + \frac{2G\nu\epsilon_0}{1-2\nu} - \left( \frac{2G\alpha(1+\nu)}{1-2\nu} + \frac{\beta\sigma_0}{2} \right) T(a). \end{aligned} \quad (6.29)$$

Once  $\sigma_r^{p1}$  and  $\sigma_\theta^{p1}$  are obtained,  $\sigma_z^{p1}$  can be calculated using the Eq.6.10.

$$\begin{aligned} \sigma_z^{p1} &= \frac{4\nu}{1-2\nu} (C_4 + \nu\epsilon_0) + 2\beta\nu \int_a^r \frac{T}{\xi} d\xi + 2\nu\sigma_0 \ln(a/r) \\ &+ [\beta\nu\sigma_0 - 2G\alpha(1+\nu)] T + 2G(1+\nu)\epsilon_0 \\ &- 2\nu \left[ \frac{2G\alpha(1+\nu)}{1-2\nu} + \frac{\beta\sigma_0}{2} \right] T(a). \end{aligned}$$

Plastic strains are obtained as

$$\begin{aligned} \epsilon_r^{p1} &= -\frac{C_3}{r^2} - \frac{2\alpha(1+\nu)}{r^2} \int_a^r \xi T d\xi + \frac{1}{2G} [2G\alpha(1+\nu) + \beta(1-\nu)\sigma_0] T \\ &\frac{a^2 [4G\alpha(1+\nu) + \beta\sigma_0(1-2\nu)]}{4Gr^2} T(a) + \frac{\sigma_0}{4Gr^2} [a^2(1-2\nu) - 2r^2(1-\nu)] \end{aligned} \quad (6.30)$$

$$\epsilon_\theta^{p1} = -\epsilon_r^{p1}, \quad (6.31)$$

$$\epsilon_z^{p1} = 0. \quad (6.32)$$

Total axial force for a space interval, i.e. from  $a$  to  $\gamma$ , is derived with the help of the integral of

$$F_z = 2\pi \int_a^\gamma r \sigma_z^{p1} dr \quad (6.33)$$

$$F_z^{p1} = 2\pi \left\{ \beta\nu\sigma_0\gamma^2 \int_a^\gamma \frac{T}{r} dr - 2G\alpha(1+\nu) \int_a^\gamma rT dr - \frac{1}{2}\nu\sigma_0[a^2 - \gamma^2 - 2\gamma^2 \ln(a/\gamma)] + \frac{(a^2 - \gamma^2)}{2(1-2\nu)} [(4G\alpha(1+\nu) + \beta\sigma_0(1-2\nu))\nu T(a) - 2G(\epsilon_0(1-\nu) + 2\nu C_4)] \right\}. \quad (6.34)$$

### 6.1.2 Plastic Region 2

In the plastic region 2, the principal stresses satisfy  $\sigma_r = \sigma_z > \sigma_\theta$ . The yield condition:

$$\sigma_r - \sigma_\theta = \sigma_z - \sigma_\theta = \sigma_{th}, \quad (6.35)$$

Tresca's yielding function in this region,

$$f_1 = \sigma_r - \sigma_\theta - \sigma_{th} = 0, \quad (6.36)$$

$$f_2 = \sigma_z - \sigma_\theta - \sigma_{th} = 0. \quad (6.37)$$

Associated flow rule

$$d\epsilon_i^p = \sum_{j=1}^2 \frac{\partial f_j}{\partial \sigma_i} d\lambda_j \quad (6.38)$$

Plastic strain increments

$$d\epsilon_r^p = \frac{\partial f_1}{\partial \sigma_r} d\lambda_1 + \frac{\partial f_2}{\partial \sigma_r} d\lambda_2 = d\lambda_1, \quad (6.39)$$

$$d\epsilon_\theta^p = \frac{\partial f_1}{\partial \sigma_\theta} d\lambda_1 + \frac{\partial f_2}{\partial \sigma_\theta} d\lambda_2 = -d\lambda_1 - d\lambda_2, \quad (6.40)$$

$$d\epsilon_z^p = \frac{\partial f_1}{\partial \sigma_z} d\lambda_1 + \frac{\partial f_2}{\partial \sigma_z} d\lambda_2 = d\lambda_2. \quad (6.41)$$

$$d\epsilon_\theta^p = -(d\epsilon_r^p + d\epsilon_z^p) \quad (6.42)$$

$$\epsilon_\theta^p = -(\epsilon_r^p + \epsilon_z^p) \quad (6.43)$$

$\sigma_z = \sigma_r$  in the stress- strain relations. Axial plastic strain can be written in terms of  $\epsilon_0$

$$\epsilon_z^p = \frac{1}{2G(1+\nu)} [-(1-\nu)\sigma_r + \nu\sigma_\theta] + [\epsilon_0 - \alpha T]. \quad (6.44)$$

Total radial and tangential strains:

$$\epsilon_r = \epsilon_r^p + \frac{1}{2G(1+\nu)} [\sigma_r - \nu(\sigma_\theta + \sigma_z)] + \alpha T, \quad (6.45)$$

$$\epsilon_\theta = -\epsilon_\theta^p + \frac{1}{2G(1+\nu)} [\sigma_\theta - \nu(\sigma_r + \sigma_z)] + \alpha T, \quad (6.46)$$

By using plastic incompressibility relation of Eq.(6.43), Eqs. (6.44)-(6.46) and geometric relations Eq.(3.6), radial and circumferential stresses can be written in terms of the displacement:

$$\sigma_r^p = \frac{2G}{(1-2\nu)} \left( \frac{\nu u}{r} + (1-\nu)u' + \epsilon_0\nu - \alpha(1+\nu)T - (1-2\nu)\epsilon_r^{p2} \right) \quad (6.47)$$

$$\sigma_\theta^p = \frac{2G}{(1-2\nu)} \left[ \frac{(1-\nu)u}{r} - (1-3\nu)u' + \epsilon_0(1-\nu) - \alpha(1+\nu)T + 2(1-2\nu)\epsilon_r^{p2} \right] \quad (6.48)$$

By using yield condition Eq.(6.35) plastic strain in  $r$  direction can be written in terms of radial displacement as

$$\epsilon_r^p = -\frac{1}{3} \left( \frac{u}{r} + \epsilon_0 - 2u' \right) - \frac{\sigma_0}{6G} (1 - \beta T) \quad (6.49)$$



Substituting stresses into the equation of motion Eq.(3.1) , one dimensional differential equation for the displacement is obtained:

$$u'' + \frac{u}{r} - \frac{u}{r^2} = \frac{\sigma_0(1-2\nu)}{2G(1+\nu)r} [\beta(rT' + 3T - 3)] + 3\alpha T'. \quad (6.50)$$

By using variation of parameters method, the governing equation is solved.

$$u_h = \frac{C_5}{r} + C_6 r \quad (6.51)$$

$$u_{par} = \frac{\beta(1-2\nu)\sigma_0}{8G(1+\nu)r} \left\{ 6r^2 \left[ \int_a^r \frac{T}{\xi} d\xi + \ln(a/r) \right] - 2 \int_a^r \xi T d\xi \right. \\ \left. - 3 \left[ (a^2 - r^2) [1 + 6G(1+\nu)\alpha T(a)] + T(a) \right] \right\} + \frac{3\alpha}{r} \int_a^r \xi T d\xi \quad (6.52)$$

where  $C_5$  and  $C_6$  are the integration constants of the plastic region 2. Total displacement is found by summation of the homogeneous and particular solutions as

$$u^{p2} = \frac{C_5}{r} + C_6 r + \frac{(1-2\nu)}{4(1+\nu)} \left\{ 3r \left[ \beta \int_a^r \frac{T}{\xi} d\xi + \ln(a/r) \right] \right. \\ \left. - \frac{1}{2r} \left[ 2\beta \int_a^r \xi T d\xi + (3 - 2\beta T(a))(a^2 - r^2) \right] \right\} \\ + \frac{3q}{r} \left( \int_a^r \xi T d\xi + \frac{(a^2 - r^2)}{2} T(a) \right) \quad (6.53)$$

$$\sigma_r^{p2} = \frac{1}{3(1-2\nu)} \{ 2G(2C_6 + \epsilon_0)(1+\nu) \\ + \sigma_0(1-2\nu) \left[ 1 + 3 \left( \beta \int_a^r \frac{T}{\xi} d\xi + \ln(a/r) \right) \right] \\ - (6G\alpha(1+\nu) + \beta\sigma_0(1-2\nu))T(a) \} \quad (6.54)$$

$$\sigma_\theta^{p2} = \frac{1}{3(1-2\nu)} \{ 2G(2C_6 + \epsilon_0)(1+\nu) \\ + \sigma_0(1-2\nu) \left[ -2 + 3 \left( \beta \int_a^r \frac{T}{\xi} d\xi + \ln(a/r) + \beta T \right) \right] \\ - [6G\alpha(1+\nu) + \beta\sigma_0(1-2\nu)]T(a) \} \quad (6.55)$$

$$\begin{aligned}
\epsilon_r^{p2} = & -\frac{C_5}{r^2} + \frac{C_6}{3} + \frac{\beta\sigma_0(1-2\nu)}{4G(1+\nu)} \int_a^r \frac{T}{\xi} d\xi \\
& - \left( 3\alpha - \frac{\beta\sigma_0(1-2\nu)}{4G(1+\nu)} \right) \frac{1}{r^2} \int_a^r \xi T d\xi + \left( 2\alpha + \frac{\beta\sigma_0(1-\nu)}{2G(1+\nu)} \right) T \\
& - \frac{(3a^2 + r^2) [6G\alpha(1+\nu) + \beta\sigma_0(1-2\nu)]}{12G(1+\nu)r^2} T(a) - \frac{2G\epsilon_0 + \sigma_0}{6G} \\
& + \frac{\sigma_0(1-2\nu)}{4G(1+\nu)} \left[ \frac{3(a^2 - r^2)}{2r^2} + \log(a/r) \right] \tag{6.56}
\end{aligned}$$

$$\begin{aligned}
\epsilon_z^{p2} = & -\frac{1}{6G(1+\nu)} \{ [4G(C_6 - \epsilon_0) + \sigma_0] (1+\nu) \\
& + 3\sigma_0(1-2\nu) \left[ \beta \int_a^r \frac{T}{\xi} d\xi + \ln(a/r) \right] \\
& + 3 [2G\alpha(1+\nu) - \beta\nu\sigma_0] T - [6G\alpha(1+\nu) + \beta\sigma_0(1-2\nu)] T(a) \} \tag{6.57}
\end{aligned}$$

$F_z^{p2}$  is calculated from  $\eta$  to  $\gamma$  as

$$\begin{aligned}
F_z^{p2} = & 2\pi \frac{\beta\sigma_0}{2} \left\{ \gamma^2 \int_a^\gamma \frac{T}{r} dr - \eta^2 \int_a^\eta \frac{T}{r} dr - \int_\eta^\gamma r T dr \right\} \\
& + \frac{\sigma_0}{4} [\gamma^2(1-2\ln(\gamma)) - \eta^2(1-2\ln(\eta))] \\
& + \frac{(\gamma^2 - \eta^2)}{6(1-2\nu)} \{ 2G(2C_6 + \epsilon_0)(1+\nu) + \sigma_0(1-2\nu)(1+3\ln(a)) \\
& - [6G\alpha(1+\nu) + \beta\sigma_0(1-2\nu)] T(a) \} \tag{6.58}
\end{aligned}$$

### 6.1.3 Plastic Region 3

For the plastic region 3, the principal stresses satisfy  $\sigma_z > \sigma_\theta$  and Tresca's yield condition is:

$$\sigma_z - \sigma_\theta = \sigma_{th}, \tag{6.59}$$

Tresca's yielding function,

$$f_1 = \sigma_z - \sigma_\theta - \sigma_{th} = 0. \tag{6.60}$$

Plastic strain increments,

$$d\epsilon_r^p = \frac{\partial f_1}{\partial \sigma_r} d\lambda_1 = 0, \quad (6.61)$$

$$d\epsilon_\theta^p = \frac{\partial f_1}{\partial \sigma_\theta} d\lambda_1 = -d\lambda_1, \quad (6.62)$$

$$d\epsilon_z^p = \frac{\partial f_1}{\partial \sigma_z} d\lambda_1 = d\lambda_1. \quad (6.63)$$

The flow rule associated with the yield condition Eq.(6.59) gives  $\epsilon_\theta^p = -\epsilon_z^p$ ,  $\epsilon_r^p = 0$ .

$$\epsilon_z^p = \frac{1}{2G(1+\nu)} (-(1-\nu)\sigma_r + \nu\sigma_\theta) + [\epsilon_0 - \alpha T]. \quad (6.64)$$

Total strains

$$\epsilon_z = \epsilon_z^p + \epsilon_z^e \quad (6.65)$$

$$\epsilon_r = \epsilon_r^e \quad (6.66)$$

$$\epsilon_\theta = -\epsilon_z^p + \epsilon_\theta^e \quad (6.67)$$

By using geometric relations Eq.(3.6), stresses can be written in terms of  $\epsilon_z^p$  as

$$\sigma_r = \frac{2G}{1-2\nu} \left[ \nu \frac{u}{r} + (1-\nu)u' + \nu\epsilon_0 - \alpha(1+\nu)T \right], \quad (6.68)$$

$$\sigma_\theta = \frac{2G}{1-2\nu} \left[ (1-\nu) \frac{u}{r} + \nu u' + (1-2\nu)\epsilon_z^p + \nu\epsilon_0 - \alpha(1+\nu)T \right], \quad (6.69)$$

$$\sigma_z = \frac{2G}{1-2\nu} \left[ \nu \frac{u}{r} + \nu u' - (1-2\nu)\epsilon_z^p + (1-\nu)\epsilon_0 - \alpha(1+\nu)T \right]. \quad (6.70)$$

Substituting Eq.s (6.70) and (6.69) into the yield condition Eq.(6.59), plastic axial strain is obtained as

$$\epsilon_z^p = -\frac{u}{2r} + \frac{\epsilon_0}{2} - \frac{\sigma_0}{4G} (1 - \beta T). \quad (6.71)$$

Substituting the stresses in the equation of motion Eq.(3.1), one dimensional differential equation in the radial direction for the plastic region 3 is obtained as:

$$u'' + \frac{u}{r} - M^2 \frac{u}{r^2} = \frac{M^2(1-2\nu)}{2Gr} \left[ 2G\epsilon_0 - \sigma_0 (1 - \beta T) + \frac{4G\alpha(1+\nu)}{(1-2\nu)} r T' \right]. \quad (6.72)$$

where  $M = \sqrt{1/(2(1-\nu))}$

Homogeneous part of the solution is

$$u_h = C_7 r^{-M} + C_8 r^M. \quad (6.73)$$

where  $C_7$  and  $C_8$  are the integration constants of the plastic region 3. For the particular solution Wronskian is calculated as

$$W(r) = \frac{2M}{r}. \quad (6.74)$$

Applying the same solution procedure , one obtains the particular solution. Summation of the homogeneous and particular solution give the final result for the displacement:

$$\begin{aligned} u^{p3} &= C_7 r^{-M} + C_8 r^M \quad (6.75) \\ &+ \frac{M}{4G} \left\{ r^M [4G\alpha(M-1)(1+\nu) + \beta\sigma_0(1-2\nu)] \int_a^r \xi^{-M} T d\xi \right. \\ &+ r^{-M} [4G\alpha(1+M)(1+\nu) - \beta\sigma_0(1-2\nu)] \int_a^r \xi^M T d\xi \\ &+ \frac{(1-2\nu)(2G\epsilon_0 - \sigma_0)}{(1-M^2)} [(1-M)a^{1+M}r^{-M} - (M+1)a^{1-M}r^M + 2Mr] \left. \right\} \\ &+ M\alpha(1+\nu)(a^{1+M}r^{-M} - a^{1-M}r^M)T(a) \quad (6.76) \end{aligned}$$

In the solution procedure, the following integrations are treated with the help of integration by parts technique:

$$\begin{aligned} \int r^{1+M} T' dr &= r^{1+M} T - (1+M) \int r^M T dr, \\ \int r^{1-M} T' dr &= r^{1-M} T - (1-M) \int r^{-M} T dr. \end{aligned}$$

Once the displacement is obtained, the stresses and strain can be calculated. Radial

plastic strain is

$$\begin{aligned}
\epsilon_z^{p3} = & -\frac{C_7}{2}r^{-1-M} - \frac{C_8}{2}r^{-1+M} + \frac{2G\epsilon_0 - \sigma_0(1 - \beta T)}{4G} \\
& - \frac{M}{8G} \left\{ r^{-1+M} [-4G\alpha(1 - M)(1 + \nu) + \beta\sigma_0(1 - 2\nu)] \int_a^r \xi^{-M} T d\xi \right. \\
& + r^{-1-M} [4G\alpha(1 + M)(1 + \nu) - \beta\sigma_0(1 - 2\nu)] \int_a^r \xi^M T d\xi \\
& + \frac{(1 - 2\nu)(2G\epsilon_0 - \sigma_0)}{(1 - M^2)} \\
& \times [2M + (1 - M)a^{1+M}r^{-1-M} - (1 + M)a^{1-M}r^{-1+M}] \} \\
& - \frac{M\alpha(1 + \nu)}{2} [a^{1+M}r^{-1-M} - a^{1-M}r^{-1+M}] T(a). \tag{6.77}
\end{aligned}$$

Radial stress is

$$\begin{aligned}
\sigma_r^{p3} = & \frac{2Gr^{-1-M}}{1 - 2\nu} [C_8r^{2M}(M(1 - \nu) + \nu) - C_7(M(1 - \nu) - \nu)] \\
& - \frac{M}{2(1 - 2\nu)} \left\{ r^{-1+M}(M(1 - \nu) + \nu) \right. \\
& \times [4G\alpha(1 + \nu)(1 - M) - \beta(1 - 2\nu)\sigma_0] \int_a^r \xi^{-M} T d\xi \\
& + r^{-1-M}(M(1 - \nu) - \nu) [4G\alpha(1 + \nu)(1 + M) - \beta(1 - 2\nu)\sigma_0] \int_a^r \xi^M T d\xi \\
& + 4G\alpha(1 + \nu) [(1/M - 2M(1 - \nu))T \\
& + [a^{1+M}r^{-1-M}(M(1 - \nu) - \nu) + a^{1-M}r^{-1+M}(M(1 - \nu) + \nu)] T(a) \} \\
& + \frac{1}{2(1 - M^2)(1 - 2\nu)} \{ 4G\epsilon_0(M^2(1 - 3\nu) + \nu) - 2\sigma_0M^2(1 - 2\nu) \\
& - M(1 - 2\nu)(2G\epsilon_0 - \sigma_0) [a^{1-M}r^{-1+M}(1 + M)(M(1 - \nu) + \nu) \\
& + a^{1+M}r^{-1-M}(1 - M)(M(1 - \nu) - \nu)] \}. \tag{6.78}
\end{aligned}$$

Tangential stress is

$$\begin{aligned}
\sigma_{\theta}^{p3} = & \frac{Gr^{-1-M}}{1-2\nu} [C_7(1-2M\nu) + C_8r^{2M}(1+2M\nu)] - \frac{M}{4(1-2\nu)} \\
& \times \left\{ r^{-1+M}(1+2M\nu) [4G\alpha(1-M)(1+\nu) - \beta\sigma_0(1-2\nu)] \int_a^r \xi^{-M} T d\xi \right. \\
& - r^{-1-M}(1-2M\nu) [4G\alpha(1+M)(1+\nu) - \beta\sigma_0(1-2\nu)] \int_a^r \xi^M T d\xi \\
& + 4G\alpha(1+\nu) [a^{1-M}r^{-1+M}(1+2M\nu) - a^{1+M}r^{-1-M}(1-2M\nu)] T(a) \\
& \left. - \frac{2}{M} [\beta\sigma_0(1-2\nu) - 4G\alpha(1+\nu)(1-2M^2\nu)] T \right\} \\
& + \frac{1}{4(1-M^2)(1-2\nu)} \{ 4G\epsilon_0(1-4M^2\nu^2) - 2\sigma_0(1-2\nu)(1+2M^2\nu) \\
& + M(1-2\nu)(2G\epsilon_0 - \sigma_0) [a^{1+M}r^{-1-M}(1-M)(1-2M\nu) \\
& - a^{1-M}r^{-1+M}(1+M)(1+2M\nu)] \}. \tag{6.79}
\end{aligned}$$

Total axial force is calculated, i.e. from  $\eta$  to  $\gamma$ , as

$$\begin{aligned}
F_z^{p3} = & \frac{C_7G(1-2M\nu)}{(1-M)(1-2\nu)} [\gamma^{1-M} - \eta^{1-M}] + \frac{C_8G(1+2M\nu)}{(1+M)(1-2\nu)} [\gamma^{1+M} - \eta^{1+M}] \\
& + \frac{1}{4(1-M^2)(1-2\nu)} \\
& \times \{ M(1-M)(1+2M\nu) [-4G(1-M)\alpha(1+\nu) + \beta\sigma_0(1-2\nu)] \\
& \times \left( \gamma^{1+M} \int_a^\gamma r^{-M} T dr - \eta^{1+M} \int_a^\eta r^{-M} T dr \right) \\
& + M(1+M)(1-2M\nu) [4G(1+M)\alpha(1+\nu) - \beta\sigma_0(1-2\nu)] \\
& \times \left( \gamma^{1-M} \int_a^\gamma r^M T dr - \eta^{1-M} \int_a^\eta r^M T dr \right) \\
& - 2 [4G\alpha(1+\nu) (1+M^2(1-4\nu)) + \beta\sigma_0(1-2\nu)(1-2M^2(1-\nu))] \int_\eta^\gamma r T dr \\
& + (\gamma^{1-M} - \eta^{1-M}) a^{1+M} M(1-2M\nu) \\
& \times [4G\alpha(1+M)(1+\nu)T(a) + (2G\epsilon_0 - \sigma_0)(1-2\nu)] \\
& - (\gamma^{1+M} - \eta^{1+M}) a^{1-M} M(1+2M\nu) \\
& \times [4G\alpha(1-M)(1+\nu)T(a) + (2G\epsilon_0 - \sigma_0)(1-2\nu)] \\
& \left. - (\eta^2 - \gamma^2) [2G\epsilon_0(1-4M^2\nu^2) + \sigma_0(1-2\nu)(1-2M^2(1+\nu))] \right\} \tag{6.80}
\end{aligned}$$

In the calculation of total axial force, the following double integrals are treated by

integration by parts technique:

$$\int_{\eta}^{\gamma} r^M \int_a^r \xi^{-M} T d\xi dr = \frac{\gamma^{1+M}}{1+M} \int_a^{\gamma} r^{-M} T dr - \frac{\delta^{1+M}}{1+M} \int_a^{\eta} r^{-M} T dr - \frac{1}{1+M} \int_{\eta}^{\gamma} r T dr, \quad (6.81)$$

$$\int_{\eta}^{\gamma} r^{-M} \int_a^r \xi^M T d\xi dr = \frac{\gamma^{1-M}}{1+M} \int_a^{\gamma} r^M T dr - \frac{\delta^{1-M}}{1-M} \int_a^{\eta} r^M T dr - \frac{1}{1-M} \int_{\eta}^{\gamma} r T dr. \quad (6.82)$$

## 6.2 Elastic-Plastic Stages and Numerical Results

Numerical results of the solution are obtained by the calculation of temperature distribution, unknown constants, and stress, strain and displacement expressions under the heat load  $q = 0.25$ . These calculations are performed by using computer codes written in Fortran Programming Language. Temperature field derived in Ch.4 is used to determine the elastic-plastic behavior of the tube. Parameters used in the calculations are: nondimensional inner radius is  $\bar{a} = 0.5$ , thermal diffusivity  $\beta = 0.2$ , and Poisson's ratio  $\nu = 0.286$ .

### 6.2.1 Purely Elastic Stage

The formulation of the elastic stage of the tube is given previously, Ch.5. Here, the heat load parameter is increased to  $q = 0.25$ . Hence, elastic stage lasts until the Tresca's yield criterion ensures at time  $\tau = 0.859001$  at the inner surface of the tube. The elastic behavior of the tube at several time steps until the the onset of plasticization is given in the following figures.

### 6.2.2 Results and Discussion for Purely Elastic Stage

By using the formulation derived in Ch.5, integration constants and axial strain are calculated and tabulated in Table 6.1. Using these values, stresses and displacement distribution of the tube are calculated at the different time steps for the analysis of

elastic behavior of the tube. The results for the stresses and displacement are shown in Figures 6.1-6.4.

Table 6.1: Axial strain and integration constants for the elastic stage

$\tau$	$\bar{\epsilon}_0$	$\bar{C}_1$	$\bar{C}_2$
0.2	0.0351	-0.0267	-0.00193
0.3	0.063	-0.0479	-0.00345
0.4	0.0932	-0.00511	-0.0709
0.6	0.15647	-0.00859	-0.11908
0.859001	0.23998	-0.18264	-0.0132

Fig.6.1 shows the radial stress distribution in the tube. Fig.6.2 shows that the tangential stress distribution during the elastic stage. Axial stress distribution in the elastic domain is depicted in Fig.6.3. Displacement distribution in the tube is also given with Fig. 6.4. As seen in these figures, the tube is stress free at the beginning of the cycle. When time is increased, the stresses start to build up in the tube. Therefore, it is searched when and where the plastic deformation starts by using the Tresca condition such that the maximum difference between the principle stresses is reached to the value of the yield stress,  $\sigma_{th}$ .

In Fig. 6.5, the stress and displacement responses versus radial coordinate are presented at the end of the elastic stage. As understood from this figure, the plastic deformation starts from the inner surface of the tube. The maximum difference between the radial and tangential stresses reach the to the value of yield stress in  $\bar{a} = 0.5$ , at time  $\tau = 0.8590001$ . Hence, in the formulation of the first plastic region, this condition is used.

The ratio of the equivalent stress to yield stress during purely elastic stage at several time steps is shown in Fig. 6.6. The elastic solution is valid until the difference of any two principle stresses reaches the temperature dependent yield limit of the material as mentioned before. When the time is increased gradually, it can be seen in Fig. 6.6 that this condition is reached at the inner wall of the tube at time  $\tau = 0.8590001$ . Fig. 6.6 also shows that the tube behaves elastically until this time. In other words, at this time, the yielding starts at the inner surface of the tube.



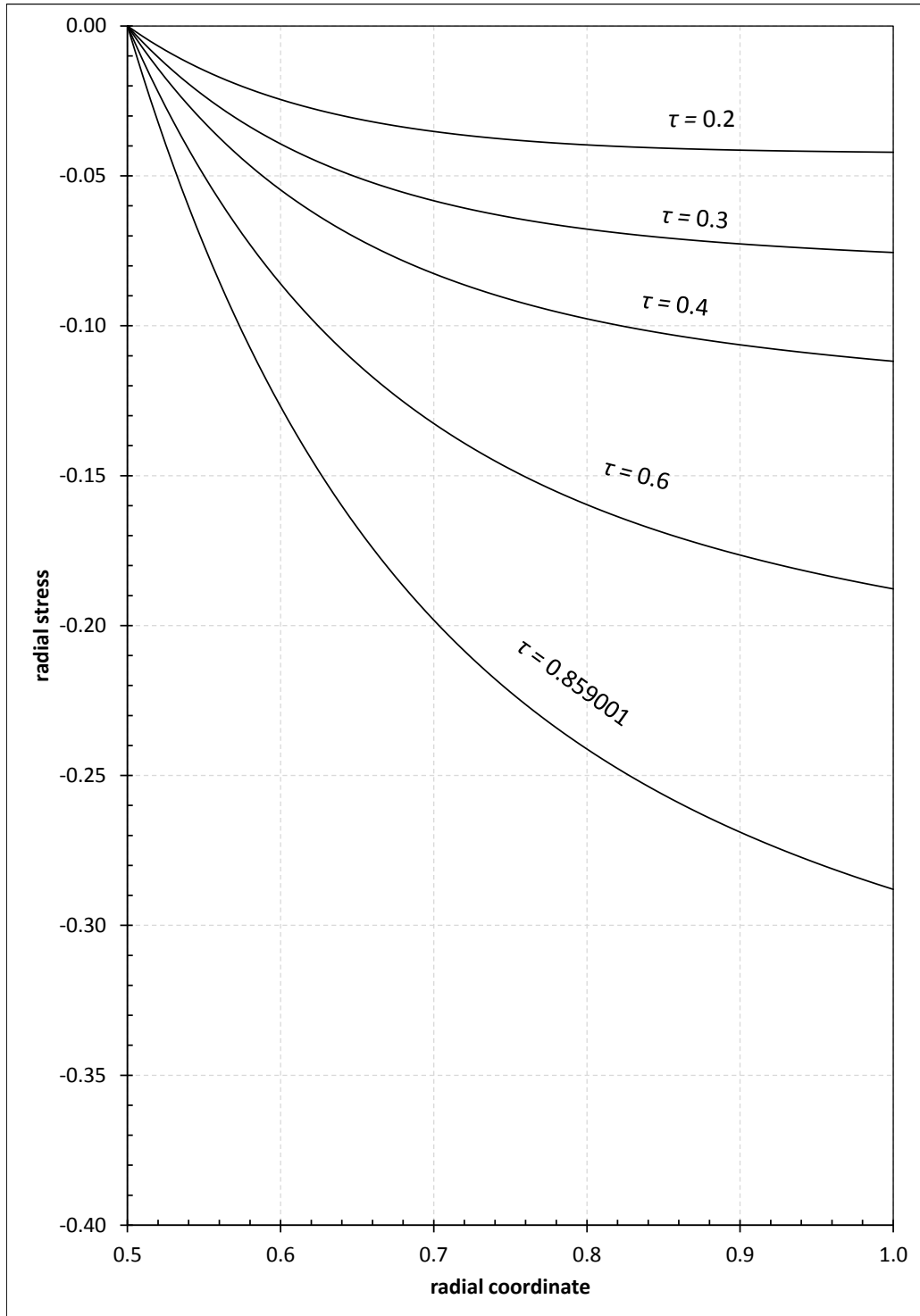


Figure 6.1: Radial stress distribution in the tube for purely elastic tube.

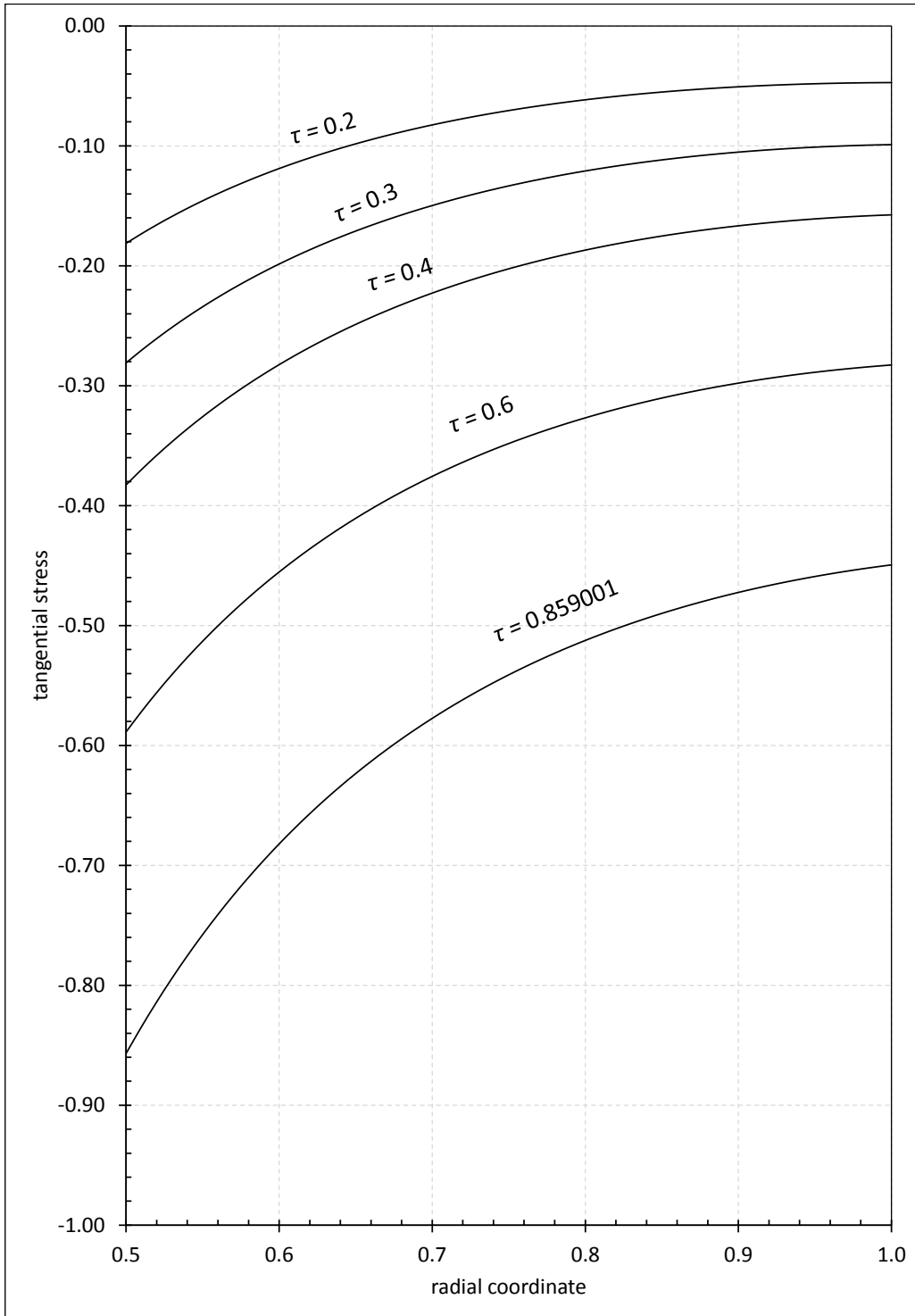


Figure 6.2: Tangential stress distribution in the tube for purely elastic tube.

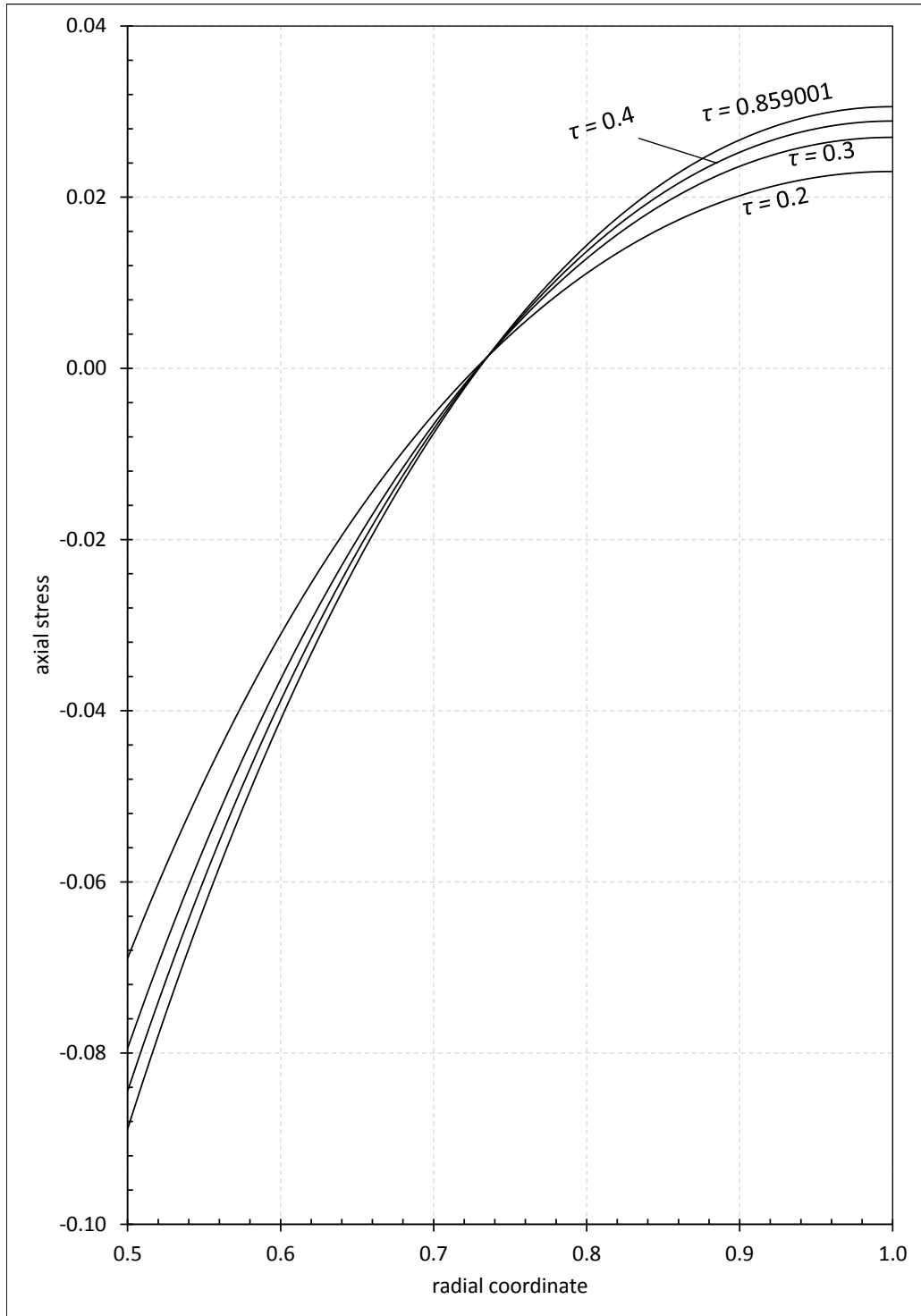


Figure 6.3: Axial stress distribution in the tube for purely elastic tube.

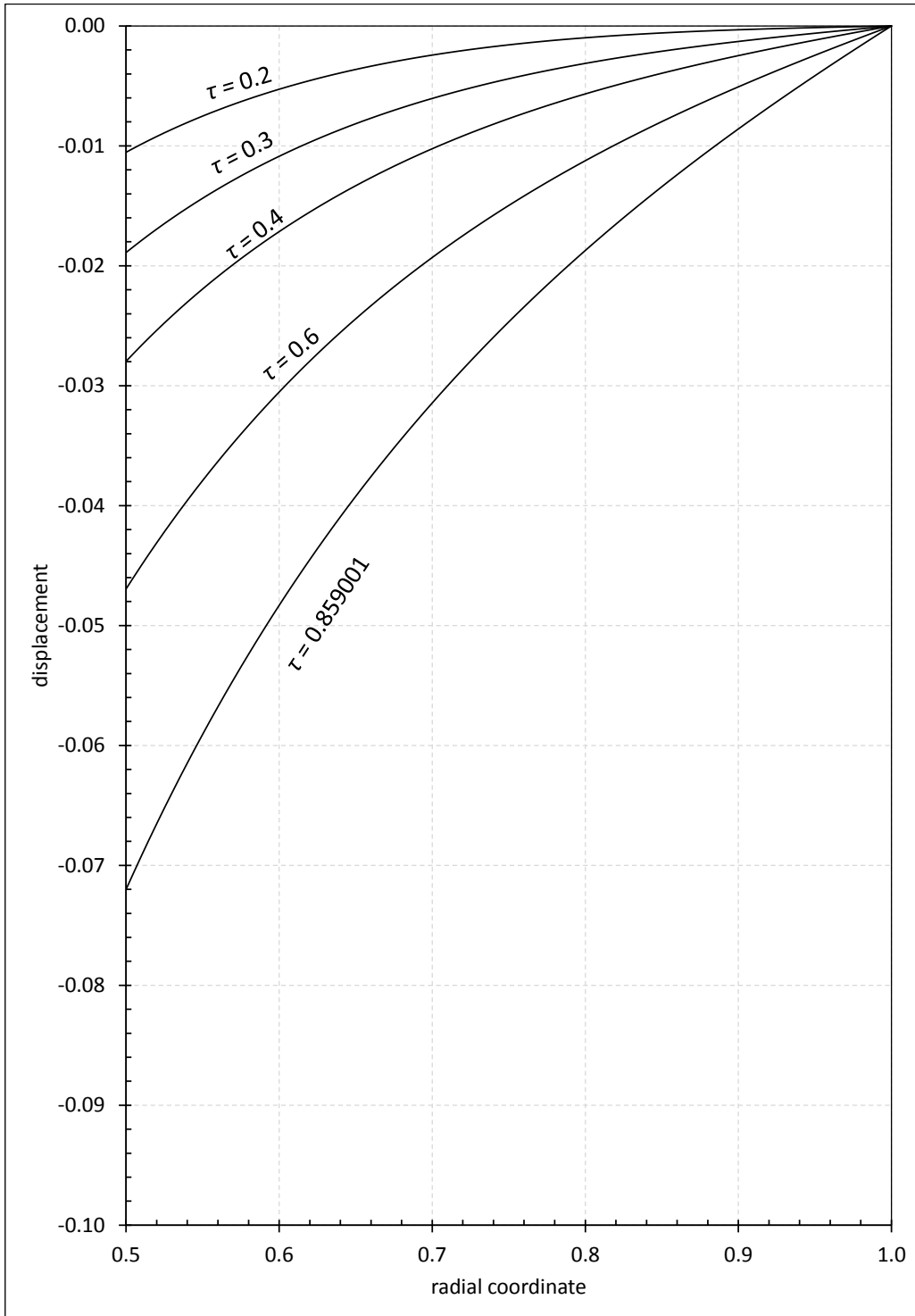


Figure 6.4: Radial displacement in the tube for purely elastic tube.

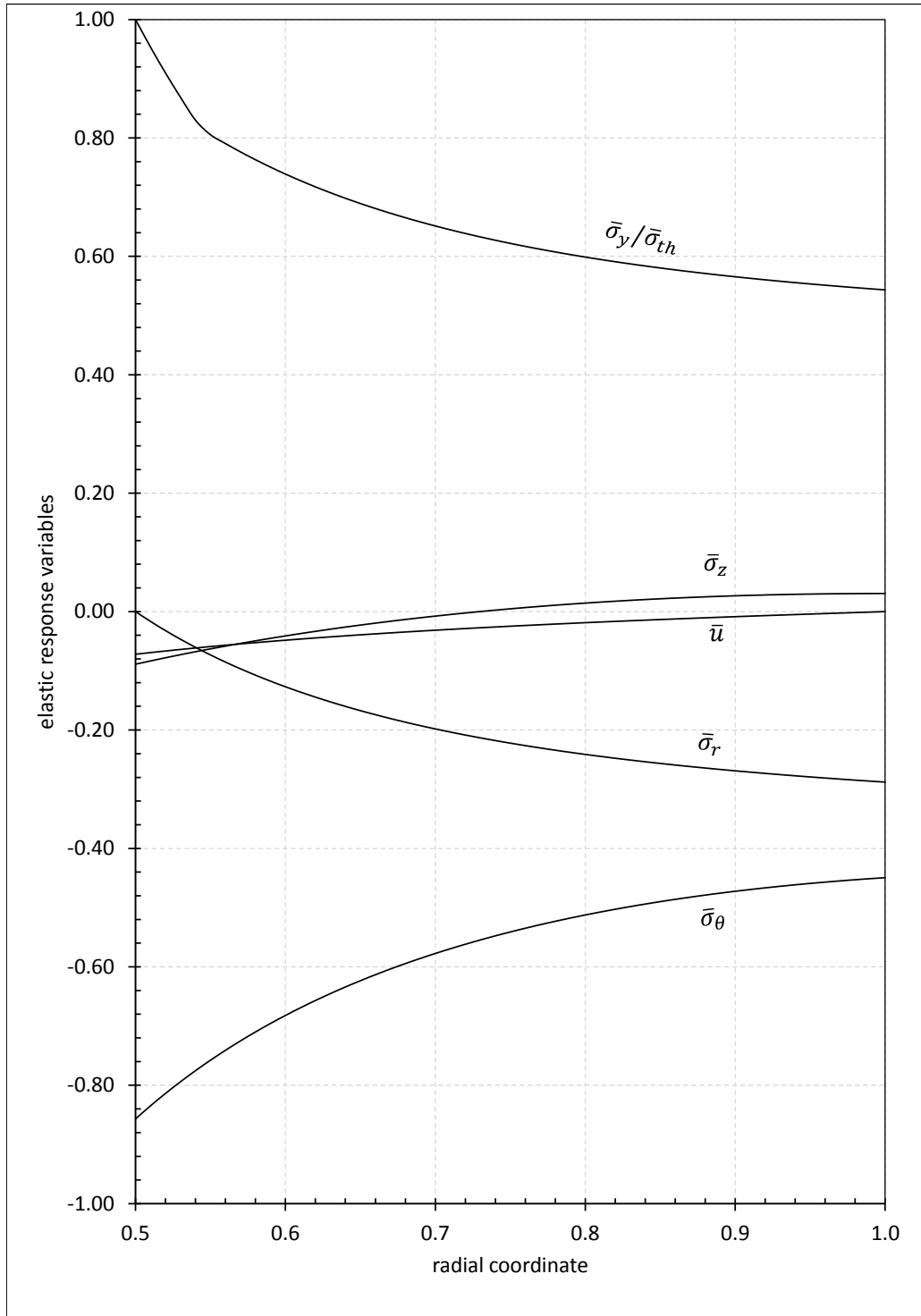


Figure 6.5: Response variables in the tube at the end of the elastic stage.

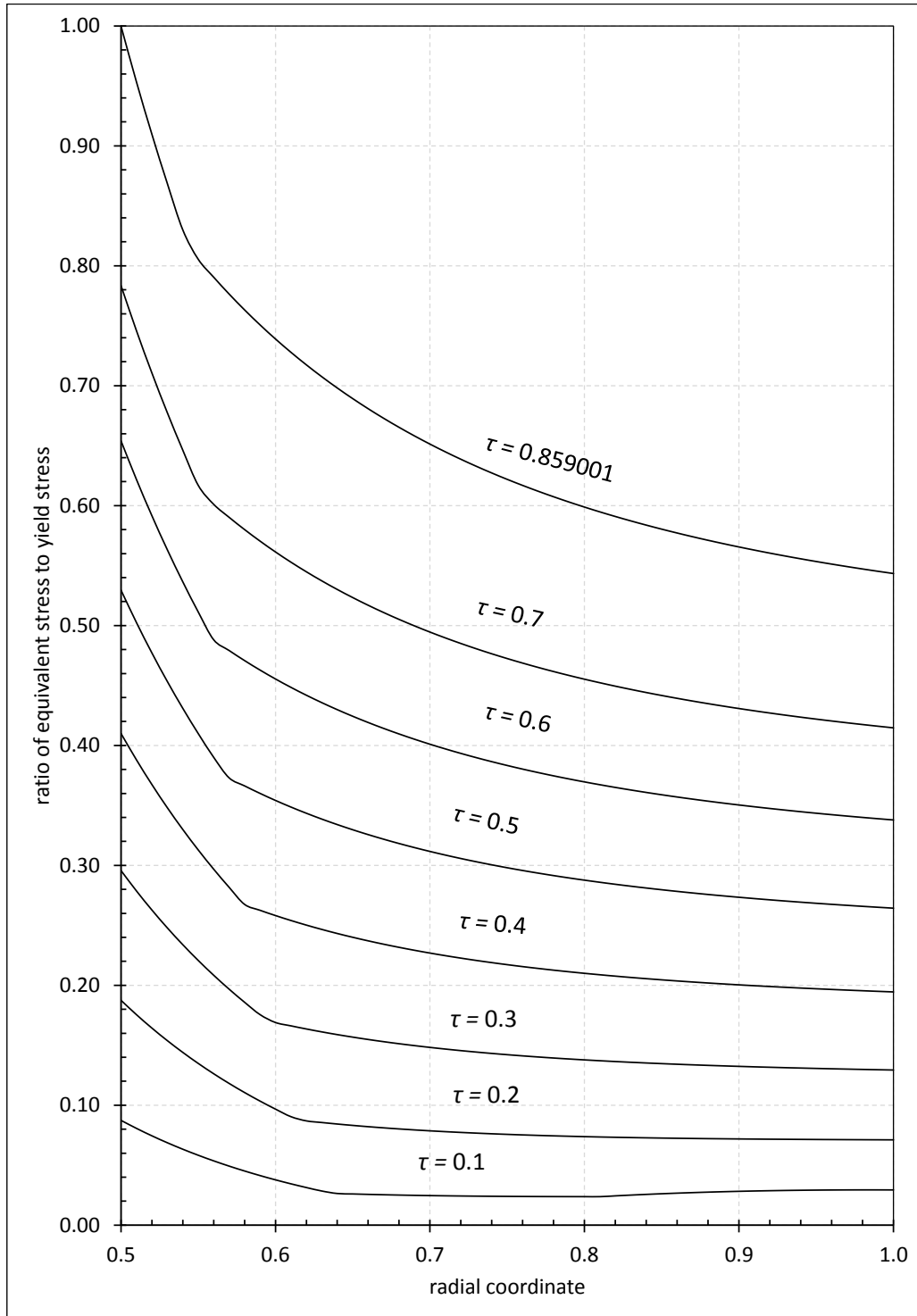


Figure 6.6: Ratio of equivalent stress to yield stress during purely elastic stage.

### 6.2.3 Elastic-Plastic First Stage

When the time is reached to the value of  $\tau = 0.8590001$ , the yield condition  $\sigma_r - \sigma_\theta = \sigma_{th}$  emerge at the inner wall due to the thermal softening of the material and plastic deformation starts. At this stage the plastic region 1 takes place between the boundary  $a$  and  $r_1$ .  $r_1$  denotes the elastic-plastic boundary and moves through the outer boundary of the tube by increasing temperature with time.

At the elastic-plastic first stage, total axial force is calculated in the elastic region between  $r_1$  and  $b$

$$\begin{aligned} F_z^e &= 2\pi \int_{r_1}^b \sigma_z^e r dr \\ &= 2\pi \left\{ -\frac{2G\alpha(1+\nu)}{(1-\nu)} \int_{r_1}^b rT dr - \frac{(r_1^2 - b^2)G}{1-2\nu} [(1-\nu)\epsilon_0 + 2\nu C_2] \right\}, \end{aligned} \quad (6.83)$$

and in the plastic region 1 between  $a$  and  $r_1$

$$\begin{aligned} F_z^{p1} &= 2\pi \int_a^{r_1} \sigma_z^{p1} r dr \\ &= 2\pi \left\{ \beta\nu\sigma_0 r_1^2 \int_a^{r_1} \frac{T}{r} dr - 2G\alpha(1+\nu) \int_a^{r_1} rT dr \right. \\ &\quad - \frac{1}{2}\nu\sigma_0 [a^2 - r_1^2 - 2r_1^2(\ln(a) - \ln(r_1))] \\ &\quad + \frac{(a^2 - r_1^2)}{2(1-2\nu)} \{ [4G\alpha(1+\nu) + \beta\sigma_0(1-2\nu)] \nu T(a) \\ &\quad \left. - 2G(\epsilon_0(1-\nu) + 2\nu C_4) \} \right\}. \end{aligned} \quad (6.84)$$

In addition to the boundary conditions, the interface conditions can be written by taking into account the continuity of stresses and displacement at the elastic-plastic boundary. Hence, boundary and interface conditions for the elastic-plastic first stage become

$$\sigma_r^{p1}(a) = 0, \quad (6.85)$$

$$u_r^e(b) = 0, \quad (6.86)$$

$$\sigma_r^{p1}(r_1) = \sigma_r^e(r_1), \quad (6.87)$$

$$u_r^{p1}(r_1) = u_r^e(r_1), \quad (6.88)$$

$$\sigma_r^e(r_1) - \sigma_\theta^e(r_1) = \sigma_{th}(r_1), \quad (6.89)$$

$$F_z^e + F_z^{p1} = 0. \quad (6.90)$$

By using the conditions Eq.s (6.85)-(6.88), the integration constants  $C_i (i = 1, 4)$  are expressed in terms of the interface radius  $r_1$ , and the axial strain  $\epsilon_0$  as

$$C_1 = \frac{1}{r_1^2 + b^2(1 - 2\nu)} \left\{ -\frac{\alpha(1 + \nu)}{(1 - \nu)} \left[ r_1^2 \int_a^b rT dr + b^2(1 - 2\nu) \int_a^{r_1} rT dr \right] - \frac{b^2 r_1^2 (1 - 2\nu) \sigma_0}{2G} \left[ \beta \int_a^{r_1} \frac{T}{r} dr + \ln(a/r_1) \right] + b^2 r_1^2 \nu \epsilon_0 \right\} \quad (6.91)$$

$$C_2 = \frac{1}{r_1^2 + b^2(1 - 2\nu)} \left\{ \frac{(1 - 2\nu) \sigma_0 r_1^2}{2G} \left[ \beta \int_a^{r_1} \frac{T}{r} dr + \ln(a/r_1) - r_1^2 \epsilon_0 \nu \right] - \frac{\alpha(1 + \nu)(1 - 2\nu)}{(1 - \nu)} \left[ \int_a^b rT dr - \int_a^{r_1} rT dr \right] \right\} \quad (6.92)$$

$$C_3 = -\frac{1}{r_1^2 + b^2(1 - 2\nu)} \left\{ 2\alpha(1 + \nu) \left[ r_1^2 \int_a^b rT dr + b^2(1 - 2\nu) \int_a^{r_1} rT dr \right] - \frac{b^2 r_1^2 (1 - \nu)(1 - 2\nu) \sigma_0}{G} \left[ \beta \int_a^{r_1} \frac{T}{r} dr + \ln(a/r_1) \right] - 2b^2 r_1^2 \nu (1 - \nu) \epsilon_0 \right\} + \frac{a^2}{4G} \{ (1 - 2\nu) \sigma_0 - [4G\alpha(1 + \nu) + \beta(1 - 2\nu) \sigma_0] T(a) \} \quad (6.93)$$

$$C_4 = \frac{1}{4G} \{ [4G\alpha\nu(1 + \nu) + \beta(1 - 2\nu) \sigma_0] T(a) - (1 - 2\nu) \sigma_0 \} - \nu \epsilon_0. \quad (6.94)$$

Defining a nondimensional parameter  $\beta = \beta/T_m$  in addition to the nondimensional and normalized variables defined in Ch5 non-dimensional form of the displacement,



stresses, plastic strain, total axial force, and integration constants are calculated.

Nondimensional form of displacement is

$$\begin{aligned}\bar{u}_r^{p1} = & \frac{\bar{C}_3}{\bar{r}} + \bar{C}_4\bar{r} + \frac{\bar{r}\bar{\beta}(1-2\nu)}{2} \int_{\bar{a}}^{\bar{r}} \frac{\bar{T}}{\xi} d\xi + \frac{2(1+\nu)q}{\bar{r}} \int_{\bar{a}}^{\bar{r}} \xi\bar{T} d\xi \\ & + \frac{(\bar{a}^2 - \bar{r}^2)(4q(1+\nu) + \bar{\beta}(1-2\nu))}{4\bar{r}} \bar{T}(\bar{a}) \\ & + \frac{(1-2\nu)(\bar{r}^2 - \bar{a}^2 + 2\bar{r}^2 \ln(\bar{a}/\bar{r}))}{4\bar{r}}.\end{aligned}\quad (6.95)$$

Nondimensional radial and tangential stresses are

$$\begin{aligned}\bar{\sigma}_r^{p1} = & \frac{2\bar{C}_4}{1-2\nu} + \bar{\beta} \int_{\bar{a}}^{\bar{r}} \frac{\bar{T}}{\xi} d\xi + \ln(\bar{a}/\bar{r}) \\ & - \left( \frac{2q(1+\nu)}{1-2\nu} + \frac{\bar{\beta}}{2} \right) \bar{T}(\bar{a}) + \frac{2\nu\bar{\epsilon}_0}{1-2\nu} + \frac{1}{2},\end{aligned}\quad (6.96)$$

$$\begin{aligned}\bar{\sigma}_\theta^{p1} = & \frac{2\bar{C}_4}{1-2\nu} + \bar{\beta} \left[ \int_{\bar{a}}^{\bar{r}} \frac{\bar{T}}{\xi} d\xi + \bar{T} \right] + \ln(\bar{a}/\bar{r}) \\ & - \left( \frac{2q(1+\nu)}{1-2\nu} + \frac{\bar{\beta}}{2} \right) \bar{T}(\bar{a}) + \frac{2\nu\bar{\epsilon}_0}{1-2\nu} - \frac{1}{2}.\end{aligned}\quad (6.97)$$

Normalized plastic strain is

$$\begin{aligned}\bar{\epsilon}_r^{p1} = & -\frac{\bar{C}_3}{\bar{r}^2} - \frac{2q(1+\nu)}{\bar{r}^2} \int_{\bar{a}}^{\bar{r}} \xi\bar{T} d\xi + \left[ q(1+\nu) + \frac{\bar{\beta}(1-\nu)}{2} \right] \bar{T} \\ & - \frac{\bar{a}^2(4q(1+\nu) + \bar{\beta}(1-2\nu))}{4\bar{r}^2} \bar{T}(\bar{a}) + \frac{\bar{a}^2(1-2\nu) - 2\bar{r}^2(1-\nu)}{4\bar{r}^2}.\end{aligned}\quad (6.98)$$

Total axial force for elastic region is calculated from  $\bar{r}_1$  to 1

$$\bar{F}_z^e = -\frac{2q(1+\nu)}{(1-\nu)} \int_{\bar{r}_1}^1 \bar{r}\bar{T} d\bar{r} - \frac{(\bar{r}_1^2 - 1)}{1-2\nu} [(1-\nu)\bar{\epsilon}_0 + 2\nu\bar{C}_2], \quad (6.99)$$

and it is obtained for the plastic region 1 from  $\bar{a}$  to  $\bar{r}_1$  :

$$\begin{aligned}
\overline{F}_z^{p1} &= \overline{\beta}\nu\overline{r}_1^2 \int_{\overline{a}}^{\overline{r}_1} \frac{\overline{T}}{\overline{r}} d\overline{r} - 2q(1+\nu) \int_{\overline{a}}^{\overline{r}_1} \overline{r}\overline{T} d\overline{r} \\
&- \frac{1}{2}\nu[\overline{a}^2 - \overline{r}_1^2 - 2\overline{r}_1^2(\ln(\overline{a}) - \ln(\overline{r}_1))] \\
&+ \frac{(\overline{a}^2 - \overline{r}_1^2)}{2(1-2\nu)} [(4q(1+\nu) + \overline{\beta}(1-2\nu))\nu\overline{T} - 2(\overline{\epsilon}_0(1-\nu) + 2\nu\overline{C}_4)]. \quad (6.100)
\end{aligned}$$

Integration constants in normalized form are

$$\begin{aligned}
\overline{C}_1 &= \frac{1}{\overline{r}_1^2 + (1-2\nu)} \left\{ -\frac{(1+\nu)}{(1-\nu)}q \left[ \overline{r}_1^2 \int_{\overline{a}}^1 \overline{r}\overline{T} d\overline{r} + (1-2\nu) \int_{\overline{a}}^{\overline{r}_1} \overline{r}\overline{T} d\overline{r} \right] \right. \\
&\quad \left. - \frac{\overline{r}_1^2(1-2\nu)}{2} \left[ \overline{\beta} \int_{\overline{a}}^{\overline{r}_1} \frac{\overline{T}}{\overline{r}} d\overline{r} + \ln(\overline{a}/\overline{r}_1) \right] + \overline{r}_1^2\nu\overline{\epsilon}_0 \right\} \quad (6.101)
\end{aligned}$$

$$\begin{aligned}
\overline{C}_2 &= \frac{1}{\overline{r}_1^2 + (1-2\nu)} \left\{ \frac{(1-2\nu)\overline{r}_1^2}{2} \left[ \overline{\beta} \int_{\overline{a}}^{\overline{r}_1} \frac{\overline{T}}{\overline{r}} d\overline{r} + \ln(\overline{a}/\overline{r}_1) - \overline{r}_1^2\overline{\epsilon}_0\nu \right] \right. \\
&\quad \left. - \frac{(1+\nu)(1-2\nu)}{(1-\nu)}q \left[ \int_{\overline{a}}^1 \overline{r}\overline{T} d\overline{r} - \int_{\overline{a}}^{\overline{r}_1} \overline{r}\overline{T} d\overline{r} \right] \right\} \quad (6.102)
\end{aligned}$$

$$\begin{aligned}
\overline{C}_3 &= -\frac{1}{\overline{r}_1^2 + (1-2\nu)} \left\{ 2(1+\nu)q \left[ \overline{r}_1^2 \int_{\overline{a}}^b \overline{T} d\overline{r} + (1-2\nu) \int_{\overline{a}}^{\overline{r}_1} \overline{r}\overline{T} d\overline{r} \right] \right. \\
&\quad \left. + \overline{r}_1^2(1-\nu)(1-2\nu) \left[ \overline{\beta} \int_{\overline{a}}^{\overline{r}_1} \frac{\overline{T}}{\overline{r}} d\overline{r} + \ln(\overline{a}/\overline{r}_1) \right] - 2\overline{r}_1^2\nu(1-\nu)\overline{\epsilon}_0 \right\} \\
&\quad + \frac{\overline{a}^2}{4} \left\{ (1-2\nu) - [4q(1+\nu) + \overline{\beta}(1-2\nu)]\overline{T}(\overline{a}) \right\} \quad (6.103)
\end{aligned}$$

$$\overline{C}_4 = \frac{1}{4} \left\{ [4q(1+\nu) + \overline{\beta}(1-2\nu)]\overline{T}(\overline{a}) - (1-2\nu) \right\} - \nu\overline{\epsilon}_0. \quad (6.104)$$

Then, the Eq.s (6.89) and (6.90) are solved by iteration to obtain the remaining unknowns  $r_1$  and  $\epsilon_0$  given in Table 6.2. Solution of temperature integral in the above equations:

$$\begin{aligned}
\int_{\bar{a}}^{\bar{r}} \frac{\bar{T}(\xi, \tau)}{\xi} d\xi &= \frac{\tau}{\tau_t} \int_{\bar{a}}^{\bar{r}} \frac{1}{\xi} d\xi + \frac{\pi}{\tau_t} \sum_{n=1}^{\infty} (1 - e^{-\bar{\lambda}_n^2 \tau}) \frac{P(\bar{\lambda}_n)}{\bar{\lambda}_n^2 F(\bar{\lambda}_n)} \int_{\bar{a}}^{\bar{r}} \frac{C_0(\xi, \bar{\lambda}_n)}{\xi} d\xi \\
&= \frac{\tau}{\tau_t} \ln(\bar{r}/\bar{a}) \\
&\quad + \frac{\pi}{\tau_t} \sum_{n=1}^{\infty} (1 - e^{-\bar{\lambda}_n^2 \tau}) \frac{P(\bar{\lambda}_n)}{\bar{\lambda}_n^2 F(\bar{\lambda}_n)} \left\{ Y_0(\bar{a}\bar{\lambda}_n) \int_{\bar{a}}^{\bar{r}} \frac{J_0(\xi\bar{\lambda}_n)}{\xi} d\xi \right. \\
&\quad \left. - J_0(\bar{a}\bar{\lambda}_n) \int_{\bar{a}}^{\bar{r}} \frac{Y_0(\xi\bar{\lambda}_n)}{\xi} d\xi \right\} \tag{6.105}
\end{aligned}$$

where  $\int_{\bar{a}}^{\bar{r}} \frac{J_0(\xi\bar{\lambda}_n)}{\xi} d\xi$ , and  $\int_{\bar{a}}^{\bar{r}} \frac{Y_0(\xi\bar{\lambda}_n)}{\xi} d\xi$  integrals were evaluated numerically by using Simpson's rule since the series analytically do not converge.

#### 6.2.4 Results and Discussion for the Elastic-Plastic First Stage

Numerical results of the solution are obtained by the calculation of temperature distribution, unknown constants, and stress, strain and displacement expressions under the same heat load  $q = 0.25$  and the parameters given in the earlier section. The numerical results of the integration constants and axial strain are tabulated in Table 6.2. Using these values, stresses, strains and displacement distribution of the tube are calculated at the different time steps for the analysis of first stage of elastic-plastic deformation in the tube. At the onset of the elastoplastic deformation, the same response variables are obtained with those of the results of the end of the elastic stage presented in Fig. 6.5. This is also the verification for the solution of the elastic-plastic first stage.

Table 6.2: Axial strain and integration constants for the elastic-plastic first stage

$\tau$	$\bar{\epsilon}_0$	$\bar{r}_1$	$\bar{C}_1$	$\bar{C}_2$	$\bar{C}_3$	$\bar{C}_4$
0.859001	0.23998	0.5	-0.18265	-0.01320	-0.01880	-0.32295
0.88	0.24676	0.50618	-0.18779	-0.01360	-0.01930	-0.32490
0.92	0.25955	0.51818	-0.19742	-0.01440	-0.02050	-0.32857
0.96	0.27219	0.53048	-0.20684	-0.01530	-0.02180	-0.33219
0.99773	0.28396	0.54238	-0.21552	-0.01630	-0.02320	-0.33558

Figures 6.7-6.14 show that the distribution of radial, tangential, axial stresses, dis-

placement, and the plastic strains in the tube at several time steps of the first elastic-plastic stage. In these figures,  $\bar{r}_1$  represents the elastic-plastic boundary.

Fig. 6.7 shows the elastic-plastic stresses and displacement distributions at the earlier time of first stage. The elastic-plastic boundary is  $\bar{r}_1 = 0.50618$  at this time. As time passes, the plastic region 1, which is between the  $\bar{a}$  and  $\bar{r}_1$ , expands to the outer wall of the tube. At time  $\tau = 0.92$ , the elastic plastic boundary is  $\bar{r}_1 = 0.51818$  as seen in Fig. 6.8, it is 0.53048 at  $\tau = 0.96$  as shown in Fig. 6.9.

The elastic-plastic boundary reaches to the value of  $\bar{r}_1 = 0.542379$  at the end of the first stage at time  $\tau = 0.99773$ . As seen in Fig. 6.10, at this time, the radial and axial stresses are equal to each other on the elastic-plastic boundary. On the other hand, as seen in Figures 6.7-6.14, the principle stresses satisfy the condition of  $\sigma_r > \sigma_z > \sigma_\theta$  at the plastic region 1.

Figures 6.11-6.14 show the propagation of the plastic radial and tangential strains at the elastic-plastic first stage of the deformation. When time elapses, radial and tangential stresses increase with the increasing temperature as shown in these figures. The maximum values of the radial and tangential stresses are observed on the inner boundary of the tube due to the applied temperature cycle to this surface.

At time  $\tau = 0.99773$ , the elastic-plastic first stage lasts and two additional plastic regions emerge at the elastic-plastic boundary  $\bar{r}_1 = 0.542379$ . After that time, the second stage of the elastic-plastic deformation starts.

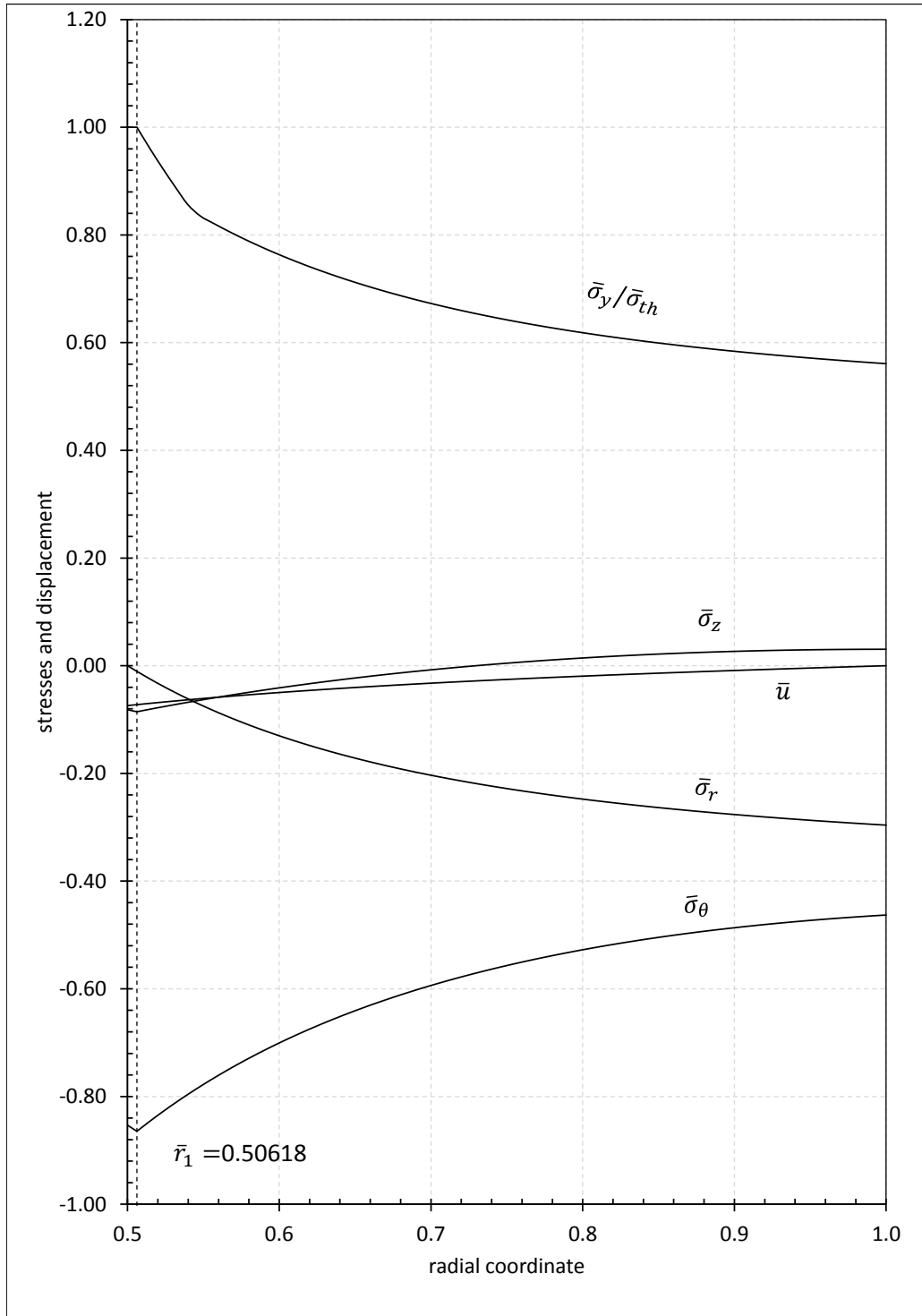


Figure 6.7: Stresses and displacement in elastic-plastic first stage at  $\tau = 0.88$

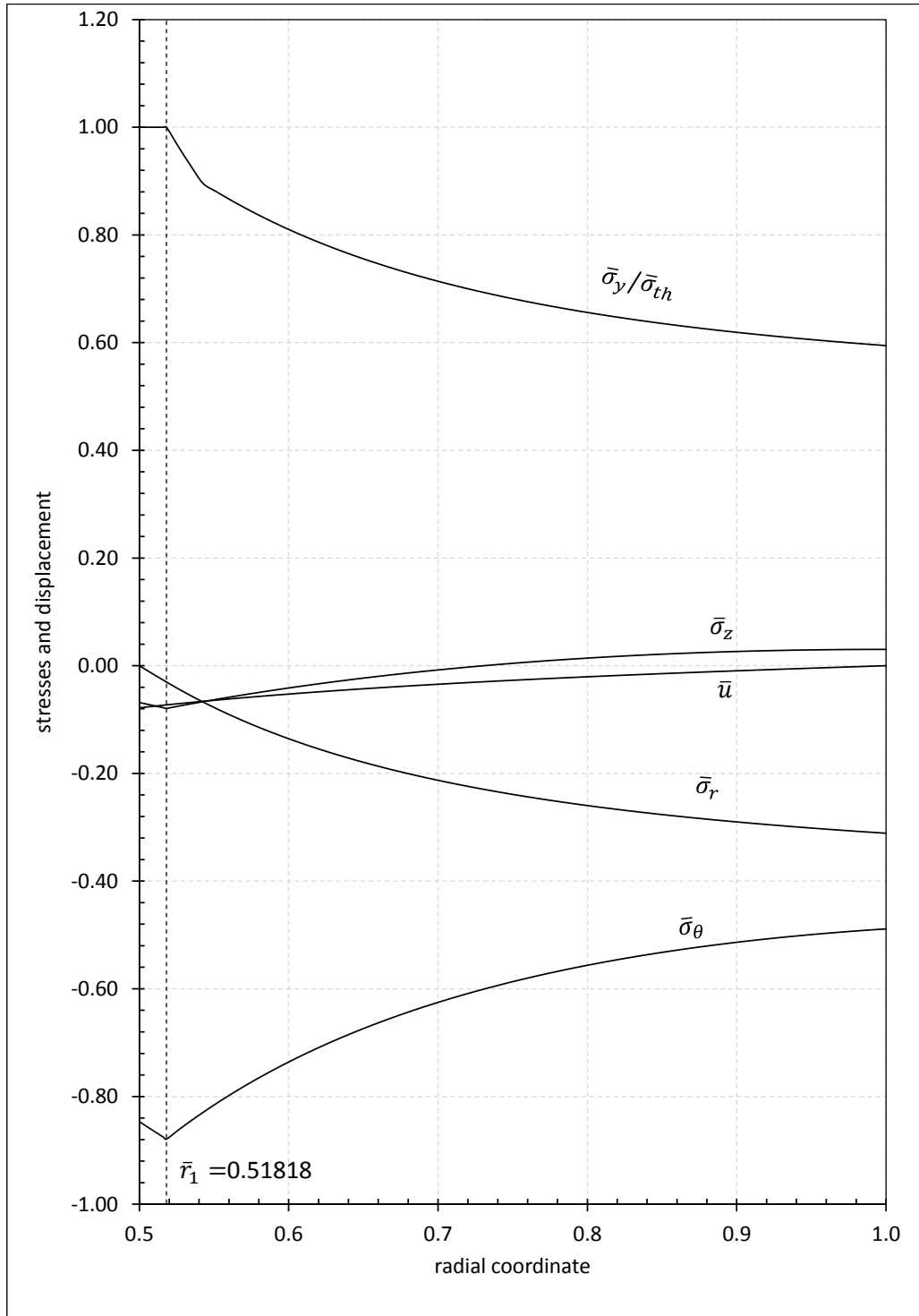


Figure 6.8: Stresses and displacement in elastic-plastic first stage at  $\tau = 0.92$

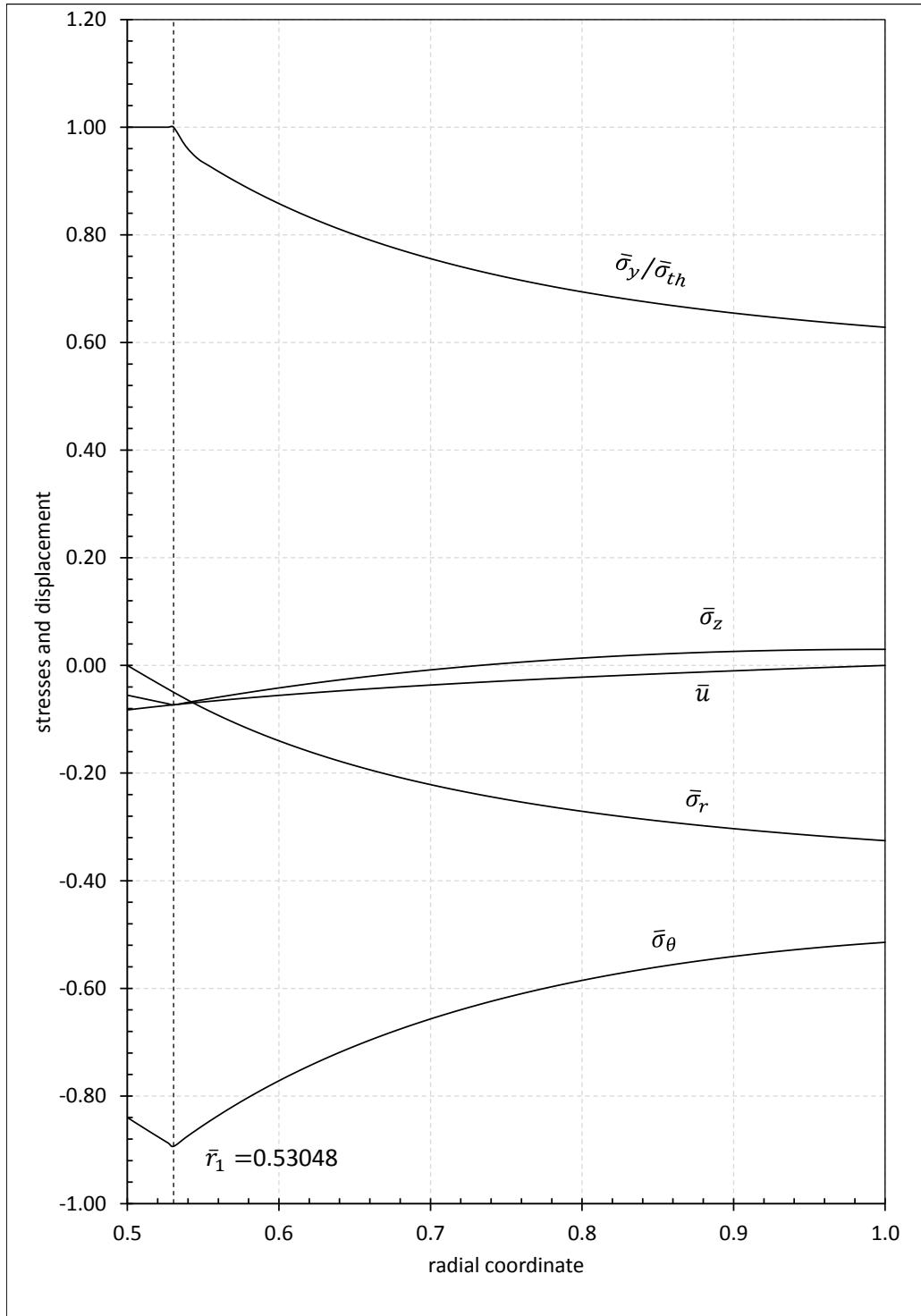


Figure 6.9: Stresses and displacement in elastic-plastic first stage at  $\tau = 0.96$

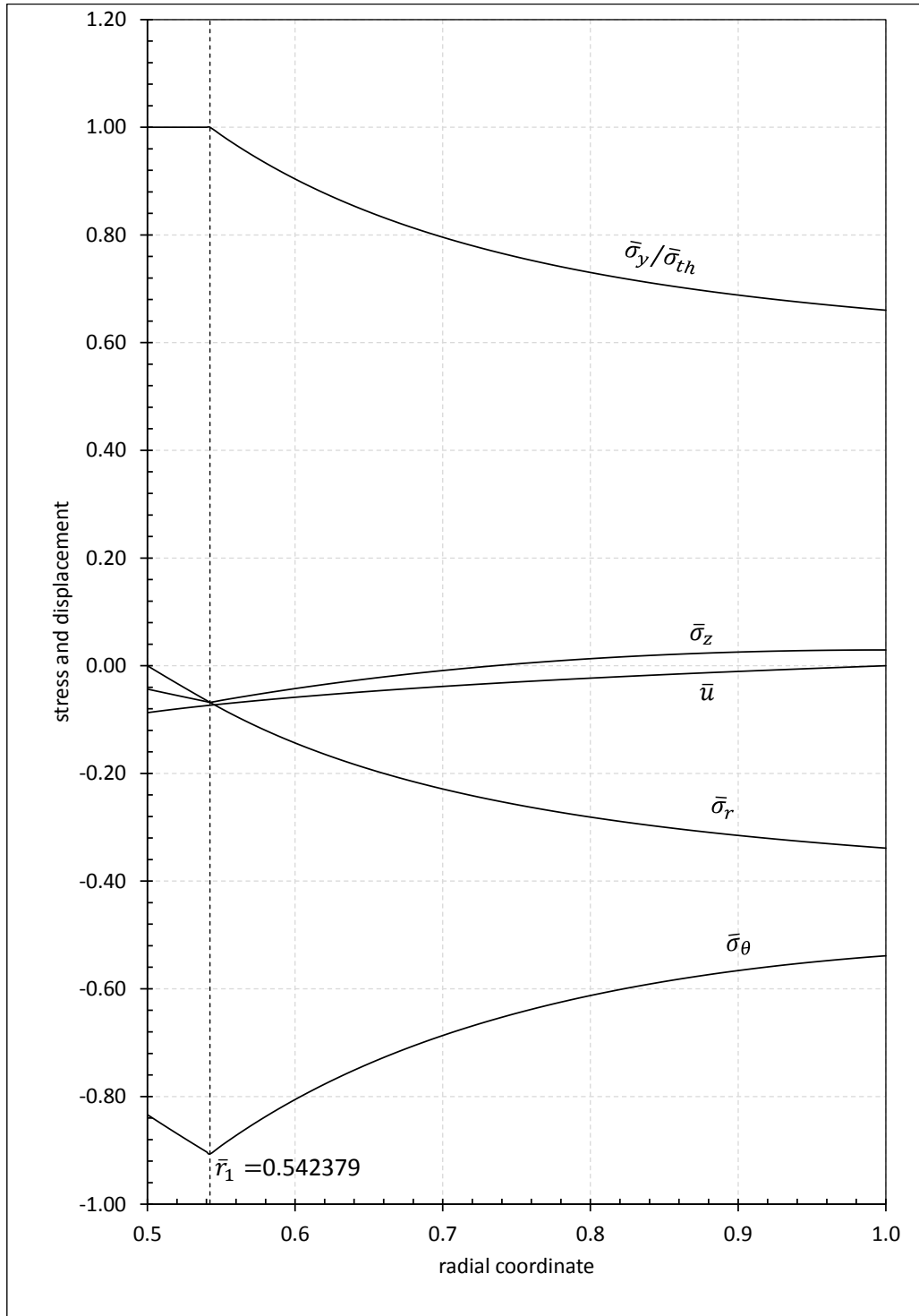


Figure 6.10: Stresses and displacement at the end of elastic-plastic first stage,  $\tau = 0.99773$



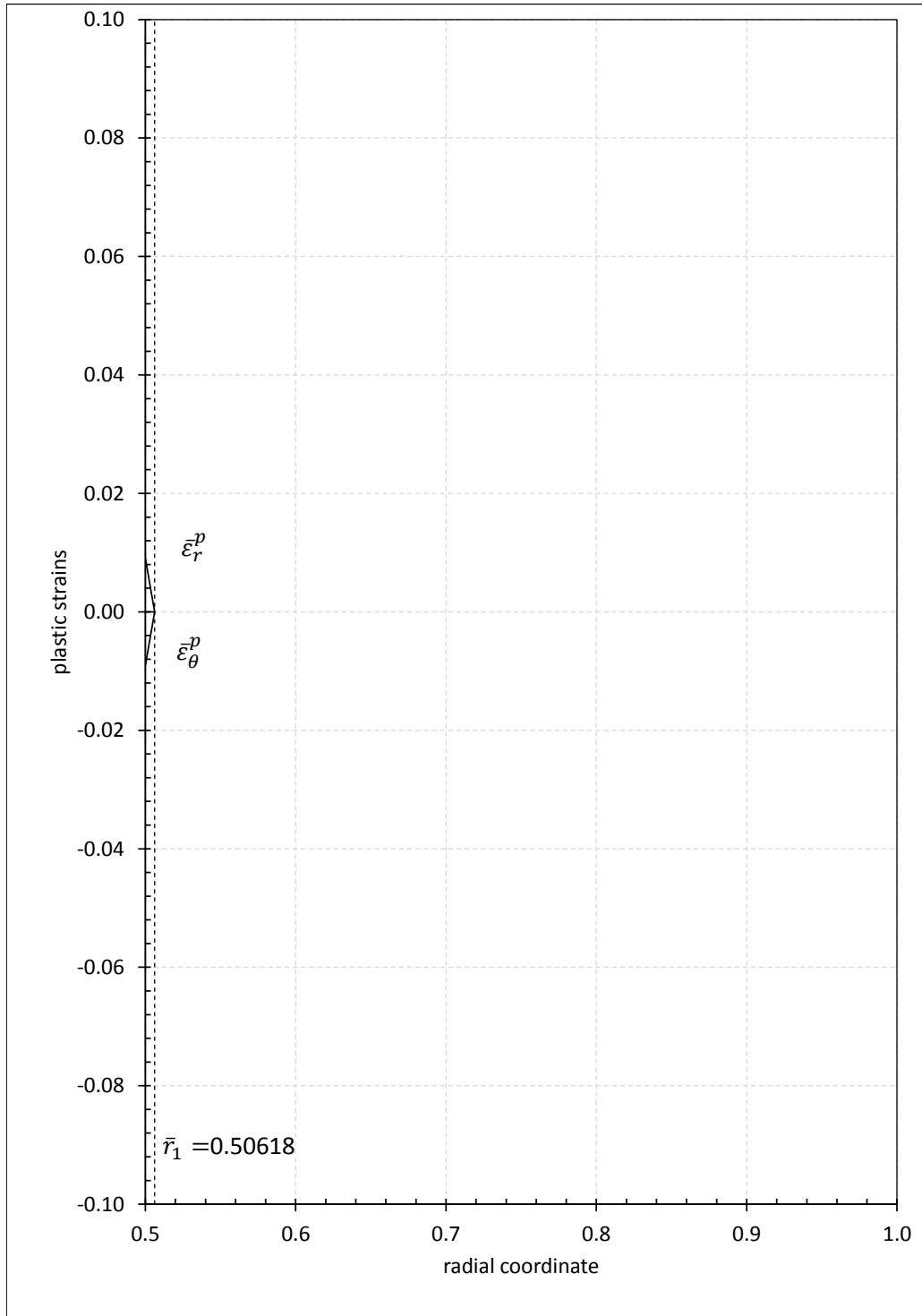


Figure 6.11: Plastic strains in elastic-plastic first stage at  $\tau = 0.88$

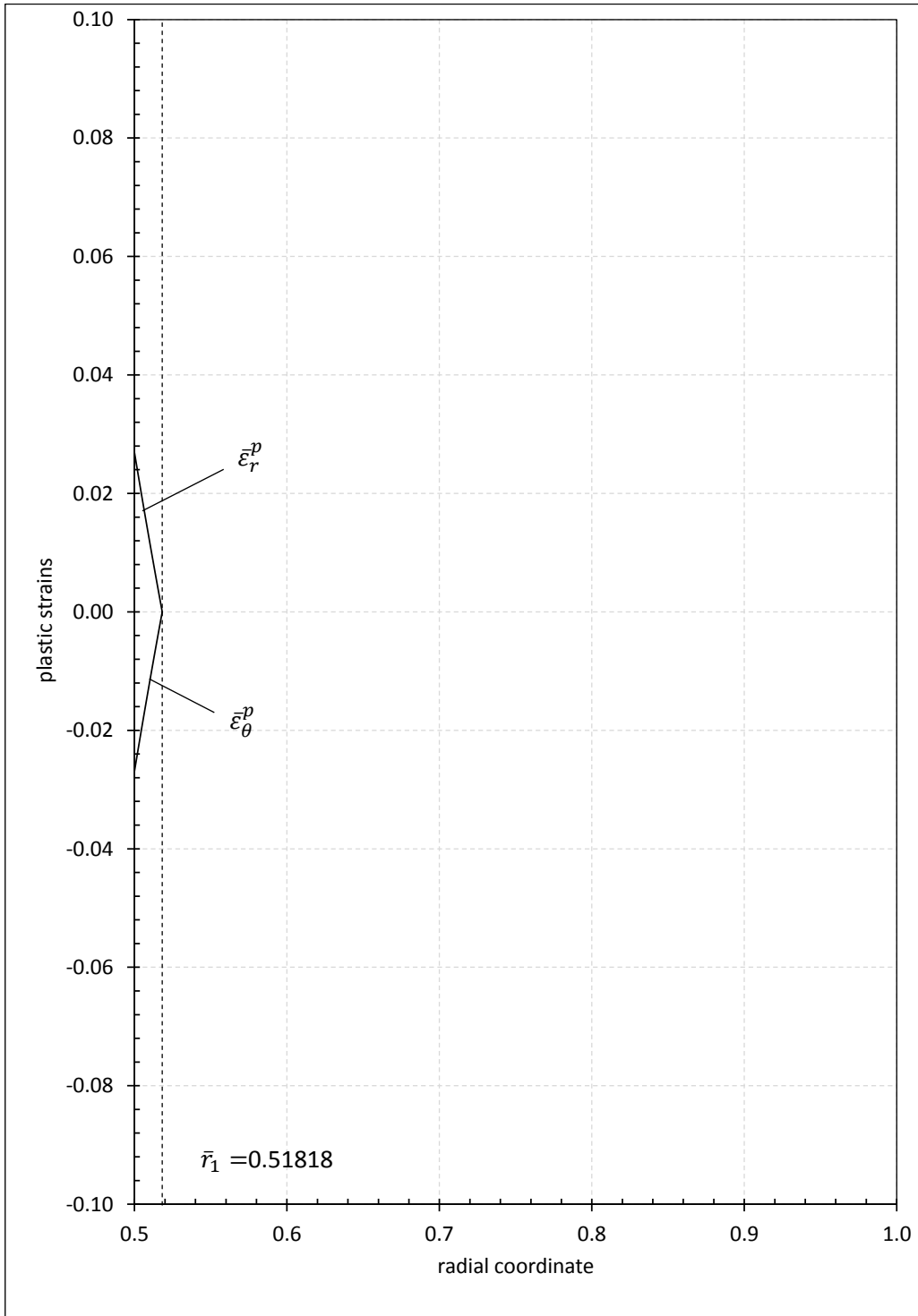


Figure 6.12: Plastic strains in elastic-plastic first stage at  $\tau = 0.92$

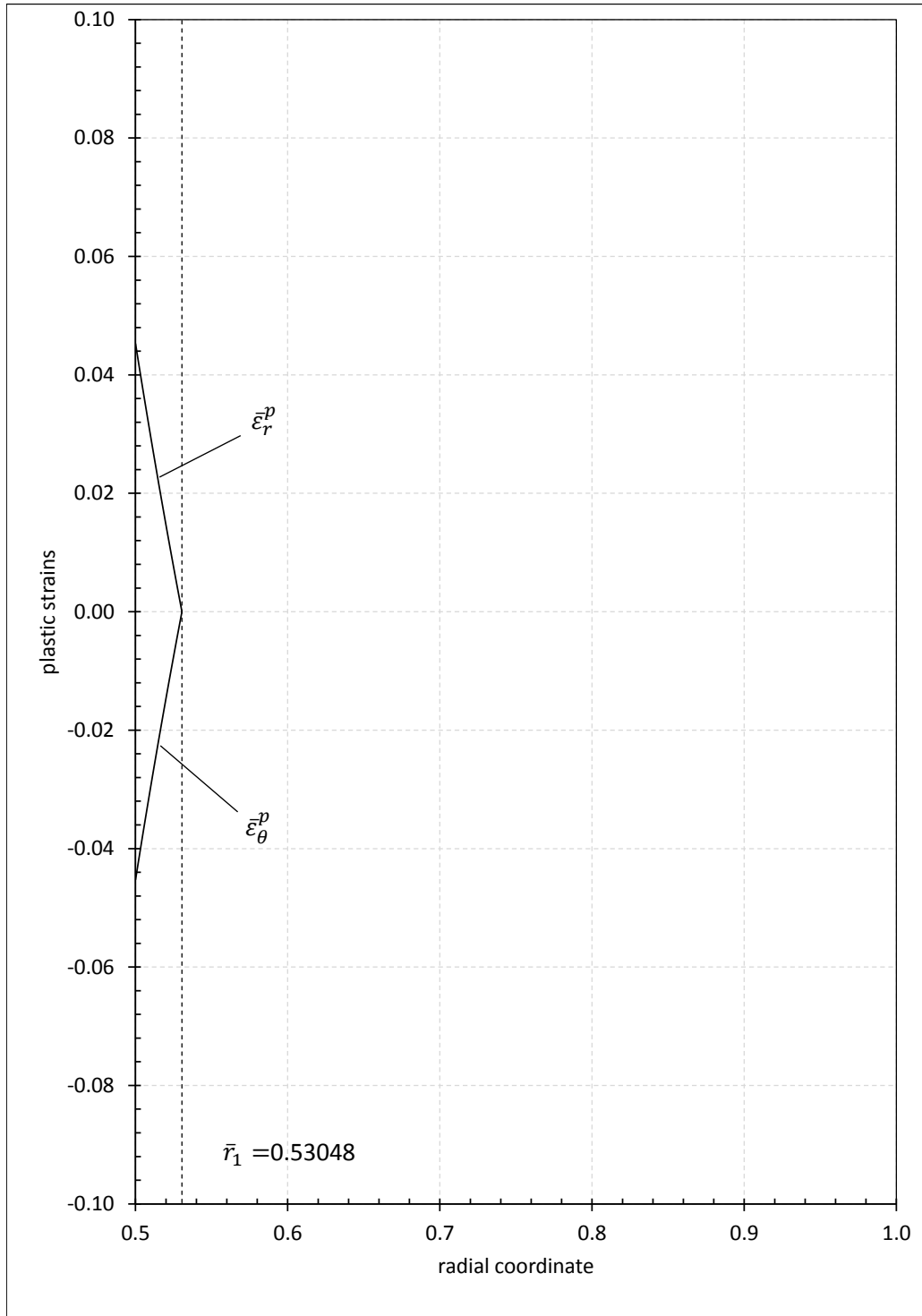


Figure 6.13: Plastic strains in elastic-plastic first stage at  $\tau = 0.96$

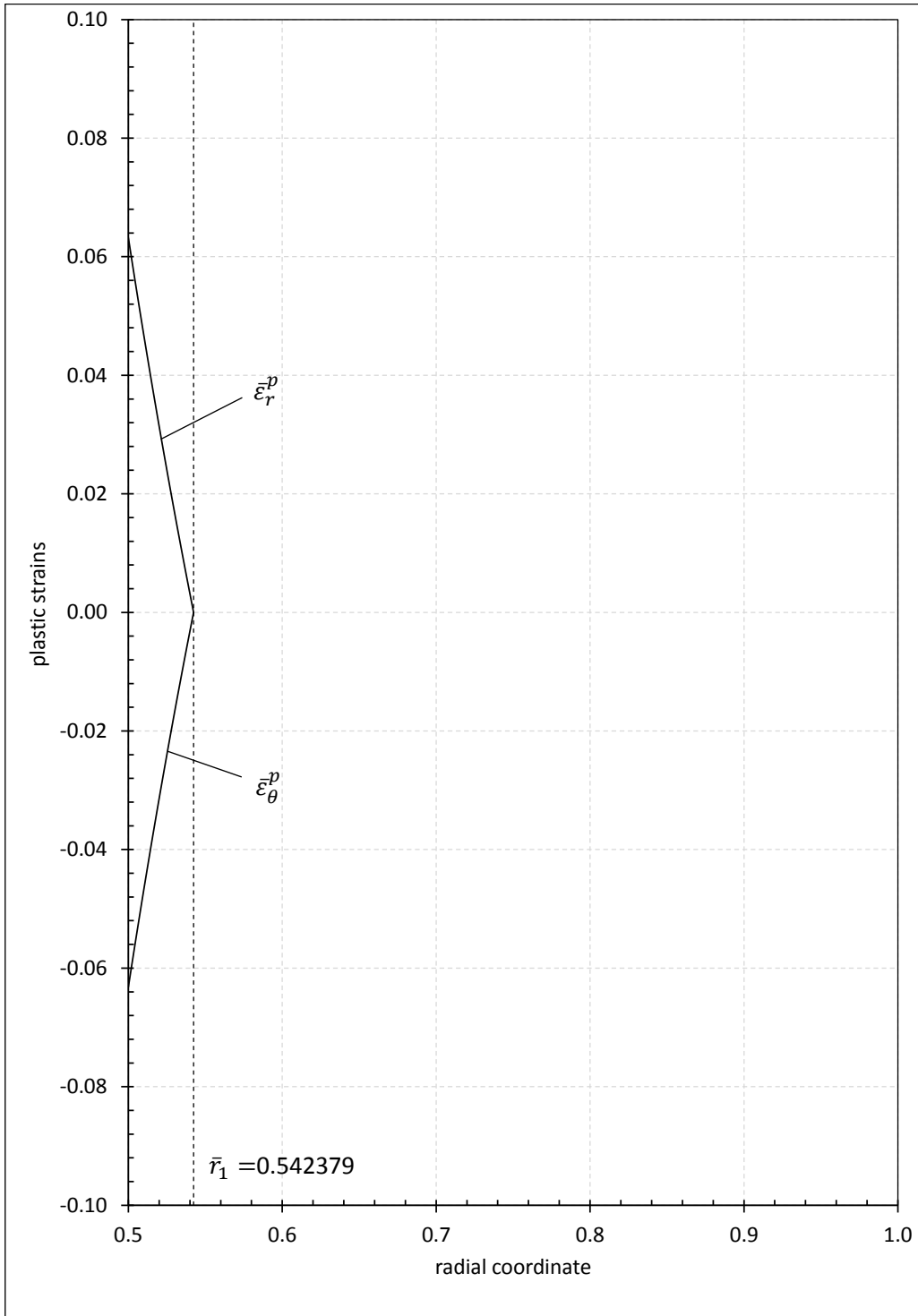


Figure 6.14: Plastic strains at the end of elastic-plastic first stage at  $\tau = 0.99773$

## 6.2.5 Elastic-Plastic Second Stage

At the second stage of elastoplastic deformation, another two plastic regions emerge at the same time at the elastic-plastic boundary and they expand through the both inner and outer sides of the tube very rapidly. Thus, there exist three plastic regions and an elastic region at this stage, which are plastic region 1 between  $a$  and  $r_1$ , plastic region 2 between  $r_1$  and  $r_2$ , plastic region 3 between  $r_2$  and  $r_3$ , and elastic region between  $r_3$  and  $b$ . Therefore, there are twelve unknowns to be calculated at this stage, eight of which are the integration constants due to the elastic and plastic regions. Three unknowns are  $r_1$ ,  $r_2$ , and  $r_3$ , which are the boundaries between the plastic regions 1 and 2, plastic regions 2 and 3, and plastic region 3 and elastic region, respectively. The remaining unknown is the axial strain,  $\epsilon_0$ .

Total axial force for the second stage of elastic-plastic deformation are the summation of the axial forces of four regions in the tube, three of which come from plastic region 1, 2, and 3 and the other from elastic region. For the elastic region, axial force calculated between  $r_3$  and  $b$  is

$$F_z^e = 2\pi \left\{ -\frac{2G\alpha(1+\nu)}{(1-\nu)} \int_{r_3}^b rT dr - \frac{(r_3^2 - b^2)G}{1-2\nu} [(1-\nu)\epsilon_0 + 2\nu C_2] \right\},$$

and for the plastic region 1, total force is calculated between  $a$  and  $r_1$  by the Eq.6.84.

Total axial force in the plastic region 2 is calculated from  $r_1$  to  $r_2$  :

$$\begin{aligned} F_z^{p2} = & \frac{\beta\sigma_0}{2} \left\{ r_2^2 \int_a^{r_2} \frac{T}{r} dr - r_1^2 \int_a^{r_1} \frac{T}{r} dr - \int_{r_1}^{r_2} rT dr \right\} \\ & + \frac{\sigma_0}{4} [r_2^2(1 - 2\ln(r_2)) - r_1^2(1 - 2\ln(r_1))] \\ & + \frac{(r_2^2 - r_1^2)}{6(1-2\nu)} \{2G(2C_6 + \epsilon_0)(1+\nu) + \sigma_0(1-2\nu)(1+3\ln(a)) \\ & - [6G\alpha(1+\nu) + \beta\sigma_0(1-2\nu)]T(a)\} \end{aligned} \quad (6.106)$$

Finally, the total axial force in the plastic region 3 is calculated between  $r_2$  and  $r_3$  as

$$\begin{aligned}
F_z^{p3} &= \frac{C_7 G(1-2M\nu)}{(1-M)(1-2\nu)} [r_3^{1-M} - r_2^{1-M}] + \frac{C_8 G(1+2M\nu)}{(1+M)(1-2\nu)} [r_3^{1+M} - r_2^{1+M}] \\
&+ \frac{1}{4(1-M^2)(1-2\nu)} \{M(1-M)(1+2M\nu) \\
&\times [-4G(1-M)\alpha(1+\nu) + \beta\sigma_0(1-2\nu)] \\
&\times \left( r_3^{1+M} \int_a^{r_3} r^{-M} T(r,t) dr - r_2^{1+M} \int_a^{r_2} r^{-M} T(r,t) dr \right) \\
&+ M(1+M)(1-2M\nu) [4G(1+M)\alpha(1+\nu) - \beta\sigma_0(1-2\nu)] \\
&\times \left( r_3^{1-M} \int_a^{r_3} r^M T(r,t) dr - r_2^{1-M} \int_a^{r_2} r^M T(r,t) dr \right) \\
&- 2 [4G\alpha(1+\nu) (1+M^2(1-4\nu)) + \beta\sigma_0(1-2\nu)(1-2M^2(1-\nu))] \int_{r_2}^{r_3} rT dr \\
&+ (r_3^{1-M} - r_2^{1-M}) a^{1+M} M(1-2M\nu) \\
&\times [4G\alpha(1+M)(1+\nu)T(a,t) + (2G\epsilon_0 - \sigma_0)(1-2\nu)] \\
&- (r_3^{1+M} - r_2^{1+M}) a^{1-M} M(1+2M\nu) \\
&\times [4G\alpha(1-M)(1+\nu)T(a,t) + (2G\epsilon_0 - \sigma_0)(1-2\nu)] \\
&- (r_2^2 - r_3^2) [2G\epsilon_0(1-4M^2\nu^2) + \sigma_0(1-2\nu)(1-2M^2(1+\nu))] \}. \quad (6.107)
\end{aligned}$$

Boundary and interface conditions for the second stage are:

$$\sigma_r^{p1}(a) = 0, \quad (6.108)$$

$$u_r^e(b) = 0, \quad (6.109)$$

$$\epsilon_z^{p2}(r_1) = 0, \quad (6.110)$$

$$u_r^{p1}(r_1) = u_r^{p2}(r_1), \quad (6.111)$$

$$\sigma_r^{p2}(r_1) - \sigma_\theta^{p2}(r_1) = \sigma_{th}(r_1), \quad (6.112)$$

$$\sigma_r^{p2}(r_2) = \sigma_r^{p3}(r_2), \quad (6.113)$$

$$u_r^{p2}(r_2) = u_r^{p3}(r_2), \quad (6.114)$$

$$\sigma_r^{p3}(r_2) - \sigma_\theta^{p3}(r_2) = \sigma_z^{p3}(r_2) - \sigma_\theta^{p3}(r_2) = \sigma_{th}(r_2), \quad (6.115)$$

$$\sigma_r^{p3}(r_3) = \sigma_r^e(r_3), \quad (6.116)$$

$$u_r^{p3}(r_3) = u_r^e(r_3), \quad (6.117)$$

$$\sigma_z^e(r_3) - \sigma_\theta^e(r_3) = \sigma_{th}(r_3), \quad (6.118)$$

and the total axial force:

$$F_z^e + F_z^{p1} + F_z^{p2} + F_z^{p3} = 0.$$

By using these twelve conditions, twelve unknowns can be calculated. Due to the fact that the analytical calculation of the unknowns is very tedious in terms of mathematical aspect, there are calculated by numerical methods with the aid of a computer program called Minpack [59].

Before the numerical calculations, in addition to the nondimensional equations of plastic region 1 derived in the first stage, nondimensional forms of the equations of plastic region 2 and 3 are obtained. Thus, the nondimensional displacement for the plastic region 2 takes the form of

$$\begin{aligned} \bar{u}_r^{p2} = & \frac{\bar{C}_5}{\bar{r}} + \bar{C}_6 \bar{r} + \frac{(1-2\nu)}{4(1+\nu)} \left\{ 3\bar{r} \left[ \bar{\beta} \int_{\bar{a}}^{\bar{r}} \frac{\bar{T}}{\xi} d\xi + \ln(\bar{a}/\bar{r}) \right] \right. \\ & \left. - \frac{1}{2\bar{r}} \left[ 2\bar{\beta} \int_{\bar{a}}^{\bar{r}} \xi \bar{T}(\xi, \tau) d\xi + (3-2\bar{\beta}\bar{T}(\bar{a}))(\bar{a}^2 - \bar{r}^2) \right] \right\} \\ & + \frac{3q}{\bar{r}} \left( \int_{\bar{a}}^{\bar{r}} \xi \bar{T}(\xi, \tau) d\xi + \frac{(\bar{a}^2 - \bar{r}^2)}{2} \bar{T}(\bar{a}) \right), \end{aligned} \quad (6.119)$$

nondimensional radial stress for plastic region 2

$$\begin{aligned} \bar{\sigma}_r^{p2} = & \frac{1}{3(1-2\nu)} \left\{ 2(2\bar{C}_6 + \bar{\epsilon}_0)(1+\nu) + (1-2\nu) \left[ 1 + 3 \left( \bar{\beta} \int_{\bar{a}}^{\bar{r}} \frac{\bar{T}}{\xi} d\xi + \ln(\bar{a}/\bar{r}) \right) \right] \right. \\ & \left. - (6q(1+\nu) + \bar{\beta}(1-2\nu))\bar{T}(\bar{a}) \right\}, \end{aligned}$$

nondimensional tangential stress for the plastic region 2

$$\begin{aligned} \bar{\sigma}_\theta^{p2} = & \frac{1}{3(1-2\nu)} \left\{ 2(2\bar{C}_6 + \bar{\epsilon}_0)(1+\nu) \right. \\ & \left. + (1-2\nu) \left[ -2 + 3 \left( \bar{\beta} \int_{\bar{a}}^{\bar{r}} \frac{\bar{T}}{\xi} d\xi + \ln(\bar{a}/\bar{r}) + \bar{\beta}\bar{T} \right) \right] \right. \\ & \left. - [6q(1+\nu) + \bar{\beta}(1-2\nu)] \bar{T}(\bar{a}) \right\}, \end{aligned} \quad (6.120)$$

nondimensional radial and axial plastic strains are

$$\begin{aligned}
\bar{\epsilon}_r^{p2} = & -\frac{\bar{C}_5}{r^2} + \frac{\bar{C}_6}{3} - \frac{\bar{\beta}(1-2\nu)}{4(1+\nu)} \int_{\bar{a}}^{\bar{r}} \frac{\bar{T}}{\xi} d\xi \\
& - \left( 3q - \frac{\bar{\beta}(1-2\nu)}{4(1+\nu)} \right) \frac{1}{\bar{r}^2} \int_{\bar{a}}^{\bar{r}} \xi \bar{T}(\xi, \tau) d\xi - \frac{2\bar{\epsilon}_0 + 1}{6} \\
& + \frac{(1-2\nu)}{4(1+\nu)} \left[ \frac{3(\bar{a}^2 - \bar{r}^2)}{2\bar{r}^2} + \ln(\bar{a}/\bar{r}) \right] \\
& - \frac{(3\bar{a}^2 + \bar{r}^2) [6q(1+\nu) + \bar{\beta}(1-2\nu)]}{12(1+\nu)\bar{r}^2} \bar{T}(\bar{a}) + \left( 2q + \frac{\bar{\beta}(1-\nu)}{2(1+\nu)} \right) \bar{\bar{T}} \quad (6.121)
\end{aligned}$$

$$\begin{aligned}
\bar{\epsilon}_z^{p2} = & -\frac{1}{6(1+\nu)} \{ [4(\bar{C}_6 - \bar{\epsilon}_0) + 1] (1+\nu) \\
& + 3(1-2\nu) \left[ \bar{\beta} \int_{\bar{a}}^{\bar{r}} \frac{\bar{T}}{\xi} d\xi + \ln(\bar{a}/\bar{r}) \right] \\
& + 3 [2q(1+\nu) - \bar{\beta}\nu] \bar{T} - [6q(1+\nu) + \bar{\beta}(1-2\nu)] \bar{T}(\bar{a}) \}, \quad (6.122)
\end{aligned}$$

and finally nondimensional total axial force for the plastic region 2 is

$$\begin{aligned}
\bar{F}_z^{p2} = & \frac{\bar{\beta}}{2} \left\{ \bar{r}_2^2 \int_{\bar{a}}^{\bar{r}_2} \frac{\bar{T}}{\bar{r}} d\bar{r} - \bar{r}_1^2 \int_{\bar{a}}^{\bar{r}_1} \frac{\bar{T}}{\bar{r}} d\bar{r} - \int_{\bar{r}_1}^{\bar{r}_2} \bar{r} \bar{T} d\bar{r} \right\} \\
& + \frac{1}{4} [\bar{r}_2^2(1-2\ln(\bar{r}_2)) - \bar{r}_1^2(1-2\ln(\bar{r}_1))] \\
& + \frac{(\bar{r}_2^2 - \bar{r}_1^2)}{6(1-2\nu)} \{ 2(2\bar{C}_6 + \bar{\epsilon}_0)(1+\nu) + (1-2\nu)(1+3\ln(\bar{a})) \\
& - [6q(1+\nu) + \bar{\beta}(1-2\nu)] \bar{T}(\bar{a}) \}. \quad (6.123)
\end{aligned}$$

Some dimensionless abbreviations are defined to express in a more easily form of the nondimensional forms of the equations for plastic region 3. These are:

$$N_1 = 1 + \nu$$

$$N_2 = 1 - 2\nu$$

$$N_3 = 1 - \nu$$



$$\begin{aligned}
K_1 &= [-4q(1 - M)(1 + \nu) + \bar{\beta}(1 - 2\nu)] \\
K_2 &= [4q(1 + M)(1 + \nu) - \bar{\beta}(1 - 2\nu)] \\
M_1 &= 1 + M \\
M_2 &= 1 - M \\
M_3 &= M(1 - \nu) + \nu \\
M_4 &= M(1 - \nu) - \nu \\
M_5 &= 1 + 2M\nu \\
M_6 &= 1 - 2M\nu
\end{aligned}$$

Bu using these abbreviations, nondimensional forms of the equations for the plastic region 3 are derived. Nondimensional displacement is

$$\begin{aligned}
\bar{u}_r^{p3} &= \bar{C}_7 \bar{r}^{-M} + \bar{C}_8 \bar{r}^M + \frac{M}{4} \left\{ \bar{r}^M K_1 \int_{\bar{a}}^{\bar{r}} \xi^{-M} \bar{T}(\xi, \tau) d\xi + \bar{r}^{-M} K_2 \int_{\bar{a}}^{\bar{r}} \xi^M \bar{T}(\xi, \tau) d\xi \right. \\
&\quad \left. + \frac{(1 - 2\nu)(2\bar{\epsilon}_0 - 1)}{M_3 M_4} [M_2 \bar{a}^{M_1} \bar{r}^{-M} - M_1 \bar{a}^{M_2} \bar{r}^M + 2M\bar{r}] \right\} \\
&\quad + Mq(1 + \nu)(\bar{a}^{M_1} \bar{r}^{-M} - \bar{a}^{M_2} \bar{r}^M) \bar{T}(\bar{a}), \tag{6.124}
\end{aligned}$$

radial and tangential stresses

$$\begin{aligned}
\bar{\sigma}_r^{p3} &= \frac{2\bar{r}^{-M_1}}{1 - 2\nu} [\bar{C}_8 \bar{r}^{2M} M_3 - \bar{C}_7 M_4] \\
&\quad - \frac{M}{2(1 - 2\nu)} \left\{ -\bar{r}^{-M_2} M_3 K_1 \int_{\bar{a}}^{\bar{r}} \xi^{-M} \bar{T}(\xi, \tau) d\xi + \bar{r}^{-M_1} M_4 K_2 \int_{\bar{a}}^{\bar{r}} \xi^M \bar{T}(\xi, \tau) d\xi \right. \\
&\quad \left. + 4q(1 + \nu) [(\bar{a}^{M_1} \bar{r}^{-M_1} M_4 + \bar{a}^{M_2} \bar{r}^{-M_2} M_3) \bar{T}(\bar{a}) \right. \\
&\quad \left. + (\frac{1}{M} - 2M(1 - \nu)) \bar{T}] \right\} \\
&\quad + \frac{1}{2M_2 M_1 (1 - 2\nu)} \{ 4\bar{\epsilon}_0 (M^2 (1 - 3\nu) + \nu) - 2M^2 (1 - 2\nu) \\
&\quad - M(1 - 2\nu)(2\bar{\epsilon}_0 - 1) [M_3 M_1 \bar{a}^{M_2} \bar{r}^{-M_2} + M_4 M_2 \bar{a}^{M_1} \bar{r}^{-M_1}] \} \tag{6.125}
\end{aligned}$$

$$\begin{aligned}
\bar{\sigma}_\theta^{p3} &= \frac{\bar{r}^{-M_1}}{1-2\nu} [\bar{C}_7 M_6 + \bar{C}_8 \bar{r}^{2M} M_5] \\
&\quad - \frac{M}{4(1-2\nu)} \left\{ -\bar{r}^{-M_2} M_5 K_1 \int_{\bar{a}}^{\bar{r}} \xi^{-M} \bar{T}(\xi, \tau) d\xi \right. \\
&\quad - \bar{r}^{-M_1} M_6 K_2 \int_{\bar{a}}^{\bar{r}} \xi^M \bar{T}(\xi, \tau) d\xi \\
&\quad + 4q(1+\nu) [\bar{a}^{M_2} \bar{r}^{-M_2} M_5 - \bar{a}^{M_1} \bar{r}^{-M_1} M_6] \bar{T}(\bar{a}) \\
&\quad \left. - \frac{2}{M} [\bar{\beta}(1-2\nu) - 4q(1+\nu)(1-2M^2\nu)] \bar{T} \right\} \\
&\quad + \frac{1}{4M_1 M_2 (1-2\nu)} \{ 4\bar{\epsilon}_0 M_5 M_6 - 2(1-2\nu)(1+2M^2\nu) \\
&\quad + M(1-2\nu)(2\bar{\epsilon}_0 - 1) [M_2 M_6 \bar{a}^{M_1} \bar{r}^{-M_1} - M_1 M_5 \bar{a}^{M_2} \bar{r}^{-M_2}] \}, \quad (6.126)
\end{aligned}$$

axial plastic strain

$$\begin{aligned}
\bar{\epsilon}_z^{p3} &= -\frac{\bar{C}_7}{2} \bar{r}^{-M_1} - \frac{\bar{C}_8}{2} \bar{r}^{-M_2} - \frac{M}{8} \left\{ \bar{r}^{-M_2} K_1 \int_{\bar{a}}^{\bar{r}} \xi^{-M} \bar{T}(\xi, \tau) d\xi \right. \\
&\quad + \bar{r}^{-M_1} K_2 \int_{\bar{a}}^{\bar{r}} \xi^M \bar{T}(\xi, \tau) d\xi \\
&\quad \left. + \frac{(1-2\nu)(2\bar{\epsilon}_0 - 1)}{M_2 M_1} [2M + M_2 \bar{a}^{M_1} \bar{r}^{-M_1} - M_1 \bar{a}^{M_2} \bar{r}^{-M_2}] \right\} \\
&\quad - \frac{Mq(1+\nu)}{2} [\bar{a}^{M_1} \bar{r}^{-M_1} - \bar{a}^{M_2} \bar{r}^{-M_2}] \bar{T}(\bar{a}) + \frac{2\bar{\epsilon}_0 - (1 - \bar{\beta} \bar{T})}{4}, \quad (6.127)
\end{aligned}$$

and nondimensional total axial force is

$$\begin{aligned}
\bar{F}_z^{p3} &= \frac{\bar{C}_7 M_6}{M_2(1-2\nu)} [\bar{r}_3^{M_2} - \bar{r}_2^{M_2}] + \frac{\bar{C}_8 M_5}{M_1(1-2\nu)} [\bar{r}_3^{M_1} - \bar{r}_2^{M_1}] \\
&\quad + \frac{1}{4M_1 M_2 (1-2\nu)} \{ M M_2 M_5 K_1 \\
&\quad \times \left( \bar{r}_3^{M_1} \int_{\bar{a}}^{\bar{r}_3} \bar{r}^{-M} \bar{T} d\bar{r} - \bar{r}_2^{M_1} \int_{\bar{a}}^{\bar{r}_2} \bar{r}^{-M} \bar{T} d\bar{r} \right) \\
&\quad + M M_1 M_6 K_2 \left[ \bar{r}_3^{M_2} \int_{\bar{a}}^{\bar{r}_3} \bar{r}^M \bar{T} d\bar{r} - \bar{r}_2^{M_2} \int_{\bar{a}}^{\bar{r}_2} \bar{r}^M \bar{T} d\bar{r} \right] \\
&\quad - 2 [4q(1+\nu) (1 + M^2(1-4\nu)) + \bar{\beta}(1-2\nu)(1-2M^2(1-\nu))] \int_{\bar{r}_2}^{\bar{r}_3} \bar{r} \bar{T} d\bar{r} \\
&\quad + (\bar{r}_3^{M_2} - \bar{r}_2^{M_2}) \bar{a}^{M_1} M M_6 [4qM_1(1+\nu) \bar{T}(\bar{a}) + (2\bar{\epsilon}_0 - 1)(1-2\nu)] \\
&\quad - (\bar{r}_3^{M_1} - \bar{r}_2^{M_1}) \bar{a}^{M_2} M M_5 [4qM_2(1+\nu) \bar{T}(\bar{a}) + (2\bar{\epsilon}_0 - 1)(1-2\nu)] \\
&\quad \left. + (\bar{r}_3^2 - \bar{r}_2^2) [2\bar{\epsilon}_0 M_5 M_6 + (1-2\nu)(1-2M^2(1+\nu))] \right\} \quad (6.128)
\end{aligned}$$

## 6.2.6 Results and Discussion for the Elastic-Plastic Second Stage

Second stage of the elastic-plastic deformation starts when the time reaches the value of  $\tau = 0.99773$ . At that time, plastic regions 2 and 3 emerge at the same time on the elastic-plastic boundary  $\bar{r}_1 = 0.542379$ . The same results are obtained for the response values of the second stage with those at the end of the elastic-plastic first stage.

Using the interface and boundary conditions, the integration constants, elastic-plastic interface radii, and the axial strain values are determined by an iterative method. These values are tabulated in Table 6.3. Using these values, stresses, plastic strains and displacement distribution of the tube are calculated at the different time steps for the analysis elastic behavior of the tube at this stage.

Table 6.3: Axial strain and integration constants for the elastic-plastic second stage

$\tau$	$\bar{\epsilon}_0$	$\bar{r}_1$	$\bar{r}_2$	$\bar{r}_3$	
1.05	0.30033	0.52585	0.55342	0.58090	
1.1	0.31639	0.50943	0.56390	0.62312	
1.12757	0.32547	0.50000	0.56958	0.64928	
$\tau$	$\bar{C}_1$	$\bar{C}_2$	$\bar{C}_3$		
1.05	-0.01781	-0.11360	-0.07375		
1.1	-0.01945	-0.11901	-0.07946		
1.12757	-0.02043	-0.12191	0.08264		
$\tau$	$\bar{C}_4$	$\bar{C}_5$	$\bar{C}_6$	$\bar{C}_7$	$\bar{C}_8$
1.05	0.10749	-0.07433	0.10971	-0.08447	0.10466
1.1	0.11718	-0.07967	0.11800	-0.08916	0.10908
1.12757	0.12245	-0.08264	0.12245	-0.09178	0.11147

In Figures 6.15-6.18, the distributions of radial, tangential, axial stresses, and the displacement are plotted at several time steps. As seen in these figures, the plastic range increases with the increasing temperature. Hence, the plastic region 2 expands to the inner surface of the tube whereas the plastic region 3 moves through the outer surface when time elapses. As a result, the plastic region 1 disappears at the end of

the elastic-plastic second stage by covering the plastic region 2.

Figures through 6.18-6.20 show the propagation of the plastic strains with time as a result of the increasing temperature. As shown in these figures, at any radial point on the tube section, the plastic strains increase with the increasing temperature.

The second elastic-plastic stage lasts until  $\tau = 1.12757$ . At this time, the radial boundary between the regions 2 and 3 is  $\bar{r}_2 = 0.56958$ , and between the plastic region 3 and the elastic region is  $\bar{r}_3 = 0.64928$ .

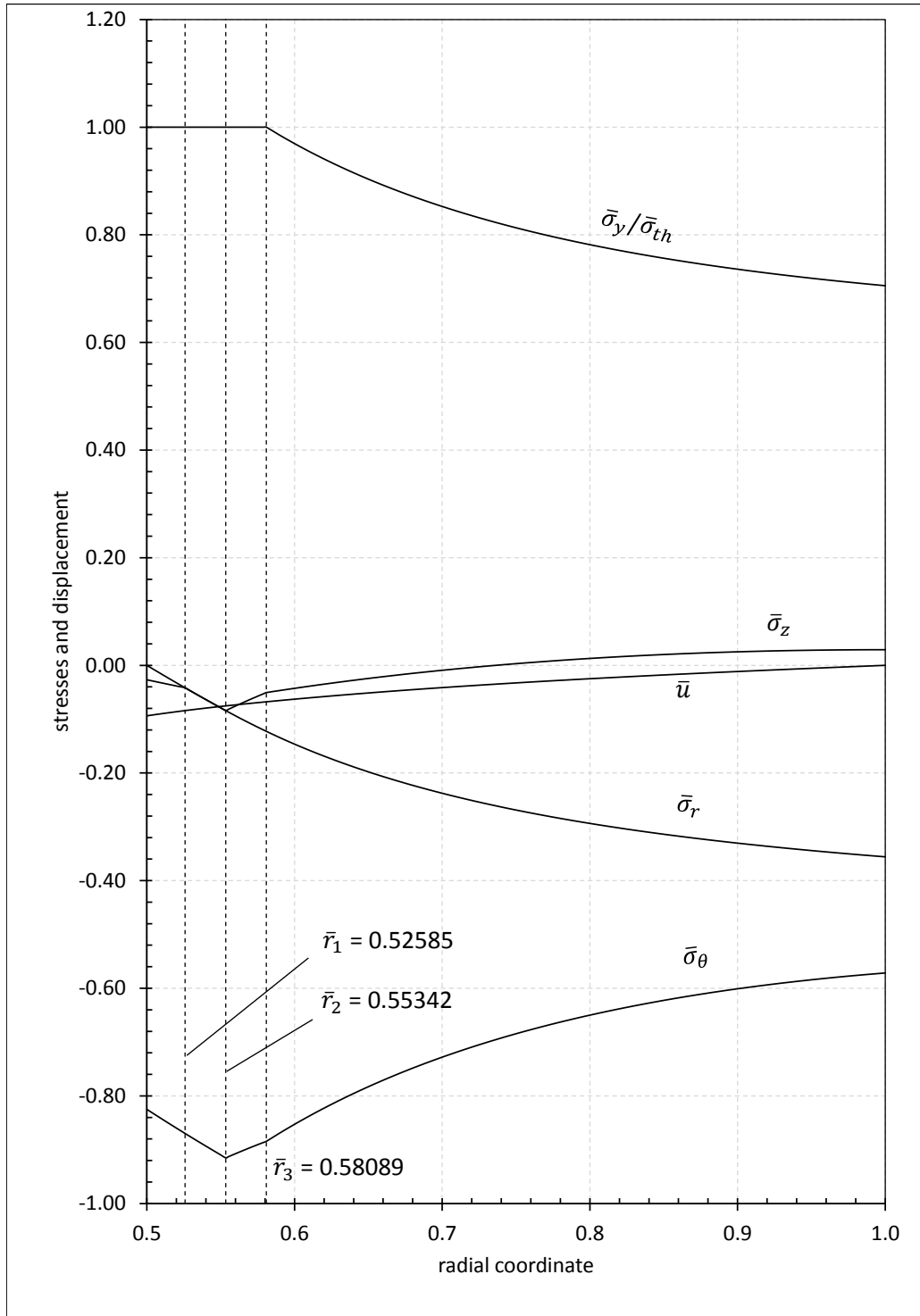


Figure 6.15: Stresses and displacement in elastic-plastic second stage at  $\tau = 1.05$

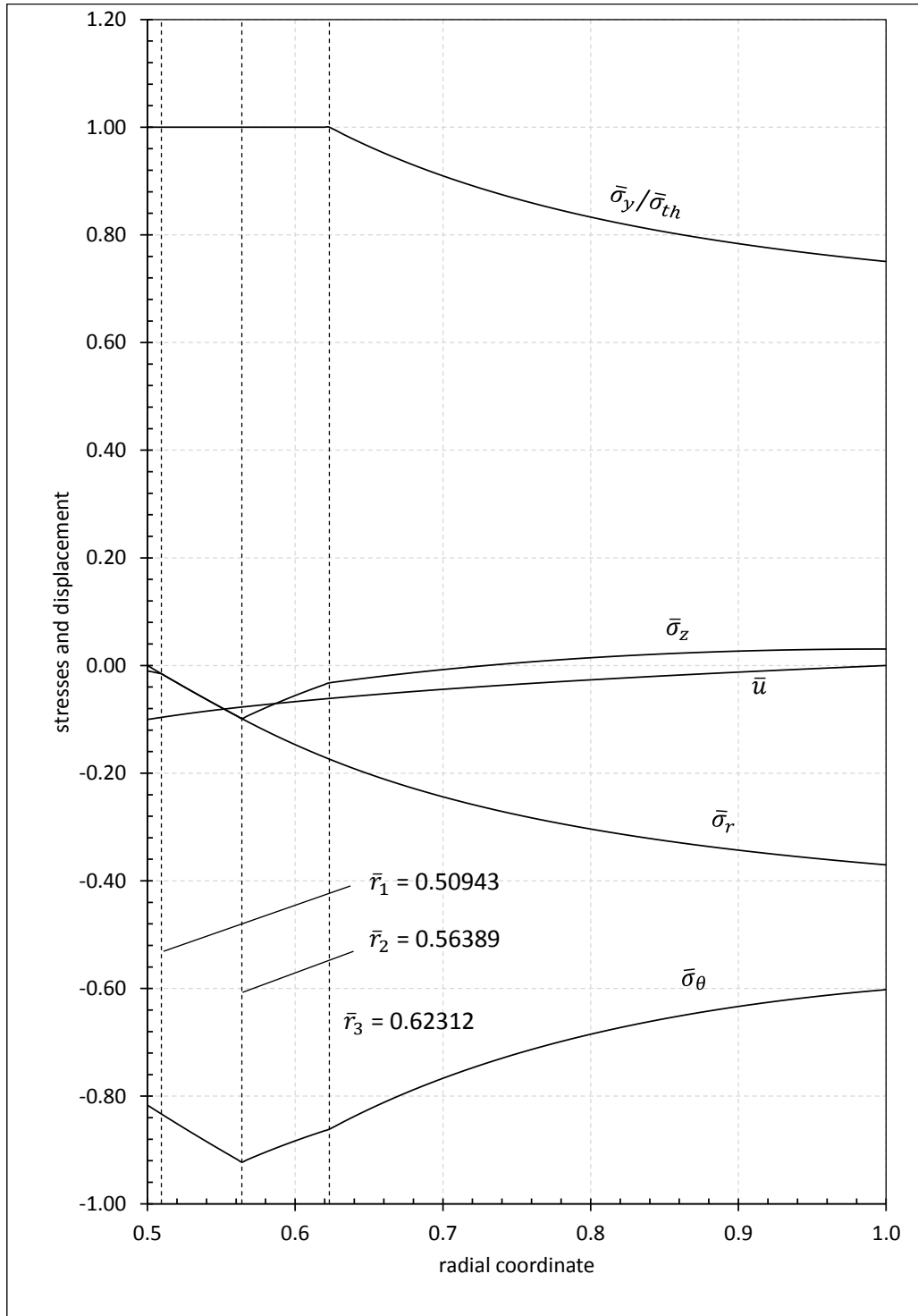


Figure 6.16: Stresses and displacement in elastic-plastic second stage at  $\tau = 1.1$

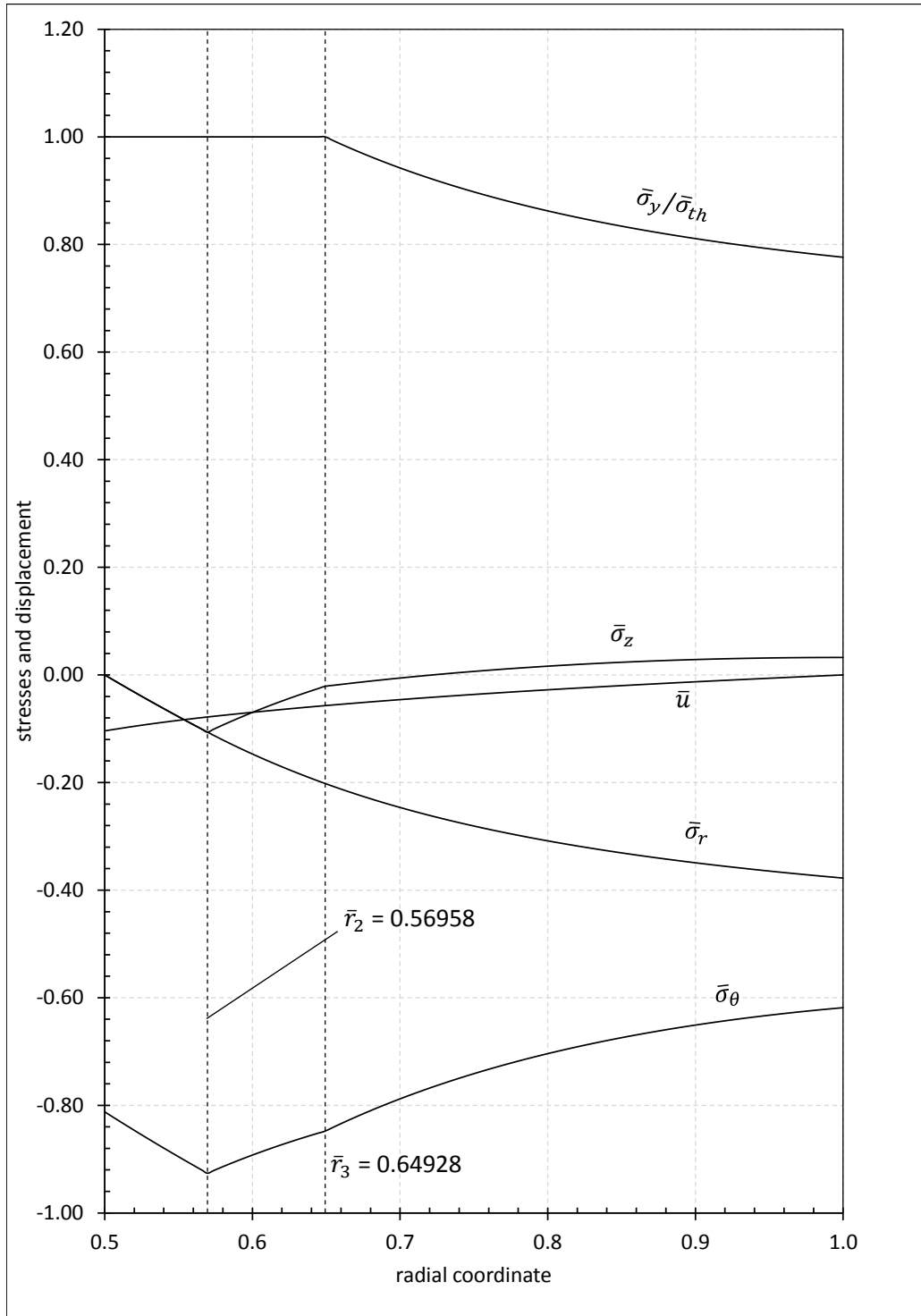


Figure 6.17: Stresses and displacement at the end of elastic-plastic second stage,  $\tau = 1.12757$

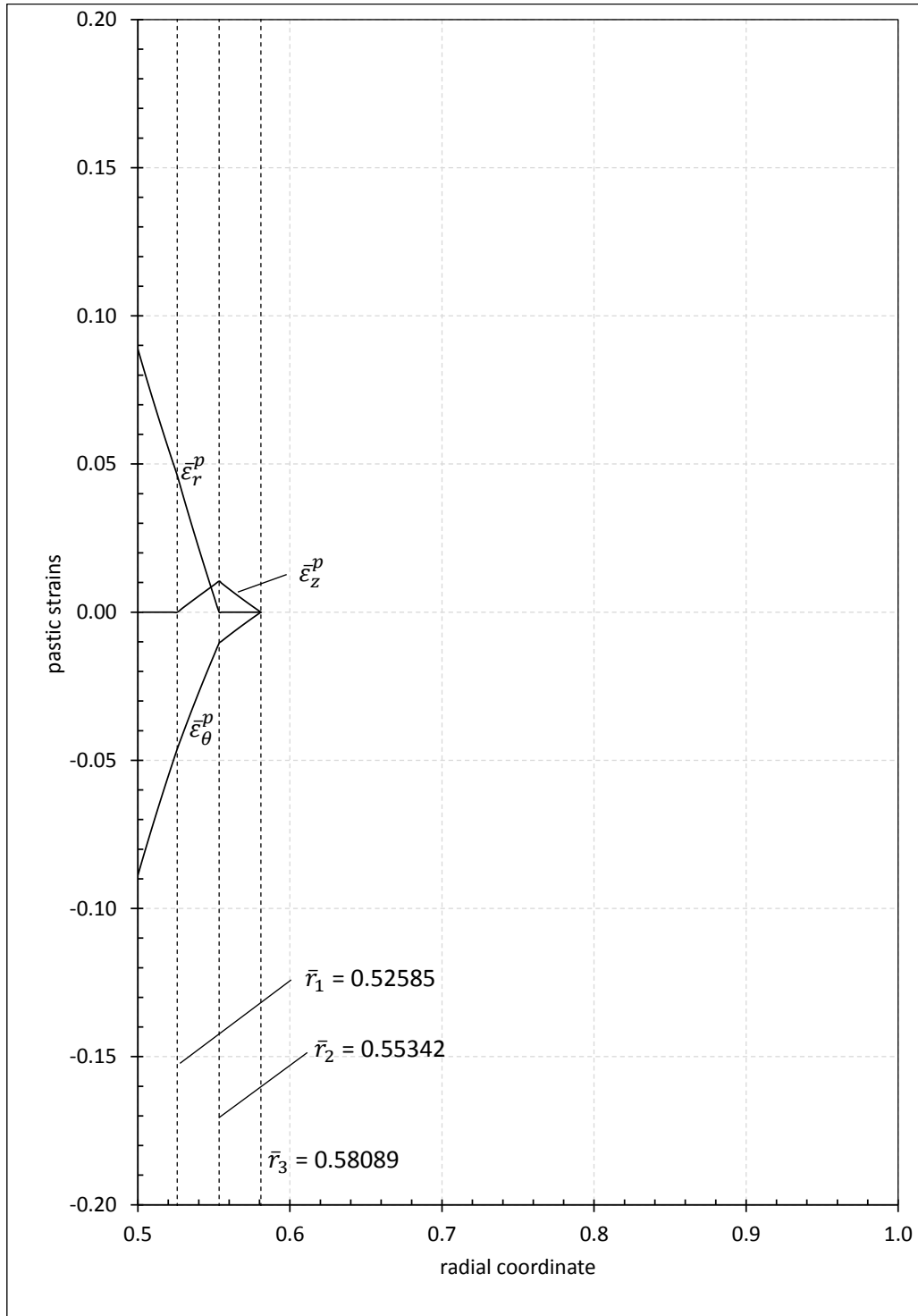


Figure 6.18: Plastic strains in elastic-plastic second stage at  $\tau = 1.05$



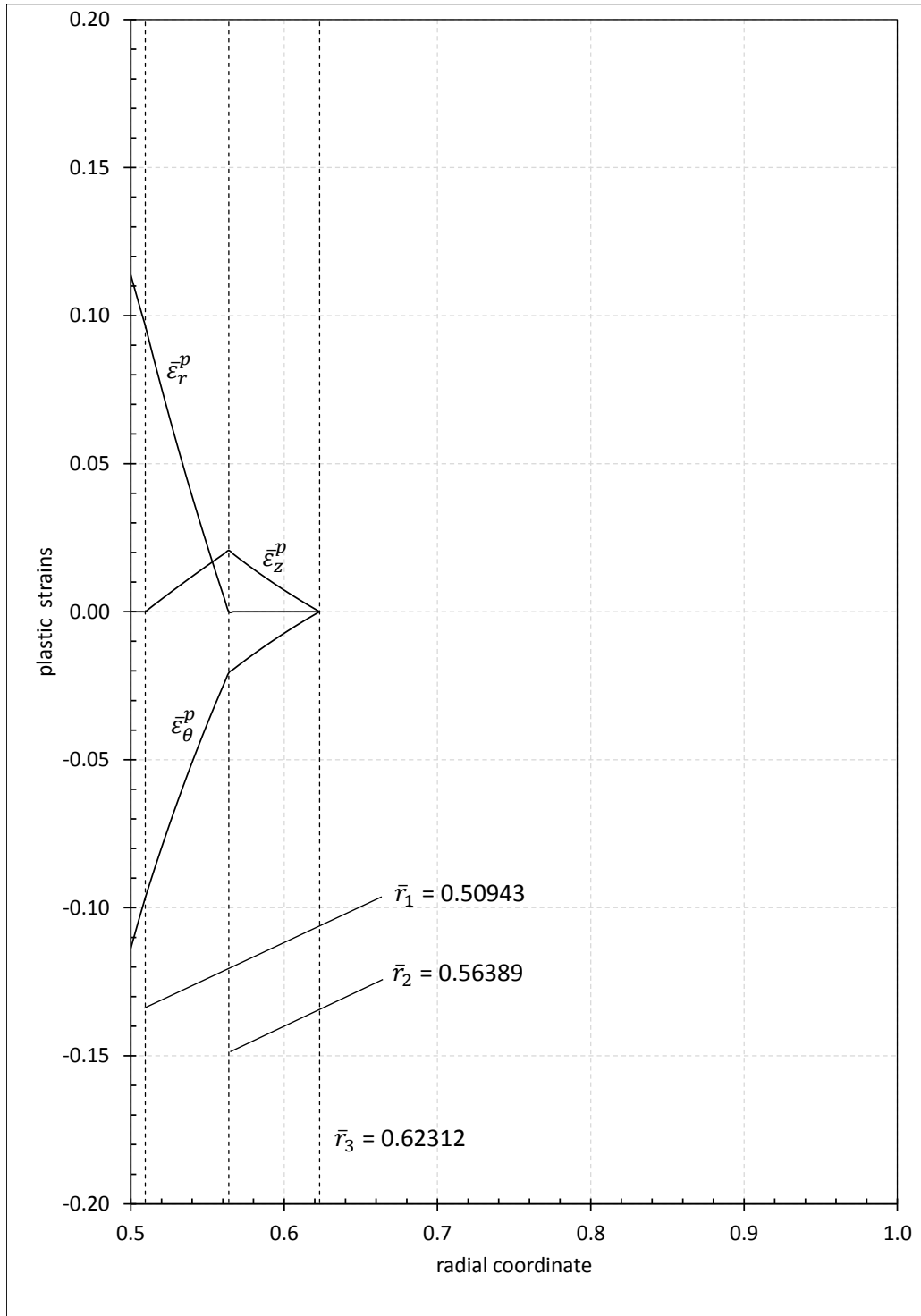


Figure 6.19: Plastic strains in elastic-plastic second stage at  $\tau = 1.1$

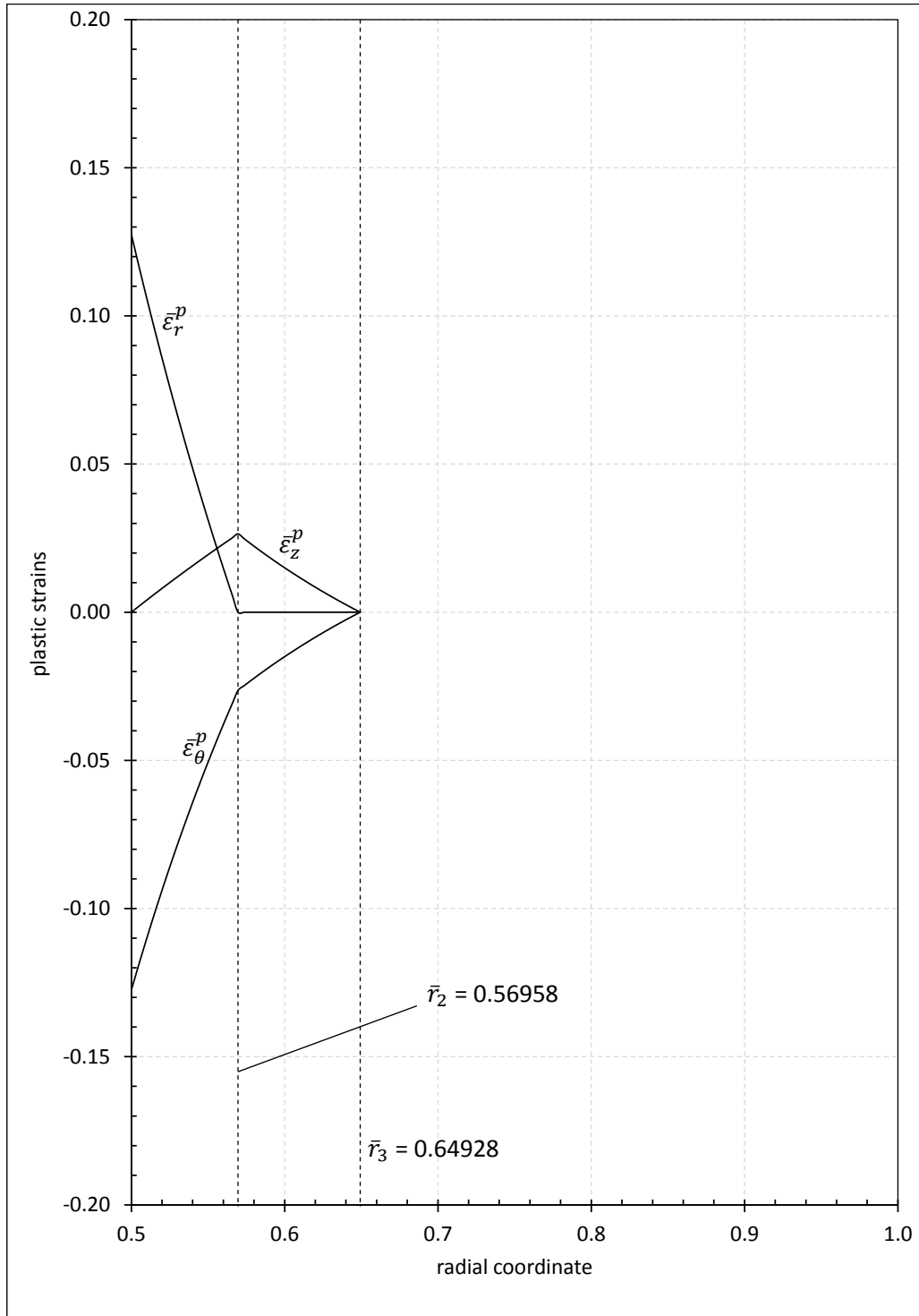


Figure 6.20: Plastic strains at the end of elastic-plastic second stage,  $\tau = 1.12757$

### 6.2.7 Elastic-Plastic Third Stage

At the end of the second stage, plastic region 2 completely covers the plastic region 1 by expanding through the inner wall. Therefore, the elastic-plastic behavior of the tube including the plastic regions 2 and 3, and an elastic region is examined at the third stage. The formulation of the plastic regions 2 and 3 are derived earlier as mentioned in the elastic-plastic second stage. However, the boundary condition at the inner surface of the tube is defined by the radial stress of the plastic region 2.

Since the plastic region 1 disappears in this stage, the total axial force is calculated by the summation of the forces of elastic region, plastic region 2 and the plastic region 3. The boundaries of  $F_z^e$  and  $F_z^{p3}$  are the same with those of in the second stage. Therefore, the axial forces derived in the second stage for the plastic region 3 and elastic region can also be used in the calculations of this stage. For the plastic region 2, it is calculated from  $a$  to  $r_2$  as

$$\begin{aligned}
 F_z^{p2} = & \frac{\beta\sigma_0}{2} \left\{ r_2^2 \int_a^{r_2} \frac{T}{r} dr - \int_a^{r_2} rT dr \right\} \\
 & + \frac{\sigma_0}{4} [r_2^2(1 - 2 \ln(r_2)) - a^2(1 - 2 \ln(a))] \\
 & + \frac{(r_2^2 - a^2)}{6(1 - 2\nu)} \{2G(2C_6 + \epsilon_0)(1 + \nu) + \sigma_0(1 - 2\nu)(1 + 3 \ln(a)) \\
 & - [6G\alpha(1 + \nu) + \beta\sigma_0(1 - 2\nu)] T(a)\} \tag{6.129}
 \end{aligned}$$

Boundary conditions for the elastic-plastic third stage are

$$\sigma_r^{p2}(a) = 0, \tag{6.130}$$

$$u_r^e(b) = 0, \tag{6.131}$$

$$\sigma_r^{p2}(r_2) = \sigma_r^{p3}(r_2), \tag{6.132}$$

$$u_r^{p2}(r_2) = u_r^{p3}(r_2), \tag{6.133}$$

$$\sigma_r^{p3}(r_2) - \sigma_\theta^{p3}(r_2) = \sigma_z^{p3}(r_2) - \sigma_\theta^{p3}(r_2) = \sigma_{th}(r_2), \tag{6.134}$$

$$\sigma_r^{p3}(r_3) = \sigma_r^e(r_3), \tag{6.135}$$

$$u_r^{p3}(r_3) = u_r^e(r_3), \tag{6.136}$$

$$\sigma_z^e(r_3) - \sigma_\theta^e(r_3) = \sigma_{th}(r_3), \tag{6.137}$$

and the total axial force is defined as

$$F_z^e + F_z^{p2} + F_z^{p3} = 0.$$

### 6.2.8 Results and Discussion for the Elastic-Plastic Third Stage

Third stage of the elastic-plastic deformation starts when the time reaches the value of  $\tau = 1.12757$  and ends at  $\tau = 1.2$ .

Integration constants and axial strain values are tabulated in Table 6.3. Using these values, stresses and displacement distribution of the tube are calculated at the different time steps for the analysis elastic-plastic behavior of the tube at this stage.

Table 6.4: Axial strain and integration constants for the elastic-plastic third stage

$\tau$	$\bar{\epsilon}_0$	$\bar{r}_2$	$\bar{r}_3$	$\bar{C}_1$	$\bar{C}_2$
1.127568	0.32547	0.56958	0.64928	-0.02043	-0.12191
1.14	0.32963	0.57211	0.66189	-0.02089	-0.12320
1.16	0.33639	0.57614	0.68337	-0.02166	-0.12526
1.18	0.34327	0.58011	0.70654	-0.02246	-0.12728
1.2	0.35028	0.58399	0.73171	-0.02329	-0.12927
$\tau$	$\bar{C}_5$	$\bar{C}_6$	$\bar{C}_7$	$\bar{C}_8$	
1.127	-0.08264	0.12245	-0.09178	0.11147	
1.14	-0.08398	0.12443	-0.09296	0.11253	
1.16	-0.08615	0.12758	-0.09487	0.11422	
1.18	-0.08833	0.13067	-0.09679	0.11589	
1.2	-0.09050	0.13369	-0.09871	0.11753	

Radial, tangential, axial stresses, and displacement distributions at several time steps of the elastic-plastic third stage are shown in Figures 6.21-6.24. The propagation of the plastic strains in the tube are depicted in Figures 6.25-6.28.

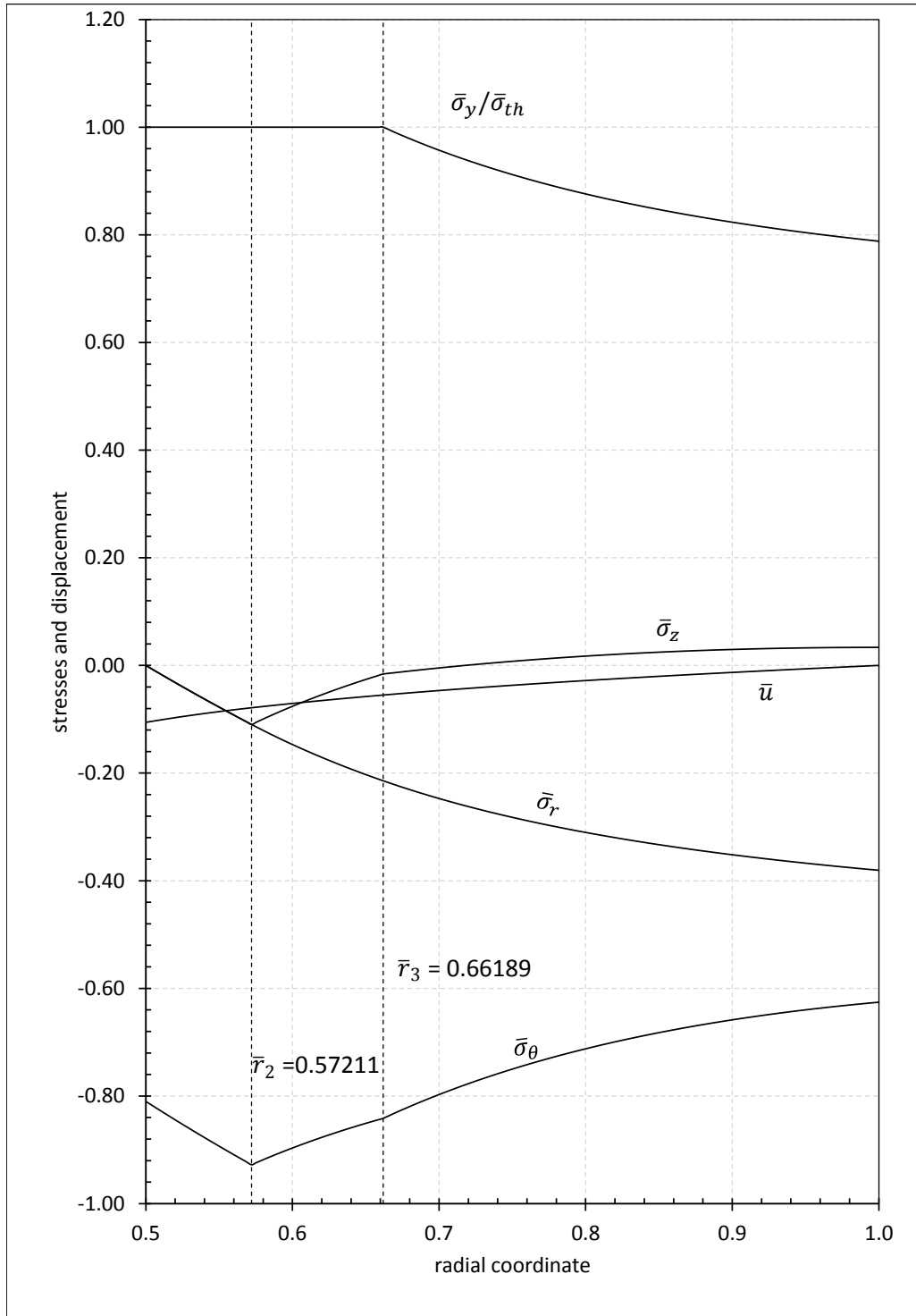


Figure 6.21: Stresses and displacement in elastic-plastic third stage at  $\tau = 1.14$

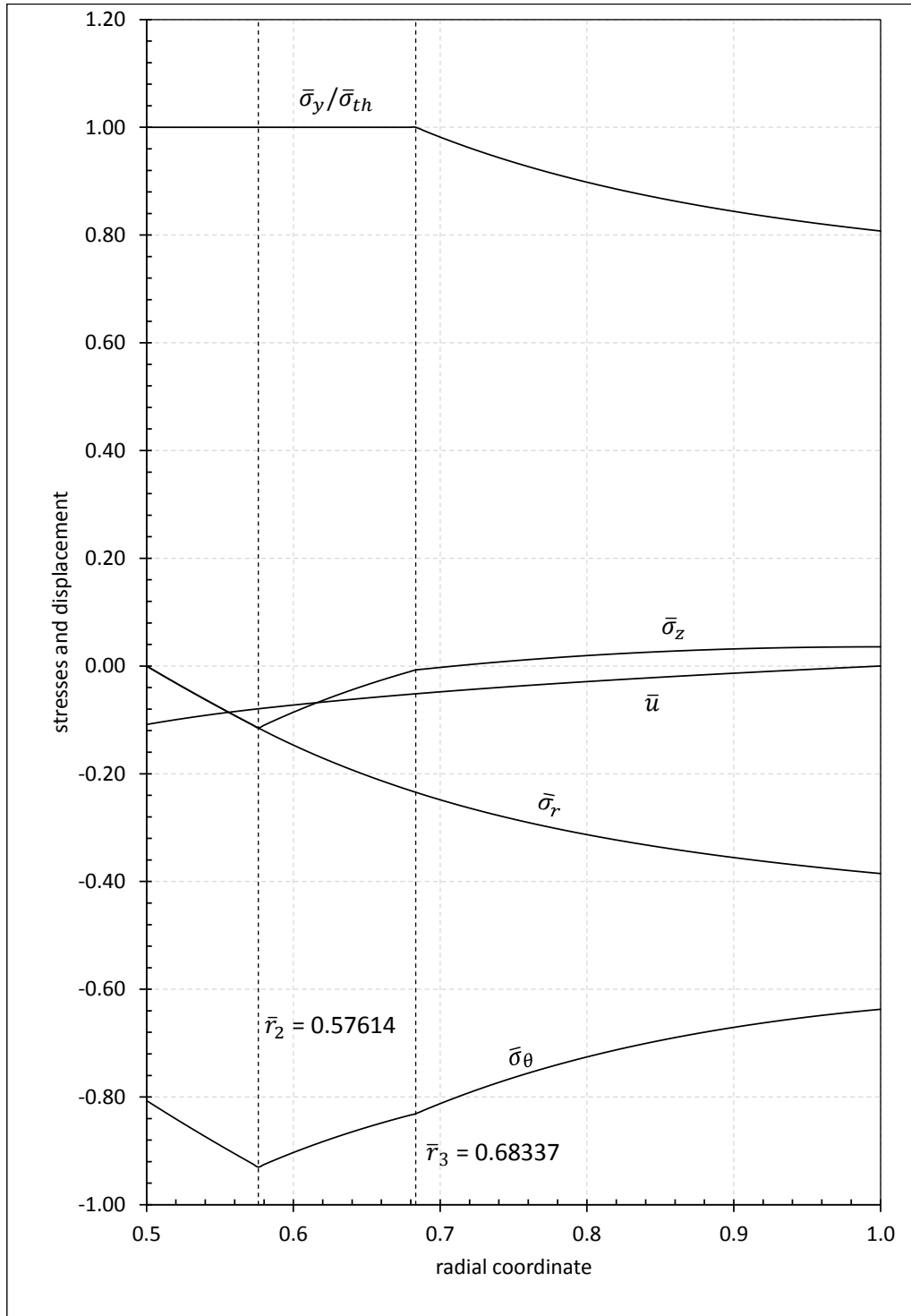


Figure 6.22: Stresses and displacement in elastic-plastic third stage at  $\tau = 1.16$

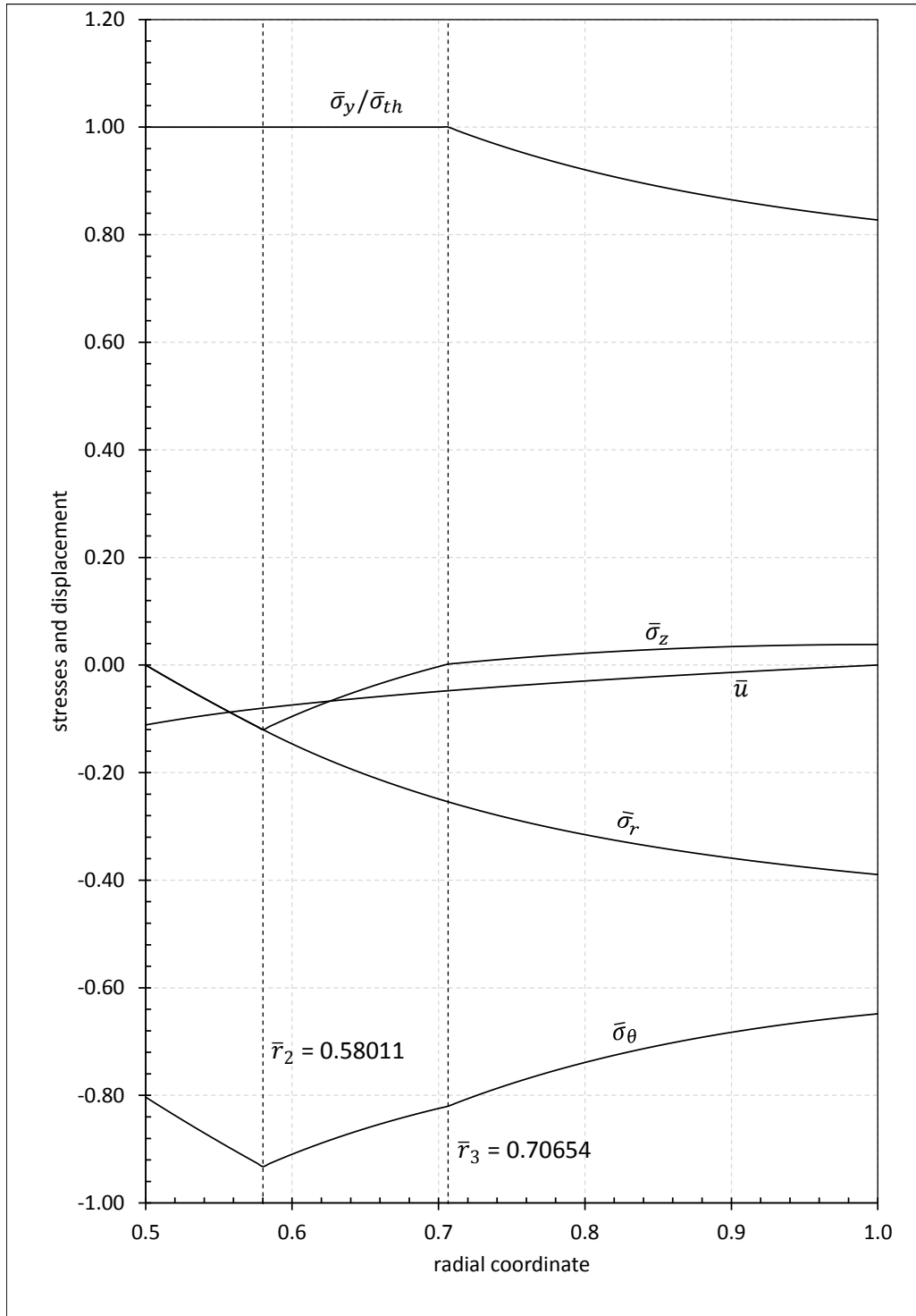


Figure 6.23: Stresses and displacement in elastic-plastic third stage at  $\tau = 1.18$

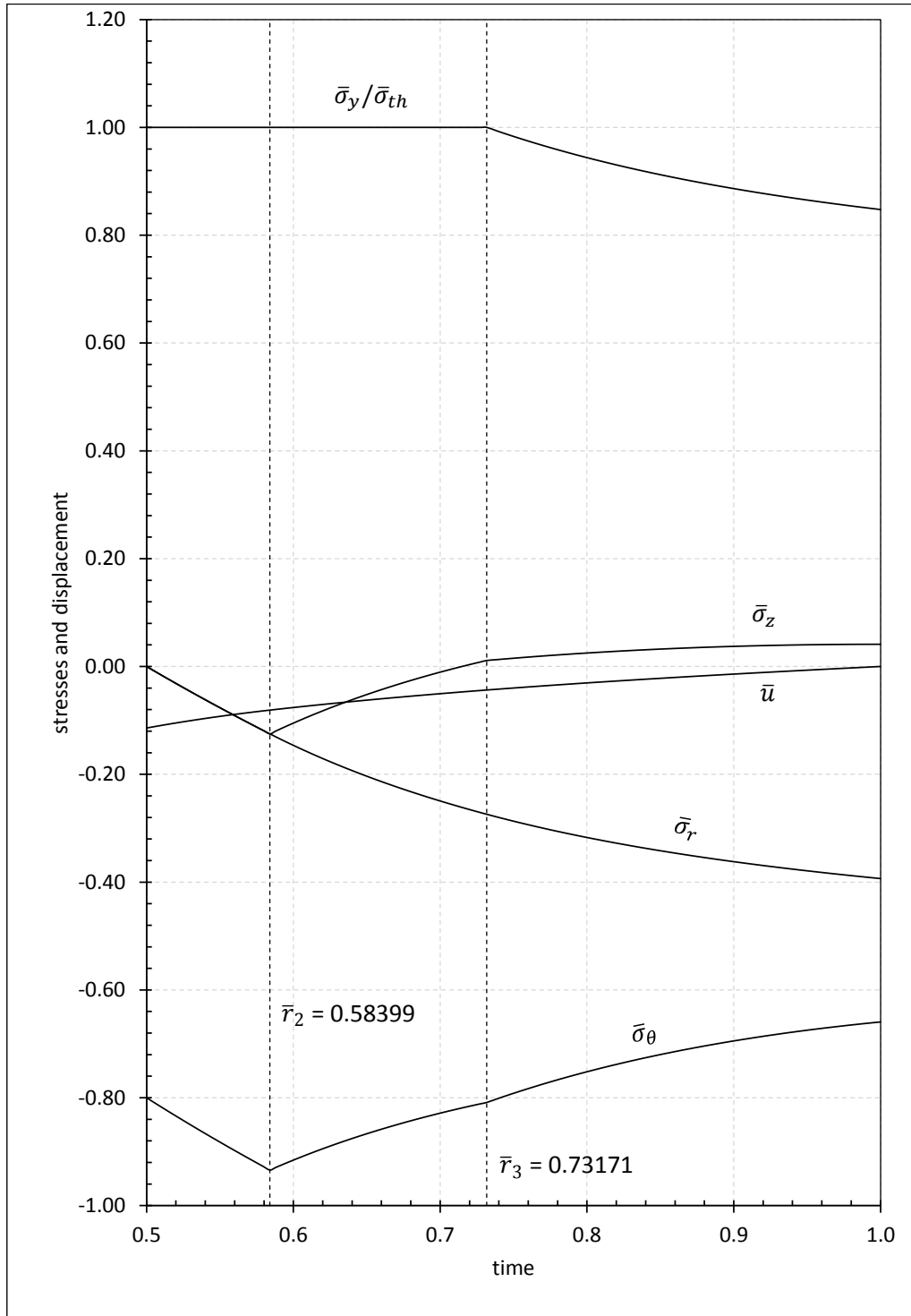


Figure 6.24: Stresses and displacement at the end of elastic-plastic third stage at,  $\tau = 1.2$



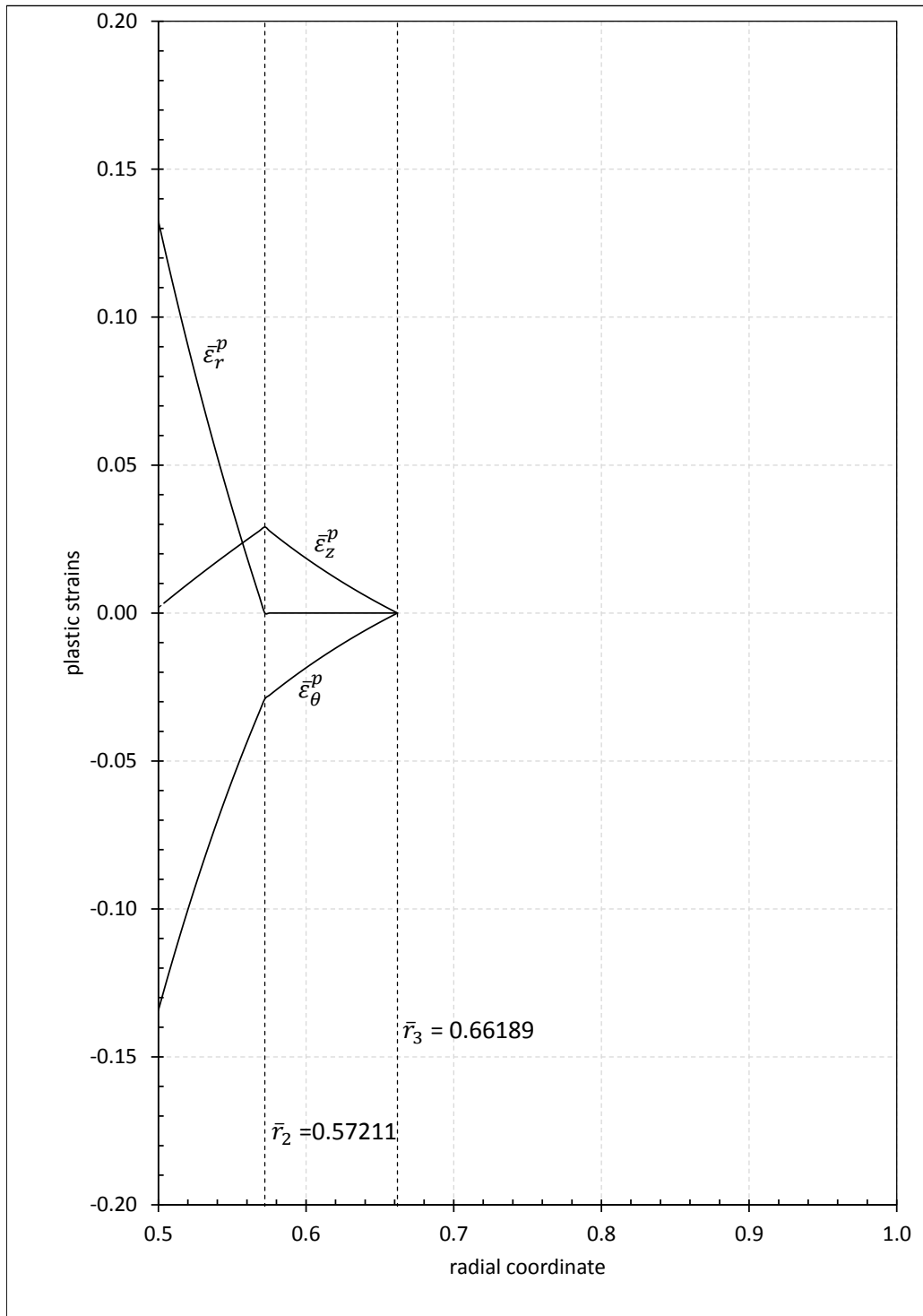


Figure 6.25: Plastic strains in elastic-plastic third stage at  $\tau = 1.14$

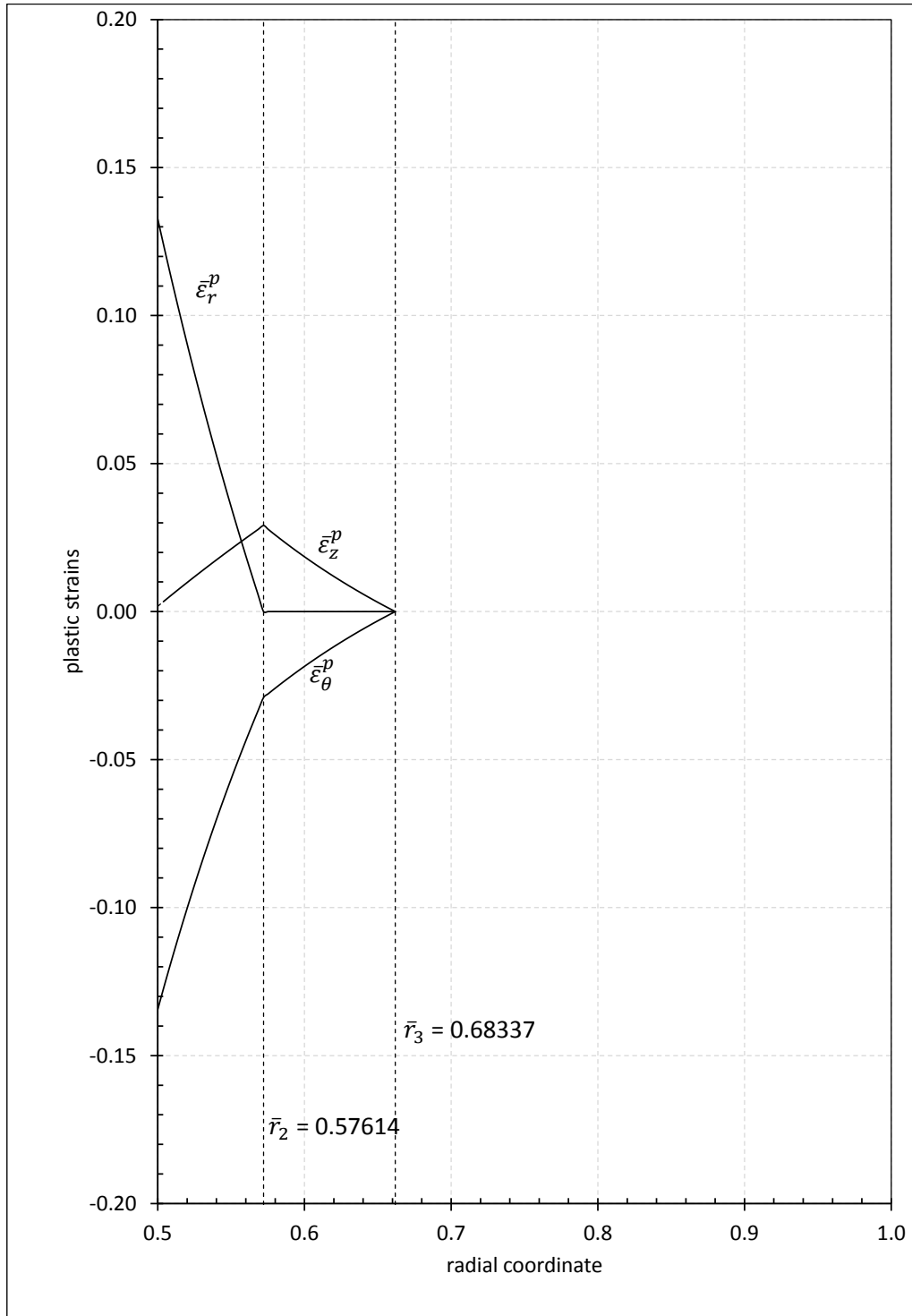


Figure 6.26: Plastic strains in elastic-plastic third stage at  $\tau = 1.16$

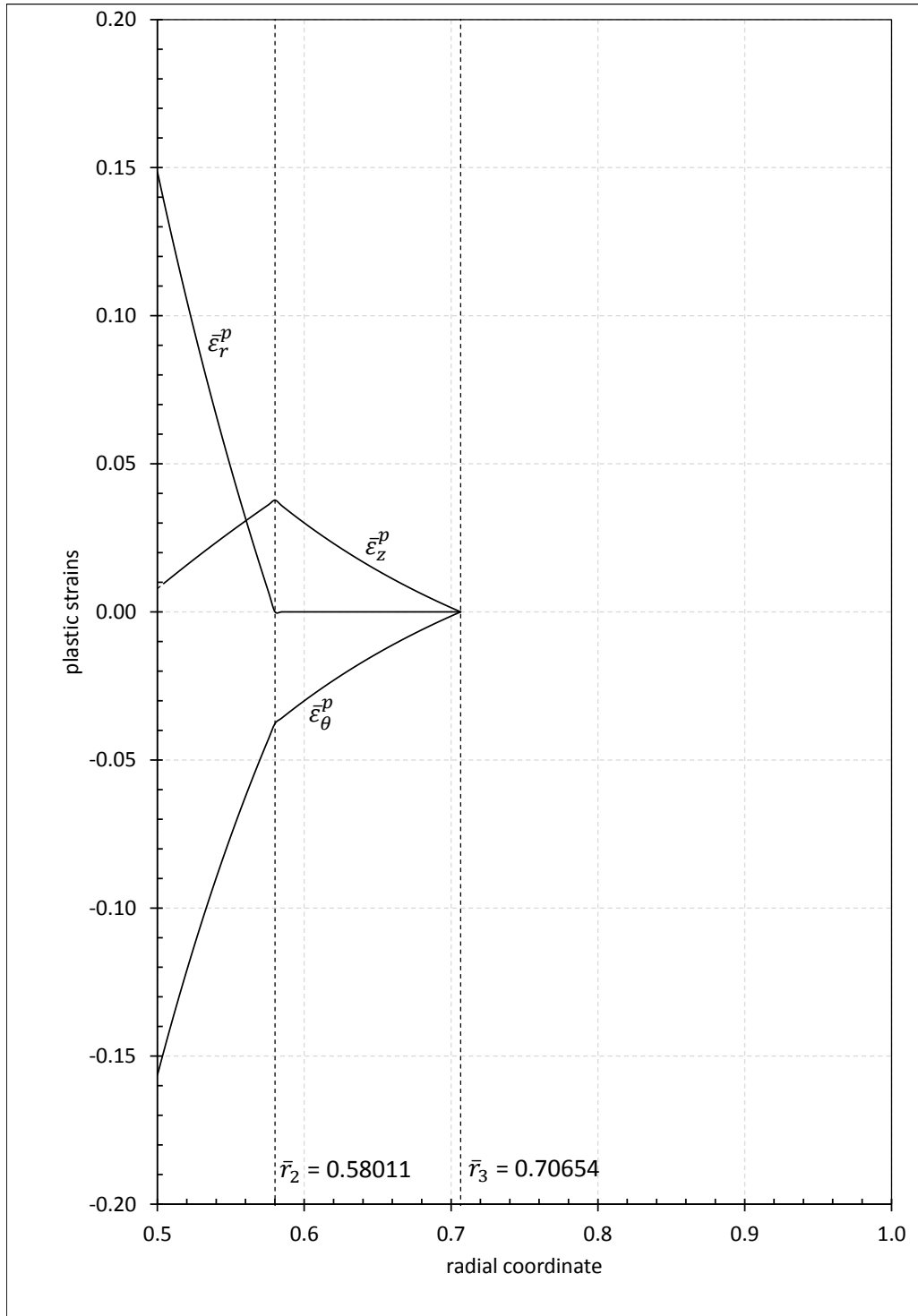


Figure 6.27: Plastic strains in elastic-plastic third stage at  $\tau = 1.18$

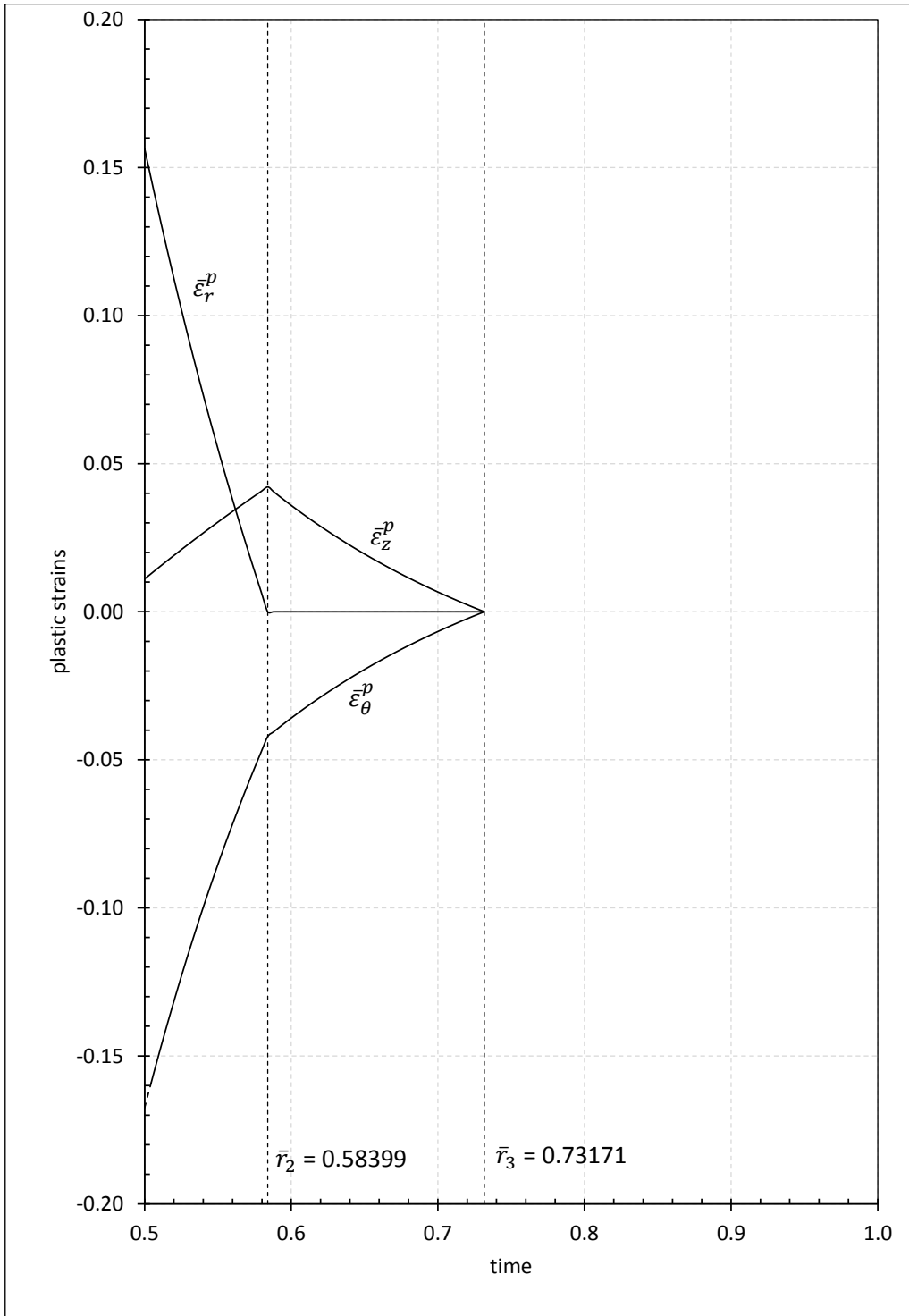


Figure 6.28: Plastic strains at the end of elastic-plastic third stage at,  $\tau = 1.2$

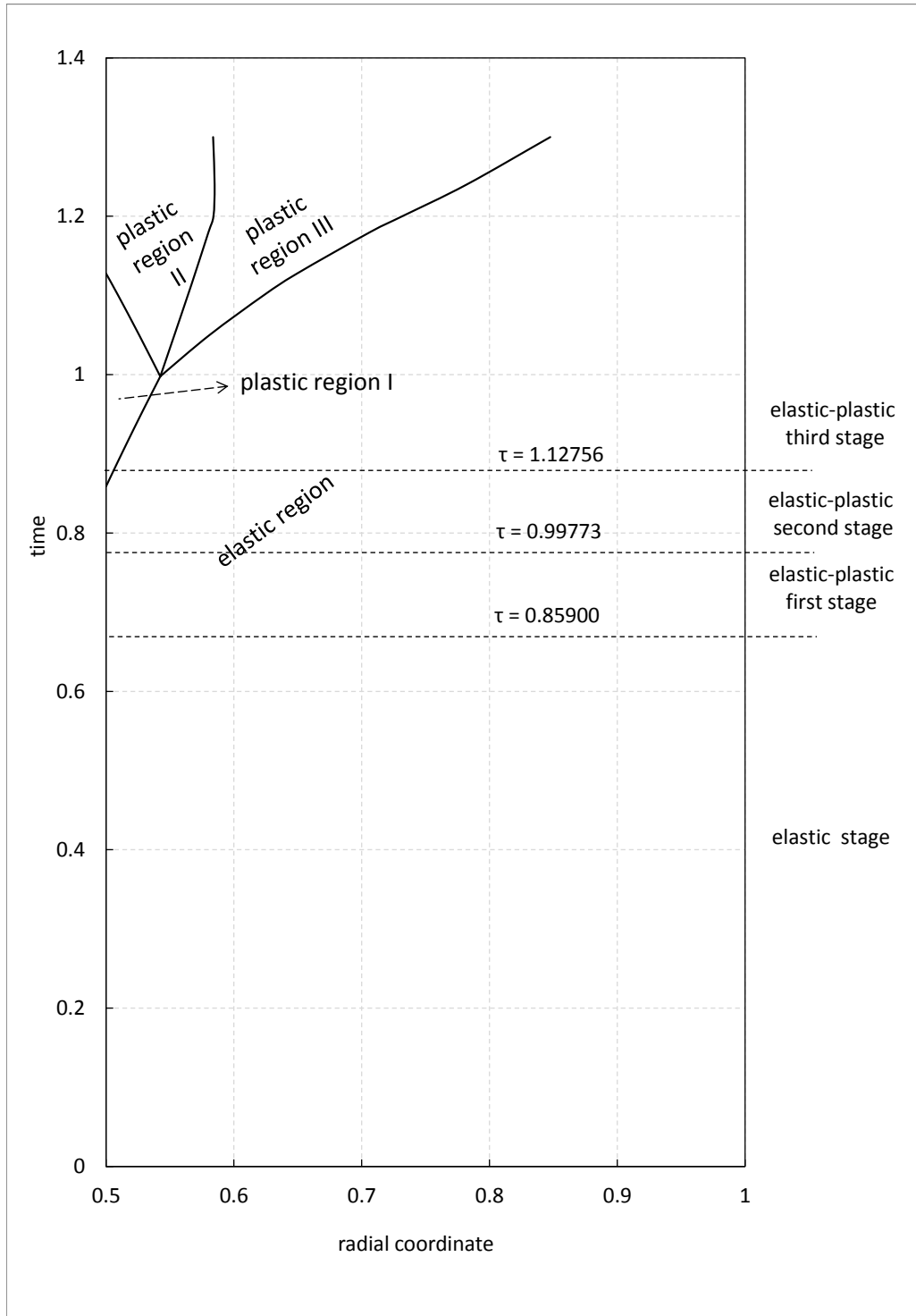


Figure 6.29: Evolution of elastic and plastic regions with respect to time.

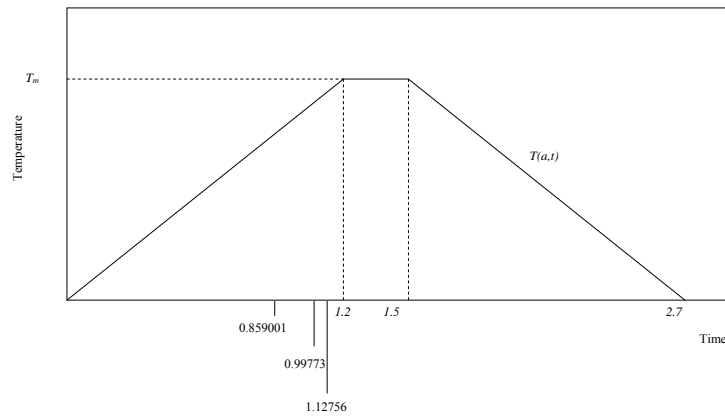


Figure 6.30: Elastic-plastic stages during temperature cycle

## CHAPTER 7

### UNLOADED STAGE

When time elapses, the expansion of the plastic regions gets slower. As seen in Fig. 6.29, the evolution of plastic region 2 through the plastic region 3 ceases at time  $\tau = 1.2$ . After that time, it turns to over the plastic region 1, it can be said that the unloading starts at this point. It is known that the plastic strains at any radial coordinate in the tube increases with the increasing temperature as a result of the plastic deformation. Hence, another point to determine the unloading point is that whether any plastic strain at any radial direction in the tube decreases or not. It may be determined by the following expression

$$\left. \frac{\partial \epsilon_i^p(r, t)}{\partial t} \right|_{t=t_u(r)} = 0. \quad (7.1)$$

It is assumed that the plastic strains at a fixed radius are frozen at the onset of the unloading and they are called as permanent plastic strain in the unloading stage. They can be expressed as

$$\epsilon_i^p(r) = \epsilon_i^{per}(r) = \epsilon_i^p[r, t_u(r)]. \quad (7.2)$$

Inversion of the Eq.(7.1) gives the interface radius,  $r_u(t)$ , between the plastic region and the unloaded region. However the calculation of this boundary is a very tedious work, it is assumed sudden unloading in the entire plastic region in the tube. Details of this assumption are given in [57].

## 7.1 Formulation of the Unloaded Region

When time elapses, the expansion of plastic regions gets slower and ceases at a time  $t = t_u$ . As a result, the borders between the plastic-plastic boundary  $r_2$  attains a stationary value at time  $\tau = 1.2$  as shown in Fig. 6.29. At that time, the radial strain ceases to increase. Therefore, in this problem, unloading starts from the inner surface of the tube and expands very rapidly to the second and third plastic region, respectively, then finally elastic region. Here, it is plausible to make a sudden unloading assumption due to the reason mentioned in [57]. Thus, the formulation of the unloaded stage can be performed as in the formulation of "elastic region", including plastic strains coming from the plastic regions 2 and 3 at time  $\tau = 1.2$ , which is the end of the elastic-plastic third stage. Therefore, keeping in mind the plastic incompressibility given by

$$\epsilon_z^{per} = -(\epsilon_r^{per} + \epsilon_\theta^{per}) \quad (7.3)$$

where the notation "per" represents *permanent*, plastic strains are taken into account as permanent in the unloaded region.

Solving Eq (3.4) for axial stress

$$\sigma_z^{per} = \nu(\sigma_r^{per} + \sigma_\theta^{per}) + 2G(1 + \nu) [\epsilon_0 + \epsilon_r^{per} + \epsilon_\theta^{per} - \alpha T].$$

Using geometric relations, and from Hooke's law, elastic stresses are written in terms of radial displacement:

$$\sigma_r^{per} = \frac{2G}{r(1 - 2\nu)} \{ \nu u + r(1 - \nu)u' - r[(1 - 2\nu)\epsilon_r^{per} - \epsilon_0\nu + (1 + \nu)\alpha T] \}, \quad (7.4)$$

$$\sigma_\theta^{per} = \frac{2G}{r(1 - 2\nu)} \{ (1 - \nu)u + r\nu u' - r[(1 - 2\nu)\epsilon_\theta^{per} - \epsilon_0\nu + (1 + \nu)\alpha T] \}. \quad (7.5)$$

Substituting the stresses into the equation of motion Eq.(3.1), the nonhomogeneous Euler equation is obtained in the radial direction as



$$r^2 \frac{d^2 u}{dr^2} + r \frac{du}{dr} - u = \frac{1 - 2\nu}{1 - \nu} r^2 \left( \frac{\epsilon_r^{per} - \epsilon_\theta^{per}}{r} + \epsilon_r^{per'} \right) - \frac{r^2 \alpha (1 + \nu)}{1 - \nu} T'. \quad (7.6)$$

Solution procedure of the elastic region is applied to obtain the general solution for the displacement for the unloaded region  $u^u$ ,

$$u^u = \frac{C_9}{r} + \frac{C_{10} r}{2} + \frac{1}{r} \left[ \frac{1 - 2\nu}{2(1 - \nu)} \left( \int_a^r \xi (\epsilon_r^{per} + \epsilon_\theta^{per}) d\xi \right. \right. \\ \left. \left. r^2 \int_a^r \frac{\epsilon_r^{per} - \epsilon_\theta^{per}}{\xi} d\xi \right) + \frac{\alpha(1 + \nu)}{(1 - \nu)} \int_a^r \xi T d\xi \right] \quad (7.7)$$

where  $C_9$  and  $C_{10}$  are integration constants.

$$\sigma_r^u = -\frac{2GC_9}{r^2} + \frac{G}{1 - 2\nu} (C_{10} + 2\nu\epsilon_0) + \frac{G}{1 - \nu} \int_a^r \frac{\epsilon_r^{per} - \epsilon_\theta^{per}}{\xi} d\xi \\ - \frac{(1 - 2\nu)G}{(1 - \nu)r^2} \int_a^r \xi (\epsilon_r^{per} + \epsilon_\theta^{per}) d\xi - \frac{2G\alpha(1 + \nu)}{(1 - \nu)r^2} \int_a^r \xi T d\xi, \quad (7.8)$$

$$\sigma_\theta^u = \frac{2GC_9}{r^2} + \frac{G}{1 - 2\nu} (C_{10} + 2\nu\epsilon_0) + \frac{G}{1 - \nu} \int_a^r \frac{\epsilon_r^{per} - \epsilon_\theta^{per}}{\xi} d\xi \\ + \frac{(1 - 2\nu)G}{(1 - \nu)r^2} \int_a^r \xi (\epsilon_r^{per} + \epsilon_\theta^{per}) d\xi \\ + \frac{2G\nu}{1 - \nu} \epsilon_r^{per} + 2G\epsilon_\theta^{per} + \frac{2G\alpha(1 + \nu)}{(1 - \nu)r^2} \left[ \int_a^r \xi T d\xi - r^2 T(r, t) \right], \quad (7.9)$$

$$\sigma_z^u = \frac{2G}{1 - 2\nu} (\nu C_{10} + (1 - \nu)\epsilon_0) + \frac{2G\nu}{1 - \nu} \int_a^r \frac{\epsilon_r^{per} - \epsilon_\theta^{per}}{\xi} d\xi \\ + \frac{2G}{1 - \nu} \epsilon_r^{per} + 2G\epsilon_\theta^{per} - \frac{2G\alpha(1 + \nu)}{(1 - \nu)} T. \quad (7.10)$$

Axial force is calculated as

$$F_z^{per} = \frac{G(b^2 - a^2)}{1 - 2\nu} [(1 - \nu)\epsilon_0 + 2\nu C_{10}] + \frac{b^2\nu}{2(1 - 2\nu)} \int_a^b \frac{\epsilon_r^{per} - \epsilon_\theta^{per}}{r} dr$$

$$\frac{2 - \nu}{2(1 - \nu)} \int_a^b r (\epsilon_r^{per} + \epsilon_\theta^{per}) dr - \frac{2G\alpha(1 + \nu)}{(1 - \nu)} \int_a^b r T dr - \quad (7.11)$$

In these equations  $C_9$ ,  $C_{10}$ , and  $\epsilon_0$  are the unknowns to be calculated. Boundary conditions for this stage are;

$$\sigma_r^{per} = 0, \quad \text{at } r = a, \quad (7.12)$$

$$u^{per} = 0, \quad \text{at } r = b, \quad (7.13)$$

$$F_z^{per} = 2\pi \int_a^b r \sigma_z dr = 0. \quad (7.14)$$

Hence, the integration constants are obtained by means of the boundary conditions as

$$C_9 = \frac{a^2}{2(a^2 - b^2)(1 - \nu)(b^2(1 - \nu) + a^2(1 + \nu))}$$

$$\times \left\{ b^2 [-b^2(1 - \nu) + a^2(1 + \nu)(1 - 2\nu)] \int_a^b \frac{\epsilon_r^{per} - \epsilon_\theta^{per}}{r} dr \right.$$

$$- b^2 [b^2(1 + (3 - 4\nu)\nu) - a^2(1 + \nu)(1 - 2\nu)] \int_a^b r (\epsilon_r^{per} + \epsilon_\theta^{per}) dr$$

$$\left. - 2\alpha(1 + \nu) [b^2(1 - \nu) - a^2(1 + \nu)] \int_a^b r T dr \right\}, \quad (7.15)$$

$$C_{10} = -\frac{b^2}{2(a^2 - b^2)(1 - \nu)(b^2(1 - \nu) + a^2(1 + \nu))}$$

$$\times \left\{ b^2 [a^2(1 - \nu(3 - 4\nu)) - b^2(1 - (3 - 2\nu)\nu)] \int_a^b \frac{\epsilon_r^{per} - \epsilon_\theta^{per}}{r} dr \right.$$

$$+ [a^2(1 + \nu) - b^2(1 - (3 - 2\nu)\nu)] \int_a^b r (\epsilon_r^{per} + \epsilon_\theta^{per}) dr$$

$$\left. + 2\alpha [a^2(1 - 3\nu) - b^2(1 - \nu)] \int_a^b r T dr \right\}, \quad (7.16)$$

$$\begin{aligned}
\epsilon_0 = & \frac{2}{a^4 - b^4 + (a^2 - b^2)^2\nu} \left\{ a^2 b^2 \nu \int_a^b \frac{\epsilon_r^{per} - \epsilon_\theta^{per}}{r} dr \right. \\
& + [b^2(1 - 2\nu) + a^2(1 + \nu)] \int_a^b r (\epsilon_r^{per} + \epsilon_\theta^{per}) dr \\
& \left. - (a^2 + b^2)(1 + \nu)\alpha \int_a^b r T dr \right\}. \tag{7.17}
\end{aligned}$$

The problem is solved for the nondimensional and normalized variables using the previously defined dimensionless and normalized variables:

$$\begin{aligned}
\bar{u}^u = & \frac{C_9}{\bar{r}} + \frac{C_{10}\bar{r}}{2} + \frac{1}{\bar{r}} \left[ \frac{1 - 2\nu}{2(1 - \nu)} \left( \int_{\bar{a}}^{\bar{r}} \xi (\bar{\epsilon}_r^{per} + \bar{\epsilon}_\theta^{per}) d\xi \right. \right. \\
& \left. \left. \bar{r}^2 \int_{\bar{a}}^{\bar{r}} \frac{\bar{\epsilon}_r^{per} - \bar{\epsilon}_\theta^{per}}{\xi} d\xi \right) + \frac{q(1 + \nu)}{(1 - \nu)} \int_{\bar{a}}^{\bar{r}} \xi \bar{T} d\xi \right] \tag{7.18}
\end{aligned}$$

where  $C_9$  and  $C_{10}$  are integration constants.

$$\begin{aligned}
\bar{\sigma}_r^u = & -\frac{2\bar{C}_9}{\bar{r}^2} + \frac{1}{1 - 2\nu}(\bar{C}_{10} + 2\nu\bar{\epsilon}_0) + \frac{1}{1 - \nu} \int_{\bar{a}}^{\bar{r}} \frac{\bar{\epsilon}_r^{per} - \bar{\epsilon}_\theta^{per}}{\xi} d\xi \\
& - \frac{(1 - 2\nu)}{(1 - \nu)\bar{r}^2} \int_{\bar{a}}^{\bar{r}} \xi (\bar{\epsilon}_r^{per} + \bar{\epsilon}_\theta^{per}) d\xi - \frac{2q(1 + \nu)}{(1 - \nu)\bar{r}^2} \int_{\bar{a}}^{\bar{r}} \xi \bar{T} d\xi, \tag{7.19}
\end{aligned}$$

$$\begin{aligned}
\bar{\sigma}_\theta^u = & \frac{2\bar{C}_9}{\bar{r}^2} + \frac{\bar{C}_{10} + 2\nu\bar{\epsilon}_0}{1 - 2\nu} + \frac{1}{1 - \nu} \int_{\bar{a}}^{\bar{r}} \frac{\bar{\epsilon}_r^{per} - \bar{\epsilon}_\theta^{per}}{\xi} d\xi \\
& + \frac{(1 - 2\nu)}{(1 - \nu)\bar{r}^2} \int_{\bar{a}}^{\bar{r}} \xi (\bar{\epsilon}_r^{per} + \bar{\epsilon}_\theta^{per}) d\xi \\
& + \frac{2\nu}{1 - \nu} \bar{\epsilon}_r^{per} + 2\bar{\epsilon}_\theta^{per} + \frac{2q(1 + \nu)}{(1 - \nu)\bar{r}^2} \left[ \int_{\bar{a}}^{\bar{r}} \xi T(\xi, t) d\xi - \bar{r}^2 \bar{T} \right], \tag{7.20}
\end{aligned}$$

$$\begin{aligned}
\bar{\sigma}_z^u = & \frac{2}{1 - 2\nu}(\nu\bar{C}_{10} + (1 - \nu)\bar{\epsilon}_0) + \frac{2\nu}{1 - \nu} \int_{\bar{a}}^{\bar{r}} \frac{\bar{\epsilon}_r^{per} - \bar{\epsilon}_\theta^{per}}{\xi} d\xi \\
& + \frac{2}{1 - \nu} \bar{\epsilon}_r^{per} + 2\bar{\epsilon}_\theta^{per} - \frac{2q(1 + \nu)}{(1 - \nu)} \bar{T}. \tag{7.21}
\end{aligned}$$

$$\begin{aligned}
\bar{C}_9 = & \frac{\bar{a}^2}{2(\bar{a}^2 - 1)(1 - \nu)((1 - \nu) + \bar{a}^2(1 + \nu))} \\
& \times \left\{ [-(1 - \nu) + \bar{a}^2(1 + \nu)(1 - 2\nu)] \int_{\bar{a}}^1 \frac{\bar{\epsilon}_r^{per} - \bar{\epsilon}_\theta^{per}}{\bar{r}} d\bar{r} \right. \\
& - [(1 + (3 - 4\nu)\nu) - \bar{a}^2(1 + \nu)(1 - 2\nu)] \int_{\bar{a}}^1 \bar{r} (\bar{\epsilon}_r^{per} + \bar{\epsilon}_\theta^{per}) d\bar{r} \\
& \left. - 2q(1 + \nu) [(1 - \nu) - \bar{a}^2(1 + \nu)] \int_{\bar{a}}^1 \bar{r} \bar{T} d\bar{r} \right\}, \tag{7.22}
\end{aligned}$$

$$\begin{aligned}
\bar{C}_{10} = & -\frac{1}{2(\bar{a}^2 - 1)(1 - \nu)((1 - \nu) + \bar{a}^2(1 + \nu))} \\
& \times \left\{ [\bar{a}^2(1 - \nu(3 - 4\nu)) - (1 - (3 - 2\nu)\nu)] \int_{\bar{a}}^1 \frac{\bar{\epsilon}_r^{per} - \bar{\epsilon}_\theta^{per}}{\bar{r}} d\bar{r} \right. \\
& + [\bar{a}^2(1 + \nu) - (1 - (3 - 2\nu)\nu)] \int_{\bar{a}}^1 \bar{r} (\bar{\epsilon}_r^{per} + \bar{\epsilon}_\theta^{per}) d\bar{r} \\
& \left. + 2q [\bar{a}^2(1 - 3\nu) - (1 - \nu)] \int_{\bar{a}}^1 \bar{r} \bar{T} d\bar{r} \right\}, \tag{7.23}
\end{aligned}$$

$$\begin{aligned}
\bar{\epsilon}_0 = & \frac{2}{\bar{a}^4 - 1 + (\bar{a}^2 - 1)^2\nu} \left\{ \bar{a}^2\nu \int_{\bar{a}}^1 \frac{\bar{\epsilon}_r^{per} - \bar{\epsilon}_\theta^{per}}{\bar{r}} d\bar{r} \right. \\
& + [(1 - 2\nu) + \bar{a}^2(1 + \nu)] \int_{\bar{a}}^1 \bar{r} (\bar{\epsilon}_r^{per} + \bar{\epsilon}_\theta^{per}) d\bar{r} \\
& \left. - (\bar{a}^2 + 1)(1 + \nu)q \int_{\bar{a}}^1 \bar{r} \bar{T} d\bar{r} \right\}. \tag{7.24}
\end{aligned}$$

## 7.2 Results and Discussion for the Unloaded Stage

At the end of the elastic-plastic deformation stages of the tube, at time  $tau = 1.2$ , unloading starts. In the computations, integrals related to the permanent plastic strains are handled by numerical integration methods [60].

Data for permanent strains collected from the third stage of the elastic-plastic deformation at  $tau = 1.2$  appear in App. A. In this data set, the plastic strains between  $\bar{a} \leq \bar{r} \leq 0.58399$  are data of plastic region 2 and between  $0.58399 \leq \bar{r} \leq 0.73171$  are plastic strains of plastic region 3 obtained from the elastic-plastic third stage. Using

Table 7.1: Axial strain and integration constants for the unloaded stage

$\tau$	$\bar{\epsilon}_0$	$\bar{C}_9$	$\bar{C}_{10}$
1.2	0.35028	-0.02240	-0.27742
1.3	0.37047	-0.02351	-0.29279
1.4	0.37996	-0.02403	-0.30001
1.5	0.38448	-0.02428	-0.30346
1.7	0.35257	-0.02250	-0.27917
1.9	0.29519	-0.01940	-0.23550
2.1	0.23209	-0.01590	-0.18747
2.3	0.16769	-0.01240	-0.13846
2.5	0.10299	-0.00883	-0.08920
2.7	0.03820	-0.00528	-0.03990

these data, the stress distributions in the tube are obtained to the end of the temperature cycle. The unknowns constants and the axial strain values are tabulated in table 7.1.

Figures 7.1-7.10 show the distribution of radial, tangential, axial stresses, and displacement. Fig. 7.11 shows that the ratio of equivalent stress to yield stress between  $\tau = 1.2$  and  $\tau = 2.7$ . As shown in this figure, because the Tresca equivalent stress exceeds the temperature dependent yield stress, the assumption is violated between the time interval  $1.2 \leq \tau \leq 1.5$ , however the difference between the equivalent stress and the yield stress, and the Tresca condition is more strict than that of the real case, the small error is expected due to this assumption.

As a result of the all calculations, the evolution of elastic, elastic-plastic and unloaded stages are depicted in Fig. 7.12. This figure is also a summary of the entire investigation of the tube. As seen in this figure, the elastic stage ends at  $\tau = 0.859001$ . This time is the onset of the plastic deformation. The tube experiences three stages in the elastic-plastic deformation. The first stage of the elastic-plastic deformation occurs between  $0.859001 \leq \tau \leq 0.99773$ , the second stage is between  $0.99773 \leq \tau \leq 1.12756$ , and third stage is between  $1.12756 \leq \tau \leq 1.2$ . After elastic-plastic deformation, at time  $\tau = 1.2$ , the unloading occurs. Finally, entire cycle is completed at  $\tau = 2.7$ .

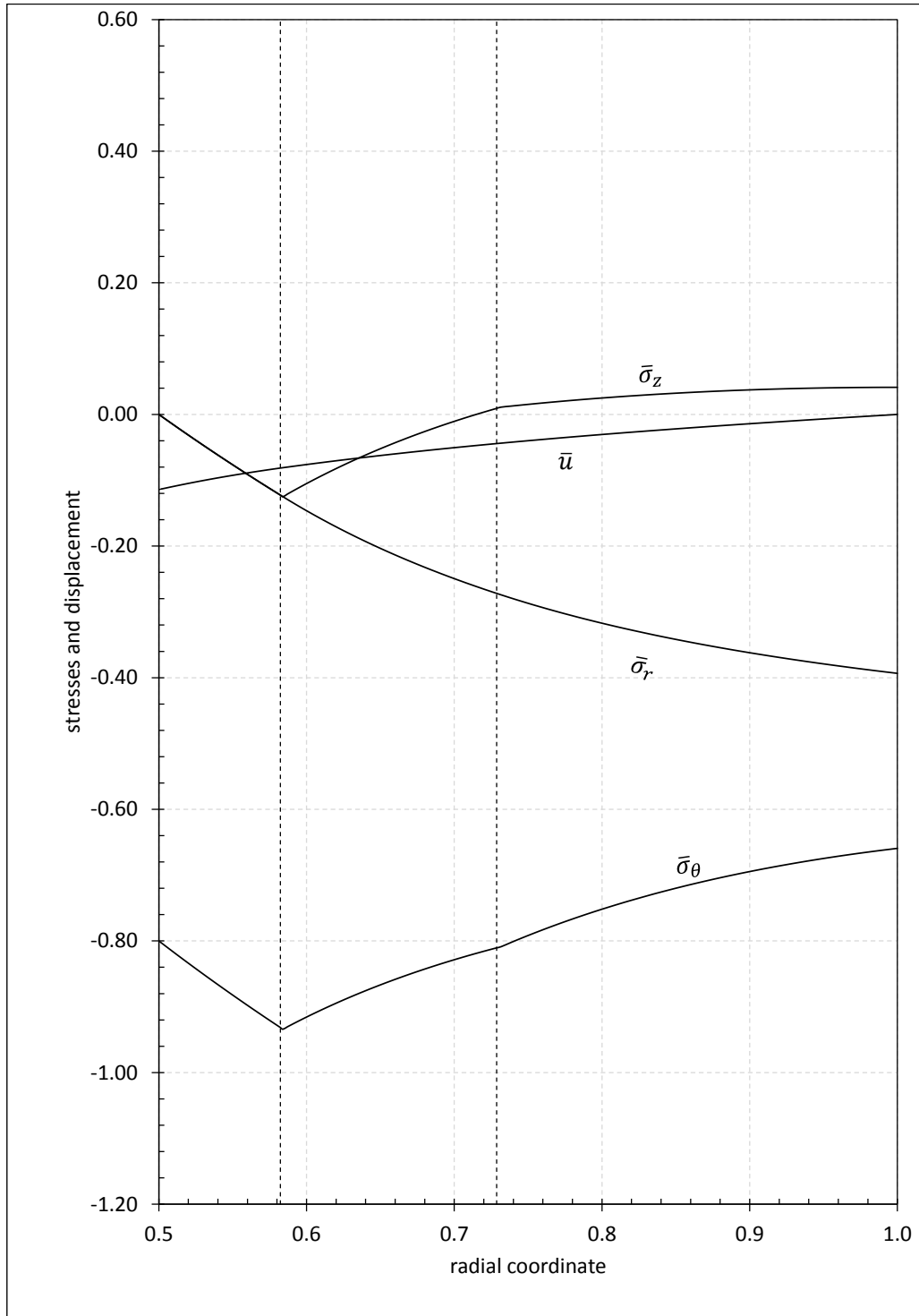


Figure 7.1: Stresses and displacement in unloaded stage at  $\tau = 1.2$

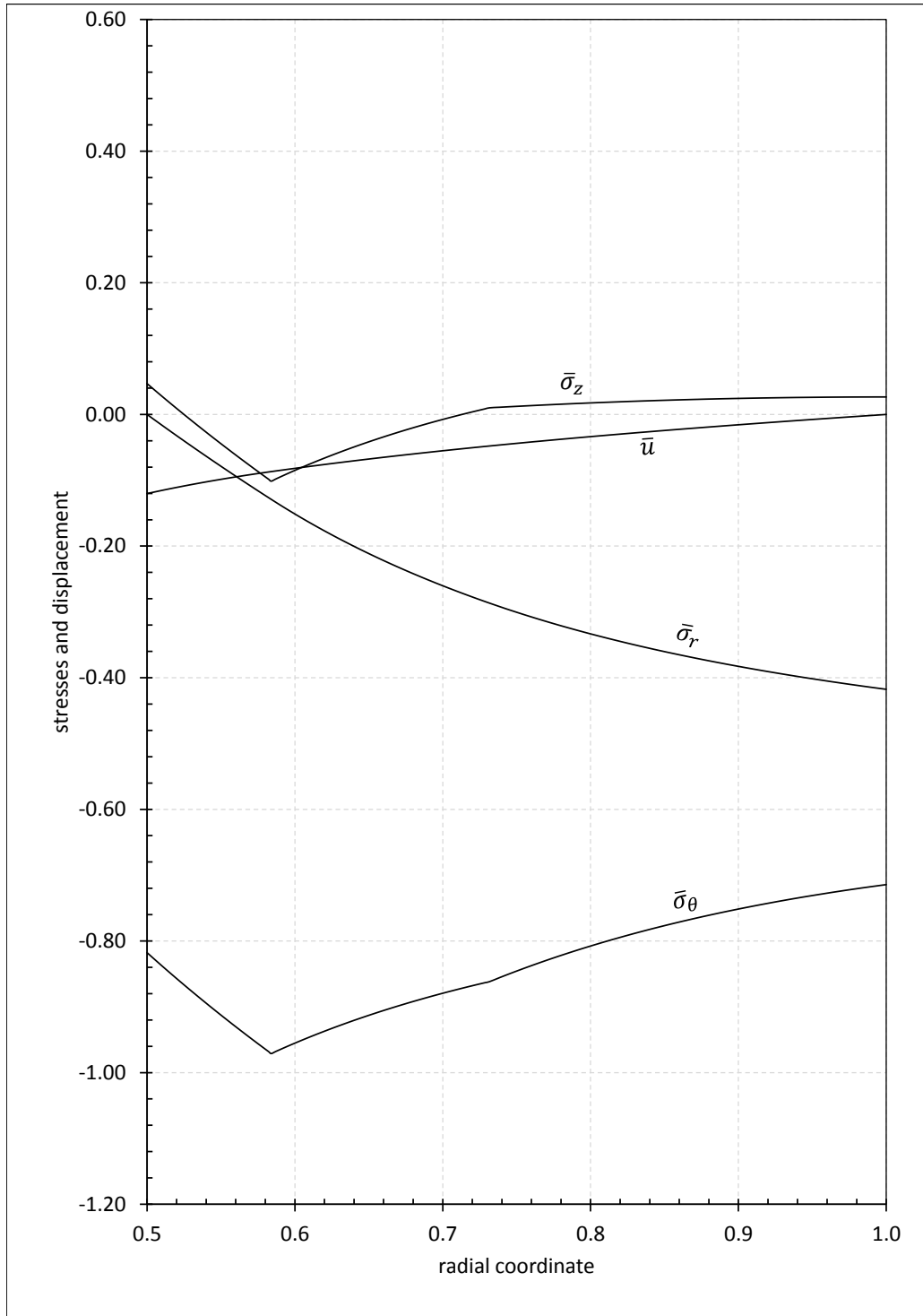


Figure 7.2: Stresses and displacement in unloaded stage at  $\tau = 1.3$

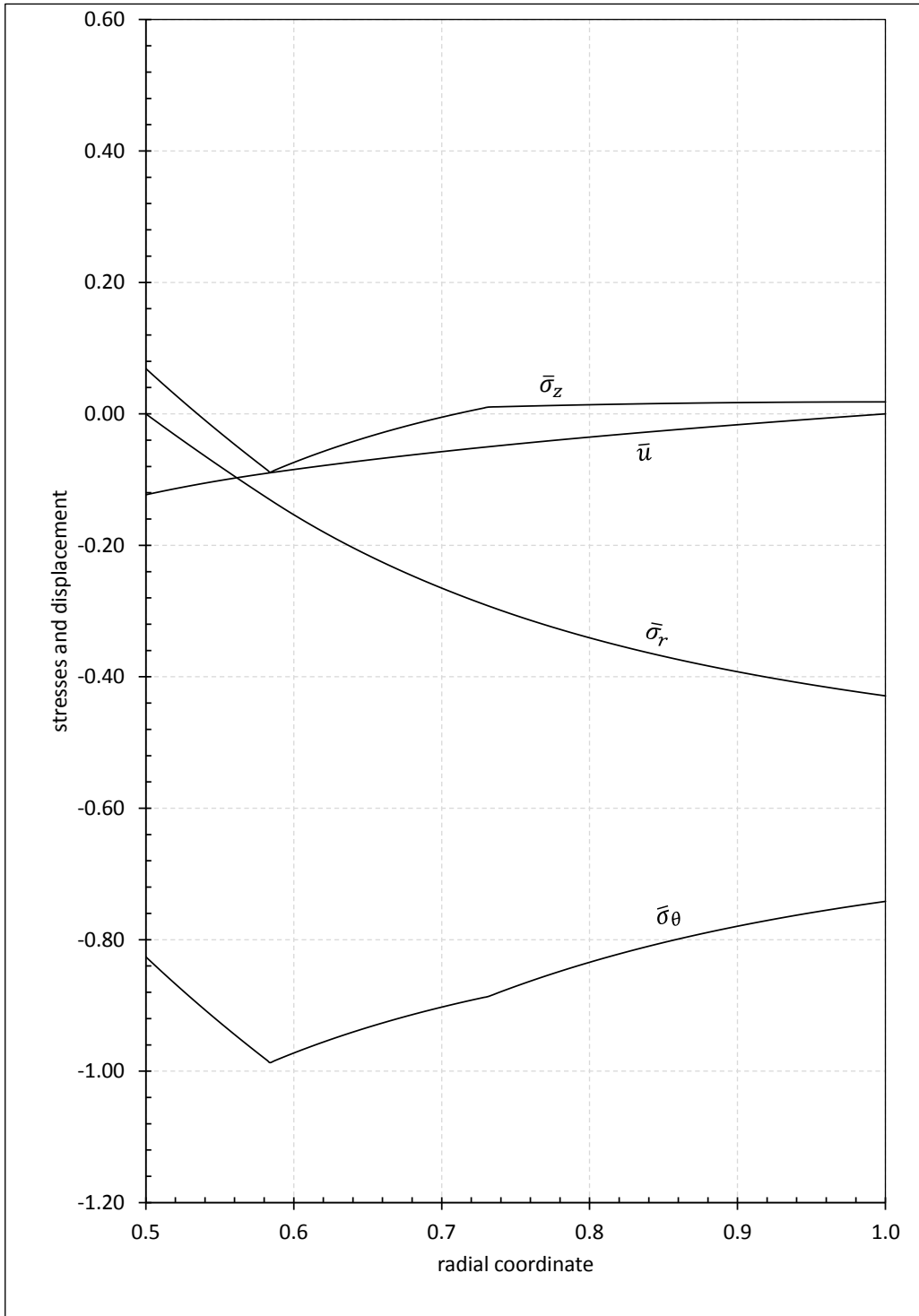


Figure 7.3: Stresses and displacement in unloaded stage at  $\tau = 1.4$



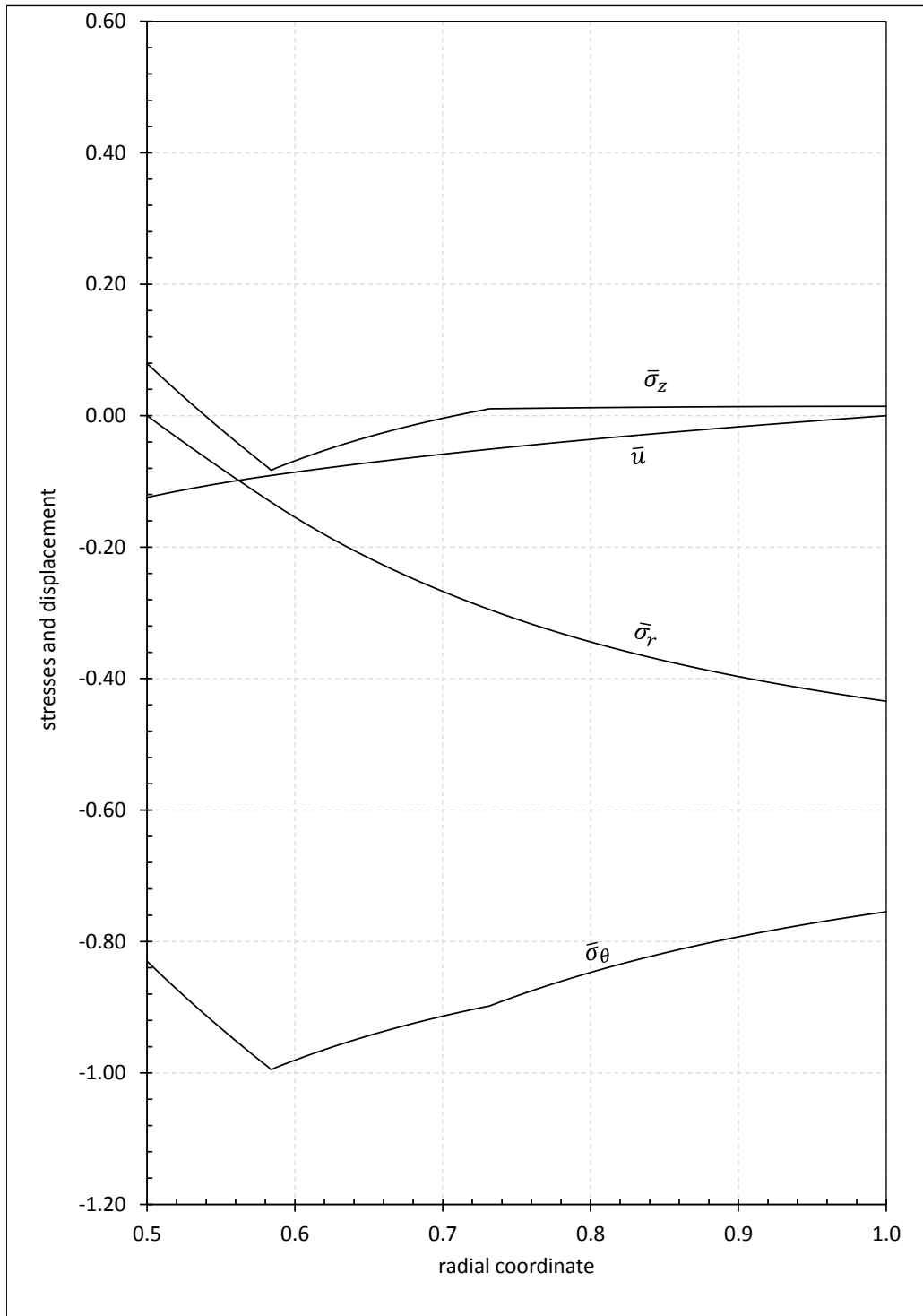


Figure 7.4: Stresses and displacement in unloaded stage at  $\tau = 1.5$

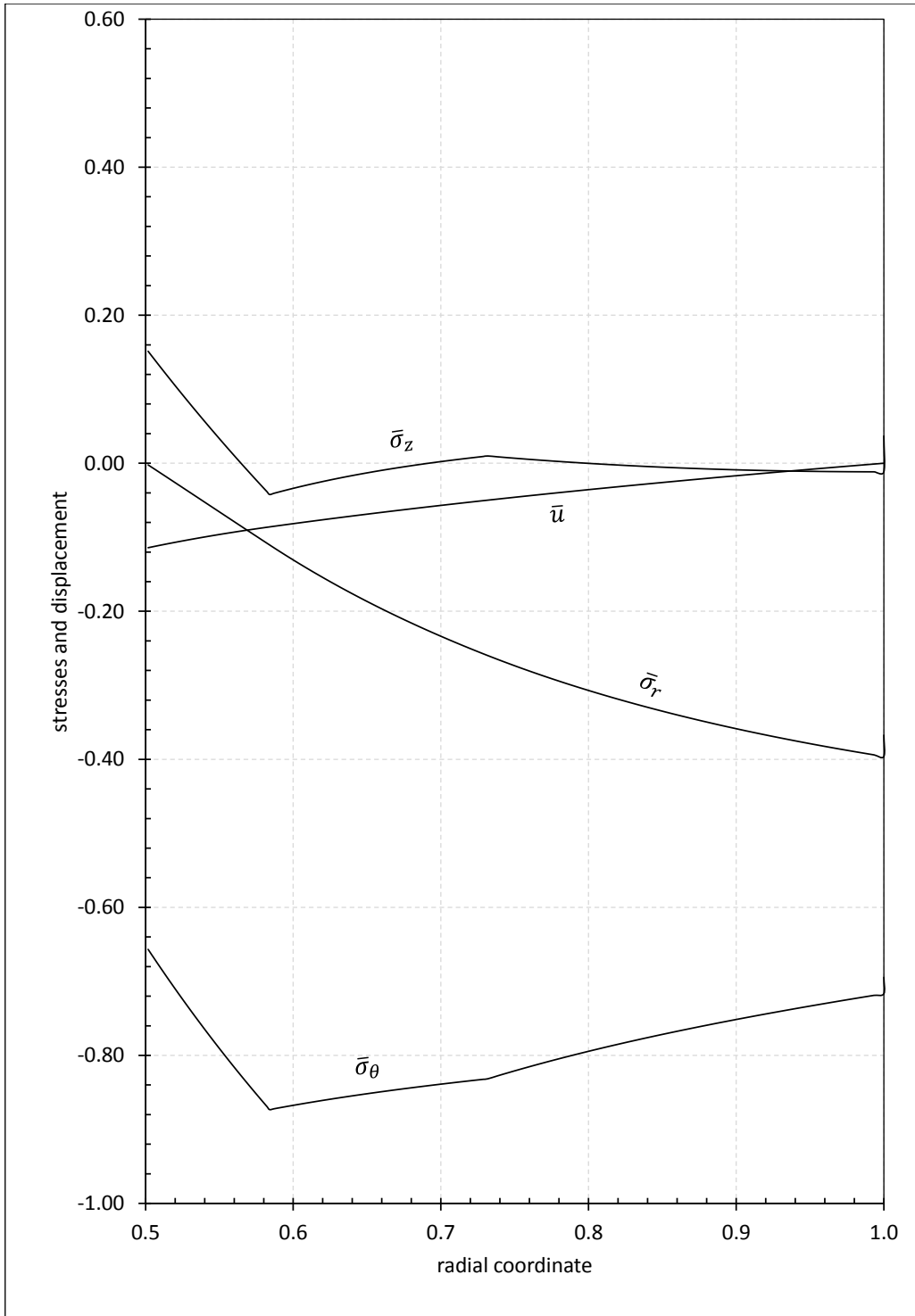


Figure 7.5: Stresses and displacement in unloaded stage at  $\tau = 1.7$

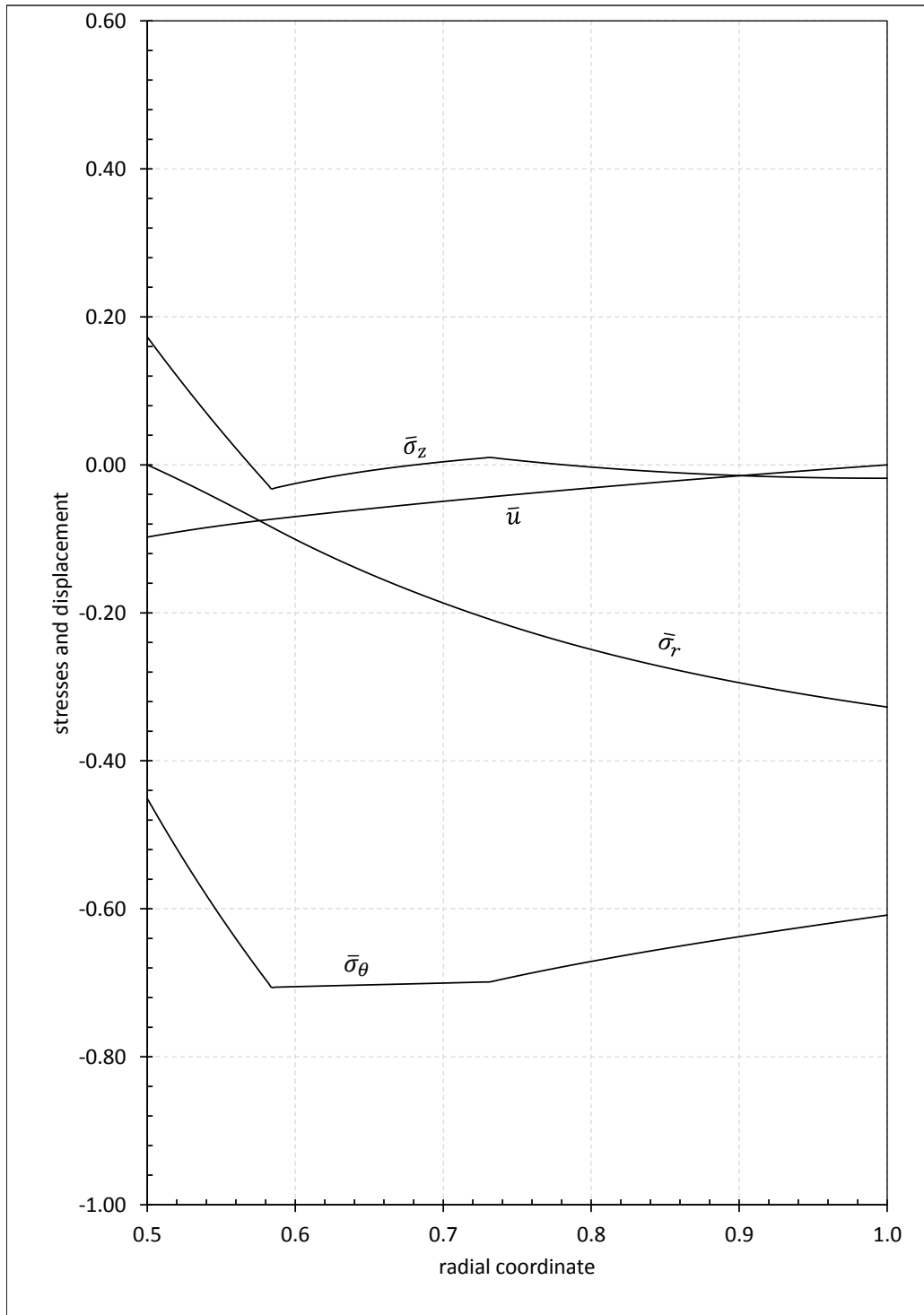


Figure 7.6: Stresses and displacement in unloaded stage at  $\tau = 1.9$

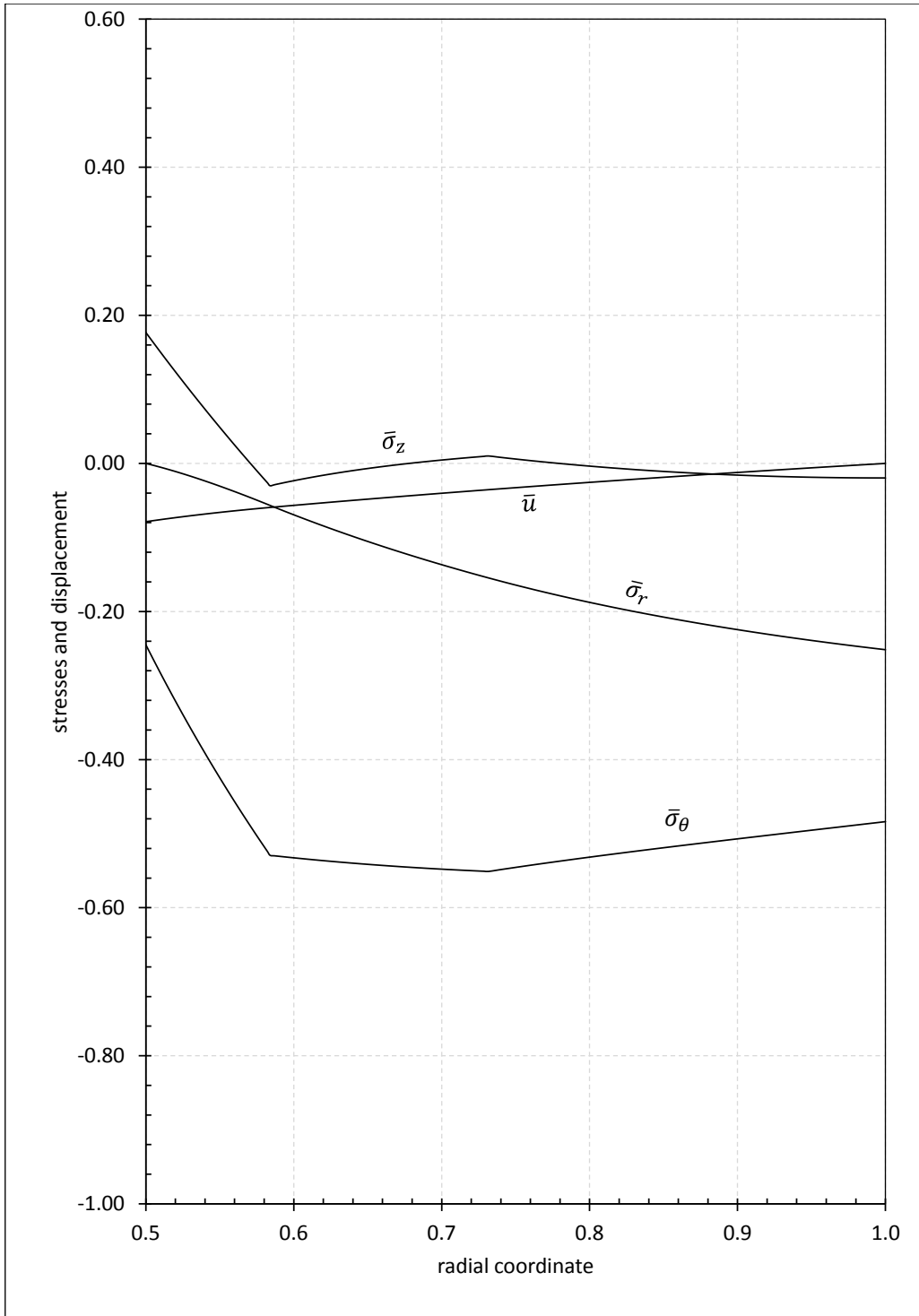


Figure 7.7: Stresses and displacement in unloaded stage at  $\tau = 2.1$

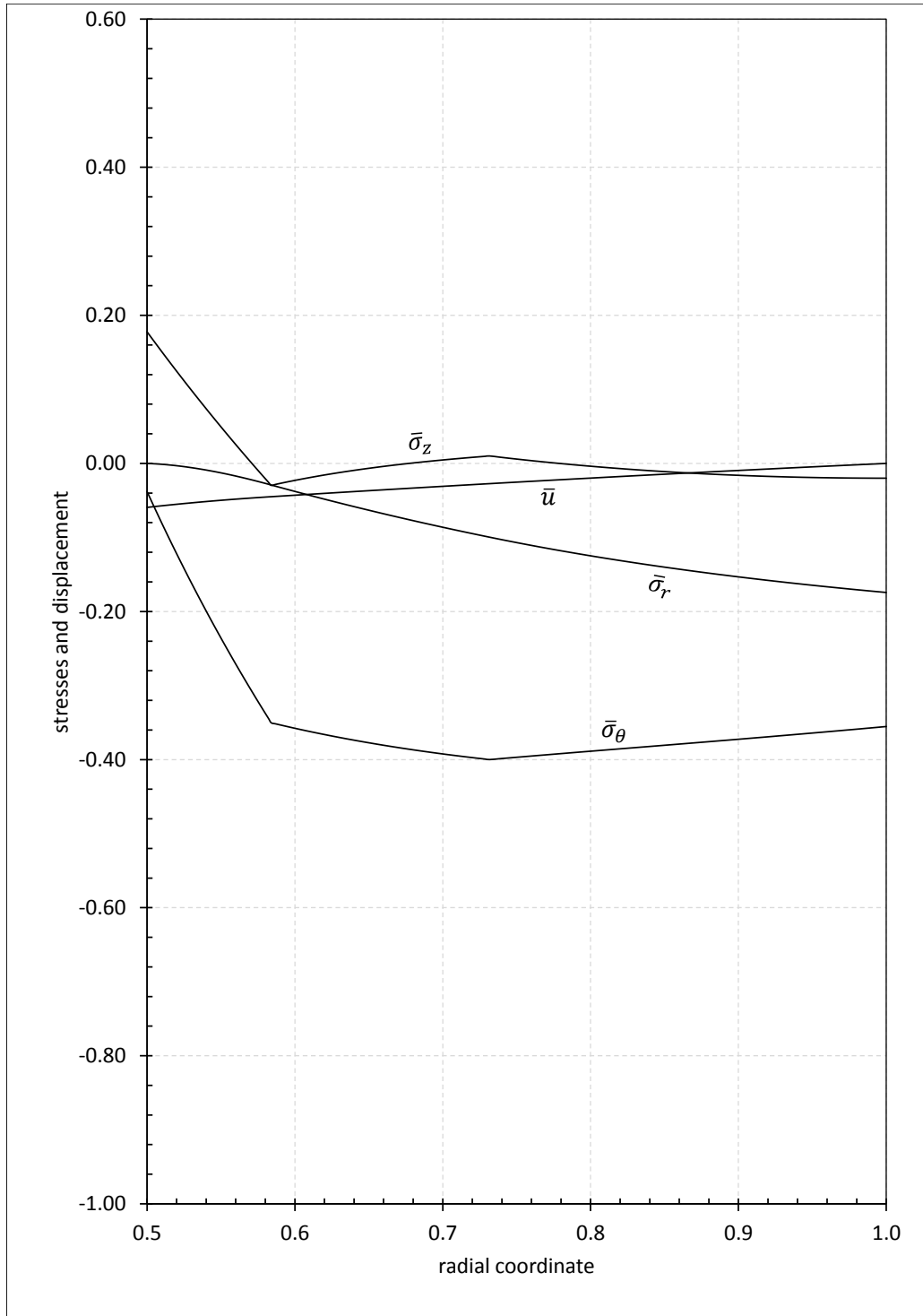


Figure 7.8: Stresses and displacement in unloaded stage at  $\tau = 2.3$

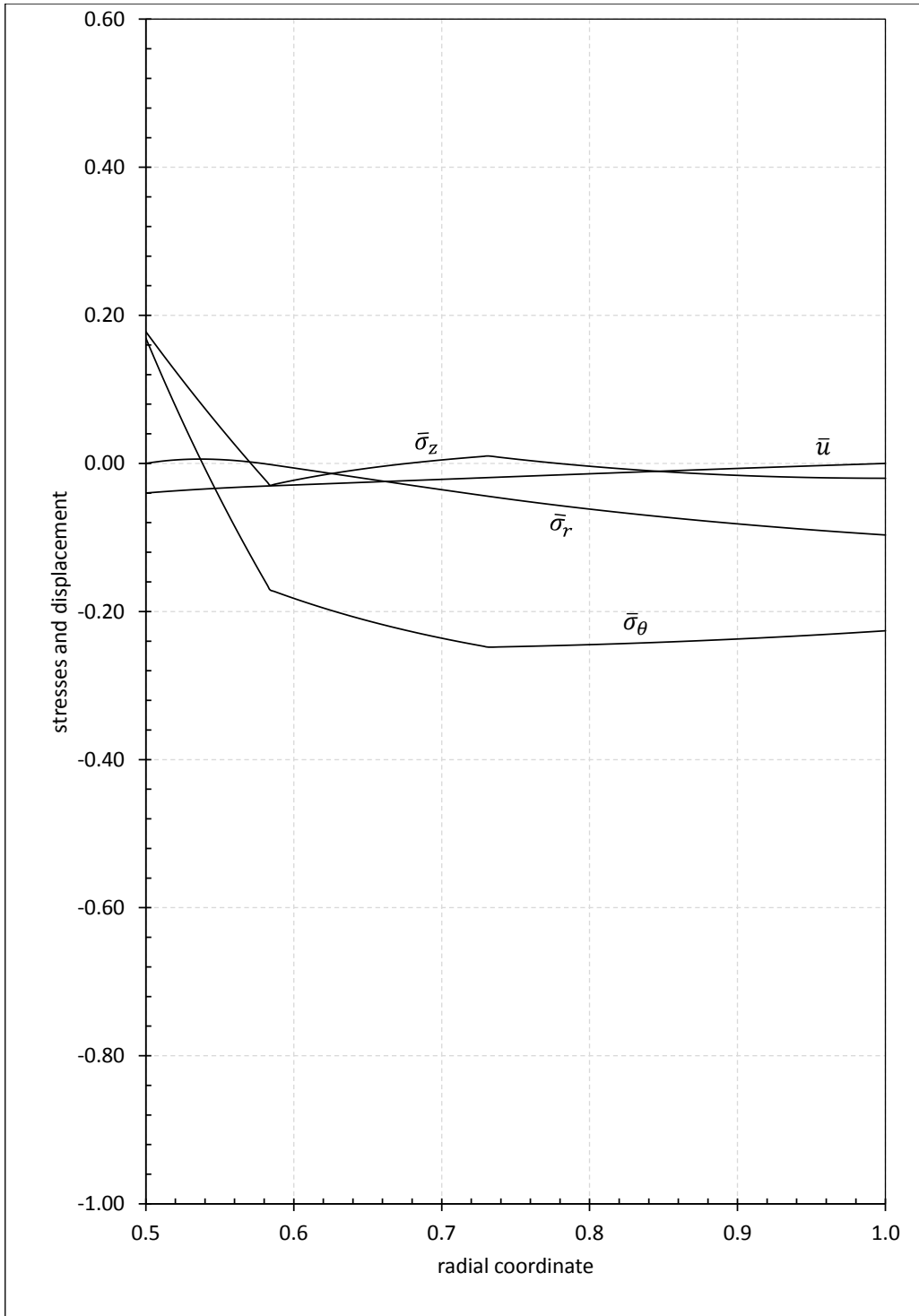


Figure 7.9: Stresses and displacement in unloaded stage at  $\tau = 2.5$

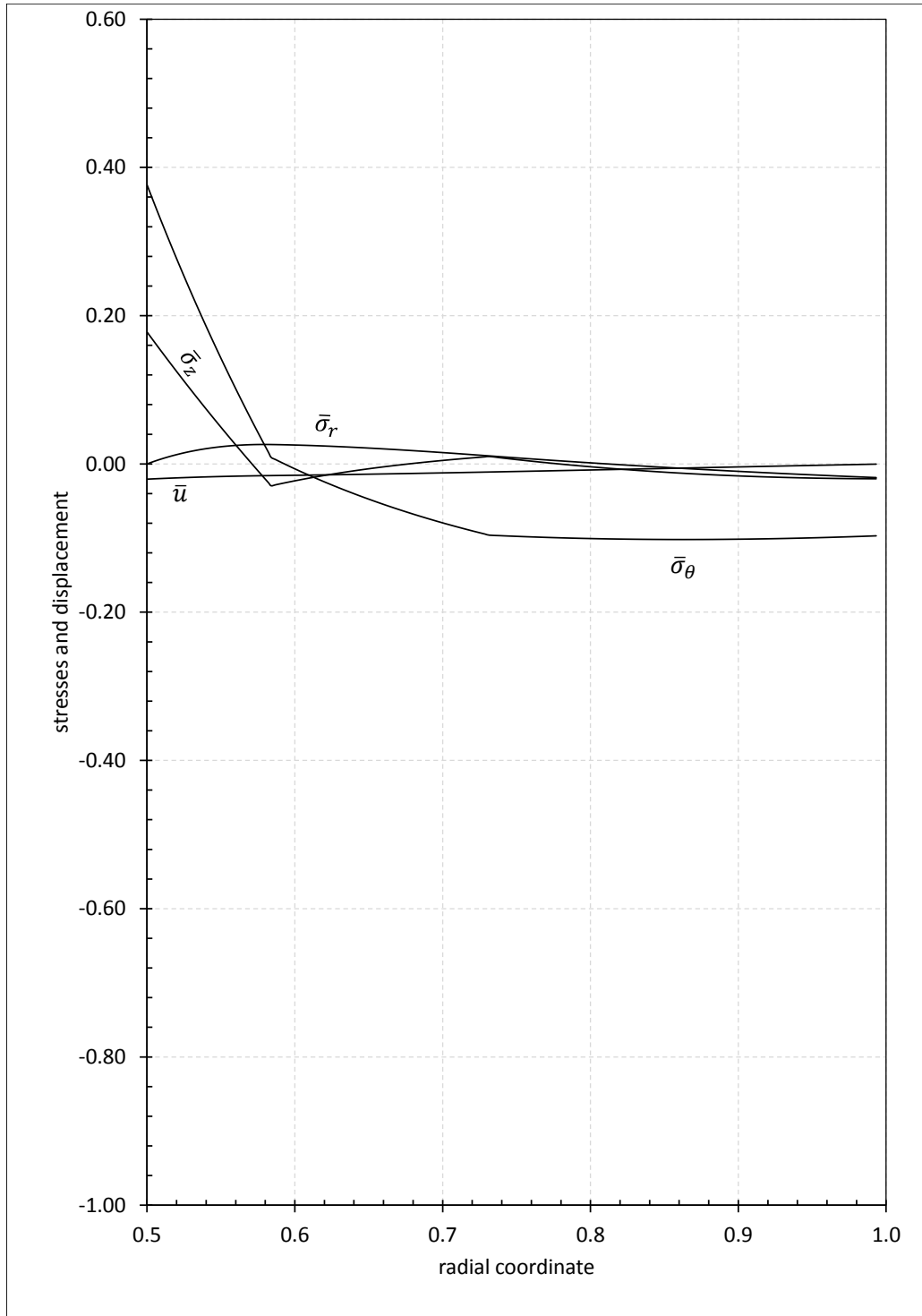


Figure 7.10: Stresses and displacement in unloaded stage at  $\tau = 2.7$

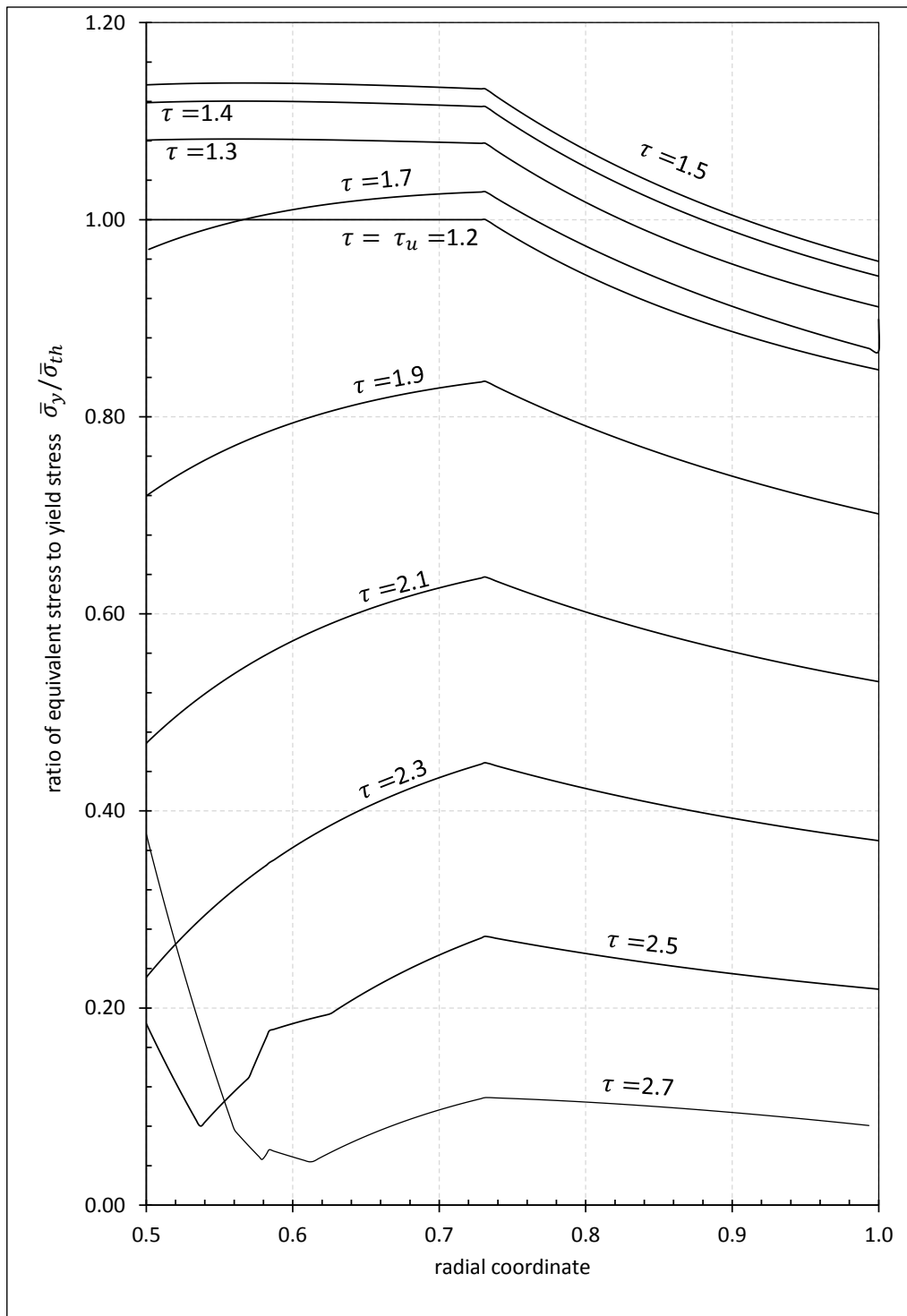


Figure 7.11: Ratio of equivalent stress to yield stress between  $\tau = 1.2$  and  $\tau = 2.7$  in unloaded stage



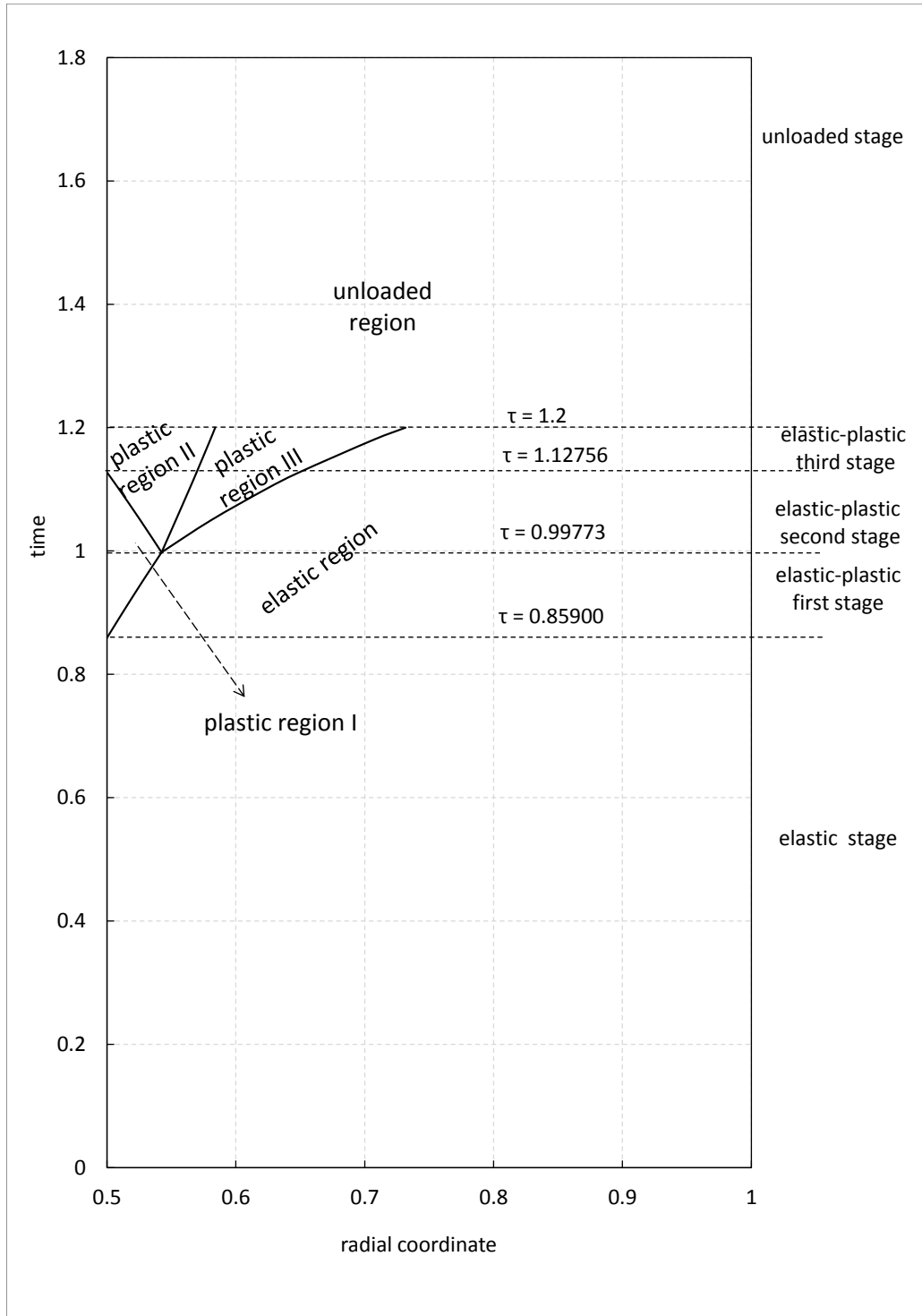


Figure 7.12: Evolution of elastic and plastic regions during the temperature cycle.



## CHAPTER 8

### SUMMARY, CONCLUSIONS AND FUTURE WORK

#### 8.1 Thesis Summary and Conclusions

In this thesis, a thermo-elastoplastic analysis of a hollow circular cylinder subject to periodical heating from its inner surface and isolated on its exterior surface is considered. As a mechanical boundary condition, the tube is stress free on the its inner wall and radially constrained from the outer wall. Since the length of the tube is very long compared to its thickness, a state of generalized plane strain condition is presumed. Small deformations theory has been taken into account. All mechanical and physical properties of the material are assumed independent of temperature. Due to the slow heating, the thermally induced wave phenomenon is vanished. End effects are ignored for such a long tube and circular symmetry is presumed.

Initially, in Ch. 4 the analytical and numerical solution of heat conduction equation is presented. Analytical results are in a good agreement with the numerical results.

Next, in Ch. 5 thermoelastic behavior of a long tube during the temperature cycle is studied and the verification of the analytical solution is made against to the numerical solution.

Additionally, in Ch. 6, analytical solutions are introduced for the tube problem by increasing the heat load parameter in order to determine the plastic behavior of the tube under temperature cycle. Firstly, the tube behaves elastic to a certain time, which is elastic stage. Then, after a certain time, the plastic deformation starts from the inner wall of the tube, which is called as elastic-plastic first stage. This plastic region is

expanded through the elastic region. When time elapses, in the plastic-elastic border, another two plastic regions (second and third plastic regions) emerge at the same time, which is named as elastic-plastic second stage. After some time, first plastic region is completely covered by the second plastic region and disappears. Second and third plastic regions are observed in the tube from the inner wall to the outer wall, while the outer wall still remains elastic, which is elastic-plastic third stage. The formulations of three plastic regions are derived separately. By this means, the stages of the tube experienced (elastic, elastic-plastic first stage, elastic-plastic second stage, and elastic-plastic third stage) are investigated.

Further, it is shown that in Ch. 7, the expansion of plastic regions gets slower and ceases when the cooling starts. For the formulation of this stage, a sudden unloading assumption is adopted. Thus, the formulation of the unloaded stage can be performed as in the formulation of elastic region including plastic strains coming from at the end of the second and third elastic regions.

At the end of these formulations, the stresses, strains and displacement distributions are plotted at different time steps of the temperature cycle. Hence, elastic and elasto-plastic behavior of the tube subjected to temperature cycle are determined.

In the mathematical aspect, the analytical treatment of tube geometry brings difficulty together compared to solid cylinder. Especially, convergence of Bessel series and handling some kind of integrals in the solution procedure are very tedious issue.

It is concluded that when a radially constrained tube subjected to a temperature cycle, the plastic deformation starts from the inner wall of the tube. Then, it is observed that the tube experiences three different plastic regions according to Tresca yield criteria. The evolution of stresses and strains in the tube are related to the temperature gradient and the loading history of the temperature.

As a result, this thesis problem contributed to the field of computational mechanics in theoretical aspect. The derived solution of thermo-elastoplastic problem of a long tube subjected to a temperature cycle is applicable for different temperature and mechanical boundary conditions.

## 8.2 Future Work

As a future work, this thesis problem may be extended:

- To investigate the effect of the temperature dependency of material properties on the thermo-elastoplastic behavior of the tube by considering a real engineering material.
- To investigate the effect of the tube thickness on the onset of plasticization.
- To investigate the elastic-plastic behavior of the tube subjected to different thermal loads such as sinusoidal temperature cycle.
- To determine the residual stresses, therefore, to analyze the behavior of the tube when the cycle is repeated.



## REFERENCES

- [1] Timoshenko S., Goodier J.N., Theory of Elasticity. 3rd ed., McGraw-Hill, New York, 1970.
- [2] Rees D.W.A., The Mechanics of Solids and Structures. McGraw Hill, New York, 1990.
- [3] Ugural A.C., Fenster S.K., Advanced Strength and Applied Elasticity. 2nd ed., Elsevier, Amsterdam, 1975.
- [4] Boley B.A, Weiner J.H., Theory of Thermal Stresses. 1st ed., Wiley Press, New York, 1960.
- [5] Arslan E., Mack W., Eraslan, A.N., Effect of a temperature cycle on a rotating elastic-plastic shaft. *Acta Mechanica* 195 (2008) 129.
- [6] Chu S.C., A Numerical Thermoelastoplastic Solution of a Thick-Walled Tube. *American Institute of Aeronautics and Astronautics (AIAA) Journal* 12:2 (1974) 176-178.
- [7] Dahl O.G.C., Temperature and stress distribution in hollow cylinders. *American Society of Mechanical Engineering Transactions* 46 (1924) 161-208.
- [8] Weiner J.H., Huddleston J.V., Transient and residual stresses in heat-treated cylinders. *Journal of Applied Mechanics of the ASME* 26 (1959) 31-39.
- [9] Landau H.G., Zwicky E.E.Jr., Transient and residual thermal stresses in an elastic-plastic cylinder. *Journal of Applied Mechanics of the ASME* 27 (1960) 481-488 .
- [10] Bland D.R., Elastoplastic thick-walled tubes of work-hardening material subject to internal and external pressures and to temperature gradients. *Journal of the Mechanics and Physics of Solids* 4 (1956) 209-220.
- [11] Perzyna P., Sawczuk A., Problems of Thermoplasticity. *Nuclear Engineering and Design* 24 (1973) 1-55 .
- [12] Valentin R.A., Carey J.J., Thermal stresses and displacements in finite, heat-generating circular cylinders. *Nuclear Engineering and Design* 12 (1970) 277-290.

- [13] Citakoglu E., Thermal stresses in a finite rod with uniform energy generation under special BCs. *METU Journal of Pure and Applied Sciences* 9 (1976) 167-187.
- [14] Ishikawa H., A thermoelastoplastic solution for a circular solid cylinder subjected to heating and cooling. *Journal of Thermal Stresses* 1 (1978) 211-222.
- [15] Ozisik M. N., *Heat Transfer. A Basic Approach*. McGraw-Hill, New York, 1985.
- [16] Ozisik M. N., *Boundary Value Problems of Heat Conduction*. McGraw-Hill, 1968.
- [17] Vedula V.R., Segall A.E., Rangarajan S.K., Technical note: Transient analysis of internally heated tubular components with exponential thermal loading and external convection. *International Journal of Heat and Mass Transfer* 41 (1998) 3675-3678.
- [18] Segall A.E., Transient analysis of thick-walled piping under polynomial thermal loading. *Nuclear Engineering and Design* 226 (2003) 183-191.
- [19] Kandula M., Transient conduction in a hollow cylinder with variable thermal conductivity. *Journal of Heat Transfer* 132:5 (2010) 0545503,1-3.
- [20] Noda N., Thermal Stresses in Materials with Temperature-Dependent Properties, in: Hetnarski R. B., (Ed.), *Thermal Stress I*, Elsevier Science. North Holland, Amsterdam (1986) 396-483.
- [21] Eraslan A.N., Argeso H., On the application of von Mises' yield criterion to a class of plane strain thermal stress problems. *Turkish Journal of Engineering and Environmental Sciences* 29 (2005) 113-128.
- [22] Eraslan A.N., Argeso H., Computer solutions of plane strain axisymmetric thermomechanical problems. *Turkish Journal of Engineering and Environmental Sciences* 29 (2005) 369-381.
- [23] Argeso H., Eraslan A.N., On the use of temperature-dependent physical properties in thermomechanical calculations for solid and hollow cylinders. *International Journal of Thermal Sciences* 47 (2008) 136-146.
- [24] Orcan Y., Gamer U., Elastic-plastic deformation of a centrally heated cylinder. *Acta Mechanica* 90 (1991) 61-80.
- [25] Orcan Y., Thermal stresses in a heat generating elastic-plastic cylinder with free ends. *International Journal of Engineering Science* 32 (1994) 883-898.
- [26] Gulgec M., Orcan Y., Elastic-plastic deformation of a heat generating tube with temperature-dependent yield stress. *International Journal of Engineering Science* 38 (2000) 89-106.



- [27] Eraslan A.N., Orcan Y., Thermoplastic response of a linearly hardening cylinder subjected to nonuniform heat source and convective boundary condition. *Mechanics Based Design of Structures and Machines* 32 (2004) 133-164.
- [28] Orcan Y., Gulgec M., Elastic-plastic deformation of a tube with free ends subjected to internal energy generation. *Turkish Journal of Engineering and Environmental Sciences* 25 (2001) 601-610.
- [29] Orcan Y., Eraslan A.N., Thermal Stresses in Elastic-Plastic Tubes With Temperature-Dependent Mechanical and Thermal Properties. *Journal of Thermal Stresses* 24:11 (2001) 1097-1113.
- [30] Eraslan A. N., Orcan Y., Computation of Transient Thermal Stresses in Elastic-Plastic Tubes: Effect of Coupling and Temperature-Dependent Physical Properties. *Journal of Thermal Stresses* 25:6 (2002) 559-572.
- [31] Mack W., Plöchl M., Transient heating of a rotating elastic-plastic shrink fit. *International Journal of Engineering Science* 38 (2000) 921-938.
- [32] Jahanian S., Sabbaghian M., Thermoelastoplastic and Residual Stresses in a Hollow Cylinder With Temperature-Dependent Properties. *Journal of Pressure Vessel Technology* 112 (1990) 85-91.
- [33] Jahanian S., Thermoelastoplastic Stress Analysis of a Thick-Walled Tube of Nonlinear Strain Hardening. *Journal of Mechanical Design* 118:3 (1996) 340-346.
- [34] Jahanian S., On the incremental growth of mechanical structures subjected to cyclic thermal and mechanical loading. *International Journal of Pressure Vessels and Piping* 71 (1997) 121-127.
- [35] Mukhopadhyay S., Kumar R., Solution of a Problem of Generalized Thermoelasticity of an Annular Cylinder with Variable Material Properties by Finite Difference Method. *Computational Methods in Science and Technology* 15:2 (2009) 169-176.
- [36] Zenkour A. M., Abbas I. A., A Generalized Thermoelasticity Problem of an Annular Cylinder. *International Journal of Thermal Sciences* 84 (2014) 54-60.
- [37] Shahani A. R., Nabavi S. M., Analytical solution of the quasi-static thermoelasticity problem in a pressurized thick-walled cylinder subjected to transient thermal loading. *Applied Mathematical Modeling* 31 (2007) 1807-1818.
- [38] Segall A. E., Thermoelastic Stresses in an Axisymmetric Thick-Walled Tube Under an Arbitrary Internal Transient. *Journal of Pressure Vessel Technology* 126 (2004) 327-332.

- [39] Kim K.S., Noda N., Green's function approach to unsteady thermal stresses in an infinite hollow cylinder of functionally graded material. *Acta Mechanica* 156:3-4 (2002) 145-161.
- [40] Radu V., Taylor N., Paffumi E., Development of new analytical solutions for elastic thermal stress components in a hollow cylinder under sinusoidal transient thermal loading. *International Journal of Pressure Vessels and Piping* 85 (2008) 885-893.
- [41] Mendelson A., *Plasticity. Theory and Application*, 1st ed., McMillan Comp., New York, 1968.
- [42] Johnson W., Mellor P.B., *Plasticity for Mechanical Engineers*. D. Van Nostrand Comp., Great Britain, 1970.
- [43] Tresca H., Memoire sur l'écoulement des Corps Solides. *Mem. Sci. Savants Acad. Sci.* 18 (1868) 733-799.
- [44] Von Mises R., *Mechanik der festen Koerper in Plastisch deformablem Zustand*, Göttinger Nachrichten Math. Phys. Klasse 1 (1913) 582-592.
- [45] Saint-Venant B., Memoire sur l'établissement des equations differentielles des mouvements interieurs operes dans les corpse solides ductiles au dela des limites ou l'elasticite pourrait les ramener a leur premier etat. *Comptes Rendus* 70 (1870) 473-480.
- [46] Prandtl L., *Spannungsverteilung in plastischen Koerpern*. 1st International Congress on Applied Mechanics, Delft (1925) 43-54.
- [47] Reuss E., *Berueckesichtigung der elastischen Formaenderungen in der Plastizitaetstheorie*. *The Journal of Applied Mathematics and Mechanics (ZAMM)* 10 (1930) 266-274.
- [48] Beer F.P., Johnston E.R., DeWolf J.T., *Mechanics of Materials*. 3rd ed., McGraw Hill, New York, 1943.
- [49] Chen W.F., Han D.J., *Plasticity for Structural Engineers*. J. Ross Pub., Ft. Lauderdale, 2007.
- [50] Hill R., *The Mathematical Theory of Plasticity*. Oxford University Press, London, 1950.
- [51] Carslaw H.S., Jaeger J.C., *Conduction of heat in solids*. 2nd ed., Clarendon Press, Oxford, 1959.
- [52] Madsen N.K., Sincovec R.F., PDECOL, General Collocation Software for Partial Differential Equations, *ACM Transactions on Mathematical Software* 5:3 (1979) 326-351.

- [53] Eraslan A. N., Kartal M. E., A Nonlinear Shooting Method Applied to Solid Mechanics: Part 1. Numerical Solution of a Plane Strain Model. *International Journal of Nonlinear Analysis and Phenomena* 2 (2005b) 31-42.
- [54] Kreyszig E., *Advanced Engineering Mathematics*. 8th ed., Wiley Press, New York, 1999.
- [55] Ziegler F., *Technische Mechanik der festen und flüssigen Körper*. Dritte, verb. Aufl., Ch. 4.3, Springer, Wien, 1998.
- [56] More J.J., Garbow B.S., Hillstom K.E., Testing unconstrained optimization software. *ACM Transactions on Mathematical Software* 7 (1981) 17-41.
- [57] Mack W., Gamer U., Zur Berechnung der Restspannungen beim Abkühlen thermisch beanspruchter elastisch-plastischer Bauteile. *Forschung im Ingenieurwesen/Engineering Research* 54 (1988) 48-52.
- [58] Mack W., Spannungen im thermisch gefügten elastisch-plastischen Querspreßverband mit elastischer Entlastung. *Ingenieur-Archiv* 56 (1986) 301-313.
- [59] Garbow B. S., Hillstom K. E., More J. J., *Minpack Project*. Argonne National Laboratory, 1980.
- [60] Davis J.D., Rabinowitz P., *Numerical Integration*. 1st ed., Blaisdell, Massachusetts, 1967.



## APPENDIX A

### DATA OF PERMANENT PLASTIC STRAINS

Table A.1: Plastic strains at  $\tau = 1.2$ .

$\bar{r}$	$\bar{\epsilon}_r$	$\bar{\epsilon}_\theta$	$\bar{\epsilon}_z$	$\bar{r}$	$\bar{\epsilon}_r$	$\bar{\epsilon}_\theta$	$\bar{\epsilon}_z$
0.50000	0.15647	-0.16753	0.01106	0.53771	0.07748	-0.10324	0.02575
0.50171	0.15250	-0.16426	0.01176	0.53942	0.07427	-0.10066	0.02639
0.50343	0.14858	-0.16103	0.01245	0.54114	0.07108	-0.09811	0.02703
0.50514	0.14469	-0.15783	0.01314	0.54285	0.06792	-0.09558	0.02766
0.50686	0.14084	-0.15467	0.01383	0.54457	0.06479	-0.09308	0.02829
0.50857	0.13703	-0.15154	0.01451	0.54628	0.06169	-0.09061	0.02892
0.51028	0.13325	-0.14845	0.01520	0.54799	0.05862	-0.08816	0.02954
0.51200	0.12951	-0.14539	0.01588	0.54971	0.05557	-0.08574	0.03017
0.51371	0.12581	-0.14236	0.01655	0.55142	0.05256	-0.08334	0.03079
0.51543	0.12214	-0.13937	0.01723	0.55314	0.04957	-0.08097	0.03141
0.51714	0.11851	-0.13641	0.01790	0.55485	0.04660	-0.07862	0.03202
0.51886	0.11491	-0.13348	0.01857	0.55657	0.04366	-0.07630	0.03264
0.52057	0.11134	-0.13058	0.01923	0.55828	0.04075	-0.07400	0.03325
0.52228	0.10781	-0.12771	0.01990	0.55999	0.03786	-0.07172	0.03386
0.52400	0.10432	-0.12487	0.02056	0.56171	0.03500	-0.06947	0.03446
0.52571	0.10085	-0.12207	0.02122	0.56342	0.03217	-0.06724	0.03507
0.52743	0.09742	-0.11929	0.02187	0.56514	0.02936	-0.06503	0.03567
0.52914	0.09402	-0.11654	0.02253	0.56685	0.02657	-0.06284	0.03627
0.53085	0.09065	-0.11383	0.02318	0.56856	0.02381	-0.06068	0.03687
0.53257	0.08731	-0.11114	0.02382	0.57028	0.02107	-0.05853	0.03746
0.53428	0.08401	-0.10848	0.02447	0.57199	0.01836	-0.05641	0.03806
0.53600	0.08073	-0.10584	0.02511	0.57371	0.01567	-0.05431	0.03865

Table A.1 (cont'd)

$\bar{r}$	$\bar{\epsilon}_r$	$\bar{\epsilon}_\theta$	$\bar{\epsilon}_z$	$\bar{r}$	$\bar{\epsilon}_r$	$\bar{\epsilon}_\theta$	$\bar{\epsilon}_z$
0.57542	0.01300	-0.05223	0.03923	0.65333	0.00000	-0.01854	0.01854
0.57713	0.01035	-0.05017	0.03982	0.65634	0.00000	-0.01769	0.01769
0.57885	0.00773	-0.04814	0.04040	0.65936	0.00000	-0.01686	0.01686
0.58056	0.00513	-0.04612	0.04099	0.66237	0.00000	-0.01603	0.01603
0.58228	0.00256	-0.04412	0.04157	0.66539	0.00000	-0.01522	0.01522
0.58399	0.00000	-0.04214	0.04214	0.66840	0.00000	-0.01442	0.01442
0.58701	0.00000	-0.04093	0.04093	0.67142	0.00000	-0.01363	0.01363
0.59002	0.00000	-0.03974	0.03974	0.67443	0.00000	-0.01285	0.01285
0.59303	0.00000	-0.03856	0.03856	0.67745	0.00000	-0.01208	0.01208
0.59605	0.00000	-0.03740	0.03740	0.68046	0.00000	-0.01133	0.01133
0.59906	0.00000	-0.03626	0.03626	0.68347	0.00000	-0.01058	0.01058
0.60208	0.00000	-0.03514	0.03514	0.68649	0.00000	-0.00985	0.00985
0.60509	0.00000	-0.03404	0.03404	0.68950	0.00000	-0.00913	0.00913
0.60811	0.00000	-0.03296	0.03296	0.69252	0.00000	-0.00841	0.00841
0.61112	0.00000	-0.03189	0.03189	0.69553	0.00000	-0.00771	0.00771
0.61414	0.00000	-0.03084	0.03084	0.69855	0.00000	-0.00702	0.00702
0.61715	0.00000	-0.02980	0.02980	0.70156	0.00000	-0.00633	0.00633
0.62017	0.00000	-0.02878	0.02878	0.70458	0.00000	-0.00566	0.00566
0.62318	0.00000	-0.02778	0.02778	0.70759	0.00000	-0.00500	0.00500
0.62620	0.00000	-0.02679	0.02679	0.71061	0.00000	-0.00434	0.00434
0.62921	0.00000	-0.02582	0.02582	0.71362	0.00000	-0.00369	0.00369
0.63223	0.00000	-0.02486	0.02486	0.71664	0.00000	-0.00306	0.00306
0.63524	0.00000	-0.02391	0.02391	0.71965	0.00000	-0.00243	0.00243
0.63825	0.00000	-0.02298	0.02298	0.72267	0.00000	-0.00181	0.00181
0.64127	0.00000	-0.02207	0.02207	0.72568	0.00000	-0.00120	0.00120
0.64428	0.00000	-0.02117	0.02117	0.72869	0.00000	-0.00059	0.00059
0.64730	0.00000	-0.02028	0.02028	1.00000	0.00000	0.00000	0.00000
0.65031	0.00000	-0.01940	0.01940				

# CURRICULUM VITAE

## PERSONAL INFORMATION

**Surname, Name:** Kaya, Yasemin

**Nationality:** Turkish (TC)

**Date and Place of Birth:** 23.08.1980, Giresun

**Marital Status:** Single

## EDUCATION

<b>Degree</b>	<b>Institution</b>	<b>Year of Graduation</b>
M.S.	METU, Engineering Sciences Dept.	2007
B.S.	Gazi University, Chemical Engineering Dept.	2003
High School	Trabzon Yomra Fen Lisesi	1997

## PROFESSIONAL EXPERIENCE

<b>Year</b>	<b>Place</b>	<b>Enrollment</b>
2006-2013	Engineering Sciences Dept./METU	Research Assistant
2011- 3 Months	TU Wien/Austria	Visiting Graduate Researcher
2010- 3 Months	TU Wien/Austria	Visiting Graduate Researcher

## PUBLICATIONS

1. Eraslan A.N., Kaya Y., Ciftci B., A computational model for partially-plastic stress analysis of orthotropic variable thickness disks subjected to external pressure, Math-

emathical Sciences And Applications E-Notes, (2014) 2: 1, 1–13.

2. Kaya Y., Eraslan A.N., Thermoelastic response of a long tube subjected to periodic heating, Mathematical Sciences And Applications E-Notes (2014) 2 : 1, 14–27.

### **International Conference Publications**

1. Eraslan A.N., Kaya Y., Ciftci B., A computational model for partially-plastic stress analysis of orthotropic variable thickness disks subjected to external pressure, 2nd International Eurasian Conference on Mathematical Sciences and Applications, Sarajevo-Bosnia and Herzegovina-2013.

2. Kaya Y., Eraslan A.N., Thermoelastic response of a long tube subjected to periodic heating, 2nd International Eurasian Conference on Mathematical Sciences and Applications, Sarajevo-Bosnia and Herzegovina-2013.

3. Eraslan A.N., Kaya Y., Varlı E., Analytical Solutions to Orthotropic Variable Thickness Disk Problems, 2nd International Eurasian Conference on Mathematical Sciences and Applications, Sarajevo-Bosnia and Herzegovina-2013.

### **National Conference Publications**

1. Eraslan A.N., Kaya Y., Değişken kalınlıklı ortotropik disk probleminin elastik analitik çözümü, 15. Ulusal Mekanik Kongresi, Isparta, Eylül 2007.

2. Eraslan A.N., Kaya Y., Termoelastik kuplaj problemlerinin hassas sayısal çözümü için bir yöntem, 13. Ulusal Mekanik Kongresi, Antakya, Eylül 2005.